Feasibility of Smart Antennas for the Small Wireless Terminals

Raqibul Mostafa

Dissertation submitted to the Faculty of Virginia Polytechnic Institute and State University in partial fulfillment of the requirements for the degree of

Doctor of Philosophy
in
Electrical and Computer Engineering

Jeffrey H. Reed, Chair
Warren L. Stutzman
William H. Tranter
Annamalai Annamalai
Hanif D. Sherali

April 25, 2003

Blacksburg, Virginia

Keywords: Transmit diversity, small wireless terminal, MIMO, vector channel measurements

Feasibility of Smart Antennas for the Small Wireless Terminals

Raqibul Mostafa

(ABSTRACT)

Smart antenna is a potential performance enhancement tool in a communications link that can be used at either end (transmitter or receiver) of the link in the form of beamforming or diversity operation. While receive smart antenna techniques and operations have matured over the years, transmit smart antenna is relatively a new concept that has seen its growth over the past few years. Both these smart antenna operations have been traditionally designed for base station applications. But with the advent of high-speed processors, transmit smart antenna can also be feasible at a small wireless terminal (SWT). This dissertation studied the feasibility of using smart antenna at a SWT. Both smart transmit and receive antennas are studied, including multiple input and multiple output (MIMO) systems, however the emphasis is placed on transmit smart antennas. The study includes algorithm developments and performance evaluations in both flat fading and frequency selective channels. Practical issues, i.e., latency and amount of feedback, related to transmit smart antenna operation are discussed. Various channel measurements are presented to assess the performance of a transmit smart antenna in a real propagation environment. These include vector channel measurements for narrowband and wideband signals, channel reciprocity, and effect of antenna element spacing on diversity performance. Real-time demonstrations of transmit smart antenna have been performed and presented, and, the applicability of the proposed techniques in the Third Generation standards and wireless local area networks (WLAN) is discussed. Receive beamforming with a small number of antenna elements (which is usually the case for a SWT) is analyzed in an interference-limited environment.

ACKNOWLEDGEMENTS

I am grateful to Allah Almighty for providing with an opportunity to pursue a doctoral degree and helping me see through to finishing this dissertation. I deeply acknowledge the support and guidance of Jeffrey H. Reed that he has provided me over the years. His profound technical insight and vision has helped to give the proper shape to this dissertation. I would like to thank Warren Stutzman and William H. Tranter for their advice in propagation measurement and filter design. I would also like to thank Annamalai Annamalai for his support in the work on selective nulling of interferers. Thanks also go to Hanif Sherali for his advice on optimization. I acknowledge the help and support of Ashok Tikku who helped me in the early stages of my research. I also thank all the MPRG students who provided such a bright academic atmosphere. Thanks go to Rich Ertel, Tom Biedka, Uwe Ringel, Zhong Hu, Nitin Mangalvedhe, Ran Gozali, Bill Newhall, Kai Dietze, Max Robert, Ramesh Pallat, James Hicks, Fakhrul Alam, Ariful Hannan and Maruf Mohammad. My heartfelt thanks are for my parents, my brother Rusho, and my wife, Farzana Ahmed who helped me through all these years to reach my goals. I also acknowledge Texas Instruments (TI) and NAVCIITI for sponsoring this research.

Table of Contents

List of Figures

List of Tables

Chapter 1

Introduction

Smart antenna systems find applications in communications systems for their potential in improving signal-to-noise ratio (SNR), link quality and reliability, and providing position location capability to user terminals. Smart antenna systems are traditionally designed for base station applications since the base station has space and enough processing power to support array processing. Smart antenna operations include diversity and beamforming (or null steering) and are predominantly used in the receive mode [JAK74], [BRE59]. Interest has recently increased in using an antenna array at the transmitter and doing beamforming in the downlink. The factor driving research interest in this direction is that if beamforming can be performed in the downlink at a base station, then the need for an antenna array at the mobile units is obviated, thus, reducing complexity and power consumption. The mobile unit form factor is not suitable for a large array size.

The use of antenna arrays at a small wireless terminal (SWT) has been viewed unfavorably because of technical difficulties. The SWT devices include (but not limited to): handset in cellular systems, wireless local area networks (WLAN) access points and user terminals, PDA, Bluetooth access points and terminals and indoor wireless fixed point to point systems. The new generation of high-speed, low power digital signal processors and miniaturized RF components facilitate computationally complex operations at the handheld terminal and supporting multiple RF chains for array processing. Use of smart antenna at the handset and performance improvement has been reported in [MOS00] and [DIE01]. Recently there have been reports of commercial prototypes of using two-element smart antenna systems for user terminals or WLAN access points [QUA01, KTF03, PAN03] and some of them are shown in Figure 1.1.

Figure 1.1. Some examples of commercial application of smart antenna at small wireless terminals (from left to right): Qualcomm QCTEST, KTF wireless PC card and Panasonic handset.

The commercial prototypes implement simple switching or selection diversity in the receive mode. More sophisticated diversity algorithms or beamforming techniques have not been implemented so far in SWTs. Additionally, transmit diversity has not been addressed for such devices. Transmit diversity is a welcome feature to use in a device that is already using receive diversity. If the end devices in a communications link are using smart antenna in the receive mode, additional benefits can be obtained by using transmit diversity at the transmitter and receive diversity at the receiver. This results in a multiple-input-multiple-output (MIMO) system that provides higher order of diversity benefits and throughput enhancement. Transmit diversity when implemented in a closed-loop fashion require feedback from the destination device (other SWT or a base station) and is thus subjected to latency and channel propagation errors. This dictates that transmit diversity techniques for SWT applications should focus on rapid convergence in order to tackle dynamic channel in addition to have simple computation for reducing processing burden. These requirements are distinctively different from those for receive diversity and need careful attention for implementing transmit diversity at the SWT. A transmit smart antenna can operate either in diversity or beamforming mode. The distinction between these two modes of operation depends on the inter-element spacing of the antenna array. In diversity mode, the spacing must be large enough (within practical limits) to yield uncorrelated signals at the antenna branches. In beamforming mode, there is an upper limit on the inter-element spacing to restrict generation of grating lobes. For a SWT form-factor, the small inter-element spacing is adequate for both diversity and beamforming operation.

The SWT can support antenna arrays of two to three elements because of the limited real estate. This poses a restriction on nulling interfering signals since an M element array can eliminate at most M-1 interfering signals. For a three elements array, this results in nulling two interferers and this may not be adequate in an interference-limited environment. In such a scenario, the technique of nulling of the dominant interfering signals can be adopted and analyzed to see the amount of improvement. This selective nulling of dominant interferers (SNDI) is an attractive feature for SWT applications. This dissertation addresses transmit smart antenna algorithm development and performance assessment for SWT applications. Practical channel measurements have been performed to test the algorithms and reported in this dissertation. Hardware demonstrations and implementation in wireless communications standards, i.e., Third Generation (3G) and WLAN IEEE 802.11 are also presented. The analysis of SNDI technique is presented.

The organization of this chapter is as follows. The classification of transmit diversity techniques and algorithms is presented in Section 1.1. An overview of existing research in this field is presented in Section 1.2. Then Section 1.3 provides with the research contributions. Section 1.4 presents the organization of this dissertation.

1.1 Classification of Transmit Diversity (TD) Techniques

The existing transmit diversity schemes can be classified from different perspectives. From the perspective of a diversity control mechanism, diversity techniques can be broadly classified as open loop techniques and closed-loop techniques.

Open loop—The open loop techniques refer to those that do not require any control mechanism or assistance from a receiver to aid in the proper functioning of the transmit diversity technique. This type of technique is simple to implement and does not require modification into existing signal format to implement feedback from receiver. Performance does not suffer from latency associated with a closed-loop system.

Closed-loop—The closed-loop systems, on the other hand, rely on some feedback information from the receiver. The feedback can be channel estimate, complex gain, or antenna selection index. The performance is generally better for a closed-loop system since it utilizes knowledge about the channel or the quality of the received signal. The issues associated with a closed-loop system are latency and errors for the feedback symbols due to channel degradation.

The existing transmit diversity techniques can also be classified according to the type of implementation: switched/selection diversity, complex weighting, and temporal processing.

Switched/Selection diversity—Switched/Selection diversity refers to simple switching between the transmit antenna elements. If the switching is done with a predefined pattern without any assistance from the receiver, then it is known as switching diversity. Simple switching is hardly ever suggested in the literature. With selection diversity, the switch position is selected using feedback from the receiver indicating the most favorable antenna. The duration of transmission with one particular antenna is determined by either the length of time-slots in Time Division Duplex (TDD) systems or the time interval of sending feedback. The advantages include low power consumption, inexpensive hardware, and simple realization. The disadvantages are omni-directional radiation of power, possibly causing interference to other users and no antenna selection update during a particular time slot in a TDD system.

Complex weighting—In the complex weighting scheme, all antennas with individual complex gains are used for simultaneous transmission. The antenna weights have to be updated fast enough to track the channel dynamics. The channel parameters are estimated before updating the weights, either by measurement or by prediction. If channel estimation is performed at the receive side, then a feedback link to the transmitter is required. The method of calculating the complex weights are usually based on the following objectives:

1. simultaneous maximization of desired signal power and minimization of interference signal power,
2. minimization of outage probability (probability that the signal-to-interference ratio (SIR) drops below certain threshold),
3. maximization of the instantaneous SNR,
4. minimization of amplitude fluctuation of the desired signal caused by interfering signals.

In general, the proposed algorithms for updating the antenna weights are complex and computationally expensive. In some cases a solution for optimum weights may not exist. Channel estimation was not considered in most reviewed papers; rather, perfect channel knowledge was assumed to obtain the complex weights. The complexity of computations (objective 1) makes real-time implementation difficult, especially in moderate to fast fading environments.

Temporal processing—Some additional temporal processing can be necessary for either countering a frequency selective channel, or encoding the information symbols in an open loop system. The second case is usually referred to as the space-time (ST) coding where the encoded symbols are assigned to different antenna elements.

1.2 Existing Transmit Diversity (TD) Techniques

The shifting of diversity operation from the receive side to the transmit side caught the attention of the research community in the early 1990s and the amount of published research has since seen a steady growth. Transmit diversity has been addressed mainly from the base station perspective though some of the proposed techniques can be implemented at the handset. The majority of the research has been devoted to solving transmit diversity problems for a flat fading channel while a few addresses transmit diversity for a frequency selective channel. Transmit diversity received a boost with the advent of ST encoding and its inclusion in the third generation or International Mobile Communications in the year 2000 (3G or IMT-2000) standard. A brief overview of key research papers is given in the following paragraphs to introduce to the readers the current state of research in this field.

Hottinen and Wichman [HOT98] discuss a transmit diversity scheme called Selective Transmit Diversity (STD), proposed for a code division multiple access (CDMA) system. The results (a two-element system with an antenna switching rate of 400Hz–1.6KHz) showed a significant bit-error rate (BER) improvement compared to a single antenna transmission.

Majmundar [MAJ] presents a technique where successive transmission slots are allocated for different antenna elements that have the strongest gain in the receive mode. The proposed technique achieves a performance gain of 2–4 dB at a BER of 10^{-2} (vehicle speed is 8 km/h). Wittneben and Kaltenschnee [WIT94] provide another realization where samples from an antenna in receive mode are fed into a minimum mean square error (MMSE) predictor (non-adaptive) and predictor output is mapped to symbol error rates for each transmit antenna. The antenna with the smallest symbol error rate predicted is chosen for the next transmission.

A simple transmit diversity scheme called partial phase combining (PPC), is proposed by Heath and Paulraj [HEA98] where relative channel phase information is quantized and fed back to the transmitter. For a 2×1 systems, the authors claim to achieve near perfect channel knowledge performance (within 1 dB) with two bits of feedback and an improvement over ideal selection diversity by 1 dB with three bits of feedback (at frame error rate (FER) of 10^{-1}).

The authors in [DAS95] consider transmit diversity schemes employing fading-resistant signal constellations that are implemented at a base station having L antennas. Transmit diversity at the base station using a linear array with equal spacing and ideal sectorized antenna elements (120^0 sector) is considered by Zetterberg and Ottersten in [ZET94]. The proposed technique is implemented by estimating the angular positions of the mobiles and using a channel allocator to decide which mobiles should use the same channel. It is shown that the actual capacity gain is largely dependent on the number of antenna elements in the array and the angular width of the locally scattered rays in the vicinity of the mobile.

The authors in [YAN98] examine the computation of downlink weighting vectors of a TDD system. They state that the weight computation has to be solved globally, across all users in the system, to get an optimal or near optimal solution. A system with an eight-element transmit array and thirty users is simulated and it is shown that transmit power can be reduced by 4.3 dB, compared to a system without the proposed scheme, to achieve an SINR of 10dB.

It is reported in [FAR98] that transmit beamforming can be done jointly in the entire network in conjunction with channel probing (frequency division duplex (FDD) system) and feedback to the base station. Since the proposed technique requires full knowledge of the channel and array responses of the entire network, the authors express concerns about its practical implementation.

Rayleigh *et. al*. in [RAY95] develop an algorithm to calculate transmit weight vectors based upon estimates of the receive vector channel for a FDD system. The authors claim that the estimates of the receive channel can be used to determine the transmit weight vector since there is a strong relationship between the average receive vector subspace and the average transmit channel subspace. Simulations suggest an increase in re-use capacity of 5–8 for a system similar to advanced mobile phone system (AMPS) or interim standard 54 (IS-54).

Lo [LO99] investigates $L \times K$ MIMO system and provides the optimal solution in a flat fading channel. Simulations indicate that the error probability decreases inversely with the $L*K$ power of the average SNR.

Mecklai and Blum [MEC95] propose a technique employing a transmit antenna array at the base station to reduce the level of interference at each user's receive antenna in a slow varying, flat fading channel.

Farsakh and Nossek [FAR95] present work on downlink beamforming and channel allocation for a multi-user system employing space division multiple access (SDMA). Their proposed technique aims to minimize total output power from a transmit array while maintaining a given SINR.

[GER94] considers the problem of minimizing the reception of signals not intended for other users. Reasonable mobile spacing requires feedback on the order of thousands of kilobytes per second, thus limiting the approach to static or slow moving receivers.

Winters [WIN94], [WIN98] proposes a scheme where a transmitter progressively delays the signal and transmits it through different antenna elements to generate frequency selective fading. The proposed technique provides performance that is close to a maximal ratio combining receive diversity system of the same order.

Papers [ALA98], [TAR98], and [ALA98] report the use of ST processing on an uncoded binary phase shift keying (BPSK) signal in a Rayleigh fading environment. Results show that the proposed scheme is 3 dB worse than Maximal Ratio Combining (MRC) at the receiver but still achieves a 15 dB diversity gain compared to a system without diversity (at a BER of 10^{-4}). The proposed detection scheme in [TAR98] does not require any channel state information at the receiver or transmitter. The authors in [HEA99] present work on an open loop transmit diversity system that incorporates joint encoding and antenna hopping.

Within the 3G standard, the newly proposed CDMA standard, known as the wideband-CDMA or W-CDMA standard, has included use of an antenna array in the transmit mode [ETS00b], [ETS98], [3GP99a], [3GP99b] and [3GP99c]. The proposed techniques use both open loop and closed-loop transmit diversity. The physical channels are designed so that the channel structure supports both modes of diversity. The authors in [HOT00] review the proposed transmit diversity schemes for the FDD version of the W-CDMA standard and propose a modified scheme (of Mode-1) to enhance the performance improvement. In paper [RAI99], the authors compare time-switched transmission diversity (TSTD) with STD implemented in a W-CDMA system.

1.3 Original Research Contribution

This report provides with a study of transmit diversity techniques for SWT applications. Contributions provided by this research include

1. New closed-loop transmit diversity algorithms,
2. Analysis and simulation of the new and existing algorithms,
3. Experiments to measure transmit diversity performance in indoor environments,
4. Hardware demonstration of transmit diversity for both narrowband and wideband signals,
5. Feasibility assessment of transmit diversity for W-CDMA and WLAN.
6. Development of reduced complexity MIMO system for indoor channels.
7. Analysis of SNDI techniques.

New Closed-loop Transmit Diversity Algorithms

This report presents new closed-loop transmit diversity techniques for both flat fading and frequency selective channels. The solutions for flat fading channels are in the form of complex weight vectors, or zero-order filters. Since a flat fading channel distorts the amplitude and phase of a transmitted signal without any additional temporal distortion, a complex weight vector suffices to compensate for the channel distortion. The solutions for a frequency selective channel, on the other hand, include filters (finite and infinite length) as this type of channel distorts both the amplitude and phase, and temporal characteristics of the transmitted signal. Both optimal and sub-optimal techniques are provided. One of the main focuses of the algorithm development and study is the convergence behavior of the algorithm. Ideally an algorithm should provide near-optimum performance within a short period of time. This aspect of fast convergence is important for a closed-loop system because of the channel dynamics and latency involved in such a system. The other focus was to develop techniques that are simple in operation and offer ease of implementation.

Analysis and Simulation of the New and Existing Algorithms

The performance improvements of the proposed techniques have been assessed from both analytical and simulation perspectives. The analysis provides closed-form solutions that in many cases have nice intuitive interpretations. Some existing techniques were also studied, and their performances was compared with the proposed techniques. Practical implementation issues were addressed for some of the proposed techniques.

Experiments to Measure Transmit Diversity Performance in Indoor Environment

Some indoor diversity measurements were carried out with hardware testbeds to characterize transmit diversity performance at the SWT for both narrowband and wideband signals. Channel reciprocity and the issue of assessing transmit diversity performance from receive diversity measurements was studied. Wideband characterization of channel magnitude response was carried out for indoor and indoor-to-outdoor channels. Experiments were performed to study the effect of inter-element spacing on envelope cross-correlation and diversity gain. For a two-element array at the handset, transmit diversity gains were assessed using indoor channel measurements.

Hardware Demonstration of Transmit Diversity for both Narrowband and Wideband Signals

Some of the proposed algorithms have been implemented and demonstrated in hardware to study the applicability of transmit diversity. Demonstrations included narrowband and wideband signals. The narrowband demonstration employed a selection-based technique. The wideband demonstration employed an equal gain combining technique with the transmitted signal having bandwidth similar to W-CDMA.

Feasibility assessment of transmit diversity for W-CDMA and WLAN

A feasibility study was performed on the transmit diversity techniques developed in this report to assess their applicability to W-CDMA and WLAN.

Development of reduced complexity MIMO system for indoor channels

A reduced complexity MIMO system has been designed for WLAN applications with a 2×2 antenna array. Feasibility of the technique in the IEEE 802.11 standard has been addressed.

Analysis of SNDI techniques

The analysis of SNDI technique as applied to a handset is presented.

1.4 Overview of the dissertation

The chapters in this dissertation are organized to present theoretical development, simulation study, measurements, and hardware demonstration.

Chapter 2 provides the theoretical background of the proposed transmit diversity techniques in a flat fading channel. Chapter 3 provides the simulation study of the proposed algorithms in Chapter 2. Practical implementation issues such as latency and the amount of feedback associated with a closed-loop system were addressed in this chapter as well.

The problem formulation and algorithm development for a frequency selective channel is provided in Chapter 4. This chapter addresses this problem using both continuous time and discrete time models. Optimal and sub-optimal structures are designed and their performances are compared in this report.

Chapter 5 provides diversity measurements from a SWT perspective in indoor channel. The measurements include a study of cross-correlation as a function of antenna spacing and the validity of reciprocal characteristics of the transmit and receive channels. A direct assessment of a 2-element transmit diversity system is presented.

Chapter 6 presents a hardware implementation and demonstration of a transmit diversity system. The transmit diversity testbeds are described along with the experiments that were carried out with them.

Chapter 7 presents algorithms and performance improvement for a reduced complexity MIMO system for flat fading channels. The space-time processing structures developed in chapter 4 are extended include MIMO systems for a frequency-selective channel.

Chapter 8 presents a brief overview of W-CDMA, the CDMA version of the newly proposed global IMT-2000 standard. W-CDMA has a provision for transmit diversity, and the proposed standards are reviewed. The applicability of the developed algorithms in the physical layer of W-CDMA is discussed. The common air interface of IEEE 802.11b is studied for implementing the proposed diversity techniques and the reduced complexity MIMO structure.

Chapter 9 presents the analysis of a smart antenna system employing SNDI technique. Performance improvement in terms of average symbol error rate and outage probability for different modulation schemes are presented.

Chapter 10 concludes the report with a summary of the research accomplishments and discusses future research directions.

Chapter 2

Transmit Diversity Techniques: Flat Fading Channel

2.1 Introduction

The development of effective transmit diversity algorithms and techniques depends on the type of channel in which a system operates, where the effectiveness of the techniques depends on the characteristics of the channel. For example, in a flat fading channel where the coherence bandwidth is larger than the signal bandwidth, diversity techniques are employed that rely on complex gain adjustment in different antenna branches. But if the channel exhibits frequency selective characteristics where signal bandwidth is comparable to coherence bandwidth, then diversity schemes require additional temporal processing (in the form of pre-coding or pre-equalization). This results in space-time processing that has recently attracted attention because of the use of wideband signals (i.e., IMT-2000 standard). This chapter presents a study and development of transmit diversity techniques at small wireless terminals (SWT) in a flat fading environment. Since an SWT usually encounters a dynamic channel, it is imperative that the proposed diversity techniques have a fast convergence property. At the same time, the techniques should include simple processing and implementation since space and battery power are constrained resources at the SWT. These two issues were the driving forces in developing the proposed transmit diversity techniques to combat flat fading at small mobile wireless devices.

Traditionally, transmit diversity has been addressed from the base station perspective and the techniques proposed in the literature vary in problem formulation, complexity, and achievable performance gain. These often require the knowledge of channel parameters or some estimate of them, and this can be an issue when the algorithm requires the downlink channels for all the mobiles. While these techniques promise varying levels of performance improvement, they do not address the convergence issue related to the proposed algorithms. Thus it is difficult to predict how much delay (in terms of number of symbols) that a technique will incur before settling on the desired optimum performance level. The level of complexity and the amount of required information may render these techniques impractical for a handset application.

The transmit diversity algorithms and techniques that are developed in this chapter focus on two criteria: simplicity in implementation and fast convergence. The proposed techniques are all closed-loop techniques as they rely on feedback from the receiver. A closed-loop approach can be justified since practical wireless communications standards leave options for feedback signal path (e.g. the 3G standard employs fast closed loop power control that operates at 1600 Hz). In addition to this, the framing structure for the 3G standard incorporates feedback information to implement closed-loop transmit diversity. There is a published research on transmit diversity techniques that employ feedback [HEA98] and [LIA95] without addressing convergence and practical issues related to latency and feedback. The effect of propagation delay on closed-loop transmit diversity techniques is addressed under simple operating scenarios in [RAG00] and on the assumption of neglecting quantization and feedback errors. Simulation study of transmit diversity concepts in W-CDMA address feedback errors and mobility [PAR00] based on the assumption of perfect channel estimate. Authors in [HOT00] discuss the mobility and feedback errors on the filtering operation on the feedback signals. Choi has analyzed the impact of different errors for a closed-loop transmit diversity system [CHO02], and the performance from a closed loop system for a $L \times M$ (L, M: number of transmit and receive antenna elements, respectively) [CHO02]. Implementation of channel estimation process and effect of envelope cross correlation are not addresses in these papers, thus, it is not clear what will be the performance improvement for a small wireless terminal in indoor environments. Since the application is for a SWT, all the techniques are developed for a two-element array at the transmitter, and in most cases, extension to more elements is straightforward.

2.2 Problem formulation

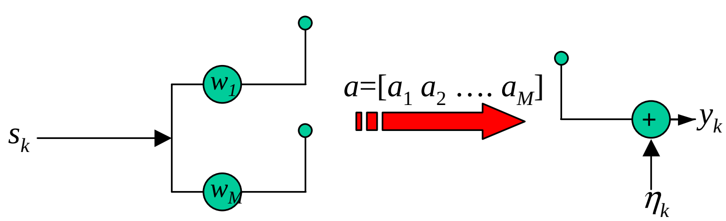

Figure 2.1 Transmit diversity block diagram.

Figure 2.1 shows a schematic diagram of a transmit diversity implementation with an antenna array of *2* elements and a single antenna receiver. The channel vector **a** (row vector) consists of individual complex channel gains a_i, from the ith element to the receiver. The information symbols at the transmitter are scaled by the complex weight vector **w** (column vector). The output at the receiver is given by

$$y_k = \mathbf{aw}s_k + \eta_k = Gs_k + \eta_k \, , \tag{2.1}$$

where s_k is the kth transmitted symbol, η_k is the kth noise sample at the receiver, and G is the gain observed at the receiver. The weight vector is chosen such that the SNR is maximized at the receiver while maintaining a constant transmit power. Mathematically,

$$\begin{aligned} &\max \; \left(\mathbf{w}^*\mathbf{a}^*\mathbf{aw}\right)\gamma_0 \\ &s.t. \quad \mathbf{w}^*\mathbf{w} = 1 \end{aligned} \, , \tag{2.2}$$

where, '*' corresponds to the hermitian transpose operation, γ_0 is the SNR for single antenna in additive white gaussian noise channel and the total transmit power is arbitrarily set to unity. Recognizing this as an eigenvalue problem, the optimal solution is known as

$$\mathbf{w}_{opt} = \frac{\mathbf{a}^*}{\|\mathbf{a}\|_2} \, . \tag{2.3}$$

Here $\|.\|_2$ refers to the norm-2 of a vector. Equation (2.3) shows that the optimal choice of the weight vector depends upon the channel vector. In a closed-loop transmit diversity system, the channel can be estimated at the receiver and made available to the transmitter through feedback. Using weight vector in (2.3) provides maximal ratio transmission (MRT) solution. There is a sub-optimal solution in which the phase of the channel vector is estimated to compute the weight vector that provides co-phasing between the individual channel gains, and this is known as equal gain transmission (EGT) solution. The proposed techniques in EGT category are

1. Bisection,
2. Gradient-based or Early-late

and, in MRT category are

1. Least square (LS),
2. Subspace method,
3. Least mean square (LMS).

2.3 Equal Gain Transmission (EGT) Techniques

The EGT techniques provide a solution for the weight vector as $\mathbf{w} = \frac{1}{\sqrt{2}}[1 \quad e^{-j\hat{\beta}}]^T$ where $\hat{\beta}$ is an estimate of the phase difference between the individual channel gains. The estimation process is based on employing a phase search technique using feedback from the receiver. The principle of the EGT techniques is to hold the gain of a weight vector constant at the transmitter and to conduct a phase search by measuring the symbol power estimate at the receiver. The receiver then assists the transmitter in updating the phase. The proposed techniques differ from the equal gain approach presented in [HEA98] in that they form an estimate of β without the assumption of perfect channel knowledge. The EGT principle can be described with reference to Figure 2.1 assuming a two-element array. When equal gain weights are used at the transmitter, the gain G can be expressed as

$$G = \frac{1}{\sqrt{2}}[|g_1| + |g_2| e^{j(\Delta\phi - \beta)}] e^{j\varphi_1}, \tag{2.4}$$

where, $g_i = |g_i| e^{j\phi_i}$ is the ith complex channel gain, $\Delta\varphi = \varphi_2 - \varphi_1$ and β is the phase difference or phase setting of the weight vector. Thus, the complex gain G is composed of a reference and a rotating vector as shown in Figure 2.2.

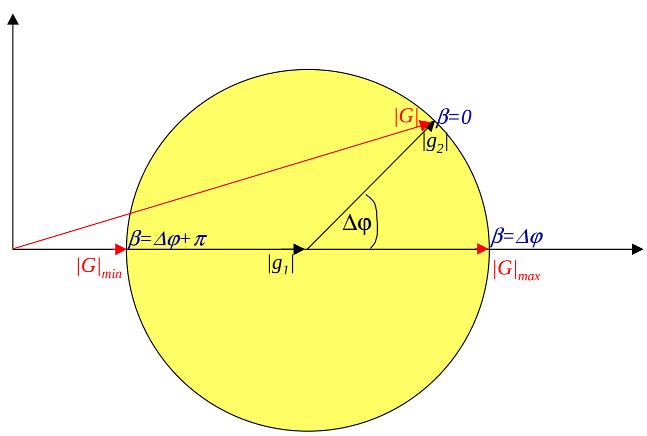

Figure 2.2. Variation of $|G|$ with β.

The magnitude of G follows a sinusoidal variation with a maximum value of $|G|_{\max}$ and a minimum value of $|G|_{\min}$. The maximum value occurs when β equals the phase difference of the channel gains or when the phases of the channel gains are perfectly matched (ideal EGT). The receiver estimates the received power for a given β and assists the transmitter in moving closer to the optimum β. The receiver can identify the optimal or sub-optimal β (as allowed by the particular search technique) by finding the maximum received power. Clearly, the optimal value for beta is $\beta \cong \phi_2 - \phi_1$ with a corresponding optimal gain of $|G_{opt}| \cong \frac{1}{\sqrt{2}}\left[|g_1| + |g_2|\right]$. One way to estimate this phase difference is to employ a simple phase scanning technique. Considering a two-element array at the transmitter, the transmitter fixes the gain of the weights for unity norm (or unity power) and adjusts the phase of one weight while keeping the phase of the other weight constant. More sophisticated search algorithms can be employed that will provide better performance than the basic phase scanning. These are discussed in the following subsections.

2.3.1. Bisection Search

The bisection search adjusts the phase of the signals transmitted from the antenna array while maintaining a constant gain, i.e., ||**w**|| =1. The transmitter initializes the weight vector **w** so that the magnitudes of the individual elements are unity and the phase of one element is a random value, $\beta \in [0,2\pi]$, with respect to the element considered as the reference element. The weight vector is further normalized so that ||**w**||= 1. The transmitter for the first iteration, k=0, transmits three successive symbols with three different phase values for the weight vector. The phase values for the three symbols are chosen so that

$$\begin{aligned} \beta_a &= \beta_k \\ \beta_b &= \beta_k + \frac{\pi}{2^k} \\ \beta_c &= \beta_k - \frac{\pi}{2^k}. \end{aligned} \tag{2.5}$$

Thus, for any iteration k, the transmitter starts with the current value β_k and computes the two other values, which are $\pm 2^{-k}\pi$ apart from the current value. The transmitter transmits the three symbols and the receiver measures the received signal power or estimates the SNR for these three symbols. The receiver then finds the symbol with the maximum strength and identifies the index of this symbol. The index is reported back to the transmitter in the feedback channel. After receiving the index corresponding to the best phase value, the transmitter uses this phase value as the current phase for the next iteration and computes the other two phase values as described before. The next three symbols are transmitted with three new phase values. The process continues until further phase adjustments yield negligible changes in phase values. Simulation results presented in Chapter 3 indicate that a total of about five iterations (or fifteen symbols) usually are sufficient to achieve a steady state output SNR since the new phase setting differs from the previous one by $\pi / 32$.

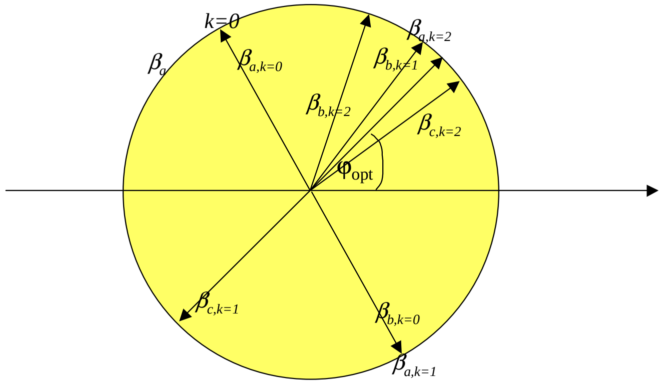

Figure 2.3. Principle of the bisection phase search technique

The bisection search is illustrated in Figure 2.3. The figure represents phase adjustments as the rotation of vectors on the periphery of a unit circle in the complex plane. The desired phase, i.e. the optimal value, is denoted as φ_{opt}. The search starts with k=0 and an initial phase of $\beta_{a,\ k=0}$. It identifies the best choice for the phase value as the one that is more aligned ($\beta_{a,\ k=0}$) with the desired value. In the next iteration with k=1, the search space is narrowed to $\frac{\pi}{2^k}$ and the best choice, that closest to the desired value ($\beta_{b,k=1}$), is found again. As the search progresses, the adaptive process converges very close to the desired phase value.

The convergence of the estimated phase close to the optimal value depends on the quality of the estimate of the received signal power. If the SNR is high, the received signal power is accurately estimated and the technique performs satisfactorily. But if the SNR is low, then the power estimates are less accurate and the technique may get stuck in a local maxima and converge to a value different from the optimal one. This problem may be alleviated by averaging over a number of symbols for each phase adjustment instead of using one symbol.

2.3.2. Gradient Search: Early-Late Technique

The search for an optimal β can be carried out by a gradient-based search. The approach borrows from the traditional early-late gate symbol synchronization technique [PRO95]. Here the transmitter successively transmits two symbols with a phase difference of $\Delta\beta$. The receiver estimates the power for the two consecutive symbols and finds the difference in power, and also the direction of the gradient. This information is relayed back to the transmitter that then decides the direction of change for updating β. The adaptive process updates β into the direction of the maximum received power. The update rate is governed by the angle step-size $\Delta\beta$. The step-size also governs convergence and residual errors both in phase and gain. For a two-element array, the beam pattern is quite broad and is not very sensitive to errors in phase; often the settling value for the gain is close to the gain achieved by ideal EGT.

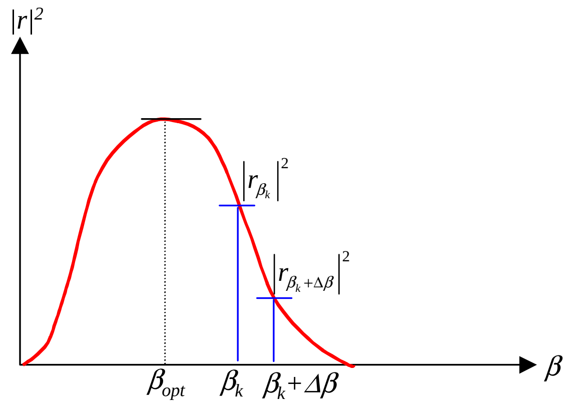

Figure 2.4. Principle of gradient-based phase search technique

This technique is illustrated in Figure 2.4. The transmitter chooses any two-phase settings as $\beta_1 = \beta_k$ and $\beta_2 = \beta_k + \Delta\beta$ and the corresponding weight vectors as

$$\mathbf{w}_1 = \frac{1}{\sqrt{2}}\begin{bmatrix}1 \\ e^{j\beta_1}\end{bmatrix} \quad and\ \mathbf{w}_2 = \frac{1}{\sqrt{2}}\begin{bmatrix}1 \\ e^{j\beta_2}\end{bmatrix}. \tag{2.6}$$

The transmitter then successively transmits symbols with two different weight vectors and the receiver measures the corresponding received signal power. The gradient is formulated as

$$\nabla_\beta = \frac{\left|r_{\beta_k}\right|^2 - \left|r_{\beta_k+\Delta\beta}\right|^2}{-\Delta\beta}. \tag{2.7}$$

where r_{β_1}, r_{β_2} refer to received signal corresponding to β_1 and β_2 respectively, and $\Delta\beta = \beta_1 - \beta_2$. This information is relayed back to the transmitter that then updates β as

$$\begin{gathered}\beta_{1,new} = \beta_1 + \mu\nabla_\beta ; \beta_{2,new} = \beta_{1,new} + \Delta\beta \\ or \\ \beta_{2,new} = \beta_2 + \mu\nabla_\beta ; \beta_{1,new} = \beta_{2,new} + \Delta\beta\end{gathered} \tag{2.8}$$

Here, $\Delta\beta$ and μ refer to angle step-size and update step-size, respectively. The transmitter then generates the weight vectors and transmits new symbols with these two weight vectors and the process is repeated. The algorithm is able to track channel dynamics without periodic initialization. For high SNR environments, the received signal power has a well-defined maxima and β can be updated toward this maxima by reliably estimating the gradient. The settling values for β may be oscillatory depending upon the step-size μ and phase offset $\Delta\beta$.

2.4 Maximal Ratio Transmission (MRT) Techniques

According to (2.3), MRT techniques require a direct or an indirect estimate of the channel vector. Lo [LO99] has shown the optimality of such a solution for a multiple-input-multiple-output (MIMO) system. His results are confined to the case of perfect channel estimation and feedback. In this paper, we build on this principle and propose techniques that generate channel estimate in a block or recursive manner. The proposed techniques are based on Least Squares (LS) or gradient estimate algorithms: Least Squares transmit diversity (LS-TD), Subspace based transmit diversity (SS-TD), Least Mean Squares (LMS) transmit diversity (LMS-TD) and Hybrid transmit diversity (H-TD).

2.4.1 Least Square transmit diversity (LS-TD)

The LS technique is adopted and modified to estimate the vector channel using weight perturbation. Both the cases of supervised and unsupervised channel estimation process are presented. In the supervised mode, a sequence of training symbols are transmitted by assigning a different but known weight vector to each of these symbols. Using this information (training sequence and weight perturbation pattern) along with the received symbols, the vector channel can be estimated at the receiver. In the unsupervised mode, both the symbol sequence and the channel gains are estimated in a recursive manner via alternating projections method.

At this point, the trade-off between speed of channel identification and transient performance of the diversity system is emphasized. For a fast identification, the channel needs to be probed, e.g., by perturbing the weight vector subject to a power constraint. The larger the amount of perturbation, the faster the identification process. Perturbed weight vectors may give rise to fluctuations in the received SNR.

The channel estimation process is illustrated first for a noiseless case. Channel estimation implies finding a scalar $c \in \mathbf{C}$ so that $c = \mathbf{aw}$. To do this, $\mathbf{w}$ needs to be varied (perturbed) for every symbol s_k to generate y_k at the receiver. For the noiseless case, the sequence of N output symbols could be written in vector notation as

$$\left[y_k....y_{k+N-1}\right]=\mathbf{a}\left[\mathbf{w}_k...\mathbf{w}_{k+N-1}\right]\begin{bmatrix} s_k & & \\ & \ddots & \\ & & s_{k+N-1}\end{bmatrix} \tag{2.9}$$

where it is assumed that the channel is stationary within the probing or estimation period. The estimated channel vector **a** is then computed by

$$\mathbf{a}=\left[y_k....y_{k+N-1}\right]\begin{bmatrix} s_k & & \\ & \ddots & \\ & & s_{k+N-1}\end{bmatrix}^{-1}\left[\mathbf{w}_k...\mathbf{w}_{k+N-1}\right]^{-1}. \tag{2.10}$$

Thus, an exact knowledge of the channel can be inferred from the knowledge of $\{\mathbf{y}_k\}$, $\{\mathbf{s}_k\}$, and $\{\mathbf{w}_k\}$. In the presence of noise, the estimate needs to be averaged over several symbols to reduce the effect of the noise. The estimated channel can be expressed as (from Appendix A2)

$$\mathbf{a}= \quad \mathbf{s}\tilde{\mathbf{Y}}\mathbf{W}^H\left(\mathbf{W}\mathbf{W}^H\right)^{-1} \tag{2.11}$$

where, $\tilde{\mathbf{Y}}$ is a diagonal matrix of received symbols, $\boldsymbol{s}$ is the training sequence, **W=**is the matrix formed from the perturbed weight vectors.

LS Estimation with Training Sequence

In this mode of channel estimation, the receiver formulates an estimate of the channel from knowledge of the weight vectors, symbol sequence, and the observed output. The use of a training sequence implies that the transmitter has to halt the information transmission periodically and to transmit a training sequence to perform the channel estimation.

Blind LS Estimation

In this mode, channel estimation includes a two-step estimation process, whereby the channel is estimated first, and with this channel-estimate, the symbol is then estimated. The iterative process is called the alternating projection method. In an alternating fashion, the channel and the transmitted symbol are estimated. The process continues until some convergence criterion is satisfied.

$$\begin{aligned} \mathbf{a}^{i+1} &= \arg\min_{\mathbf{a}} \left(\sum_{k=1}^{N} (y_k - \mathbf{a}\mathbf{w}_k s_k^i)^2 \right) \\ s_k^{i+1} &= \arg\min_{s_k} \left(\sum_{k=1}^{N} (y_k - \mathbf{a}^{i+1}\mathbf{w}_k s_k)^2 \right) \end{aligned} \tag{2.12}$$

A corresponding algorithm for the blind LS technique follows.

Step 1:

Pick s_0 arbitrarily or assume it to be known. Let i=1.

Step 2:

Solve for the channel estimation:

Let $\mathbf{a}^{i+1} = \arg\min \left\| \mathbf{s}^i \tilde{\mathbf{Y}} - \mathbf{a}\mathbf{W} \right\|_2^2$.

Then the solution is $\mathbf{a}^{i+1} = \mathbf{s}^i \tilde{\mathbf{Y}} \mathbf{W}^H \left(\mathbf{W}\mathbf{W}^H \right)^{-1}$. (See Appendix A2.)

Solve the symbol estimation:

Let $\mathbf{s}^{i+1} = \arg\min \left\| \mathbf{s}\tilde{\mathbf{Y}} - \mathbf{a}^{i+1}\mathbf{W} \right\|_2^2$.

However, this is not an LS problem as the symbols belong to a certain class of values, i.e., they have a finite alphabet property. BPSK signals represent one particular case where $s_k \in \{1, -1\}$. The solution to this problem is the sequence that solves the following problem

$$\min_{s_1, s_2, \cdots s_N} \left\| (s_1 y_1 - c_1)\,(s_2 y_2 - c_2) \cdots\cdots (s_N y_N - c_N) \right\|_2^2 \quad \text{where} \quad c_i = \mathbf{a}_i \mathbf{w}$$

or

$$\min_{s_1, s_2, \cdots s_N} \left| (s_1 y_1 - c_1) \right|^2 + \cdots\cdots\cdots \left| (s_N y_N - c_N) \right|^2 .$$

The solution for each s_k can be found by finding the symbol in each summation term that minimizes the respective squared difference term.

Step 3:

Let $i = i + 1$ and go to step 2 until convergence.

2.4.2 Subspace TD (SS-TD)

The power iterations method is based on projecting an arbitrary weight vector $\mathbf{w}_0$ onto the channel vector $\mathbf{a}^H$. The resulting vector $\mathbf{v}$ of the projection operation is [GOL93]

$$\mathbf{v} = \frac{\mathbf{a}^H \mathbf{a}}{\mathbf{a}\mathbf{a}^H} \mathbf{w}_0 . \tag{2.13}$$

Thus, $\mathbf{v}$ is aligned with $\mathbf{a}^H$ and the optimum weight vector $\mathbf{w}_{opt}$ can be re-written as

$$\mathbf{w}_{opt} = \frac{\mathbf{v}}{\|\mathbf{v}\|_2}. \tag{2.14}$$

Since $\mathbf{w}_{opt}$ still requires channel knowledge, which is not known, the optimum weight vector cannot be computed yet. However, recognizing that the gradient of the cost function $J(\mathbf{w}) = \mathbf{w}^H\mathbf{a}^H\mathbf{a}\mathbf{w}$, taken with respect to $\mathbf{w}^H$ and evaluated at $\mathbf{w}_0$, is

$$\nabla_{\mathbf{w}^H} J(\mathbf{w})\Big|_{\mathbf{w}=\mathbf{w}_0} = \nabla_{\underline{w}^H} \mathbf{w}^H\mathbf{a}^H\mathbf{a}\mathbf{w}\Big|_{\mathbf{w}=\mathbf{w}_0} = \mathbf{a}^H\mathbf{a}\mathbf{w}_0. \tag{2.15}$$

The optimum weight vector can be expressed in terms of the gradient of the cost function that can be evaluated numerically as

$$\mathbf{w}_{opt} = \frac{\nabla J(\mathbf{w}_0)}{\|\nabla J(\mathbf{w}_0)\|_2}. \tag{2.16}$$

Expressing the weight vector in terms of the real and imaginary weight components

$$\mathbf{w} = \begin{bmatrix} w_1 \\ \vdots \\ w_M \end{bmatrix} = \begin{bmatrix} w_1^R + jw_1^I \\ \vdots \\ w_M^R + jw_M^I \end{bmatrix} \tag{2.17}$$

and expanding the gradient of the cost function results in

$$\nabla J(\mathbf{w}) = \begin{pmatrix} \dfrac{\partial J}{\partial w_1^R} \\ \vdots \\ \dfrac{\partial J}{\partial w_M^R} \end{pmatrix} + j \begin{pmatrix} \dfrac{\partial J}{\partial w_1^I} \\ \vdots \\ \dfrac{\partial J}{\partial w_M^I} \end{pmatrix} \tag{2.18}$$

Each of the terms $\dfrac{\partial J}{\partial w_1^R} \ldots \dfrac{\partial J}{\partial w_M^R}, \dfrac{\partial J}{\partial w_1^I} \ldots \dfrac{\partial J}{\partial w_M^I}$ can be estimated using numerical derivative as follows:

$$\frac{\partial J}{\partial w_1^R} \approx \frac{J\begin{pmatrix} \left(w_1^R + \Delta\right) + jw_1^I \\ \vdots \\ w_M^R + jw_M^I \end{pmatrix} - J\begin{pmatrix} w_1^R + jw_1^I \\ \vdots \\ w_M^R + jw_M^I \end{pmatrix}}{\Delta}. \tag{2.19}$$

Apparently the estimate depends on the amount of perturbation Δ in conjunction with the additive noise in the system. If the background noise is high relative to Δ, then the estimate of the cost function is not likely to be reliable and Δ should be chosen with a larger value. Another observation is that $2M$ different weight perturbations are needed to estimate the gradient of the cost function. Each perturbation requires the transmission of multiple symbols. The more symbols are used, the more reliable the estimate. Hence, the estimation of the gradient requires a considerably high number of symbols to be transmitted. An advantage of the subspace method is its unsupervised operation.

2.4.3 LMS-TD

LMS is a stochastic gradient-based algorithm and as such requires an estimate of $\nabla J(\mathbf{w})$. The recursive weight update can be expressed as

$$\mathbf{z}_k = \mathbf{w}_k + \mu \hat{\nabla} J(\mathbf{w}_k)\,. \tag{2.20}$$

So, the weights are computed with

$$\mathbf{w}_{k+1} = \frac{\mathbf{z}_k}{\left\|\mathbf{z}_k\right\|_2}\,. \tag{2.21}$$

The stability and speed for LMS-type algorithms depend on the step-size μ. In general, the step-size is chosen to be small and thus the LMS approach is slow. The advantage with the LMS method is that it can work blindly, i.e., without the use of a dedicated training sequence.

2.4.4 Hybrid TD

A hybrid method can be devised where the Subspace method is used in the initial iterations, and, then the LMS technique is used for final convergence. The Subspace method provides a direct estimate of the optimal weight vector from gradient measurements, and, is thus expected to provide substantial performance improvement within the first couple of gradient estimates. Then the system will switch to the LMS technique to gradually approach the optimal point. This combines good transient characteristics of the Subspace method and the stable steady state performance of the LMS to offer a more efficient technique than either of the two.

2.5 Conclusions

Closed-loop transmit diversity techniques have been developed for a flat fading channel with multiple antenna elements at the transmitter and a single element at the receiver. The weight vector adjusts the gain in each antenna element at the transmitter array to maximize the receive signal strength at the receiver (or SNR). The techniques were developed to provide fast convergence and simplicity in operation and implementation. The proposed techniques are classified into two groups: EGT and MRT. The EGT techniques rely on adjusting the phase of transmitted signals to achieve co-phasing or in other words coherent combining at the receiver. The feedback information is small and comprises either phase-index or a quantized phase-value. The MRT techniques generate weight vectors that operate on both the amplitude and phase of the transmitted signals. The amount of feedback is usually a complex weight vector the size of which depends on the number of antenna elements. The convergence time of the subspace and LMS are expected to be larger than that of the LS technique.

Chapter 3

Simulation Study of Transmit Diversity in a Flat Fading Channel

3.1 Introduction

This chapter investigates performance of the proposed transmit diversity techniques presented in Chapter 2 for a two-element array by simulation studies. The vector propagation channel was assumed to undergo i.i.d. Rayleigh fading. Furthermore, the vector channel gain was assumed to be stationary during the probing or channel estimation period. This setting may be justified from the W-CDMA standard of IMT-2000, where it is assumed the estimation period occurs (for the power control loop) within one slot and the channel is stationary for a slot period. Performance assessment addressed the followings:

1. convergence,
2. diversity gain,
3. capacity (normalized throughput) and
4. practical implementation issues.

The convergence behavior was studied by generating snapshots of convergence or learning curves and estimating the number of symbols required to achieve performance within 5% or less of the optimal SNR value. Diversity gain was assessed from outage probability curves (or cumulative distribution function, CDF) through Monte Carlo simulations. The CDF function at value x defines the probability that a random number has a value of x or less. The diversity gains are usually evaluated at 1% or 10% in the CDF plots. Capacity enhancement from the proposed techniques was evaluated and compared with single antenna system. Some key proposed techniques were studied for implementation in W-CDMA standard and the impact of practical issues i.e., quantization error, latency and feedback error, on the performance was also evaluated.

3.2 Convergence: EGT Algorithms

3.2.1 Bisection (BS) Search and Early-Late (EL) Algorithm

For the Bisection method, the total number of symbols dedicated for phase adjustment has been set at thirty so that the number of iterations is set at ten with three symbols for each iteration. The estimate of received signal power is done on a per-symbol basis. For the Early-Late method, the value of the phase difference ($\Delta\beta$) is set at 15° and the update rate (μ) is set at 0.3. These two parameters can be made adaptive to better enhance the performance. The convergence curves presented in the upper subplot of Figure 3.1 illustrate the variation of the received SNR with number of symbols for the Bisection method at a fixed SNR (γ_0) of 15 dB. The optimal SNR for this snapshot is shown as a straight line. The plot reveals that convergence is approached within 15-20 iterations. The lower subplot of Figure 3.1 shows a snapshot of the variation of the overall gain for the Early-late method from each phase setting (β_1 and β_2). The stepped nature of the curves is due to the fact that there are several symbols associated with each SNR measurement for each setting. The plots show that convergence is attained within 90-100 symbols.

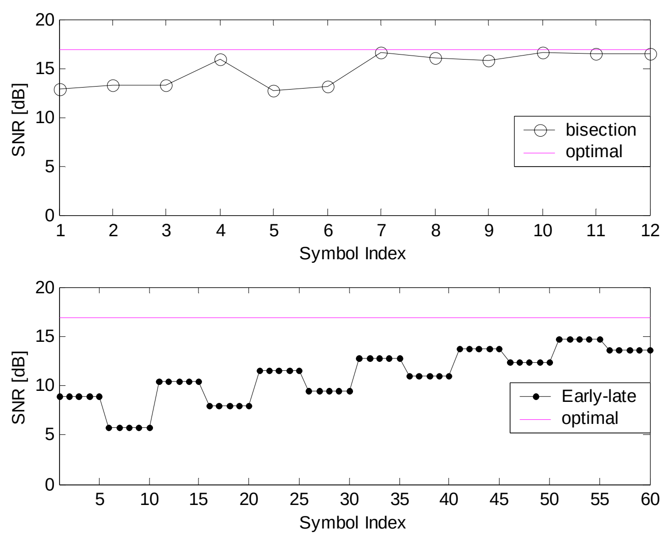

Figure 3.1. Convergence plots for Bisection method; Early-late method $\Delta\beta$ =15° and μ= 0.3.

3.3 Convergence: MRT Techniques

3.3.1 LS-TD

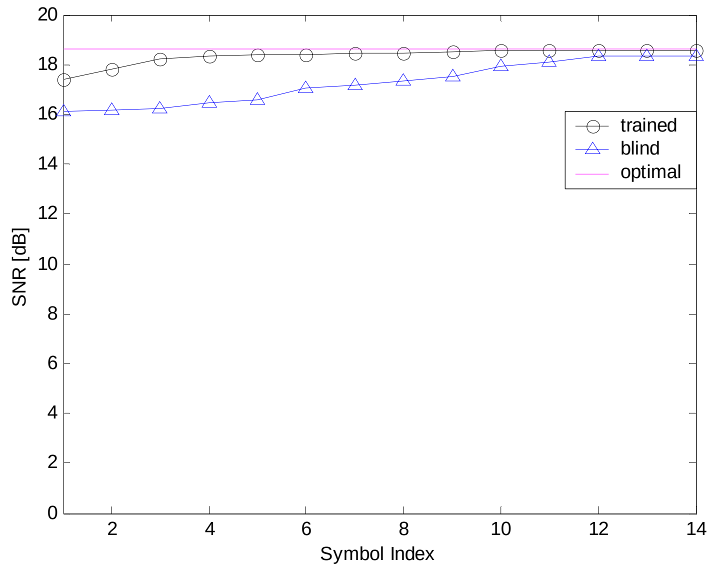

Figure 3.2. Convergence curve for the LS technique.

Figure 3.2 shows convergence plots generated from an ensemble of snapshots using both the trained and blind mode of LS technique for 15 dB SNR. The optimal performance is shown as a straight line. Both the modes of LS technique show good convergence behavior with the trained mode being better than the blind one. The learning curves show that the LS techniques converge within 5-10 symbols for the trained mode and 15-20 symbols for the blind mode.

3.3.2 Subspace Method

For the subspace method, it is necessary to compute the gradient of the SNR through weight perturbation to obtain the optimum weights (Equation 2.28). The perturbation is carried out on the real and imaginary components of each elemental weight in the weight vector **W**, and for a two-element array, the total number of perturbations is four. This results in a total of five SNR estimates. Figure 3.3 shows a typical convergence example for one particular channel realization.

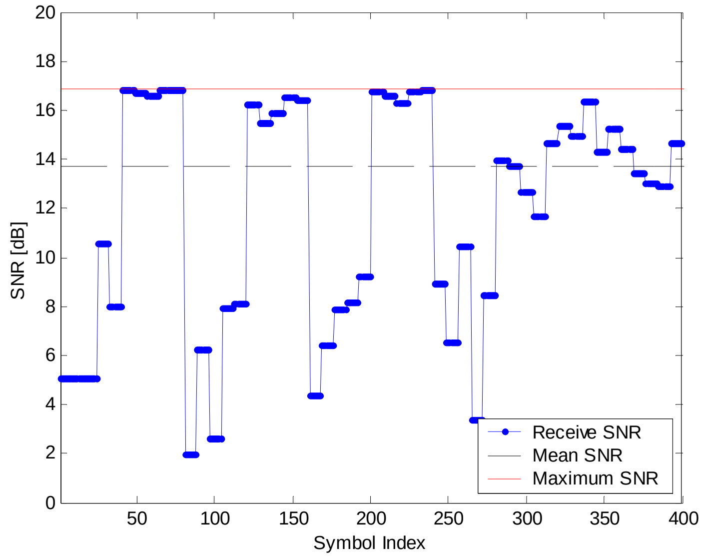

Figure 3.3. Convergence curve for the Subspace method

Each estimate of SNR for the Subspace method is obtained from averaging over a period of eight symbols resulting in a step-like variation in the plot. The weight vector for the subspace method is updated at the end of every fifth step (considered as a single iteration). The algorithm achieves near-optimal performance after one iteration from about 40 symbols. The oscillatory behavior is due to the fact that the gradient estimate is accurate at locations in the cost function surface where it has a high value, i.e., far from the optimal point, and, it is degraded when it has a small value, i.e., in the vicinity of the optimal point. Thus, approaching the optimal value, where the gradient is relatively flat, the next set of iterations yield a poor estimate of the weight vector. Advantageously the algorithm achieves close optimal performance after single iteration. Thus, the algorithm is fast and depends only upon the number of symbols used for the signal strength observations. Since the algorithm is based on the gradient estimation (signal strength), it does not require knowledge of the channel nor the transmitted symbols.

3.3.3 LMS-TD

In the LMS technique, the gradient of the SNR is estimated and the weight vector is updated with a finite step-size as shown in Equation 2.33. Here the characteristics of conventional LMS apply, and thus the step-size determines the rate of convergence as well as the stability of the algorithm. The advantage of this approach is that if the gradient estimate is erroneous due to noise, the effect on the overall performance is small as long the majority of the gradient estimates point toward the optimum. The SNR performance does not degrade as much as in the subspace method. Also, this technique does not explicitly require channel knowledge or knowledge of the symbols. Figure 3.4 illustrates a convergence example for one particular channel realization.

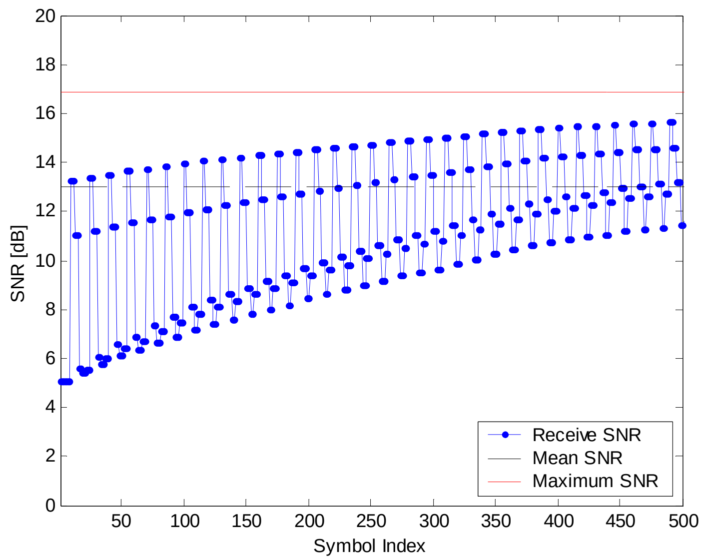

Figure 3.4. Convergence curve for the LMS method.

An average of three symbols is used to estimate each derivative term. Here the trade-off is between a relatively fast convergence with highly variable SNR output and a slower convergence with more stable SNR output at the receiver. The amount of weight perturbation as well as the LMS step-size is chosen relatively high for fast convergence. Even then, it needs more than 200 symbols until convergence is reached. This rate may not be acceptable for a practical system implementation (i.e., the proposed IMT-2000 standard) in conjunction with computation time and feedback latency.

3.3.4 H-TD

The convergence plot for Hybrid method is shown in Figure 3.5. The figure shows that by using Subspace method, the performance reaches around the optimal one. Then the technique switches to LMS for slowly approaching the optimal point. With this approach, the receive SNR does not encounter either wide fluctuation as in Subspace method or slow gradient ascent as in LMS method.

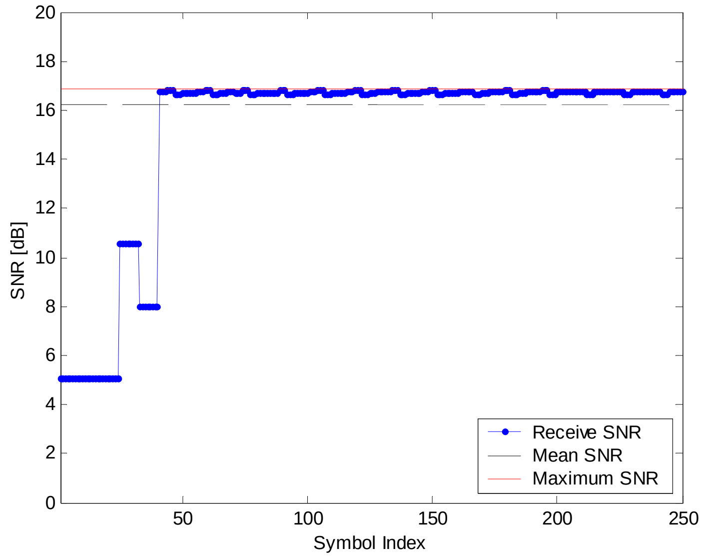

Figure 3.5. Convergence plot for the Hybrid method.

3.4 Diversity Gain

The diversity gain from the two EGT techniques (BS and EL) and three MRT techniques (Hybrid, supervised and blind LS) was assessed by Monte Carlo simulation and was compared with the optimal as well as a single antenna system. The operating SNR (γ_0) was set at 20 dB. Stationary channel with i.i.d. Rayleigh distribution was assumed, and, for each technique, the number of samples was chosen so that the technique attained convergence. Figure 3.6 shows the outage probability plots from the results generated from simulation. At 1% outage level, all the proposed techniques provide substantial gain, with the supervised LS (from MRT) and the Bisection (from EGT) being better than the single antenna case by more than 10 dB and about 10 dB, respectively.

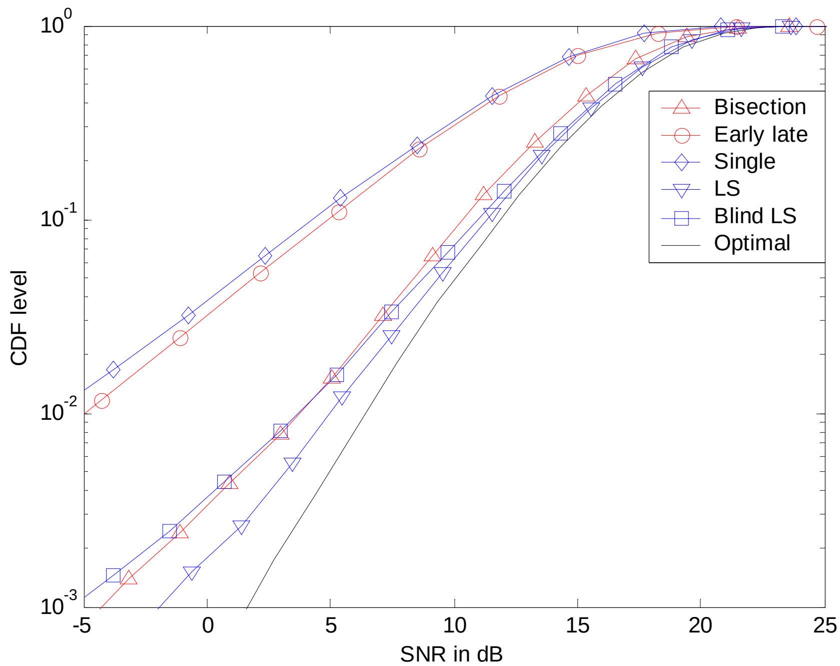

Figure 3.6. Diversity gain from the proposed transmit diversity techniques

The mean SNR improvement has been computed and is presented in Table 3.1. The EGT techniques are shown in shaded area. From the table it can be seen that the trained LS provides the best performance, offering a gain of about 3 dB over the single antenna system. Among the EGT methods, the Bisection shows good performance and falls behind the trained LS method by little more than 1 dB. All the proposed methods show performance improvement over a single antenna system.

Table 3.1 Statistical comparison of performance improvement

Method	Mean (dB)
Single Antenna	16.1
Bisection	17.8
Early-late	17.0
Hybrid	18.1
Trained LS	19.1
Blind LS	18.6
Ideal MRT	19.13

3.5 Channel Capacity

Channel capacity in the information theoretic sense refers to the spectral efficiency that is defined as bits/sec/Hz. For high-speed communications system it is desirable that the throughput be maximized for a given bandwidth. A discussion on the use of multiple antenna elements to increase channel capacity is provided in the seminal paper by Foschini and Gans [FOS98]. This section uses the analytical expressions of capacity in that paper and presents simulation results to compare the improvement in channel capacity by using the proposed transmit diversity techniques. For a Rayleigh fading channel, the expression for capacity for a MIMO system is given by

$$C = \log_2 \det\left[I_{n_R} + \left(\frac{SNR}{n_T} \right) HH^* \right] \tag{3.1}$$

where n_R and n_T refer to the number of elements on the receiver and transmitter side, SNR is the signal-to-noise ratio for each antenna branch in the receiver, H is the channel matrix and * is the complex conjugate operation. The matrix H is of size $n_R \times n_T$ and each element h_{ij} refers to the channel gain from the transmitter antenna element j to the receiver antenna element i. For a transmit diversity system, this expression reduces to

$$C = \log_2 \left[1 + \left(\frac{SNR}{n_T} \right) \sum_{j=1}^{n_T} \left| h_j \right|^2 \right] \tag{3.2}$$

Note that the total SNR is distributed over the n_T transmit antenna elements. This is because of the practical implementation issue where the total transmit power is distributed equally among the antenna branches through a RF splitter. This expression holds for optimal combining where the channel gains are estimated perfectly and used on the transmitter side. However, the transmit diversity schemes in this dissertation involve using weight vector at the transmitter and thus the expression needs to be modified to incorporate this factor. The modified expression is proposed as

$$C = \log_2 \left[1 + \left(\frac{SNR}{n_T} \right) \mathbf{w}^* \mathbf{h} \right] \tag{3.3}$$

where **w** and **h** represent the weight and channel vector respectively. Under the assumption of perfect channel estimation, this modified expression reduces to expression (3.2).

The converged weight vectors from different TD techniques are used in (3.3) to compute capacity. Figure 3.7 shows the complementary CDF (CCDF) plot of the capacity resulting from some of the transmit diversity techniques. The single antenna case provides the baseline for performance comparison.

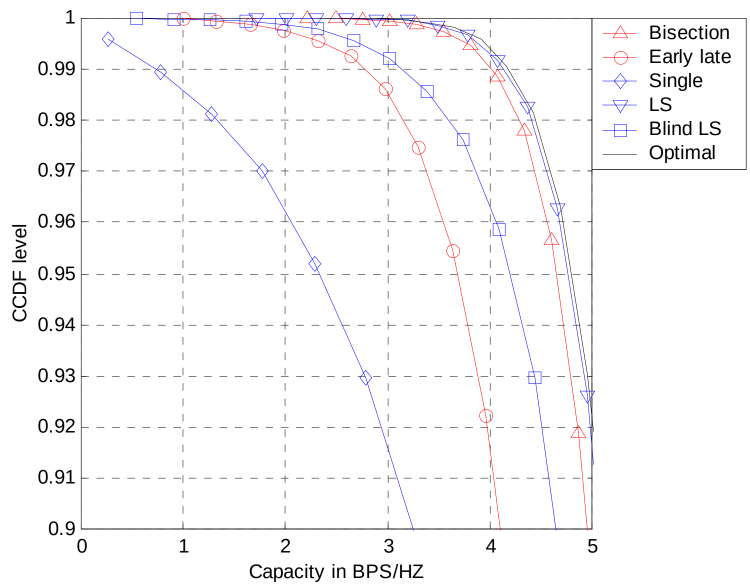

Figure 3.7. Capacity plots of the proposed transmit diversity techniques.

It can be noted from the plots that the TD techniques provide capacity enhancement over the single antenna case when the channel undergoes fading and the capacity for a single element is low. At 5% outage probability (or 0.95 CCDF level), the capacity values for the proposed techniques along with the single antenna element are read off the plots and are presented in Table 3.2.

Table 3.2. Capacity values for different techniques at 5% outage probability

Technique	Capacity (BPS/Hz)
Single antenna	2.4
Early-late	3.7
Blind LS	4.2
Bisection	4.65
Trained LS	4.75
Optimal	4.8

It is clear that when the system operates at high CCDF level such as 0.95, the proposed diversity schemes provide a capacity enhancement over a single antenna system. The minimum enhancement is 1.3 bps/Hz for the early-late system while the maximum is 2.35 for the trained LS. However, as channel conditions improve, the capacity improves for a single antenna system and the enhancement diminishes for the TD system. This is due to the fact that the transmit diversity systems are penalized in terms of total transmit power per antenna branch. Eventually, the single antenna system outperforms the diversity schemes for capacity beyond around 6 bps/Hz as shown in Figure 3.8. This sets the guideline for operating smart transmit antenna system in terms of capacity enhancement: when channel conditions are satisfactory use single antenna system but when channel conditions degrade, switch to an appropriate transmit diversity scheme.

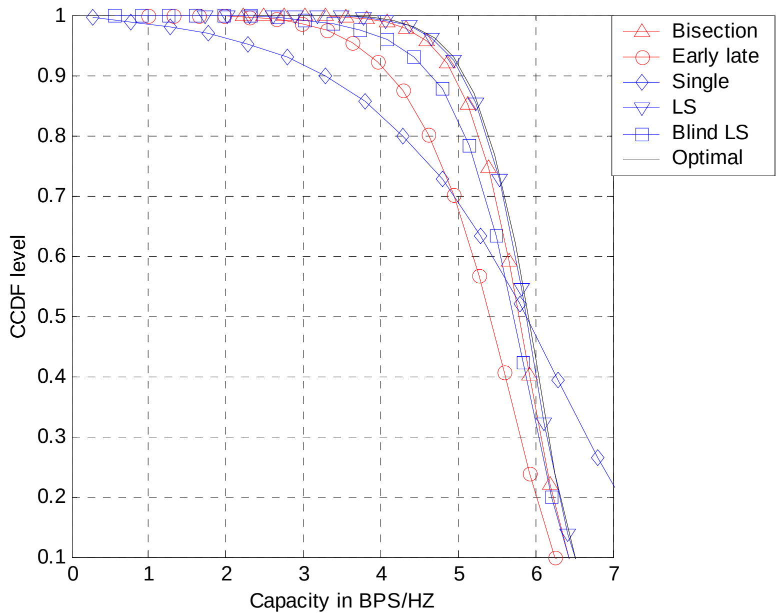

Figure 3.8. Capacity plots of the proposed transmit diversity techniques.

3.6 Implementation Issues

All transmit diversity algorithms developed in the previous chapter have one common characteristic: they all require feedback. In the theoretical development, it was always assumed that the channel variation was negligible, instantaneous feedback was possible, and enough bandwidth was available to feed all the weight elements without quantization back to the transmitter. Needless to say, such a setting represents a highly idealized environment and hardly conforms to any practical propagation environment. A practical environment exhibits channel dynamics that includes fading, finite propagation delays and feedback channel degradation and occurrence of errors. In addition to these, quantization of weight vector into a finite number of bits will be required to accommodate the feedback information in physical channels (data and/or control channels) in any practical wireless system. Thus it is imperative to address these practical implementation issues and test the proposed transmit diversity algorithms under these real-life propagation constraints. These issues are summarized in Figure 3.9.

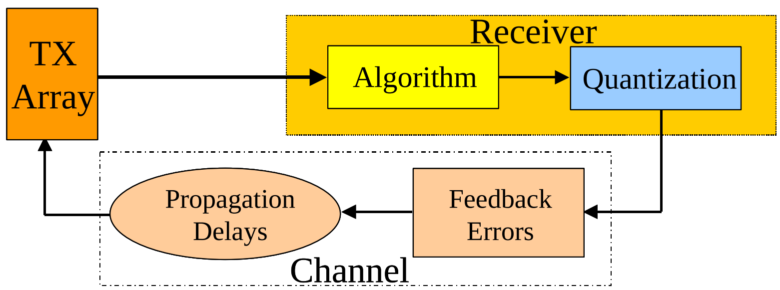

Figure 3.9. Closed-loop operation and sources of errors.

The algorithm section in Figure 3.9 provides optimal weight vector for any given technique, which is then quantized into a finite number of bits as permitted by feedback payload. Due to imperfection in the reverse link, this quantized weight vector can suffer bit errors, and experiences finite propagation delay before arriving at the transmitter. The forward channel (from transmitter to the receiver) is modeled with a fading envelope at certain mobility whereas the feedback channel is characterized with a specific probability of error. Thus, even though an optimal weight vector may be estimated, but the propagation conditions along with implementation constraints do not allow the system to operate under optimal conditions. The impact of the operating constraints on performance are discussed in the following subsections.

3.6.1 Limited Amount of Feedback: Application of Quantization

The amount of feedback may be a limiting factor for transmit diversity schemes because it depends directly on the number of antenna elements and on the number of bits assigned to each weight value (real and imaginary components). The simplest form of quantization is the uniform quantization. However when the PDF of the channel gains is known, more sophisticated quantization techniques, for example, the optimum non-uniform quantizer can be found by using the Lloyd-Max-Algorithm. However, quantization is a non-linear operation and always introduces errors in the quantized information. The impact of these errors is not easily predictable, but simulations give insight into how severe the system performance is degraded.

Table 3.3 summarizes the SNR degradations from non-quantized values (infinite precision) found from Monte-Carlo simulations with the following simulation parameters:

- 5000 trials with new channel parameters (magnitudes and phases) in each trial,
- blind LS channel estimation operating on BPSK modulated symbols,
- 50 symbol observation window length for channel estimation,
- $(\gamma_0) = 12\ dB$.

Table 3.3. Impact of feedback quantization on system performance

	Different Channels/ SNR Degradation			
Quantization	Rayleigh Fading *2bits for magnitude 3bits for phases*	Ricean Fading *2bits for magnitude 3bits for phases*	Rayleigh Fading *3bits for magnitude 3bits for phases*	Ricean Fading *3bits for magnitude 3bits for phases*
Uniform Quantization	.19 dB	.19 dB	.152 dB	.165 dB
Non-Uniform Quantization	.16 dB	.17 dB	.148 dB	.161 dB
Improvement Non-Uniform vs. Uniform	.02 dB	.015 dB	.0043 dB	.0043 dB

Two main conclusions can be drawn from Table 3.3. First, the performance degradation due to quantization is small compared to errors introduced by channel estimation. With only a few bits, e.g., ten to twelve bits, the channel can be reliably reported to the transmitter. Second, the difference between uniform and non-uniform quantization is marginal. To save computational complexity, it is sufficient to quantize uniformly.

3.6.2 Channel Dynamics and Latency

Introduction

In the following simulation studies, the framing structure of W-CDMA standard is used as a representative signal format for the model in Figure 3.9. The overall latency, ΔL associated with a closed-loop application, uplink power control mechanism, is given in [ETS00] and it can be inferred that the maximum ΔL comes out to be around 1-2 slots for practical cell radii. ΔL, in general, can be expressed as ΔL = $(2\tau_p + \tau_1 + \tau_2)$, where τ_p is the propagation delay, τ_1, τ_2 are processing delays at the receiver and transmitter, respectively. Using the slotted transmission of

W-CDMA as a reference model provides realistic values of 1-2 slots for ΔL. In this study, latency values of 1 and 5 slots, representing both practical and pessimistic estimates, are used to test the proposed algorithms. Two speeds are considered: pedestrian speed at velocity V = 3 mi/h and low mobile speed at V = 10 mi/h, and fading channels were generated at the slot rate (1500 Hz) using Rayleigh fading channel simulator with the maximum Doppler corresponding to this velocity. The time coherence of the channel is assumed to span more than a slot at this low mobility. This assumption is reasonable as can be seen from Figure 3.10 that shows a particular snapshot of the fading envelopes along with the slot structure. Two different feedback error rates $p_e \in \{0.01, 0.05\}$ were considered. The operating SNR is assumed to be 20 dB.

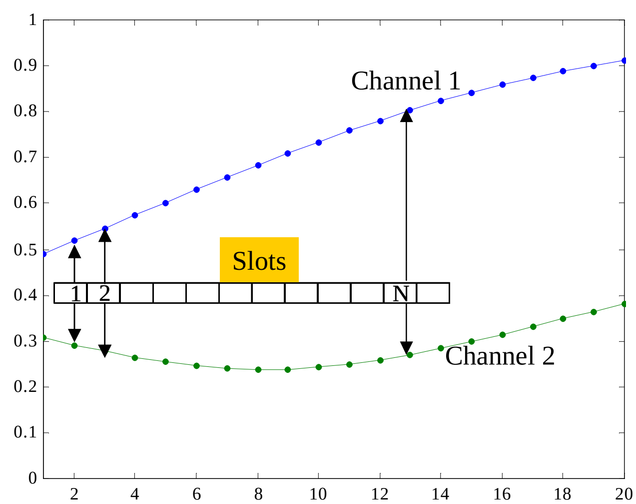

Figure 3.10. Fading envelope snapshot in terms of amplitude vs. slot number.

The techniques that were tested under practical implementation constraints were the Bisection method from EGT category, and both trained and blind forms of LS from the MRT category. An iteration of the Bisection technique follows a closed-loop path from the receiver through the channel to the transmitter array, and thus, convergence characteristics and overall performance are subject to distortions arising from the practical constraints. On the other hand, the LS technique works in a block mode, and thus, is subject to distortions only once per probing process. The feedback information for the Bisection method is an integer value, $i \in \{1,2,3\}$ that can be quantized by two bits. For the LS technique, the feedback information is the estimated weight vector whose magnitude and phase information for each component can be quantized to finite number of bits. The feedback payload in this investigation accommodates 2 bits for magnitude and 3 bits for phase for each component in the weight vector. It is worthwhile to mention at this point that the W-CDMA standard allocates 1 bit for quantization for mode 1 and 1 bit for magnitude, and 2 bits for phase for mode 2 in the closed-loop category. Based on the initial findings on quantization study in Section 3.6, it was decided to use uniform quantization with the above bit allocations. Three independent simulations were carried for these three techniques and the results, expressed as mean receive SNR in dB, are presented in Tables 3.4-3.5. The ideal LS techniques in Tables 3.4 refer to the proposed LS techniques excluding the errors shown in Fig 3.9.

Table 3.4.1. Performance from LS (trained) with practical implementation constraints; V= 3 MPH

V= 3 MPH Latency, ΔL	p_e	Actual LS (blind)	Ideal LS (blind)	Actual LS (trained)	Ideal LS (trained)	1-antenna	Ideal MRT
1	0.01	18.27	18.54	18.31	18.58	15.74	18.68
	0.05	17.69	18.54	17.77	18.58	15.74	18.68
5	0.01	17.53	17.73	18.28	18.56	15.74	18.68
	0.05	17.16	17.75	17.76	18.56	15.74	18.68

Table 3.4.2. Performance from LS (trained) with practical implementation constraints; V= 10 MPH

V= 10 MPH Latency, ΔL	p_e	Actual LS (blind)	Ideal LS (blind)	Actual LS (trained)	Ideal LS (trained)	1-antenna	Ideal MRT
1	0.01	15.76	15.98	16.6	16.85	14.08	17.02
	0.05	15.37	16.01	16.06	16.85	14.08	17.02
5	0.01	15.67	15.88	16.45	16.71	14.07	17.01
	0.05	15.29	15.89	15.89	16.72	14.07	17.01

For both the versions of LS techniques at mobile speed of 3 mph, it can be seen from Table 3.4.1 that they are relatively insensitive (excluding the effects of small variability) to practical channel conditions and always provide substantial gains over the single-antenna system. It is observed that for any particular value of ΔL, the performance degradation for the actual output from the ideal output from the LS techniques is about 0.2-0.3 dB for error rate of 1% and about 0.6-0.8 dB for 5%. Even then, the performance improvement is about 2 dB and 1.5 dB over the single antenna case for the trained and the blind LS respectively. For a mobile speed of 10 mph that is higher than the pedestrian speed, the results from Table 3.4.2 show the general performance trends for both the LS techniques as found in Table 3.4.1. At ΔL = 5 and p_e= 5%, there is a gain of about 1.3 dB and 1.8 dB over the single antenna system for the blind and the trained LS respectively. The relative insensitivity of the performance of the algorithms with different mobile speeds is attributed to the block processing nature of these algorithms.

Table 3.5.1. Performance from Bisection with practical implementation constraints; V= 3 MPH

V= 3 MPH Latency, ΔL	p_e	Bisection	1-antenna	Ideal MRT
1	0.01	15.69	13.69	16.68
	0.05	15.58	13.69	16.68
5	0.01	15.26	13.69	16.68
	0.05	15.19	13.69	16.68

Table 3.5.2. Performance from Bisection with practical implementation constraints; V= 10 MPH

V= 10 MPH Latency, ΔL	p_e	Bisection	1-antenna	Ideal MRT
1	0.01	14.14	12.1	15.63
	0.05	14.07	12.1	15.63
5	0.01	12.44	12.12	15.64
	0.05	12.39	12.12	15.64

The Bisection method is also relatively robust to channel dynamics and latency effects at the mobile speed of 3 mph as can be seen from Table 3.5.1. The results show small degradation (~ 0.1 dB) with error rate for any ΔL, and degradations of about 0.4 dB with ΔL for any error rate. At the high end of latency and error rate, the Bisection method is able to provide a gain of about 1.5 dB. Table 3.5.2 shows that for speed of 10 mph, the technique provides a gain of about 2 dB for ΔL = 1 irrespective of error rate. The technique is more sensitive to ΔL than the error rate and at the extreme settings of these two parameters; the performance is marginally above the single antenna case. This is to be expected since each iteration of the technique involves closed-loop feedback and the occurrence of errors will cause the algorithm to diverge to a wrong solution altogether. In addition to this, higher values of latency will further worsen the performance. However, the results show that under reasonable operating constraints and in low mobility environment, the proposed techniques provide substantial performance improvement over single-antenna systems.

Note that the latency associated with indoor wireless channels is smaller than the latency considered in this study [PRA98]. Thus, indoor channels will provide a vantage scenario for the algorithms under consideration. Indoor channels are dominated by fast fading characteristics, but very small values of latency coupled with small error rate will provide a vantage scenario for the algorithms under consideration. For indoor applications, the impact of the transmit diversity algorithms will be substantial and the resulting performance improvement in fading channels will weigh in favor the implementation of these algorithms.

3.7 Conclusions

In this Chapter, the techniques proposed in Chapter 2 have been tested for their performance improvement by simulation. Both the convergence and the SNR performance improvement have been studied. The EGT techniques have been shown to provide substantial improvement over a single antenna system. The bisection method provided the best performance both in terms of convergence and SNR among this class of techniques, and it is approximately within a dB of the best ideal technique (ideal MRT). Among the MRT techniques, the supervised LS-TD technique provides the best performance and almost achieves the upper bound of an ideal MRT technique. The convergence behavior of the MRT techniques, other than the LS-TD, falls short when compared to EGT techniques. The EGT techniques also outperform the MRT techniques regarding the amount of feedback (the feedback in the EGT case is often a phase index compared to a full complex vector for the MRC case). The implementation issues regarding the proposed techniques have been addressed. The latency associated with LS and BS techniques, has been studied for a dynamic channel. Relatively coarse quantization (to accommodate feedback information) has been found to have small impact on the SNR performance of LS technique.

The inherent drawback associated with these techniques is that the signal may undergo substantial amplitude fluctuations, which may make the received signal too low for proper detection. One way to overcome this problem is to transmit at a higher power during the training period for proper detection and estimation of the optimal weight vector and then reduce the transmit power during information transmission with the optimal weight vector.

Chapter 4

Spatio-Temporal Processing: Transmit Diversity in the Frequency Selective Channel

4.1 Introduction

For a frequency-selective channel, transmit diversity implementations include filters at each antenna element at the transmitter to counter the temporal distortion introduced by such a channel. In addition, there may be filters at the receiver. In such a case, joint optimization is sought for involving all the filters.

Transmit diversity techniques in a frequency selective channel have been addressed in the literature. One common technique is to convert a flat fading channel into a frequency selective channel by introducing delays [WIN94], [WIN98], [BON99], [DES00] or phase rotations in different antenna elements in the transmitter array [WEE93], [HIR92]. Another class of temporal processing with an antenna array, commonly known as a Space-Time processing, has attracted much interest for its use on the transmitter side [ALA98] and [TAR98]. The main emphasis of these techniques is to devise an efficient coding scheme (temporal processing) and to assign transmitted symbols to different antenna elements (spatial processing). These techniques focus on a flat fading channel, but extensions to a frequency selective channel can be found in [LIN00]. Temporal processing along with transmit diversity has been addressed in the form of modulation diversity in which each antenna branch processes the incoming signal with different modulation filters [WIT93].

Although the papers mentioned above address frequency selective channels or spatio-temporal processing at the transmitter, they do not address the joint optimization of both transmit and receive filters for performance enhancement. This chapter addresses this issue directly and presents theoretical expressions for optimum performance. Some sub-optimum structures are proposed alongside that are more convenient for implementation. Joint optimization of transmit and receive filters for a single antenna system has been addressed in [BER67]. It discusses a joint design of transmit and receive filters that minimizes the MSE between the transmitted and estimated symbols given a constant transmit power and without any excess bandwidth. This approach was followed up and extended to include joint transmit/receive diversity for a multiple-input/multiple-output (MIMO) system [YAN94a], [YAN94b]. These proposed techniques provide closed-form expressions that are not quite intuitive and not easy to relate to physical parameters, e.g., channel response either in time or frequency domain. The analysis undertaken in this chapter is similar to these techniques in principle but differs significantly in terms of closed-form solutions. The filter design and joint optimization were done in frequency domain for a continuous time model. The contributions in this chapter are as follow: 1. Optimal solutions for both MSE and distortion-free SNR (DSNR) are derived, 2. These expressions relate channel parameters (e.g. multipath profile) to performance in a straightforward manner, 3. Some sub-optimal filter structures are proposed that can be more suitable for implementation, and 4. Since practical implementations (in a handset or base station) would require digital processing, some discrete time structures were proposed and investigated. For the discrete time structures, the issue of feedback was addressed.

This chapter begins with optimum and sub-optimum techniques for optimizing DSNR and MSE in frequency domain. Then filter design in the discrete time domain is presented and several sub-optimum structures are derived. Simulation results are provided to study the performance improvement from the different techniques.

4.2 Problem Formulation and Analysis

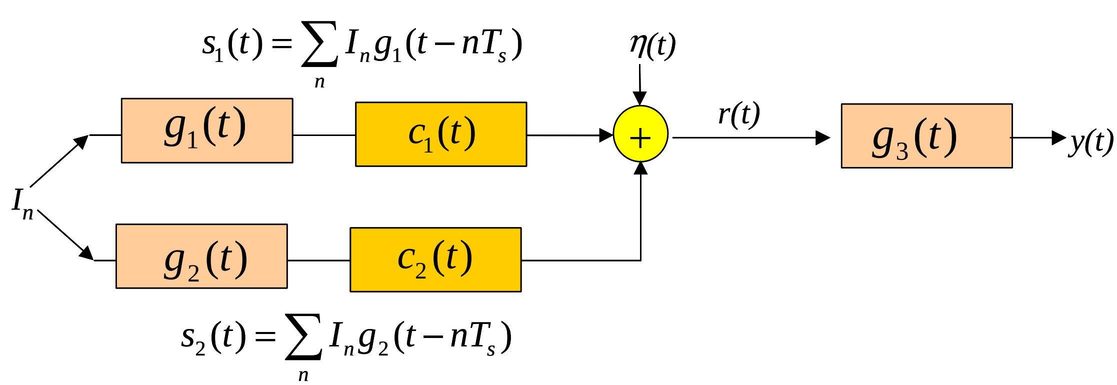

Figure 4.1. Transmit diversity system modeled in a continuous time domain

A two antenna transmit diversity system modeled in continuous time domain is shown in Figure 4.1. The information symbols, denoted by I_n with duration T_s, pass through the pulse shaping filters $g_1(t)$ and $g_2(t)$ to generate the signals (modulated) $s_1(t)$ and $s_2(t)$. Due to the filtering operation, these signals contain contributions from more than one information symbol I_n, and thus they are correlated with numerous input symbols. The transmitted signals pass through frequency selective channels $c_1(t)$ and $c_2(t)$ that may be expressed as finite impulse response filters having the form

$$c(t) = |c_0| e^{j\phi_0} + |c_1| e^{j\phi_1} \delta(t - t_1) + ... + |c_n| e^{j\phi_n} \delta(t - t_n)\,. \tag{4.1}$$

This, in general, conforms to a typical wireless channel where frequency selectivity arises from delayed multipath signal propagation. Receiver front-end noise $\eta(t)$ is added to the received signal to generate $r(t)$, which is passed through a receive filter $g_3(t)$, acting as an equalizing filter. All filters are considered to be ideal filters, i.e., infinite length filters. The goal here is to employ a filter, $g_3(t)$, which will optimize performance for given $g_1(t)$ and $g_2(t)$, and then to further optimize the system by adjusting the transmit filters. This provides a joint solution to the optimization problem. Maximum performance is achieved if all three filters are jointly optimized.

The input symbols $\{I_n\}$ are assumed to be wide sense stationary with autocorrelation function $R(k)$ and power spectral density $\Phi(f)$. The power spectral density of $s_i(t)$ can be written as

$$\Phi_{S_i}(f) = \frac{1}{T_s} |G_i(f)|^2 \, \Phi_I(f)\,. \tag{4.2}$$

where, $G_i(f)$ is the Fourier Transform of $g_i(t)$. The signals $s_i(t)$ can be restricted so that their equivalent bandpass representations occupy a certain bandwidth W. This can be achieved by restricting the pulse shapes $g_i(t)$ so that

$$G_i(f) = 0 \;\; for\; |f| > \frac{W}{2}\,. \tag{4.3}$$

Let R denote the information rate defined as T_s^{-1}. The ratio of the bandwidth of the pulse shape filters to that of the information symbols is expressed by bandwidth expansion factor, B_e, defined as $B_e = W/R = WT_s$.

The received signal can be expressed as the superposition of two transmitted signals that are convolved with their respective channels:

$$r(t) = c_1(t) * s_1(t) + c_2(t) * s_2(t) + \eta(t)\,. \tag{4.4}$$

Here $\eta(t)$ is modeled as white Gaussian noise power spectral density of N_0. The received signal is first passed through a matched filter that is matched to equivalent channel response of

$$h(t) = c_1(t) * g_1(t) + c_2(t) * g_2(t)\,. \tag{4.5}$$

The output from the matched filter is sampled at the symbol rate T_s. The resulting discrete-time signal is passed through a linear shift invariant filter with impulse response b_k to generate an estimate of the kth symbol,

$$\hat{I}_k = I_k q_0 + \sum_{n \neq 0} I_{k-n} q_n + \nu_k\ , \tag{4.6}$$

where $\{q_n\}$ are coefficients resulting from combining all the filters and sampling them appropriately. The additive term ν_k represents colored noise resulting from passing $\eta(t)$ through the receiver filter.

Performance can be enhanced by designing the transmit and receive filters so that the quality of the estimate of the transmitted symbol is improved. Equation 4.6 shows that the estimate is comprised of the scaled value of the actual symbol, contributions from other symbols (inter-symbol interference (ISI)), and additive colored noise. Performance enhancement can be based on two criteria, such as peak distortion and mean squared error (MSE) defined as:

$$D = \sum_{n \neq 0} |q_n|\,. \text{ (peak distortion)} \tag{4.7}$$

$$MSE = E\left[\left|I_k - \hat{I}_k\right|^2\right]. \text{ (MSE)} \tag{4.8}$$

4.2.1 Peak Distortion Solution

The peak distortion can be made zero by employing an appropriate infinite length filter [PRO95]. That results in zero distortion for the symbol estimate and a SNR of

$$SNR = \frac{d^2}{T_s N_0} \cdot \left(T_s \int_{-\frac{1}{2T_s}}^{\frac{1}{2T_s}} \frac{df}{\sum_n \left| H\left(f + \frac{n}{T_s} \right) \right|^2} \right)^{-1} \tag{4.9}$$

where $H(f) = G_1(f) \cdot C_1(f) + G_2(f) \cdot C_2(f)$ and $d^2 = E|I_k|^2$. The term $H(f + n/T_s)$ refers to the folded spectrum with respect to the Nyquist band. The distortion-free SNR (4.9) can be further maximized by shaping the transmit filters properly. The optimization process needs to be carried out under the constraint that the total transmit power remains constant:

$$\frac{1}{T_s}\int_{-\frac{1}{2T}}^{\frac{1}{2T}}\sum_n\left(\left|G_1\left(f+\frac{n}{T}\right)\right|^2+\left|G_2\left(f+\frac{n}{T}\right)\right|^2\right)\Phi_I(f)\,df=P_{av} \qquad (4.10)$$

The maximum DSNR is given as

$$SNR_{opt}=\frac{P_{av}T_s}{\sigma^2W}\left(T_s\int_{-1/2T_s}^{1/2T_s}\frac{\sqrt{\Phi_I(f)/d^2}\,df}{\max\limits_n\sqrt{\left|\hat{C}_1\left(f+\frac{n}{T}\right)\right|^2+\left|\hat{C}_2\left(f+\frac{n}{T}\right)\right|^2}}\right)^{-2} \qquad (4.11)$$

where $\hat{C}_i(f)=\begin{cases}C_i(f) & |f|\le\frac{W}{2}\\ 0 & else\end{cases}.$

The proof of (4.11) is given in Appendix B1. The result for an optimum DSNR shows that the optimization is carried over the folded spectrum even when the signal spans a bandwidth of $R=T_s^{-1}$. At each frequency f, the SNR is optimized for the index n where the norm of the channel vector is maximized. The optimized transmit filters result in having structures that are discontinuous over the range ($-W/2,W/2$) and that have a total span of R. Such structures may render the transmit filters difficult to implement.

One special case can be considered for this expression: let $\Phi_I(f)=d^2$, and the channels have flat fading characteristics, i.e., $C_i(f)=c_i$ for all f, i=1,2. In this case, the expression for SNR becomes $SNR_{opt}=\frac{P_{av}T_s}{\sigma^2}\left(|c_1|^2+|c_2|^2\right)$. This expression for optimal SNR is consistent with what one would expect for a two-element transmit diversity in a flat fading case. In this case, SNR_{opt} reduces to the SNR from ideal MRC that is optimal for a flat fading channel.

To alleviate the problem of implementing optimum transmit filters, one may resort to some sub-optimum filter structures. The resulting SNR is, in general, less than the optimum SNR. The two structures that are proposed in the following sections rely on the inversion of frequency response of the channel vector. Generating filters that have the inverse frequency response of the propagation channel is a relatively benign problem compared to implementing optimal transmit filters.

The first sub-optimal structure, *Sub-opt$_I$*, incorporates pulse shapes at the transmitter that have an inverse frequency response of the respective channels. In other words, the filters are chosen such that $G_i(f)=\frac{\alpha_i}{\hat{C}_i(f)}$ holds. Figure 4.2 shows the proposed structure.

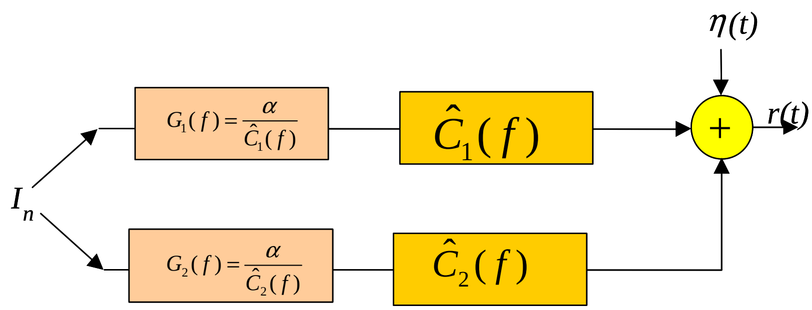

Figure 4.2. Sub-Optimal Structure I (*Sub-opt$_I$*): canceling ISI in each transmitter individually

The frequency response of $G_1(f)$ and $G_2(f)$ is the scaled inverse of the channel frequency responses $\hat{C}_1(f)$ and $\hat{C}_2(f)$, respectively. The scaling is necessary to satisfy power constraint. The corresponding expression for SNR is given by

$$SINR_{sub-optI}=\frac{P_{av}T_s}{W\sigma^2}\cdot\left(\left(\frac{1}{W}\int_{-\frac{W}{2}}^{\frac{W}{2}}\frac{\sqrt{\Phi_I(f)/d^2}df}{\left|\hat{C}_1(f)\right|^2}\right)^{-1}+\left(\frac{1}{W}\int_{-\frac{W}{2}}^{\frac{W}{2}}\frac{\sqrt{\Phi_I(f)/d^2}df}{\left|\hat{C}_2(f)\right|^2}\right)^{-1}\right). \quad (4.12)$$

The proof of (4.12) can be found in Appendix B2. The second sub-optimal structure, *Sub-opt$_{II}$*, is designed such that the overall spectral characteristics of the channel appear flat. This means that the transmit filters are chosen such that $H(f)$ is given by $H(f)=G_1(f)\cdot\hat{C}_1(f)+G_2(f)\cdot\hat{C}_2(f)=\alpha$.

The resulting SNR is then given by

$$SINR_{sub-optII}=\frac{P_{av}T_s}{\sigma^2W}\cdot\left(\frac{1}{W}\int_{-\frac{W}{2}}^{\frac{W}{2}}\frac{\sqrt{\Phi_I(f)/d^2}df}{\left|\hat{C}_1(f)\right|^2+\left|\hat{C}_2(f)\right|^2}\right)^{-1} \quad (4.13)$$

(Proof is given in Appendix B3).

4.2.2 MSE Solution

The analysis presented in this section follows the same general principle as in the peak distortion case. An optimum equalizer b_k is assumed at the receiver, and the resulting optimum MSE, in this case, is given by [PRO95]

$$MSE = T_s \sigma^2 W T_s \int_{-\frac{1}{2T_s}}^{\frac{1}{2T_s}} \frac{\Phi_I(f)\,df}{\Phi_I(f) \sum_n \left| H\left(f + \frac{n}{T_s}\right)\right|^2 + \sigma^2 W T_s} . \tag{4.14}$$

This expression of MSE can be minimized to achieve the optimum or minimum MSE (MMSE) with proper choice of transmit filters. The problem now can be formulated to optimize the transmit filters to minimize the MSE subject to the power constraint. It turns out that a closed-form analytical solution to this problem is not always possible due to the nonlinear nature of the problem. Rather, an iterative search is proposed along the MSE surface to locate the optimal solution (see references [Yan94a], [BER67]). A lower bound on the MMSE can be derived and is presented as (proof given in Appendix B4)

$$MMSE \geq d^2 \left(T_s \int_{-1/2T_s}^{1/2T_s} \sqrt{\frac{\Phi_I(f)/d^2}{\hat{a}(f)}}\,df \right)^2 \Bigg/ \left(\frac{P_{av} T_s}{\sigma^2 W} + T_s \int_{-1/2T_s}^{1/2T_s} \sqrt{\frac{\Phi_I(f)/d^2}{\hat{a}(f)}}\,df \right)^2 \tag{4.15}$$

$$\hat{a}(f) = \max_n \sqrt{\left|\hat{C}_1\left(f + \frac{n}{T}\right)\right|^2 + \left|\hat{C}_2\left(f + \frac{n}{T}\right)\right|^2}$$

4.2.3 Results

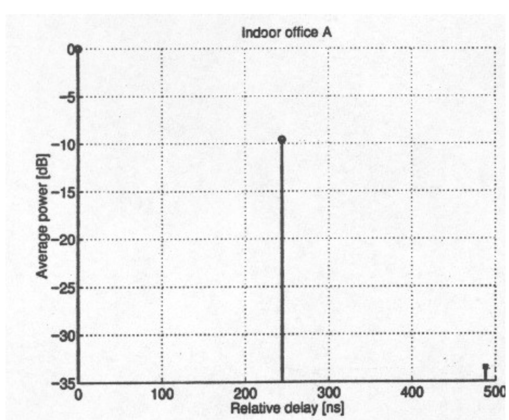

Figure 4.3.WCDMA Indoor channel A

In this section, the optimal and sub-optimal solutions in (4.11)-(4.13) are evaluated in WCDMA type-A indoor channel for a two-element transmitter array. This channel (see Figure 4.3) is proposed by 3G standards body for modeling indoor propagation for a bandwidth of 5 MHz. Rayleigh fading is assumed for all the three multipaths and a total of 500 realizations of the channel are used for this study. The signal bandwidth is assumed to be 1 MHz resulting in $B_e = 5$. The receiver noise power corresponded to a SNR of 12 dB (signal power of symbols $\{I_k\}$).

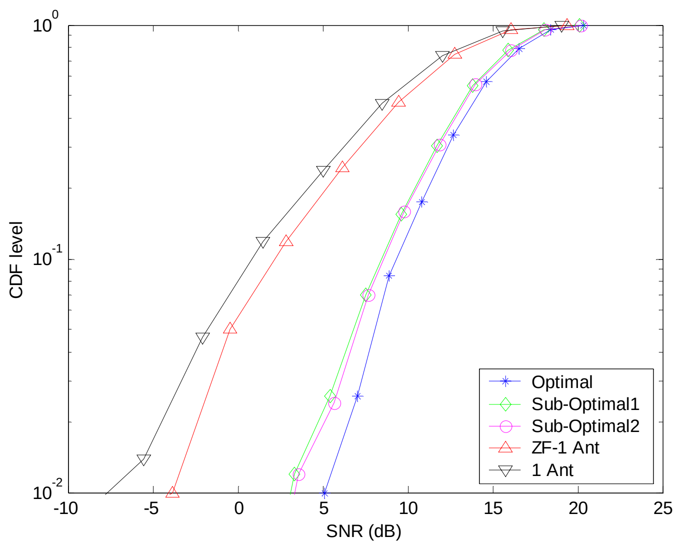

Figure 4.4. CDF plots of SNR achieved from different structures.

The ensemble of SNRs generated from the simulations are presented in CDF plots in Figure 4.4. A single antenna case employing zero-forcing equalization was considered for comparison with the proposed solutions (termed ZF-1 Ant). The CDF plots show that the optimal structure outperforms all other structures providing a diversity gain of about 12 dB over the single antenna without equalization and about 9 dB over the single antenna with ZF equalization at an outage probability level of 10^{-2}. Both the sub-optimal solutions provide about the same performance with a degradation of about 2 dB from the optimal solution at the same outage probability level.

4.3 Discrete Time Sub-Optimal Filter Structures

The optimum filters presented in the previous sections provide maximization of distortion-free SNR for the peak distortion case. The receiver is equipped with an ideal, infinite length equalizer for the optimum structures. The resulting transmit filters are described in the frequency domain, and from an implementation point of view, these filters need to be transformed to the time domain and sampled at the symbol rate. Analyses from the previous sections have shown that the optimum filters are difficult to realize because of their frequency characteristics, and sub-optimal filters that have inverse frequency response of the channel filters may prove difficult to realize because of noise enhancement during inversion process. Furthermore, the wireless channels often turn out to be simple delay-gain or finite-impulse response (FIR) filters and the inverse of these filters require infinite-impulse response (IIR) filters, which can have stability problems. When these filters are implemented in the form of discrete-time filters with finite number of coefficients, performance is already degraded from the optimal level (even from the sub-optimal level for sub-optimal structures) because of the finite-length approximation. Thus practical implementation issues indicate the desirability of designing the filters directly in the discrete time domain. The problem may be equivalently stated in the sampled signal domain with an appropriate discrete time model. The shortcoming of this approach is that since the filters are already in finite-length forms, the resultant performance may not be optimal. But since the optimal filters lose their optimality when converted to finite-length discrete time structures, this problem can be overlooked. The following sections present an equivalent discrete time model of the problem and the necessary formulations.

4.3.1 Evolution to Discrete Time (DT) Model from Continuous Time (CT) Model

The use of a finite length filter necessitates recasting the problem formulation in the discrete time domain and deriving the optimal solutions for the filters. To analyze the optimization problem in discrete time, it is imperative to understand the inter-relation between the continuous-time and discrete time models and derive the transition from the former model to the latter. This section deals with the transition between the two representations.

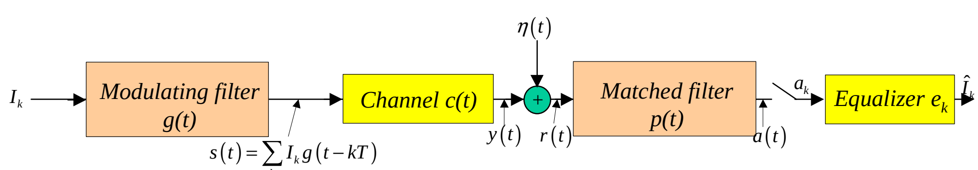

Figure 4.5. Continuous time system model

Figure 4.5 shows the block diagram of the continuous time representation of a communications system that operates in a frequency selective channel and employs an equalizer to counter the ISI effect of the channel. The information symbols are assumed to be independent of each other, i.e., mathematically, $E\left[I_k\right]=0, \quad E\left[I_k I_j^*\right]=\delta_{k-j}$.

The modulating filter $g(t)$ provides the pulse shape to the information symbols and is bandlimited to W, i.e., $\left|G(f)\right|=0 \quad for \left|f\right|>\frac{W}{2}$.

Since the filter $g(t)$ is band limited, by Nyquist's theorem, it can be expressed in terms of sampled values as

$$g(t)=\sum_k g_k \operatorname{sinc} \pi W\left(t-\frac{k}{W}\right) \text{with } g_k=g\left(\frac{k}{W}\right). \tag{4.16}$$

The sampling period T is assumed to be some integer multiple of the inverse of the filter bandwidth W as $T=m/W$. The additive noise $n(t)$ is assumed to be bandpass white gaussian noise (WGN) and has the following spectral density

$$\Phi_n(f)=\begin{cases}\sigma^2 & |f|\leq\frac{W}{2} \\ 0 & else\end{cases}. \tag{4.17}$$

The continuous time model description of the communications system illustrated in Figure 4.5 can be shown to have the discrete time representation as shown in Figure 4.6.

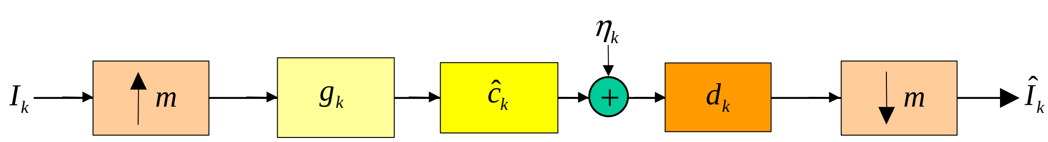

Figure 4.6. Equivalent discrete time system model

The discrete time model shows that the information symbols need to be upsampled m times before they are applied to the discrete time pulse shaping filter g_k. All the filters including the multipath channel are assumed to be sampled at this higher rate. The filters at the transmitter and the receiver, g_k and d_k, form fractionally spaced equalizers (FSE). In this model, the following equalities hold:

$$g_k=g\left(\frac{k}{W}\right), \eta_k=\eta\left(\frac{k}{W}\right)$$

$$\hat{c}_k=\hat{c}\left(\frac{k}{W}\right) \quad \text{where } \hat{c}(t)=\int c(\tau)\operatorname{sinc}\left(\pi W\left(t-\tau\right)\right)d\tau$$

or $\hat{C}(f) = \begin{cases} C(f), & |f| \le \frac{W}{2} \\ 0, & else \end{cases}$.

The proof of the validity of the discrete time model is given in a series of propositions in Appendix B5.

4.3.2 Fractionally Spaced Equalizers

In developing the discrete time models, it was assumed that the signal was oversampled m times and the resulting filters had tap settings at a fraction of the symbol duration. This results in the filters having a form of fractionally spaced equalizers. Figure 4.7 shows transmit diversity setup with fractionally spaced filters.

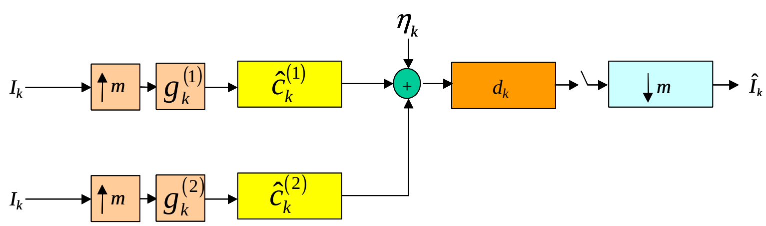

Figure 4.7. Transmit diversity system modeled in discrete time domain

From Figure 4.7, the bandwidth expansion factor becomes $B_e = WT_S = m$. The incoming information symbols are over-sampled m times (by zero padding with m-1 zeros) to generate the sequence s_k. The over-sampled sequence is then filtered by fractionally spaced filters $g_k^{(i)} = g_i(t = k/W), i = 1, 2$. The transmitted sequence passes through the channel filters that have sampled impulse response $\hat{c}_k^{(i)} = \hat{c}_i(t = k/W), i = 1, 2$. The received signal comprises of individual transmitted signal and additive receiver noise and is expressed as

$$r_k = h_k * s_k + \eta_k; \quad h_k = \hat{c}_k^{(1)} * g_k^{(1)} + \hat{c}_k^{(2)} * g_k^{(2)}$$

The received signal r_k is passed through the receive filter b_k and down-sampled by m times to get the signal at the symbol rate. The estimate for the information symbol at the kth instant can be written as

$$\hat{I}_k = I_k q_0 + \sum_{n \ne 0} I_{k-n} q_n + \nu_k \text{ with } q_n = \sum_j d_j h_{nm-j}; \quad \nu_k = \sum_j d_j \eta_{km-j}. \tag{4.18}$$

The transmit power constraint can be written as

$$\frac{1}{m} \sum_n R_{I,n} \left[\sum_k g_{k-nm}^{(1)} (g_k^{(1)})^* + g_{k-nm}^{(2)} (g_k^{(2)})^* \right] = P_{av}. \tag{4.19}$$

With the development of the discrete time model and the reformulation of the necessary expressions, the optimization criteria must be specified. Among different options, the minimum peak distortion and maximum SINR criteria are chosen for this problem.

4.3.3 Peak Distortion

Let the transmit and receive filters as well as the channel filters be duration-limited as follows:

$$g_k^{(i)} = 0 \quad |k| > M; \quad b_k = 0 \quad |k| > N; \quad \hat{c}_k^{(i)} = 0 \quad k < 0, k > L \,.$$

This results in a finite length filter for h_k :

$$h_k = 0 \quad k < -M,\, k > M + L \,.$$

From this, one can show that the coefficients for filter $\{q_n\}$ are restricted in length as $q_n = 0$ for $n < (-M-N)/m$ and n > $(M+N+L)/m$. This implies that the number of nonzero coefficients of $\{q_n\}$ is at most $\left\lfloor \frac{2(M+N)+L}{m} \right\rfloor + 1$. If N is chosen such that $N \geq \frac{M+L/2}{m-1}$ then the number of equalizer coefficients $\{b_n\}$, 2N+1, is greater than the number of nonzero parameters for $\{q_n\}$ and the distortion D can be made zero. Thus with a FSE the distortion can be made zero even when the receiver equalizer has finite length.

To analyze the performance of a structure working on peak distortion, let the following vectors be defined as

$$\begin{aligned} \mathbf{b} &= \left[b_{-N} \; b_{-N+1} \cdots\cdots b_N \right]^T \\ \mathbf{x}_n &= \left[h_{nm+N} \; h_{nm+N-1} \cdots\cdots h_{nm-N} \right]^* . \end{aligned} \tag{4.20}$$

Here [ ]* means a complex conjugate or Hermitian transpose operation. Then we have $q_n = \mathbf{x}_n^* \mathbf{b}$. Now the optimization problem is defined as to maximize the receive SNR $d^2|q_0|^2/E|v_k|^2$ subject to the constraint that $q_n = 0$ for $n \neq 0$. This implies that $\mathbf{b}$ has to be orthogonal to all $\mathbf{x}_n$ for $n \neq 0$. In addition, $\mathbf{b}$ has to be aligned with that part of $\mathbf{x}_0$ that is orthogonal to all $\mathbf{x}_n$, $n \neq 0$. In this case, the maximum DSNR can be expressed as

$$DSNR = \frac{d^2}{N_0} \mathbf{x}_0^* \left(\mathrm{I} - \mathbf{X} \left(\mathbf{X}^* \mathbf{X} \right)^{-1} \mathbf{X}^* \right) \mathbf{x}_0 \tag{4.21}$$

(proof in Appendix B6) where the matrix $\mathbf{X}$ has as its columns all nonzero vectors $\mathbf{x}_n$, $n \neq 0$. Now this DSNR can be optimized with respect to the transmit filters by shaping the pulses $g_k^{(i)}, i = 1, 2$

subject to the power constraint. This renders itself as a nonlinear optimization problem where a closed loop solution is difficult to obtain.

4.3.4 SINR optimization

Optimization of the SINR with respect to the shaping filters is discussed and several sub-optimal structures are proposed in this section. The analytical formulation of the sub-optimal solutions is provided. The proposed structures are investigated by simulation to study the performance improvement.

The output at the receiver is comprised of a scaled desired symbol and interference arising from ISI and filtered noise. Maximizing the SINR means maximizing the signal power of the desired signal $|q_0|^2$ relative to the power of all interference signals $|q_j|^2$ and the noise power. The maximization of SINR is subject to the power constraint at the transmitter. The SINR at the receiver for this transmit diversity system can be expressed as

$$SINR = \frac{|q_0|^2}{\sum_{j\neq 0}|q_j|^2 + \sum_i |d_i|^2 N_0} \tag{4.22}$$

where W is the channel bandwidth and N_0 is the noise power.

The optimization problem can be formulated as

$$\begin{aligned} &\max_{g^{(1)},g^{(2)},d} && \frac{|q_0|^2}{\sum_{j\neq 0}|q_j|^2 + \sum_i |d_i|^2 N_0} \\ &\text{subject to} && \frac{1}{T_s}\sum_k \left|g_k^{(1)}\right|^2 + \left|g_k^{(2)}\right|^2 = 1. \end{aligned} \tag{4.23}$$

The power constraint is normalized to unity in the expression above. The formulation described above is a joint optimization problem with respect to the filters g_k and d_k and solving it provides the global optimal solution. But this results in a non-linear constrained optimization problem that is quite difficult to solve analytically. One sub-optimal approach is to decouple the joint optimization problem can be decoupled into two separate optimization problems involving transmit and receive filters, respectively. The approach is to treat either the transmit or receive filter as constant and optimize the SINR over the other. Then the optimized filter(s) is(are) held at this given solution and the other filter(s) is(are) then optimized. This two-stage optimization process may need to be iterated until some convergence criteria are satisfied. The corresponding algorithm is described in the following steps:

1. Fix d_k and optimize over g_k;
2. Fix g_k at this optimized value and optimize over d_k;
3. Go to step 1 and repeat until convergence is reached.

With this two-stage iterative optimization approach, three different sub-optimal structures have been proposed and investigated. The structures differ with respect to the length of the filters at the transmitter and the receiver.

Structure 1: There are filters at the transmitter and the receiver, and the system has the same representation as shown in Figure 4.7.

Structure 2: Here the shaping filter at the receiver is omitted. The filters that combat ISI are all assumed to be at the transmitter.

Structure 3: Here the shaping filter at the transmitter is reduced to zero-order filters. In other words, the transmit filters do not have any delay and act as a weight vector. The receiver is equipped with an equalizer.

The difference in the proposed sub-optimal structures can also be illustrated with respect to the type of processing carried out at the transmitter and the receiver. In structure 1, space-time processing is performed at the transmitter while temporal processing is performed at the receiver. Structure 2 provides space-time processing at the transmitter but no additional processing at the receiver. In structure 3, the transmitter performs spatial processing while the receiver performs temporal processing.

The other key difference in these proposed structures is the amount of feedback involved. The optimization process is carried out solely at the receiver, and the transmit filter coefficients are then fed back to the transmitter. The amount of feedback will depend upon the length of the respective filters and may be prohibitive for a practical system if a large number of transmit filter coefficients are involved. Among the proposed structures, structure 1 is expected to provide the best performance, but it involves finite length filters at the transmitter and thus a certain amount of feedback. On the other hand, structure 3 involves the smallest transmit filter length and thus the least amount of feedback. Thus, if the performance degradation of structure 3 compared to structure 1 is acceptable, then it is more feasible to resort to structure 3 from practical point of view.

Structure 1

As described in the previous section, the optimal solution for the transmitter filters is found by holding the receiver filter coefficients at any arbitrary level. With the optimized transmit filters held at their optimal values, the receiver filter is then optimized. This sequential update process may need to be iterated several times before some convergence criterion is satisfied. The following section provides the analytical expression for the sub-optimal receive and transmit filter coefficients for this sub-optimal approach.

Assuming d_k is fixed and filter g_k is of finite length $2L$ $\left(g_k = 0 \ \forall |k| > L\right)$, then coefficients q_j can be expressed as

$$q_j = \sum_{i=-L}^{L} g_i^{(1)} \left(\sum_n \hat{c}_{jm-n-i}^{(1)} d_n \right) + \sum_{i=-L}^{L} g_i^{(2)} \left(\sum_n \hat{c}_{jm-n-i}^{(2)} d_n \right). \tag{4.24}$$

Defining the vectors $\mathbf{g}$ and $\mathbf{p}_j$ as

$$\begin{aligned} \mathbf{g} &= \left[g_{-L}^{(1)} \cdots g_{L}^{(1)} \quad g_{-L}^{(2)} \cdots g_{L}^{(2)} \right]^T \\ \mathbf{p}_j &= \left[\sum_n \hat{c}_{jm-n+L}^{(1)} d_n \cdots \sum_n \hat{c}_{jm-n-L}^{(1)} d_n \quad \sum_n \hat{c}_{jm-n+L}^{(2)} d_n \cdots \sum_n \hat{c}_{jm-n-L}^{(2)} d_n \right]^H, \end{aligned} \tag{4.25}$$

(4.24) can be re-written as $q_j = \mathbf{p}_j^H \mathbf{g}$ and the problem formulation in (4.23) changes to

$$\begin{aligned} &\max \quad \frac{\mathbf{g}^H \mathbf{p}_0 \mathbf{p}_0^H \mathbf{g}}{\mathbf{g}^H \mathbf{X} \mathbf{g}} \\ &s.t. \quad \mathbf{g}^H \mathbf{g} = T \end{aligned} \tag{4.26}$$

where $\mathbf{X}$ is a matrix constructed by

$$\mathbf{X} = \sum_{j \neq 0} \mathbf{p}_j \mathbf{p}_j^H + \frac{\sigma^2 W}{T} \sum_i |d_i|^2 \mathbf{I} \,. \tag{4.27}$$

The solution for the optimal transmit filters is expressed as

$$\mathbf{g}_{opt} = \sqrt{T}\,\frac{\mathbf{X}^{-1}\mathbf{p}_0}{\left\|\mathbf{X}^{-1}\mathbf{p}_0\right\|_2} \tag{4.28}$$

(a complete derivation can be found in Appendix B7). Keeping $\mathbf{g}_k$ fixed at $\mathbf{g}_{opt}$ and optimizing the SINR with respect to d_k leads to an expression for an optimal filter d_{opt}. Interchanging g_k with d_k in the previous equations describes the optimization process for the receive filter. Note that due to the power constraint, the matrix $\mathbf{X}$ reduces to

$$\mathbf{X} = \sum_{j \neq 0} \mathbf{p}_j \mathbf{p}_j^H + \sigma^2 W \mathbf{I}\,. \tag{4.29}$$

The solution is similar to the one obtained for $\mathbf{g}_k$ and is given by

$$\mathbf{d}_{opt} = \mathbf{X}^{-1}\mathbf{p}_0\,. \tag{4.30}$$

The maximum achievable SINR is then

$$SINR = \mathbf{p}_0^H \mathbf{X}^{-1} \mathbf{p}_0\,. \tag{4.31}$$

Structure 2

Structure 2 is the same as structure 1 with the filter at the receiver omitted. Thus the optimization process is limited to the transmitter filters only. The optimized SINR has the expression shown in (4.31). No further optimization is carried out at the receiver.

Structure 3

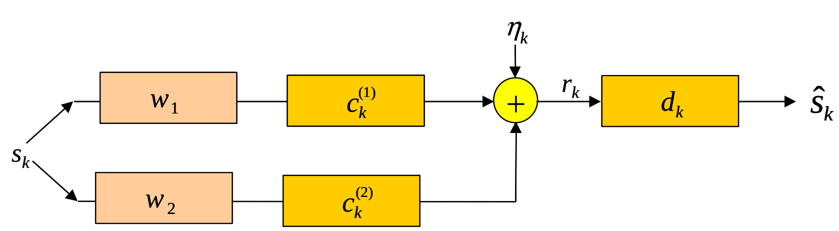

Figure 4.8. Block diagram of structure 3.

Figure 4.8 represents the block diagram of structure 3, which is also a modified version of structure 1 and it is derived by collapsing the transmit filters to zero-order filters. In other words, the transmit filters reduce to a simple weight vector that defines the complex gain for each diversity branch. This is similar to the arrangement of transmit diversity for a flat-fading channel. The receiver is equipped with a filter to combat ISI. Thus the joint space-time processing is separated into spatial processing at the transmitter and temporal processing at the receiver. Here the optimization process is carried out by first optimizing the receive filter while keeping the weight vector constant and then optimizing the weight vector with the optimized receive filter. This two-stage optimization may need to be iterated several times for the algorithm to settle to some local optimal point. The two-stage optimization process is first carried out on the receive filter. Assuming any weight vector $\mathbf{w}_k$ at the kth instant, the optimum filter at the receive is given by

$$\mathbf{d}_{opt} = \frac{\left[\sum_{k\neq 0}\mathbf{p}_k\mathbf{p}_k^H + \sigma^2\mathbf{I}\right]^{-1}\mathbf{p}_0}{\left\|\left[\sum_{k\neq 0}\mathbf{p}_k\mathbf{p}_k^H + \sigma^2\mathbf{I}\right]^{-1}\mathbf{p}_0\right\|_2} \tag{4.32}$$

With this given optimal receive filter, the optimal weight vector is given as

$$\mathbf{w}_{opt} = \frac{\left[\sum_{k\neq 0}\mathbf{q}_k\mathbf{q}_k^H + \sigma^2\mathbf{I}\right]^{-1}\mathbf{q}_0}{\left\|\left[\sum_{k\neq 0}\mathbf{q}_k\mathbf{q}_k^H + \sigma^2\mathbf{I}\right]^{-1}\mathbf{q}_0\right\|_2}. \tag{4.33}$$

The derivations for the optimal solutions are given in Appendix B8. With this optimal weight vector, the vectors $\mathbf{p}_k$ in the expression (4.32) change, thus the optimal $\mathbf{d}$ needs to be recomputed. With the new computed $\mathbf{d}$, the optimal weight vector can be recomputed. This alternate optimization is iterated until some convergence criteria are satisfied.

4.3.5 Results

The section present performance improvement of the sub-optimal discrete-time structures. Two metrics are studied: convergence behavior and diversity gain. The vector multipath channel that has been used in the convergence study is comprised of a 13-tap filter that has an impulse response and pole-zero description as shown in Figures 4.9 (a) and (b).

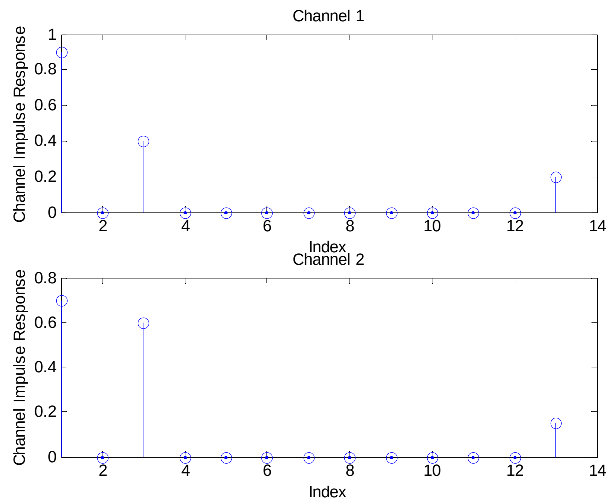

Figure 4.9 (a). Impulse response of the simulated channels.

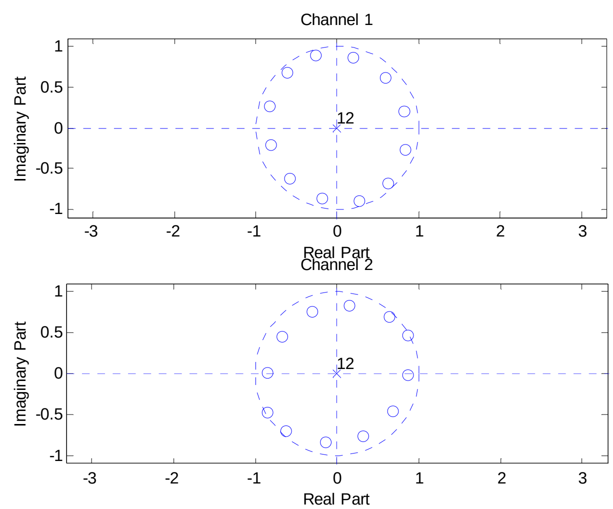

Figure 4.9 (b). Pole-Zero description of the simulated channels.

The convergence behavior of the different sub-optimal filters for this particular channel is shown in Figure 4.10. In this simulation, the length for all the filters is set at twenty and the operating SNR is chosen as 20 dB. The un-equalized channels from each transmit antenna is shown for comparison. From the plots, sub-optimum structure 2 provides the highest SINR without any transient behavior. The other structures require 30 iterations before gradually converging to 19 dB. The plots reveal that optimizing three filters jointly (sub-optimal 1) is not efficient compared to the other two structures. Structure 2 does not require any iteration but feedback payload can be high depending on the value of K (the same holds for structure 1). Structure 3 performs within a couple of 2 dB of structure 2 but requires feedback of only 2 complex numbers. Thus, in practical applications, structure 3 may provide an ideal compromise between complexity and performance improvement.

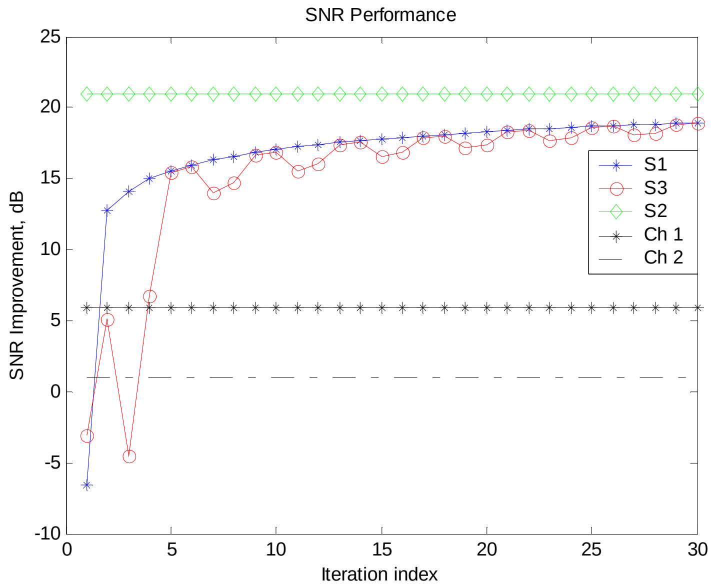

Figure 4.10. Snapshot of SINR convergence from different structures.

The designed filters should mitigate the channels so that the overall channel between the information symbols and the estimated symbols collapse into a single filter with an approximately Dirach delta like response. The performance of different filters is shown in terms of this overall impulse response in Figure 4.11. The plots in this figure show that all the structures remove the ISI effectively from the received signal.

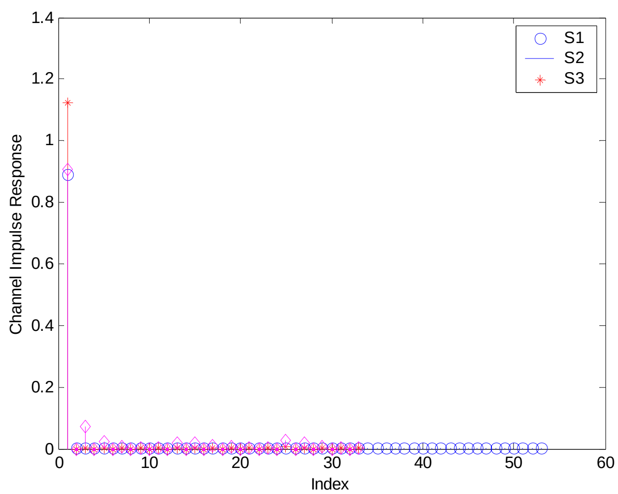

Figure 4.11. Overall impulse response.

The diversity gains of the sub-optimal structures have been evaluated for WCDMA indoor channel (Figure 4.3) and are plotted in Figure 4.12. The plots yield that structures 2 and 3 are better than structure 1.

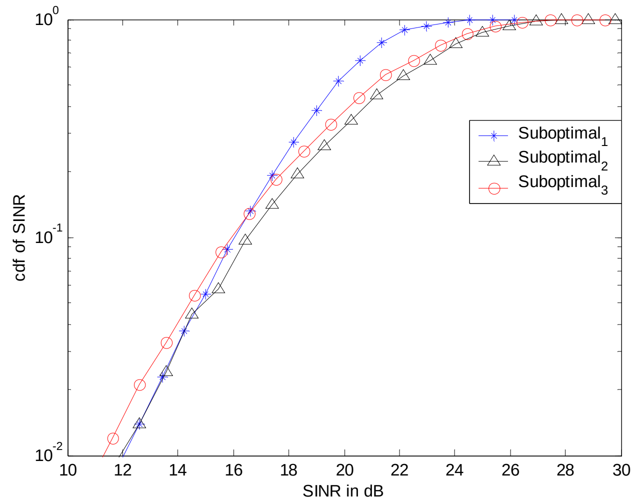

Figure 4.12. CDF plots of output SINR from different structures.

4.4 Conclusions

In this chapter, transmit diversity techniques for a frequency selective channel have been proposed and evaluated. The techniques have been based on optimizing DSNR and MSE for a given frequency selective channel. The analysis regarding the optimal solution was carried out in frequency domain for the signals with excess bandwidth. The analysis also shows that the optimal solution reduces to a MRC solution when the channel becomes frequency non-selective. Several sub-optimal solutions were also developed that seem more convenient for practical realization. Then discrete time analysis resulted in finite length filters that optimize the performance, and several sub-optimal structures were proposed. The discrete time sub-optimal filters provide better performance than a single antenna system. Simulation studies point out an interesting result: while structure 3, a simple weight vector at the transmitter supported by an equalizer at the receiver, performs substantially better than a single antenna system, is slightly behind structure 2, which has filters at the transmitter. However, structure 3 requires several iterations before providing a converged solution.

In all the techniques, it is assumed that the frequency selective vector channel is known at the receiver. The estimates of the channel coefficients can be made available at the receiver by a suitable pilot-assisted channel estimation technique such as the least squares technique. The amount of feedback and the dynamic nature of the wireless channel may restrict the use of these techniques to a low mobility channel or a fixed point-to-point application.

Chapter 5

Diversity Measurements at the Handset

5.1 Introduction

The diversity measurements presented here include vector propagation measurement both for narrowband and wideband signals at the mobile terminal in an indoor channel in order to study channels and assess diversity performance at the mobile. This will allow us to study the impact of mutual coupling between the antenna elements on diversity performance. The channel characteristics may be quite different for a narrowband signal and a wideband signal, and thus diversity performance may differ for these two different signals. Channel measurements for both these types of signals are helpful in assessing a particular diversity system for these two different signals. Section 5.1 presents a study of channel reciprocity at the handset. The concept of reciprocity is useful in channel measurements as the diversity performance of transmit diversity system can be inferred from a receive diversity system. Section 5.2 presents a study of the effect of antenna spacing on the mutual coupling or envelope cross-correlation properties of a closely spaced antenna array system. Section 5.3 presents indoor vector channel measurements for a wideband signal. Section 5.4 presents narrowband transmit diversity measurements in an indoor channel.

5.2 Reciprocity Measurements at the Handset

5.2.1 Introduction

Radio propagation channels to exhibit reciprocal behavior in that the channel characteristics from the transmitter to the receiver are the same as from the receiver to the transmitter. Thus the behavior of the channel is not affected if the role of the transmitter and receiver is interchanged. This behavior is certainly restricted by the fact that carrier frequency has to be the same in both uplink and downlink. Exceptions to channel reciprocity may arise from certain propagation effects, such as diffraction, that tend to be asymmetrical, i.e., the effect is different in different directions. Channel reciprocity is an advantage for a TDD system that employs an antenna array. If reciprocity holds for an indoor vector propagation channel, then one can assess (or estimate) the diversity performance of a transmit diversity system from receive diversity measurements that have the same system configurations. This estimation will save time and resources by avoiding the need to build a separate system to evaluate diversity performance from the transmit side.

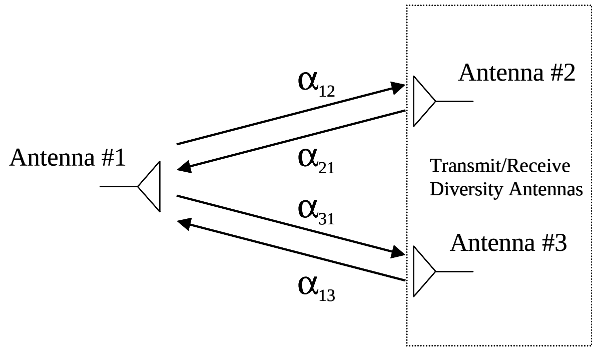

Figure 5.1. Schematic representation of channel reciprocity

In Figure 5.1, channel reciprocity dictates that the instantaneous transfer characteristics of the channel remain unchanged when the role of the receive and transmit antenna elements are functionally interchanged, i.e., $\alpha_{ij}=\alpha_{ji}$ where α_{ij} is the channel gain from antenna i to antenna j. Thus, the diversity performance is expected to be the same for a receive diversity system (antenna #1 transmits and antenna #2 and #3 receive) and a transmit diversity system.

5.2.2. Measurement System

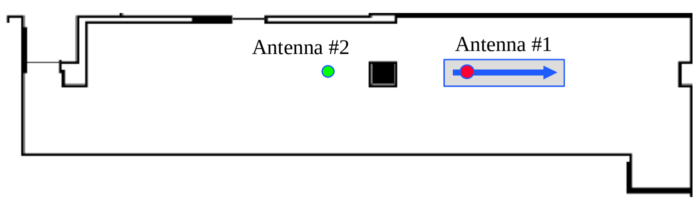

Figure 5.2. Measurement setup for the single antenna experiments

The measurement setup is shown in Figure 5.2. The measurements were taken at the DSP lab of the Mobile and Portable Radio Research Group (MPRG). The system included a two-element antenna array system and a single antenna system. Each antenna element is a quarter wavelength monopole mounted on a ground plane. The inter-element spacing in the antenna array is half-wavelength. The carrier frequency is set at 2.050 GHz and the desired signal is a sinusoidal tone at 1 kHz. Antenna #1 is moved along a track covering a distance of 2 m in increments of 2.9 mm (5 motor steps). The distance over which the array moved was sampled at discrete intervals and the array collected received signals at each of these spatially sampled points. At a certain position on the track, the array was kept stationary while it collected signals over a period of time

T. At each location, 5,000 samples were collected at a 100 kHz sampling rate. The signals collected over this interval were averaged to reduce the effect of noise and to provide a better estimate of the signals received at that point. The array was then moved to the next position and the collection process was repeated. Proceeding in this manner, a set of received signals was obtained as a function of discrete sampled spatial points. The signals were stored in complex form (I and Q) from which the envelope information could be extracted and subsequently, fading characteristics could be observed. There are two different measurement setups that were used to perform the experiments.

In the first setup, only two single antenna systems were used as transmitter and receiver and they were placed on opposite sides of a building column to ensure non-line-of-sight (NLOS) propagation. The goal of this set of experiments was to verify channel reciprocity for a single antenna system before moving onto the antenna array system. Antenna 2 was stationary while antenna 1 was moved along a track. In the first set of experiments, antenna #1 was the transmitter and antenna #2 was the receiver. This provided the gain $\alpha_{12}(t)$. In the second set of experiments, antenna #2 was the transmitter and antenna #1 was the receiver to yield $\alpha_{21}(t)$. Figure 5.3 shows the normalized envelope measurements of the channel gains in both directions. The horizontal axis of the graphs in the figure is converted to the distance traversed on the track. This implies that $\alpha_{12}(t)$ or $\alpha_{21}(t)$ can be equivalently described as $\alpha_{12}(d)$ or $\alpha_{21}(d)$ where d is the distance crossed on the track.

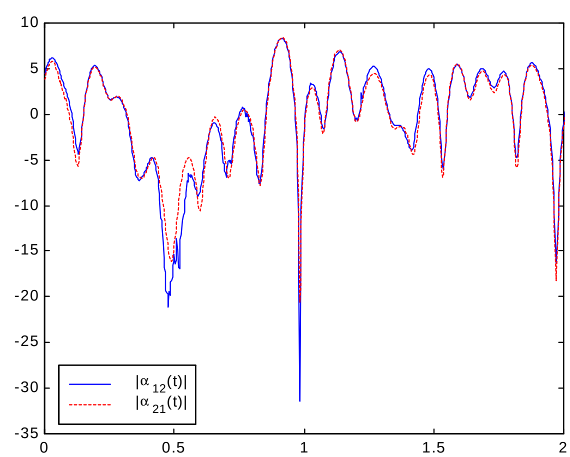

Figure 5.3. Fading envelopes for the single antenna measurements

The envelope cross-correlation coefficient defined as follows was studied for the measured data:

$$\rho_e = \frac{E\left[(e_i-\mu_i)(e_j-\mu_j)\right]}{\sqrt{E\left[(e_i-\mu_i)(e_i-\mu_i)^*\right]E\left[(e_j-\mu_j)(e_j-\mu_j)^*\right]}} \tag{5.1}$$

where e_i and e_j are individual envelope measurements and μ_i and μ_j are the sample means of the respective envelopes. The cross-correlation coefficient between the two measured envelopes was 0.99, denoting a very close match.

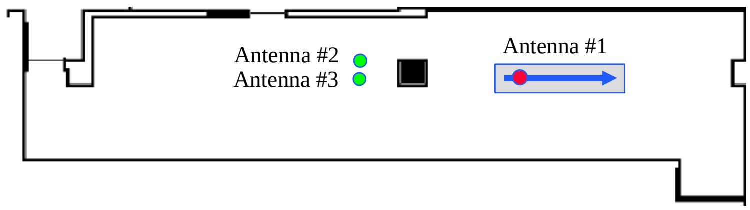

Figure 5.4. Measurement setup for the antenna array experiments

After verifying channel reciprocity for a single antenna system, different setups were used to verify the channel reciprocity for an antenna array system. Figure 5.4 shows the setup in which a two-element antenna array and a single antenna were used. Single antenna #1 was moved along the track while the antenna array (#2 and #3) was stationary. In the first experiment, antenna #1 acted as the transmitter and the antenna array was the receiver. This generated receive diversity channel measurements. In the next experiment, the antenna array transmitted while antenna #1 received. An RF toggle switch allowed transmission from both antenna #2 and #3 at each location of spatial sampling. This is shown in Figure 5.5.

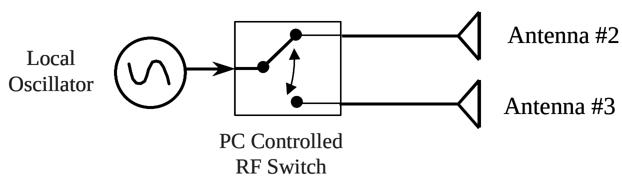

Figure 5.5. Selecting antenna elements for transmission with an RF switch

A dc voltage of 12 volts activated the switch and connected the switch to any one antenna. When the dc voltage was removed, the switch was deactivated and connected to the other antenna. The toggling command was issued from a central PC that controlled the measurement system.

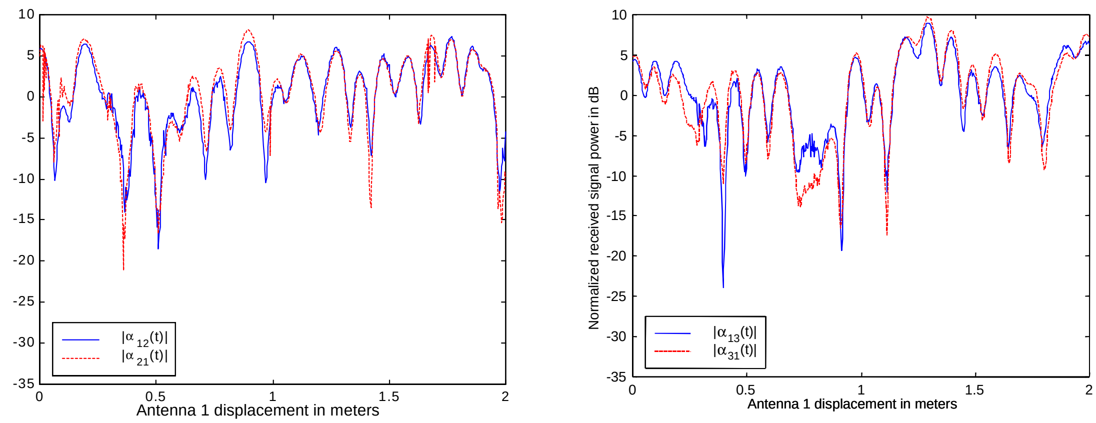

Figure 5.6. Fading envelopes for antenna array measurements

Figure 5.6 shows the measured envelopes from this setup. Propagation channels between antenna #1 and the antenna array reveal a nearly perfect reciprocal behavior. The toggling of the RF switch at the antenna array introduces small measurement errors as can be seen from the graph of $\alpha_{31}(t)$. The envelope cross-correlations between antenna #1 and #2, and between antenna #1 and #3 are 0.95 and 0.96, respectively. These values corroborate the visual similarity between the relevant envelopes shown in Figure 5.6.

The channel measurements presented so far reveal reciprocity for a narrowband indoor channel. The fading envelopes along with the correlation coefficients support this observation. The fading envelopes can be further processed to study comparison of diversity performances between a transmit and receive diversity system. The envelopes are combined using a selection diversity algorithm, and the CDF plots are generated for individual signals and the combined signals. The CDF plots for the receive diversity system are shown in Figure 5.7 and those for the transmit system are shown in Figure 5.8.

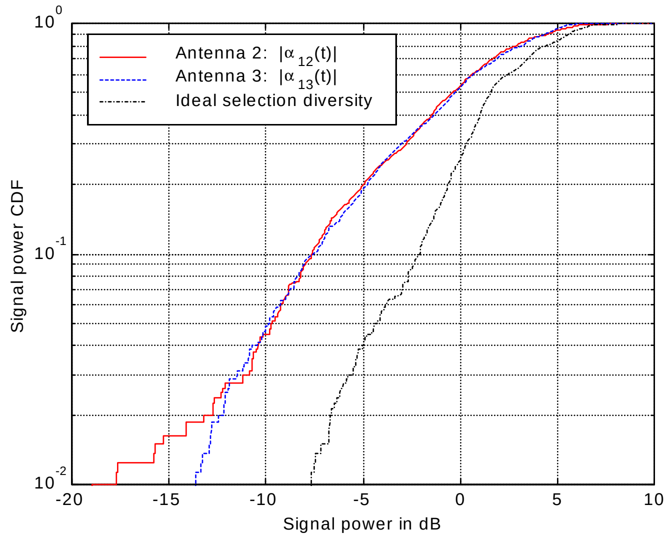

Figure 5.7. CDF plots for receive diversity

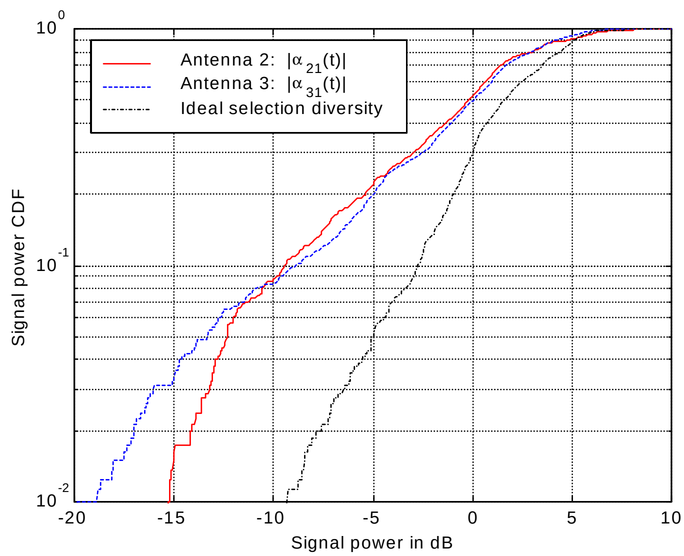

Figure 5.8. CDF plots for transmit diversity

Figure 5.7 shows that the diversity gain at the 10% CDF level is about 6 dB for a receive diversity system. Figure 5.8 reveals that the transmit diversity with the same system is little more than 6 dB at the same CDF level. The diversity plots also confirm the reciprocal behavior of the indoor propagation channel at the handset.

5.3 Study of Envelope Correlation with Antenna Spacing

5.3.1 Introduction

Antenna arrays can be easily accommodated in a base station because space is not a constraint. Sufficient decorrelation of the received signals is obtained when the inter-element spacing is about 8–10λ, where λ is the carrier wavelength. A mobile handset offers little space to accommodate antenna arrays because of its compact size. The antenna elements need to be closely spaced at the handset, and at close inter-element spacing, the mutual coupling between the signals on the elements may make them correlated and hamper diversity performance. The effect of antenna spacing on the envelope cross-correlation has been analyzed to follow a Bessel function variation with an increase of correlation with decreasing spacing [JAK74]. The usual value of 0.5λ reported in the literature provides small correlation but results in an element spacing of about 16 cm at cellular bands and about 8.33 cm at PCS bands. The commonly accepted rule of spacing (0.5λ) is thus seen to prohibit antenna array application at a mobile terminal at cellular bands and even at PCS bands compared to the form factor of typical user terminal. But Rodney Vaughan [VAU91] has shown that tighter than conventional spacing is possible because the correlation does not increase as much as predicted. Measurements reported in [OGA94], [MAN96], and [DIE00] also show that the envelope correlation as a function of antenna spacing follows a smoother curve than predicted from theory. These results are promising for the feasibility of a closely spaced antenna array system at the handset.

This section presents measurements to investigate the effect of antenna spacing on envelope cross-correlation in an indoor environment. The studies here consider this effect in the azimuth plane only. Two different orientations of handset motion, inline and broadside, were considered. These two orientations represent the two extreme orientations with respect to transmitter, and the average orientation is somewhere in between the two. Thus the average performance is expected to be between the measured performances of these two orientations. The measurements were carried out for a two-element array at the handset at an RF carrier frequency of 2.05 GHz.

5.3.2 Experiment Setup

The experiment was conducted in the DSP lab of the MPRG. The transmitter was positioned behind a column so there was no direct propagation path or line-of-sight (LOS) to the receiver (see Figure 5.2). The two-element array was positioned on the track and was connected to the RF chains by coaxial cables. The data collection principle is the same as described in Section 5.2.2. The averaged signals from the two branches were stored in the host PC.

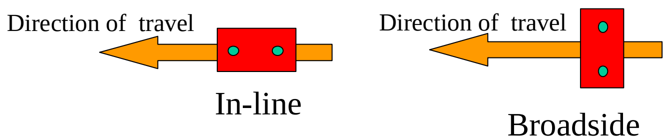

Figure 5.9. Different orientations for correlation measurements

Two different orientations were studied: inline and broadside (see Figure 5.9). With inline orientation, the array axis parallel to the direction of motion. With broadside orientation, the axis of the array was perpendicular to the direction of motion, making the array broadside relative to the transmitter.

For each array orientation, the spacing between the elements was varied, the array was moved along the track, and data was collected. The inter-element spacing was drawn from the set {0.5,0.4,0.3,0.2,0.1} of wavelength. Thus measurements corresponding to five different element spacings and two different orientations yielded a total of ten measurements.

5.3.3 Results

For each measurement set, signals from the two elements were processed to extract the envelope information. Figures 5.10 and 5.11 show the envelope characteristics of the received branch signals (dB vs. sample index) for an inline orientation with $d/\lambda = 0.5$ and 0.1, respectively.

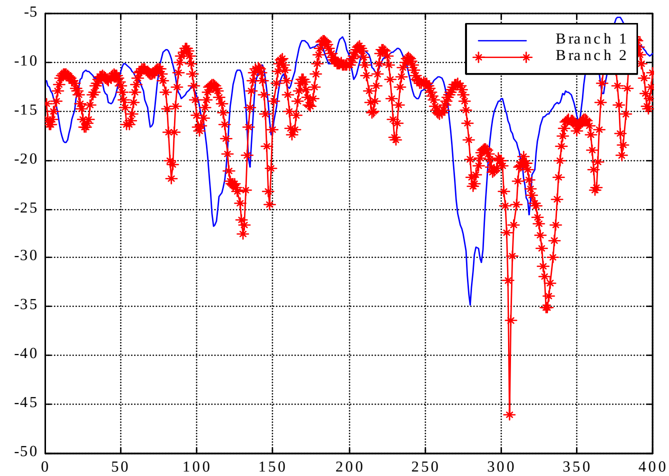

Figure 5.10. Fading envelopes for inline measurements with $d/\lambda = 0.5$

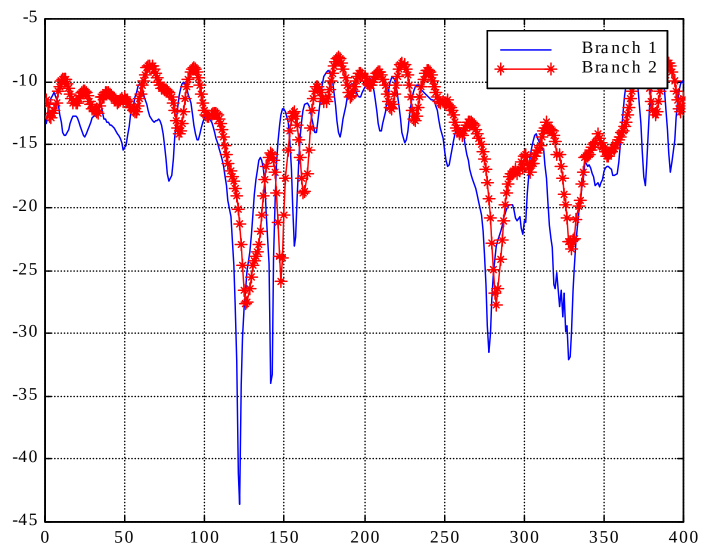

Figure 5.11. Fading envelopes for inline measurements with $d/\lambda = 0.1$

For inline measurements, it is expected that the envelope waveforms would be correlated to some extent since the elements are inline and one element follows the other. This correlation is in addition to the mutual coupling that exists between the closely spaced antenna elements. For $d/\lambda = 0.5$, the waveforms from the elements exhibit some similarity in the behavior. As expected, this is more prominent when $d/\lambda = 0.1$. Even then, the fading characteristics in terms of fade depths are different, which may be attributed to pattern distortion that results from having the elements in close proximity and the mutual coupling between them that distorts the resulting pattern. The resemblance between the waveforms for a particular value of d/λ for a specific orientation can be quantified in terms of the envelope correlation coefficient, ρ_e. Figure 5.12 shows the fading envelope when the array is broadside at d/λ=0.1. The figure shows that even at that close spacing, the fading envelopes on the two elements are different and there is no pronounced resemblance as in the case of inline orientation.

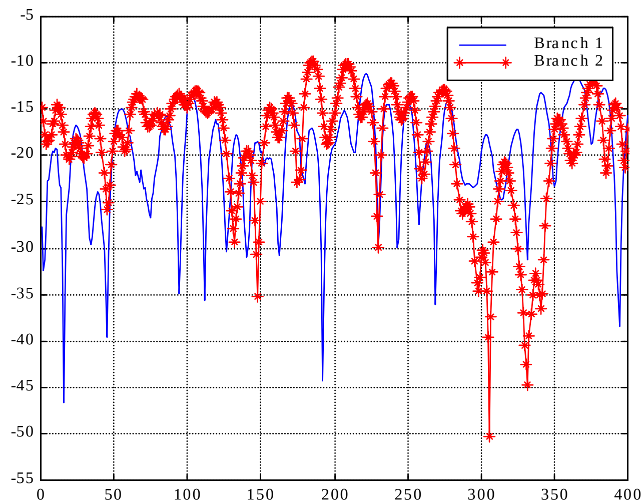

Figure 5.12. Fading envelopes for broadside measurements with d/λ= 0.1

5.3.4 Diversity calculation

A selection diversity scheme is assumed for diversity reception, and the diversity gain was calculated at the 1% CDF level. Tables 5.1 and 5.2 present the value of ρ_e and diversity gain for in-line and broadside orientation, respectively. The rule of thumb is that at ρ_e = 0.7, the diversity gain is greatly diminished. Table 5.1 also confirms a similar notion as can be seen from the reduction of diversity gain from 10 dB (d/λ=0.5) to 2 dB (d/λ=0.1).

Table 5.1. Inline Orientation

Antenna Spacing d/λ	Correlation Coefficient, ρ_e	Diversity Gain @ 1% CDF level, dB
0.5	0.41	~10
0.4	0.52	~6
0.3	0.57	~4
0.2	0.66	~3
0.1	0.64	~2

Table 5.2 shows that the correlation between the elements is relatively insensitive to antenna spacing. The very small value of correlation at 0.2-wavelength spacing is attributed to a measurement error of unknown nature. From both tables, it can be concluded that the antenna spacing in an antenna array can be quite close at the handset without sacrificing substantial performance gain.

Table 5.2. Broadside Orientation

Antenna Spacing d/λ	Correlation Coefficient, ρ_e	Diversity Gain @ 1% CDF level, dB
0.5	0.17	~ 6
0.4	0.18	~9
0.3	0.14	~5
0.2	0.006	~7
0.1	0.16	~8

The proposed transmit diversity techniques in Chapter 2 have been tested with the measured vector channels. The results in terms of average receive SNR are shown in Tables 5.3 and 5.4. The single antenna case is represented by choosing the fading profile from one channel of the array.

Table 5.3. Average receive SNR in inline orientation.

Element spacing, d/λ	ρ_e (Inline)	LS (trained) (dB)	LS (blind) (dB)	Bisection (dB)	Single antenna (dB)	Optimal (dB)
0.5	0.41	12.9	12.9	12.5	10.7	13.4
0.4	0.52	13.7	13.6	13.2	12.1	14.0
0.3	0.57	14.3	14.2	13.8	12.7	14.6
0.2	0.66	13.9	13.2	13.6	11.9	14.3
0.1	0.64	12.3	12.1	11.9	8.7	12.7

Table 5.4. Average receive SNR in broadside orientation.

Element spacing, d/λ	ρ_e (Broadside)	LS (trained) (dB)	LS (blind) (dB)	Bisection (dB)	Single antenna (dB)	Optimal (dB)
0.5	0.17	11.5	11.3	10.7	7.8	12.0
0.4	0.18	10.3	9.4	9.5	6.5	10.9
0.3	0.14	10.3	10.0	9.7	6.5	10.9
0.2	0.01	10.0	9.7	9.2	5.5	10.6
0.1	0.16	7.9	6.9	7.4	4.2	8.7

Table 5.3 provides the computed gains in the inline orientation for different antenna element spacing. The results show that with increasing separation, the correlation coefficient decreases but the performance varies within small margins. The performance peaks at a spacing of 0.3 and tapers off gradually in either direction of increasing/decreasing spacing. From Table 5.4, it is observed that the correlation values are relatively insensitive to inter-element spacing, and the performance for all the techniques improve with increasing separation. This improvement is most prominent going from $d/\lambda = 0.1$ to 0.2, and small for other changes. The effect of antenna separation on diversity performance for both the inline and broadside orientations can be explained in the context of pattern distortions that arise from closely spaced radiating elements. Radiation pattern measurements in the azimuth plane for two dipoles with $d/\lambda \in \{0.1, 0.3, 0.5\}$ are shown in Figure 5.13 [DIE01]. The plots show patterns from both electromagnetic modeling (by using NEC software) and measurements. Here, the black dots represent antenna locations and the patterns correspond to the left element (marked as centered black dot). The patterns for the right element are assumed to be symmetrical, reflected across the center point of the array.

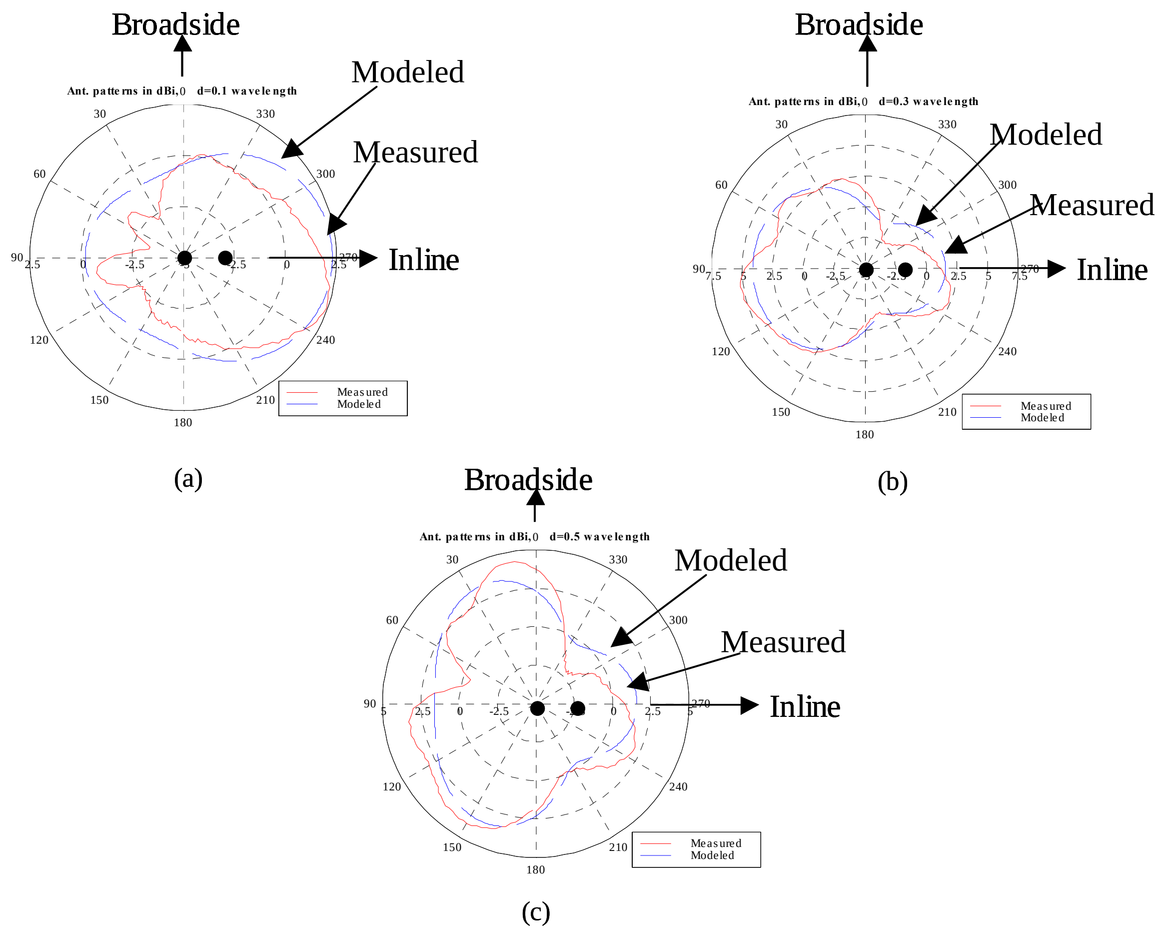

Figure 5.13. Radiation pattern measurement plots for different inter-element spacing; (a) d/λ=0.1, (b) d/λ=0.3, and (c) d/λ=0.5 [DIE01]. The black dots represent antenna locations.

Both the measured and modeled plots show that the patterns become distorted and assume a directional shape instead of an omni-directional one. The directivity of the patterns is aligned with the axis of the array in most cases, and the maximum gain varies for different separations. The maximum gain for inline orientation occurs at spacing of 0.3 (= 5 dB; along the horizontal axis) and for other two spacing, the maximum gain is approximately the same (about 2.5 dB). In the broadside orientation, maximum gain occurs for 0.5 spacing. These observations explain why the diversity gain is maximized at 0.3 spacing for inline orientation, and 0.5 spacing for broadside orientation. Also, note that, for broadside orientation, the gain in the broadside direction increases from 0 dB to 2.5 dB when d/λ changes from 0.1 to 0.3, which explains the prominent increase in diversity performance. These results indicate that the proposed diversity techniques benefit from sufficient signal decorrelation at a tightly spaced array in indoor environments, and render themselves feasible for small wireless devices.

5.4 Wideband Propagation Measurements

5.4.1 Introduction

The channel measurements reported so far in this chapter were conducted for a narrowband signal in indoor environments. Indoor wireless communication channels provide small delay spread in the multipath components and thus provide a coherence bandwidth that is usually larger than the signal bandwidth. Conventional diversity combining schemes can be employed in such a flat fading channel. But the same environment may be frequency selective for a wideband signal, and common diversity schemes may not be applicable due to the temporal distortion in signals arising from frequency selectivity of the channel. In contrast, an outdoor-to-indoor channel usually shows frequency selectivity for a signal bandwidth that otherwise experiences flat fading in an indoor channel. This section presents direct measurement results of spectral characteristics of an indoor and outdoor-to-indoor channel near the PCS and ISM bands.

Wideband channel measurements for single channel [LOM98] and multi-channel transmitters and receivers [EGG00] provide useful information but they do not address coherence bandwidth and cross-correlation coefficient for an antenna array in wideband indoor channels. Such measurements can be performed by channel sounding with wideband signals [ADN00] or by frequency sweeping using a network analyzer and inverting the measured spectral information to get the temporal characteristics [KAR99]. In both methods, accurate and sophisticated equipment is required to obtain adequate time resolution in the power delay profile (PDP) measurements. But simpler approaches can be adopted if one is interested in only the fading envelopes and coherence bandwidth of the channel. Furthermore, for an antenna array, the method provides envelope cross-correlation information between antenna elements, a parameter that is important from diversity performance perspective. This section presents one such approach that uses an antenna array testbed to sweep across a spectrum of 10 MHz bandwidth at 2.05 GHz carrier frequency and uses the collected data to generate information on coherence bandwidth in both indoor and outdoor-to-indoor channels. Frequency-dependent envelope cross-correlation coefficients across the elements are computed for the indoor channel. Furthermore, the results are useful for small wireless terminals or handsets since the inter-element separation is kept at half-wavelength, which corresponds to about 7.5 cm at 2.05 GHz carrier frequency.

5.4.2 Indoor Channel

5.4.2.1 Measurement Setup

The measurement system was set up in the DSP lab of the MPRG as shown in Figure 5.14. The transmitter consisted of a signal generator connected to a monopole antenna on a ground plane. The antenna was mounted on a linear track. The receiver system was comprised of two different linear antenna array systems. One array was a two-element antenna array of monopole elements with three-eighths of wavelength spacing (antenna 1 and 2). The other array was a six-element linear array with half wavelength inter-element spacing (antenna 3 to 8). The two arrays were placed at different locations to spatially sample the received signal over a wider area.

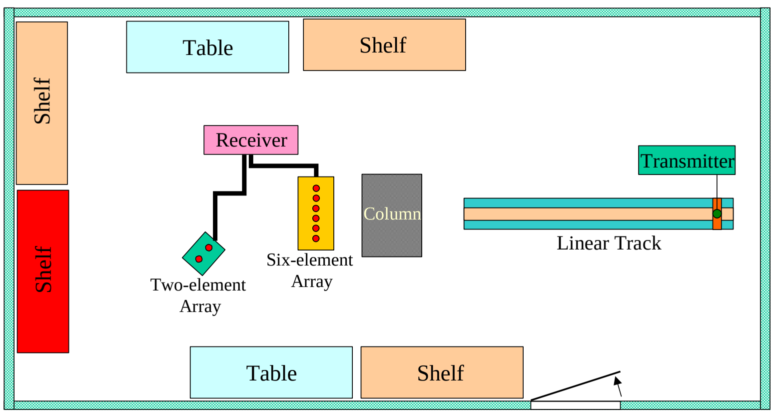

Figure 5.14. Measurement setup for indoor wideband measurements

The transmitted signal was a 2.05 GHz signal with the signal of interest being a tone at 1 KHz. The wideband measurement was implemented by varying the RF carrier in steps of 0.5 MHz and adjusting the local oscillator (LO) signal frequency at the receiver so that the intermediate frequency (IF) signal was always at the designated value of 68 MHz. This allowed for changing the RF carrier over the pass band of the RF front-end bandpass filter without altering the IF filters. The RF carrier frequency was swept from 2045 MHz to 2055 MHz spanning a total spectrum of 10 MHz. For each discrete carrier frequency, the transmitter traversed a distance of 2.5 meters along a prescribed path dictated by the position and orientation of the track. For each complete traversal of the transmitter on the track, signals were collected by all eight receiving antenna elements and the envelope information was stored on the host PC. This collection of data was repeated for all the carrier frequencies and resulted in a database of information from two different antenna arrays for each traversal of the transmitter.

5.4.2.2 Results

The collected data was processed offline to generate fading envelopes as a function of three parameters: antenna elements, distance and frequency. Due to the large volume of the database, it is not possible to display the collected data over the required bandwidth for all eight elements. Figure 5.15 shows a three-dimensional plot of the fading envelope as a function of distance and frequency for antenna element 1. Along the distance dimension, the received signal envelope exhibits the usual fading characteristics that are encountered in an indoor channel. Along the frequency axis for a given location of the transmitter (i.e., for a given value on the distance axis), the envelope is nearly flat showing very little variation in the amplitude. That shows the relative insensitivity of the channel with respect to the spectrum of the signal. This conclusion also holds true for other antenna elements except for element 2. The plot for element 2 is shown in Figure 5.16. The plot reveals some frequency selective fading across the total span of the band. This behavior is unclear at this moment and may be attributed to the components in the RF chain for this antenna element.

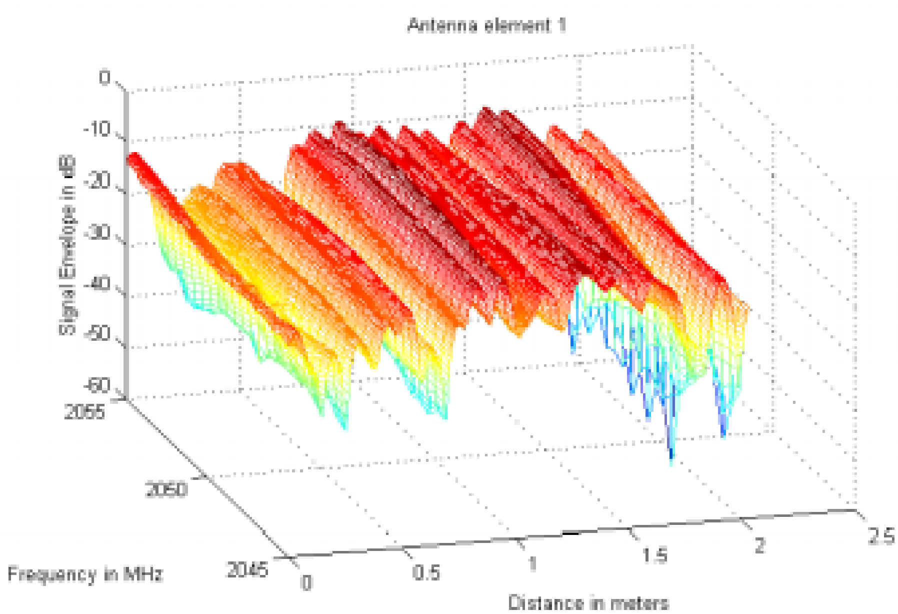

Figure 5.15. Three-Dimensional plot for element 1.

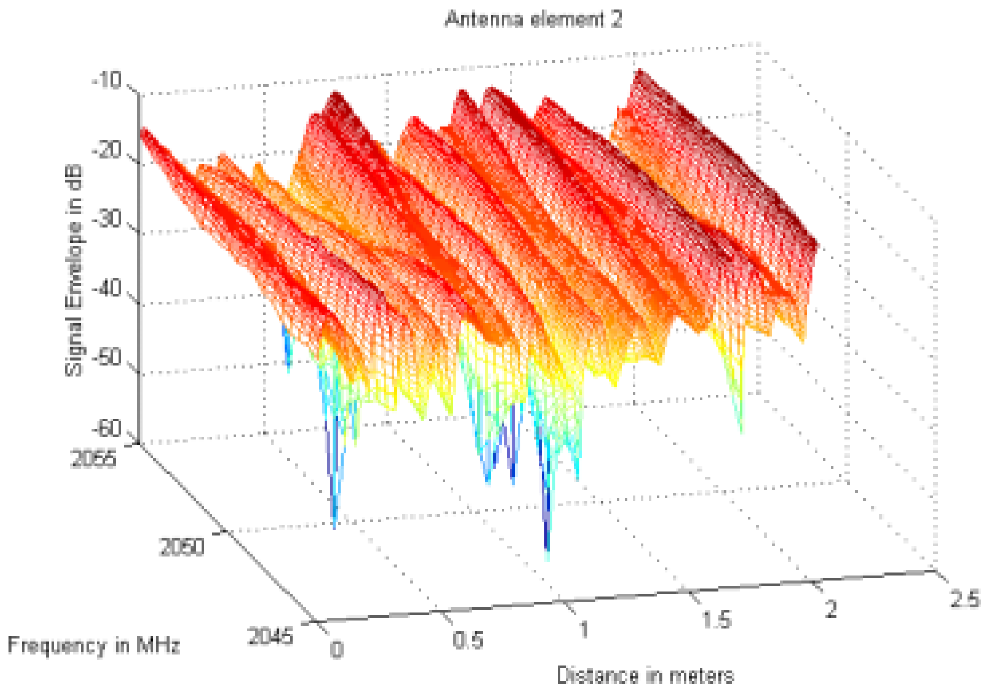

Figure 5.16. Three-Dimensional plot for element 2.

The envelope correlation coefficient was studied for the received signals on different antenna elements. For a specific antenna element, the correlation coefficient was calculated as a function of the frequency separation. This quantifies spectral coherence or the degree of “flatness” of the complete spectrum of the signal and thus indicates the nature and extent of flatness of a flat fading channel. Figure 5.17 shows such a frequency dependent correlation coefficient for all eight elements of the two different arrays.

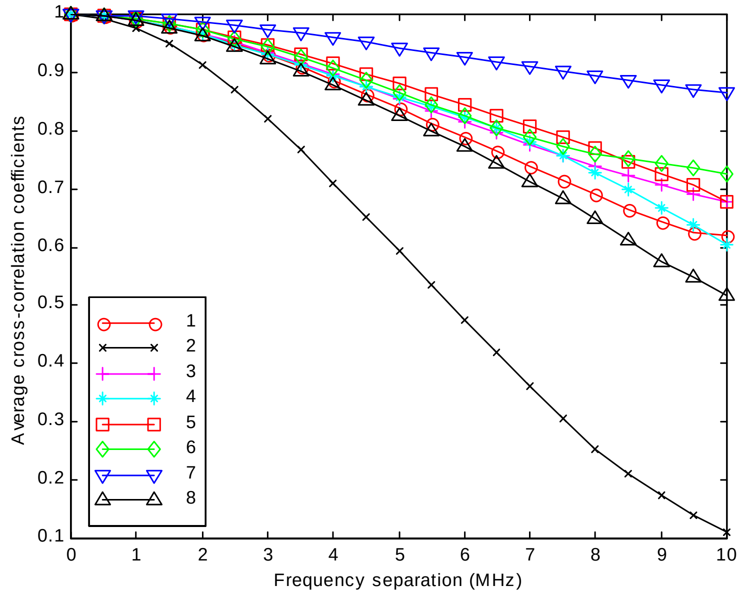

Figure 5.17. Envelope correlation coefficients as a function of frequency for all the elements

From the figure, it can be seen that for all the elements except element 2 of the two-element array, the correlation coefficient decreases only slightly from 1.0 to 0.6. For element two, which is a dipole antenna, the correlation drops noticeably as separation of frequency increases. This behavior, which is different from other elements, may be attributed to the RF chain connected to it because the bandpass RF filter component may have degraded over time. Excluding element two, the correlation curves indicate that the indoor channel provides a flat fading channel over 10 MHz bandwidth. If the coherence bandwidth is defined as the bandwidth over which the envelope cross-correlation is 0.6 or greater, then the value of coherence bandwidth can be found from the plots as presented in Table 5.5 below.

Table 5.5. Coherence bandwidth for different antenna elements

Element number (#)	Coherence Bandwidth (MHz)
1	≈ 10
2	5
3	> 10
4	10
5	> 10
6	> 10
7	> 10
8	≈ 8

Table 5.5 shows that in most elements, the bandwidth is 10 MHz or greater, and this is typical of an indoor channel. Thus conventional diversity combining techniques can be easily applied to existing narrowband systems (i.e., GSM, PHS, and PACS) as well as the proposed wideband W-CDMA systems.

Figure 5.18 shows the correlation curve as a function of frequency between element 1 and other elements. A particular value of correlation coefficient was evaluated at a specific frequency by taking the cross-correlation between the fading envelopes of two elements. All the plots show a low value of correlation across the spectrum of 10 MHz and the amount of change is also small. This shows that the signals on different antenna elements are weakly correlated in the frequency domain, and coupled with the fact that large coherence bandwidth implies very small delay-spread, conventional narrowband diversity techniques can be effectively used on a wideband signal in such an environment.

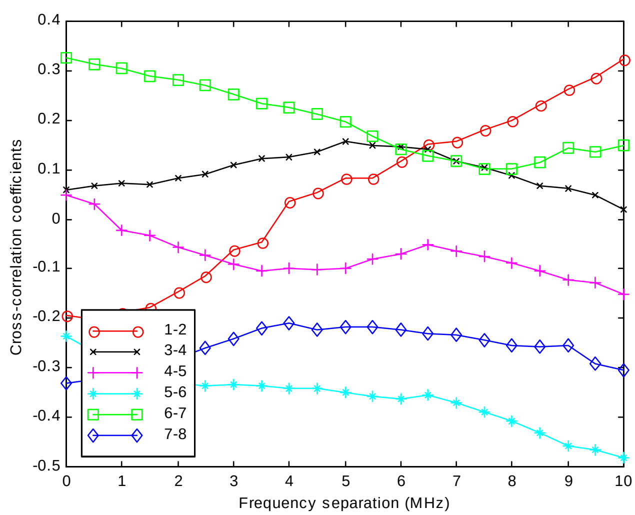

Figure 5.18. Cross-correlation between antenna elements as a function of frequency

5.4.3 Outdoor to Indoor Channel

5.4.3.1 Description

This experiment follows the same general principle as in the indoor measurement case. Here due to difficulty in setup, the receiver is comprised of a single antenna (rather than an array) moving on the linear track. A signal generator located on the roof of Whittemore Hall transmitted a signal with a power of approximately 30 dBm from a vertical dipole antenna. The receiver was located in the MPRG DSP lab in the new engineering building (NEB), which is next to Whittemore Hall (see Figure 5.19). For this experiment, one channel of the receiver was connected to a single vertical monopole antenna that was moved along a 2.8 m linear track.

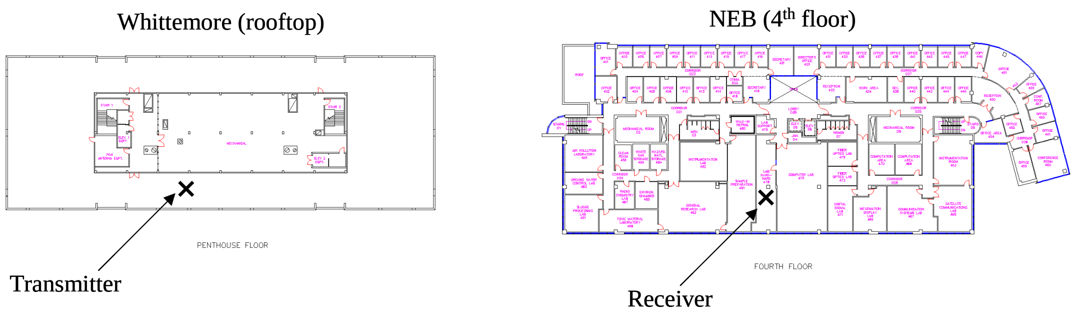

Figure 5.19. The floor plan of the measurement scenario.

The same RF parameters were used as in the indoor case. A total of 10 MHz bandwidth was spanned by performing the measurements at 500 kHz intervals from 2.050 to 2.060 GHz. Each measurement lasted approximately five minutes. The measurement at one frequency was repeated to determine whether the channel varied with time.

5.4.3.2 Results

The approximate coherence bandwidth was determined by calculating the envelope cross-correlation of signal envelopes measured at different frequency offsets. For repeated measurements at a single frequency, the envelope cross-correlation was approximately 0.89, indicating some variability in the channel from one measurement to the next.

Figure 5.20 shows a 3D plot of fading envelopes as a function of frequency offset and receiver displacement on the track. Compared to Figure 5.15, which shows the 3D plot for antenna 1 in indoor case, the spectral variations at a particular location are quite large. A visual inspection of the figure reveals the overall frequency selective nature of the channel.

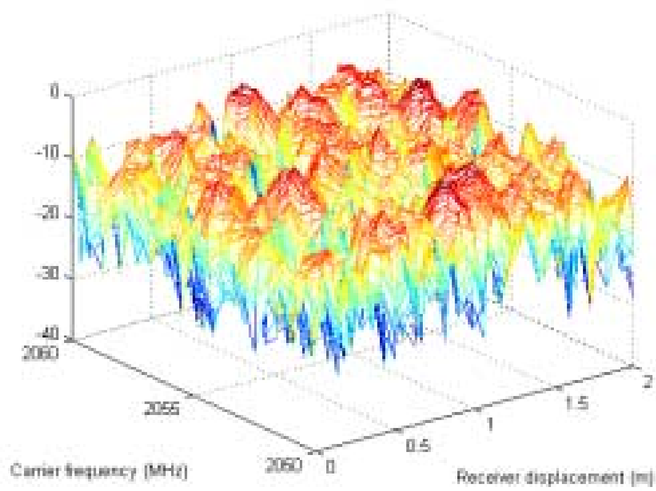

Figure 5.20. 3D plot of signal strength for outdoor-to-indoor channel.

A scatter plot of the cross-correlation values is shown in Figure 5.21. As shown in the figure, for this experiment the coherence bandwidth appears to be between 500 kHz and 1 MHz. The measurements conducted were sufficient to determine that the coherence bandwidth of this channel was much less than the 5 MHz bandwidth planned for W-CDMA of 3G wireless systems. The measured coherence bandwidth exceeds the bandwidth of systems such as GSM, PHS, and PACS. This indicates that narrowband measurements could be used to estimate the diversity or adaptive combining performance of such systems in this channel. Otherwise, some temporal processing (equalization) is needed to remove the spectral distortion arising out of small coherence bandwidth.

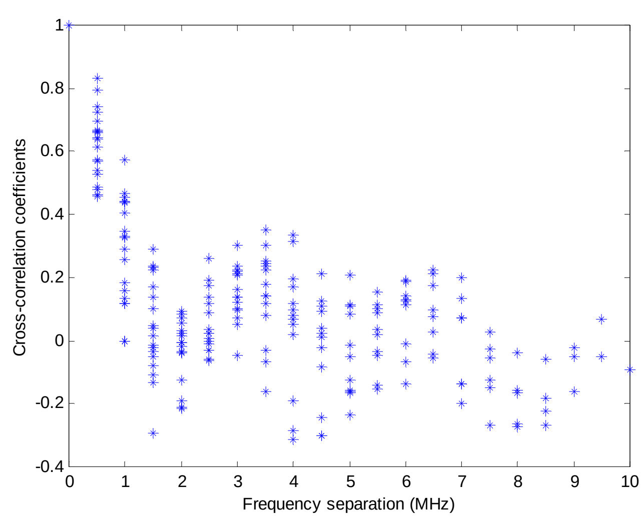

Figure 5.21. Frequency dependent envelope cross-correlation coefficients for outdoor-to-indoor channel.

5.5 Transmit Diversity Measurements for an Indoor environment

5.5.1 Introduction

Measurements have been carried out for a two-element antenna array at the handset and reported here. This section presents narrowband transmit diversity measurements conducted in an indoor environment at a RF carrier of 2.05 GHz. A description of the measurement setup and data collection methodology is presented, followed by post-processing of the data. A discussion of the effect of different diversity schemes implemented on these measured channel envelopes is also presented.

5.5.2 Experimental Setup

The experimental setup was designed to carry out transmit diversity measurements in an indoor environment. A two-element antenna array comprised of monopoles was used at the transmitter. The inter-element spacing was 3/8 RF wavelength where the RF carrier was set at 2.05 GHz with 1 KHz offset. The transmitter was set at one side of the MPRG DSP Lab and receiver on the other as shown in Figure 5.22.

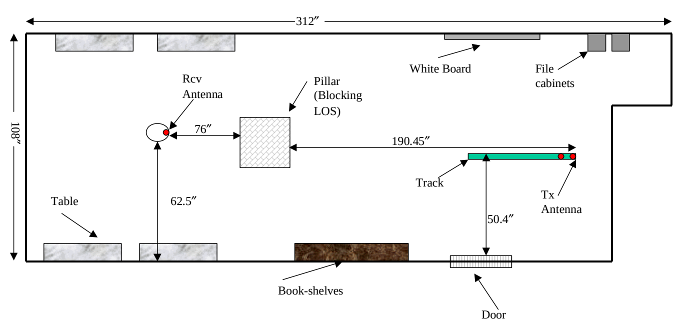

Figure 5.22. Measurement environment.

The antenna array at the transmitter was mounted on a platform on a linear track. The track system helped to realize a controlled experiment where the array traversed a predefined distance for all the test runs. The receiver was setup in such a way that an NLOS fading channel was realized between the transmitter and the receiver. The measurements were taken by starting the platform containing the antenna array from a starting point on the track and collecting data for a certain duration of time. Data was collected by connecting transmitter output port to one element in the array while keeping the other open and moving the array across the track. Several measurements were taken with the same setup to examine the repeatability of the waveforms. Then the transmitter connection was switched to the other element, keeping the former open, and the measurements were repeated. The receiver stored only the magnitude information or the envelope of the complex channel. In essence, the measurements represented indoor vector channel measurements where the receiver was stationary and the transmitter was in motion.

5.5.3 Measurement Parameters

The RF carrier has been set to 2.05 GHz with 1 KHz offset. The receiver collected data at a 100 KHz sampling rate, and the collected samples were decimated by a factor of twenty. Since the measurement setup was limited in storage capacity and to take data over a larger period of time, decimation was performed. This resulted in collecting 30,000 samples within the duration of six seconds. The array moved over the track at 11.5cm/sec and the time required to traverse one wavelength was 1.272 sec. Hence 6000 samples are collected per wavelength, which is sufficiently high since only twenty to thirty samples per wavelength is enough for proper measurement.

5.5.4 Data Collection

As described in Section 5.3.2, two orientations were studied: inline and broadside. The leading element is termed as element 2 while the lagging one is termed element 1 (see Figure 5.23). In either case, only one element of the array was excited at a particular run.

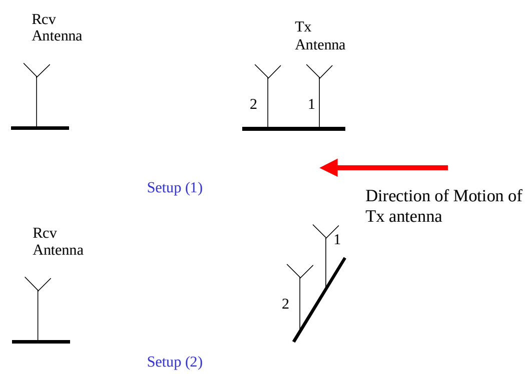

Figure 5.23. Different antenna array setups.

For a particular setup (inline or broadside), two different types of measurements were done: i) one antenna element was excited while the other element was kept open, ii) one antenna element was connected while the other element was removed from the array (only one element being present). Six measurements were taken in each category resulting in a total of twenty-four measurements for a particular setup. The purpose of the six measurements was to remove any undesirable variability that may corrupt or distort a certain measurement. Three measurements were selected out of these six by studying the envelope cross-correlation coefficient (ρ_e) between the recorded waveforms. The selected waveforms had ρ_e value 0.9 or higher as shown in Table 5.6.

Table 5.6. Cross-correlation coefficients of the measured waveforms

Setup	Active Element	Other Element	$\rho_{1,2}$	$\rho_{1,3}$	$\rho_{2,3}$
1	1	Present	0.95	0.97	0.96
	1	Absent	0.98	0.95	0.97
	2	Present	0.99	0.99	0.99
	2	Absent	0.995	0.99	0.99
2	1	Present	0.97	0.91	0.90
	1	Absent	0.98	0.98	0.98
	2	Present	0.94	0.98	0.97
	2	Absent	0.96	0.97	0.99

5.5.5 Results

<u>Inline Measurements</u>

Figures 5.24(a) and 5.24(b) present the average fading envelopes for element 1 and element 2 for an inline motion of the array. Figure 5.24(a) shows the fading channel from element 1 with or without the presence of the second element, and Figure 5.24(b) shows the same from element 2. From the figures, it can be seen that the presence of an open-circuited antenna element acts as a parasitic load on the active element and causes the average level to deviate from the single element case. This may be caused by pattern distortion from the presence of the open-ended second element. The effect of the distortion is different for the two antennas excited separately. When element 1 is active, the effect of element 2 is to reduce the average level.

The receiver is almost in the direction of motion, and element 2, being the leading element, acts as a load to reduce the received power level. On the other hand, when element 2 is active, the presence of element 1 reinforces the average received power level. This has a significant impact on selection transmit diversity operation: when the antenna element providing the best received signal power is selected, the element facing the receiver in an inline orientation will almost be selected (neglecting the body effects).

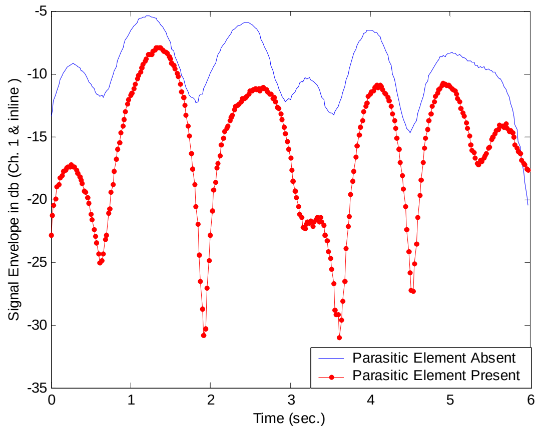

(a) Element 1

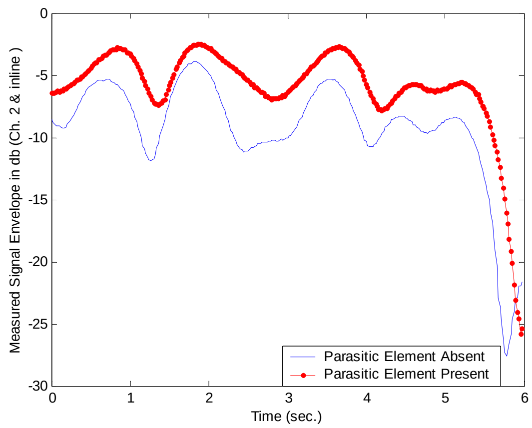

(b) Element 2

Figure 5.24. Average fading envelope for inline motion.

Figure 5.25 shows the average fading envelope vector when both elements are present. The difference in the average level of the two channel measurements is attributed to the pattern distortion effect of the inactive element as discussed before.

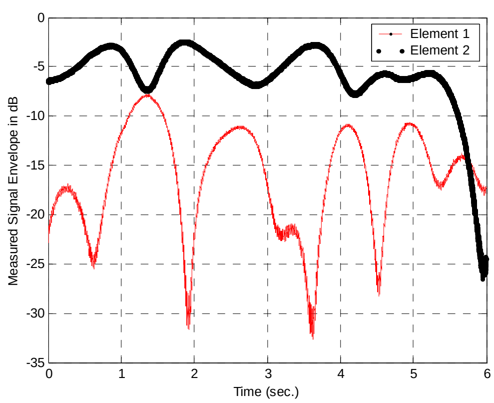

Figure 5.25. Fading envelope measurement for inline orientation.

Broadside Measurements

This section presents the average fading channel envelope for broadside orientation. Figures 5.26 (a) and (b) represent the fading envelopes for channel 1 and channel 2 respectively. The figures reveal that the presence of a parasitic or an inactive element in a broadside orientation has a less prominent effect than in an inline orientation. Element 1 shows more or less the same kind of behavior, but element 2, which was nearer to the wall reveals somewhat different fading characteristics. The average level, in both the cases, is insignificantly affected by the inactive element.

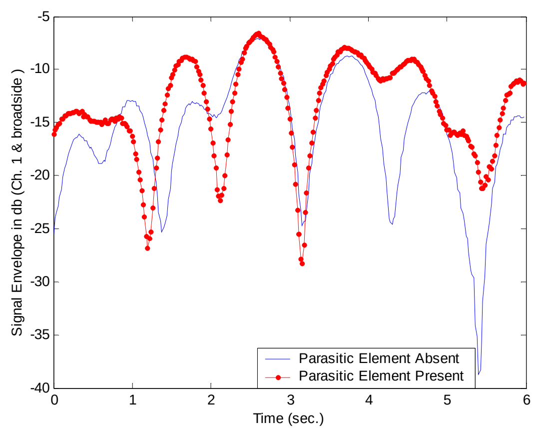

(a) Element 1

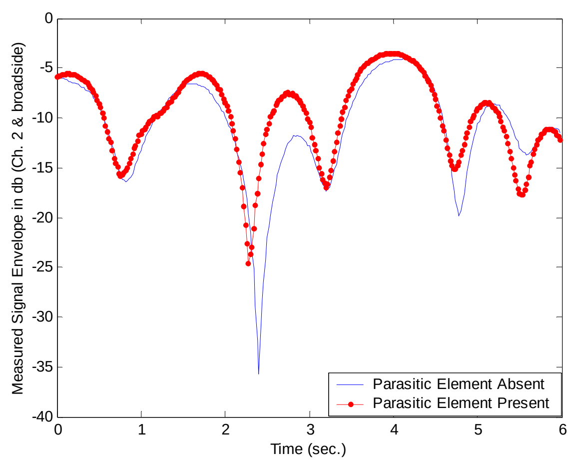

(b) Element 2

Figure 5.26. Average fading envelope for broadside motion.

Figure 5.27 presents the average vector channel measurements when both the elements are present. The difference in the average level of the received signals is much smaller than in the inline case.

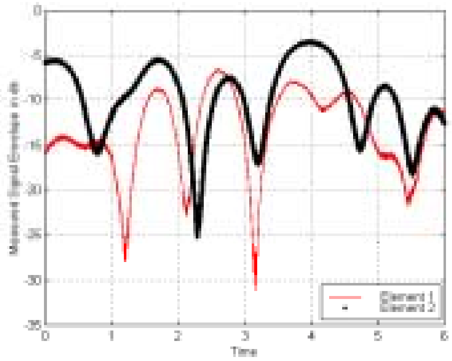

Figure 5.27. Vector channel measurement for broadside orientation.

The received envelope in both inline and broadside measurement can be explained with reference to the pattern measurement [DIE01] of an individual element as shown in Figure 5.28 (repeated here from Figure 5.13c).

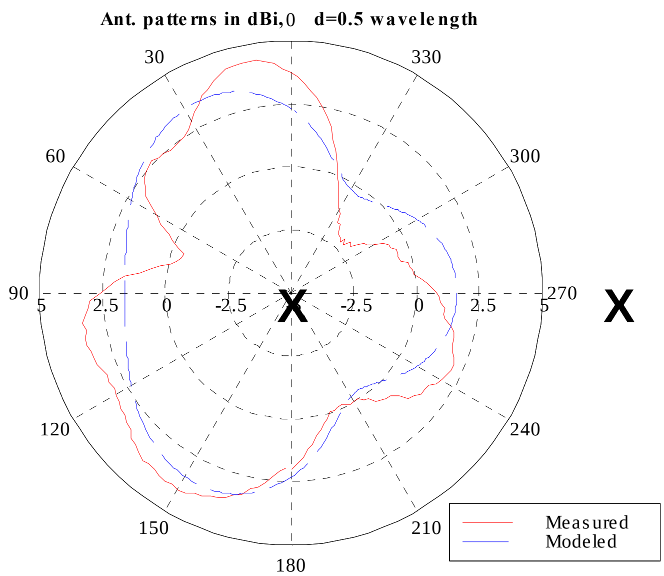

Figure 5.28 Individual pattern measurement [DIE01].

Figure 5.28 is the radiation of a dipole antenna element, and it is assumed that the same general pattern would hold for a monopole on the ground plane. The plot indicates the pattern distortion on an element resulting from the presence of another element at a distance of 0.5λ. The pattern would be otherwise isotropic if there were no closely spaced antenna element. The resulting pattern distortion in turn would affect propagation characteristics and consequently diversity performance of an antenna array. The effect of pattern distortion on the diversity performance of the two-element array placed in an inline orientation can be described with reference to Figure 5.29.

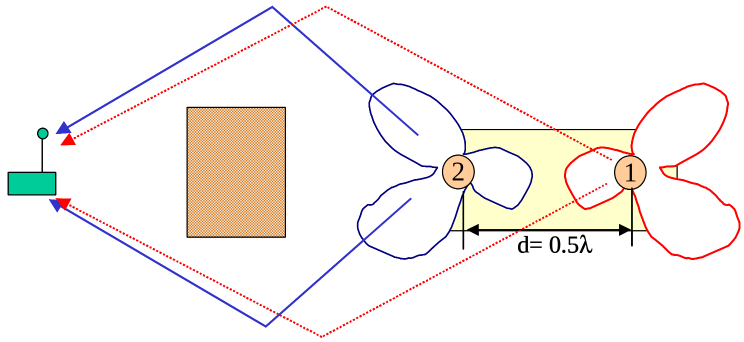

Figure 5.29 Signal propagation from each element with pattern distortion for inline orientation

Figure 5.29 shows the antenna array in an inline orientation with a rough sketch of radiation patterns around the individual elements. The figure also shows the placement of the receiver behind the column that is blocking LOS propagation. The signal is propagated by reflecting off the local scatterers. Signal propagation with respect to the radiation pattern of the elements show that element 2 has a larger gain in the direction of the receiver than element 1. Thus measurement of signal strength will reveal that element 2 provides a signal level that has a higher mean level than that does element 1. This is verified by the recorded waveforms as shown in Figures 5.24 and 5.25.

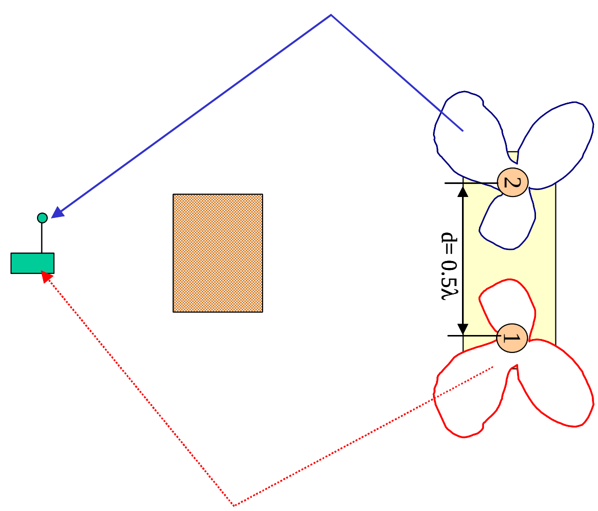

Figure 5.30 Signal propagation from each element with pattern distortion for broadside orientation

Figure 5.30 shows the antenna array in broadside orientation with the resultant radiation pattern from the individual elements. From the figure, it can be seen that now both elements have close gains from the radiation patterns and mainly the local scatterers in the environment dominate the channel gains in individual paths. Thus it is expected that the difference in received signal strength for each element will not be as diverse as in the inline case. This is also verified in Figures 5.26 and 5.27.

Table 5.7 summarizes the vector channel measurements in terms of the cross-correlation coefficient and average received signal power. For an inline orientation, the value of ρ_e between the two elements is around 0.28, which is much smaller than the value predicted by classical theory. The difference in mean received signal strength is about 10 dB. The value of ρ_e for broadside motion is about 0.5 and the difference in received signal strength is less than 4 dB.

Table 5.7. Summary of measurements

Setup	Envelope Cross-Correlation	Mean Power, Element 1 (dB)	Mean Power, Element 2 (dB)
Inline	0.28	-16.16	-5.99
Broadside	0.49	-9.78	-13.48

5.5.6 Diversity Gain

The measured fading envelopes can be processed for diversity implementation. Figure 5.31 shows the schematic setup that is intended for a transmit diversity operation.

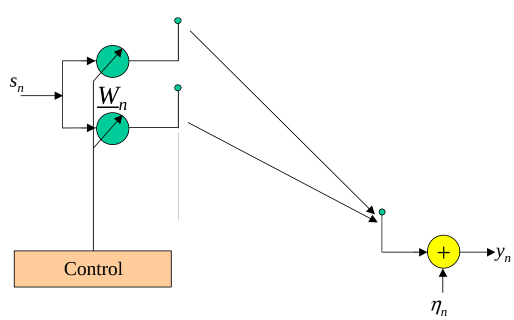

Figure 5.31. Transmit diversity implementation.

In the setup above, the received signal e_0 can be expressed in terms of input signal e_i as

$$e_o = (w_1 g_1 + w_2 g_2) e_i \tag{5.2}$$

where, g_1 and g_2 represent individual complex channel gains (from element 1 and 2) and w_1 and w_2 constitute the weight or scaling vector at the transmitter. Channel measurements as described in the previous sections could substitute for the channel gains (g_1 and g_2), and it is assumed that these measurements are available at the transmitter. It is also assumed that the signal at the transmitter is unity power signal, i.e., $|e_i|^2 = 1$.

In this section, the diversity gain that can be obtained from transmit diversity operation will be assessed with the measurements of the waveforms. This computation of diversity gain incorporates the underlying assumption of perfect channel knowledge and instantaneous feedback from the receiver. This indicates the ideal transmit diversity gain that is possible for a narrowband system. Three diversity schemes are studied here: selection, equal gain and maximal ratio. The necessary formulations for the three schemes are presented below.

1) *Selection*: The received power in this case is

$$|e_o|^2 = |g_1|^2 \ or \ |g_2|^2 \tag{5.3}$$

2) *Equal gain combining*: The weight vector **w** =[w_1 w_2] is so chosen that the transmitted signals are co-phased at the receiver and **w** is normalized to unity. The received power can be expressed as

$$|e_o|^2 = \frac{1}{2}\left[|g_1| + |g_2|\right]^2 \tag{5.4}$$

3) *Maximal Ratio*: In this case the weight vector is chosen as the complex conjugate of the channel gain. The received signal power then becomes

$$|e_o|^2 = |g_1|^2 + |g_2|^2 \tag{5.5}$$

Using the above expressions for diversity operation, the received waveforms have been generated for different diversity schemes at the transmitter. The diversity gain achieved from different schemes is assessed in terms of CDF of the received power level. The CDF plots for inline and broadside orientation are shown in Figures 5.32 and 5.33.

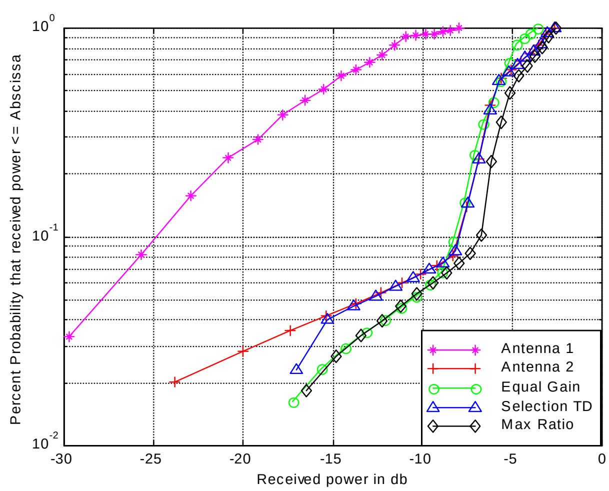

Figure 5.32. CDF plot for inline orientation.

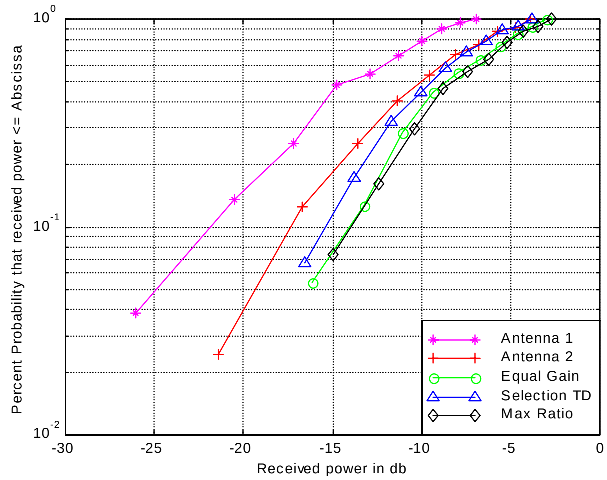

Figure 5.33. CDF plot for broadside orientation.

For inline orientation, the combined received signal is almost always the stronger signal (element 2) for the selection diversity scheme because of the difference in the mean level of the channel envelopes. The diversity gain mainly stems from the stronger channel envelope. For broadside orientation, the difference between the mean received powers from the two elements is reduced and the diversity gain is higher than the inline orientation. The diversity gain with the maximal ratio scheme for the measured waveforms is computed with respect to both channels at a CDF level of 10% is presented in Table 5.8.

Table 5.8. Diversity Gains for different orientations

Orientation	Diversity gain from element 1(dB)	Diversity gain from element 2 (dB)
Inline	18	1
Broadside	7.8	3.3

The results in Table 5.8 show the effect of unbalance in mean signal power between different antenna elements on the achievable diversity gain from the measurement system. In inline orientation, this unbalance is about 10 dB (see Table 5.5), and thus a single antenna system based on the stronger element (element 2 in this case) is as good as the diversity system. In broadside orientation, the unbalance is much smaller (about 4 dB) and the diversity output is better than the best single antenna system (element 2 in this case) by a larger margin than for inline orientation. The power unbalance is mainly caused by array orientation, individual antenna pattern, and pattern distortion resulting from the effect of mutual coupling. Note that the diversity measurements are limited to the azimuth plane only and are based on perfect and instantaneous feedback from the receiver.

5.6 Conclusions

This chapter presented diversity measurements for a mobile terminal in an indoor environment. The measurements were carried out to address three basic propagation related issues: i) channel reciprocity at the mobile terminal, ii) effect of antenna spacing on signal correlation, and iii) wideband diversity measurements. Channel reciprocity was verified for a single antenna system and subsequently, for an antenna array system. Fading envelopes were generated and recorded by moving a single antenna system on a linear track. The diversity performances based on the measurements show that both receive and transmit diversity systems exhibit similar behavior. Thus, an existing receive diversity system can be employed to infer the performance of a similar transmit diversity system without building new systems and designing new experiments.

The effect of inter-element spacing on the mutual coupling behavior was measured for a mobile terminal. The inter-element spacing was varied and fading envelopes were recorded for two different orientations of the handset. Measurements show that at 0.1λ spacing, the correlation is 0.64 for inline orientation and for broadside orientation, this value is 0.16 at the same spacing. For inline orientation, the value of correlation increased from 0.41 to 0.64 and diversity gain (selection) decreased from 10 to 2 as spacing was decreased from 0.5λ to 0.1λ. For the broadside case, both correlation and diversity gain were relatively insensitive to variation in spacing. The impact of element spacing on the average receive SNR from some of the proposed transmit diversity techniques was studied. Low values of correlation coefficients indicate that the elements can be tightly spaced at the handset without significantly degrading diversity performance. This would allow implementation of diversity operation efficiently at the SWT without widely spaced arrays.

The wideband measurement was performed by adjusting the RF carrier frequency to span a total bandwidth of 10 MHz while keeping the IF signal frequency at a fixed value. Two different environments, indoor and outdoor-to-indoor, were investigated. For the indoor channel, a mobile transmitter was employed and the received signal was collected with two different antenna array subsystems. For the outdoor channel, the transmitter location was fixed and data was collected by a single antenna receiver moving on the track. During the course of the measurements, only the envelope information of the received signals was stored. The signals collected over all the different elements reveal the relative flat fading nature of the indoor channel. The coherence bandwidth was found to be about 10 MHz. Such a large coherence bandwidth for an indoor channel suggests that conventional diversity combining schemes may still be useful as such a channel minimally affects the temporal features of the signals. Outdoor-to-indoor measurements showed that the channel possesses some frequency selective characteristics. Coherence bandwidth was between 0.5MHz and 1 MHz for this channel. It can be concluded that conventional diversity schemes still apply for existing narrowband systems but may not apply for the proposed W-CDMA system.

A direct measurement of narrowband transmit diversity at the mobile terminal. Fading envelopes have been measured for two different orientations of the transmitter array. The presence of an adjacent element in the array is found to produce a difference in mean received power level and is mainly attributed to the pattern distortion effect. The inline orientation of the transmitter array is sensitive to this distortion effect. This in turn affects the diversity performance. The broadside orientation has been found to be relatively insensitive to this effect.

Chapter 6

Hardware Demonstration of Transmit Diversity

6.1 Introduction

This chapter presents hardware implementations of both narrowband and wideband diversity systems. These implementations provide direct and practical assessments of performance of a given diversity system. Diversity performance can be predicted from simulations or can be estimated indirectly from vector channel measurements, but a hardware implementation provides the actual performance that is achieved by a system in a given environment. This chapter presents the implementation of a narrowband transmit diversity system first, followed by the same for a wideband system.

6.2 Narrowband Transmit Diversity Implementation

6.2.1 Introduction

A narrowband transmit diversity system has been implemented and demonstrated for an indoor channel. The demonstration was developed and tested in the MPRG DSP lab. Later on, the implementation was demonstrated at the 1999 MPRG/Virginia Tech Symposium on Wireless Personal Communications. The performance demonstration involved transmitting an audio signal (playback from an audio tape) through the transmit diversity system and observing the quality at the output of a single antenna receiver.

6.2.2 Measurement Setup

A two-element antenna array was used as the transmitter array and a single element system as the receiving system (see Figure 6.1). The diversity system operated on a simple switching algorithm where only one antenna was transmitting at any given instant. The receiver measured the signal power from the elements and provided the antenna selection message through a wired feedback channel.

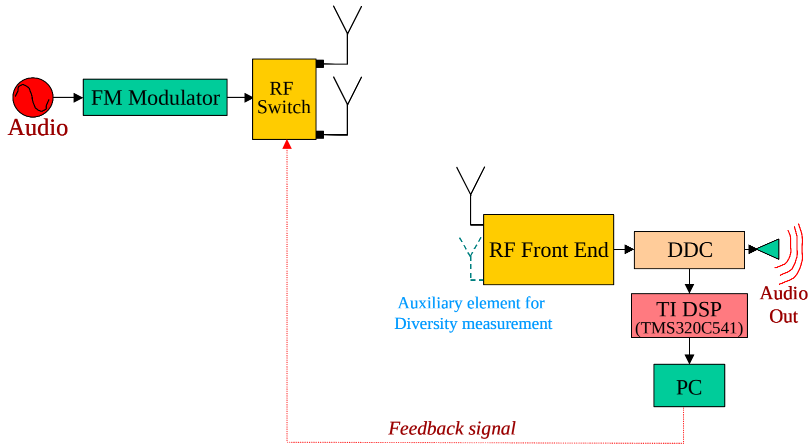

Figure 6.1. Demonstration setup for narrowband transmit diversity.

The transmitter section consisted of an audio source, an FM modulator, and a RF switch. The audio signal was modulated in FM, and the modulated RF carrier of 2.05 GHz was provided to the RF switch. The RF switch connected the modulated signal to either of the antenna elements depending upon the feedback signal from the receiver.

The receiver system consisted of an RF front end and a digital downconverter (DDC). The DDC had an on-board FM demodulator that was used to demodulate the received signal. The received signal was collected in blocks of N symbols by a DSP (TI TMS320C541) and was transferred to the host PC. A switching algorithm, implemented on Matlab platform, processed the data. The algorithm measured the signal power of a block of N received signal samples and computed the average as E_{avg}. The average was compared to a preset threshold E_{th} and a switching command was issued accordingly. The threshold was estimated by observing the average signal strength below which the audio quality was considered unacceptable. The algorithm is explained as follows.

Switch to any arbitrary antenna element.

If ($E_{avg} < E_{th}$) *then*

    switch to the next element

else

    continue with the current active element.

End.

The feedback system was implemented by running a cable from the parallel port of the host PC to an RF switch. The feedback signal was two different voltage levels that corresponded to the switching voltages of the RF switch.

6.2.3 Discussions

In this set up, the audio quality of the received signal provided a qualitative assessment of the diversity system. The locations of the transmitter and the receiver were varied and both direct LOS and NLOS propagation were studied. For a slowly varying channel (moving the receiver antenna at a slow walking pace), the diversity system almost always provided better performance than a single element system. This was also verified by looking at the received signal strengths that were higher due to diversity operation. But as the relative motion between the transmitter and the receiver was increased, the diversity performance decreased because the receiver, in collecting the data and running the algorithm, was not able to keep up with the dynamic nature of the channel. The time coherence of the channel was not long enough to permit reliable diversity operation at high relative motion.

The RF switching at the transmitter introduces phase discontinuity of the modulated audio signal, and this is translated in the receiver output signal as a clicking sound. This switching effect needs to be minimized as it causes a major source of disturbance in an audio application. The threshold level and the block size of data along with the mobile speed determine the switching frequency. These parameters need to be dynamically optimized to reduce the amount of switching and provide a performance improvement.

6.3 Wideband Transmit Diversity Implementation

6.3.1 Introduction

This section presents a hardware demonstration of transmit diversity at the mobile terminal in an indoor channel. The bandwidth of signal transmission was 5 MHz, which is similar to the one proposed for W-CDMA. A closed-loop transmit diversity technique based on simple phase scanning between the antenna elements was implemented.

6.3.2 Overview of Phase Scanning Technique

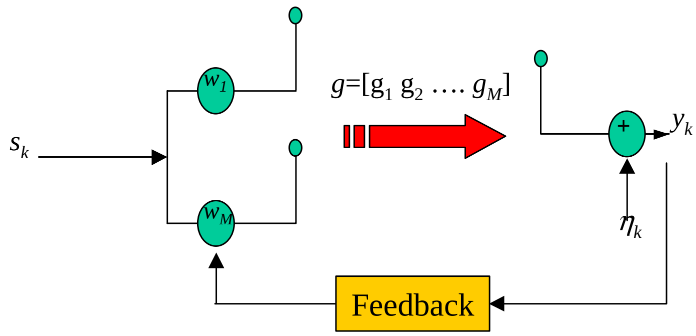

Figure 6.2. Block diagram of a transmitter diversity system

The phase scanning technique can be described with reference to Figure 6.2. A flat fading channel is assumed. The received signal can be expressed as

$$y_n = [w_1 |g_1| e^{j\theta_1} + w_2 |g_2| e^{j\theta_2}] s_n + \eta_n , \tag{6.1}$$

where, the symbols have the usual conventions (presented earlier in Chapter 2). When equal gain weights are used at the transmitter, an overall gain G can be expressed as

$$G = [|g_1| + |g_2| e^{j(\theta - \Delta\phi)}] e^{j\theta_1} , \tag{6.2}$$

where, $\theta = \theta_2 - \theta_1$ and $\Delta\phi$ is the phase difference or phase setting of the weight vector. The gain, G, is seen to be maximized when the phase setting at the transmitter is equal to the phase difference of the channel gain vector. One way to estimate this phase difference is to employ a simple *phase scanning* technique. Considering a two-element array at the transmitter, the transmitter fixes the gain of the weights and adjusts the phase of one weight while keeping the phase of the other weight constant. The phase adjustment occurs in discrete steps of $\Delta\varphi$, where $\Delta\varphi$ denotes the step-size of a uniform phase quantization between 0 and 2π. This results in a quantized search in the phase space where the granularity is defined by the step size.

The receiver measures the power level for each discrete phase setting and identifies the setting with the maximum power and its associated index. This index is then fed back to the transmitter. The transmitter then selects this phase index and keeps it for data transmission before resuming a fresh search. This periodic search helps to track channel variation. Reliable power or SNR estimate is important for this technique. The presence of noise and interference may degrade power estimate and thus may degrade the performance of the diversity scheme.

6.3.3 Measurement Setup

The setup for the hardware demonstration is shown in Figure 6.3. The figure shows different components associated with the setup: the transmitter, antenna array, receiver, and feedback system.

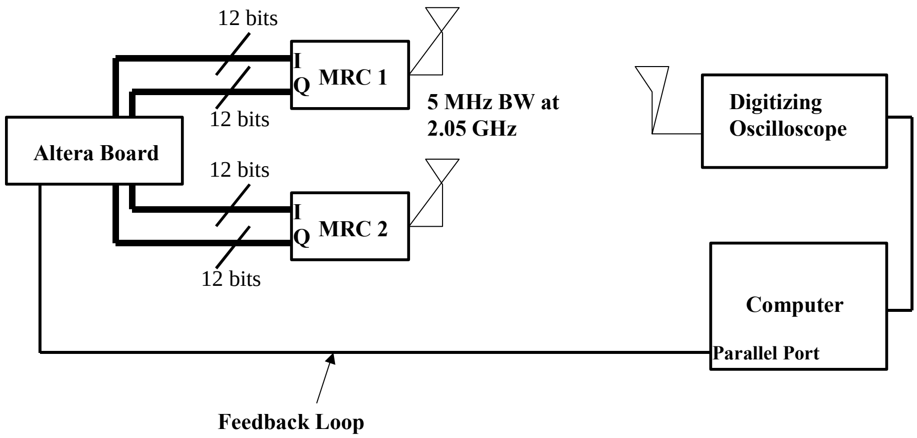

Figure 6.3. Setup for hardware demonstration

Transmitter setup

The transmitter setup includes a data generation module and an RF front-end to support array operation. The data generation module is based on an complex programmable logic device (CPLD) board based on Altera 10K. Miniature Radio Codecs (MRC) from Rockwell-Collins were used as the RF front-ends. The Altera board interfaces to the digital to analog converters on the MRC modules. It provides a 12-bit I and Q word to each MRC radio. The MRCs take these digital words and convert them to a corresponding RF signal with BPSK modulation centered at a 2.05 GHz with a bandwidth of 5 MHz.

The transmitter sends an initial set of training symbols each with different antenna weights as depicted in Figure 6.4. For the first eight symbols, the weight on antenna 1 is held constant (at W_{11}) while the phase on the second element is varied in increments of 45° (e.g. W_{21},W_{22}, ...W_{28}) while maintaining the same amplitude as antenna 1. The set of *I* and *Q* levels that are used for each antenna element is shown in Figure 6.4. Table 6.1 lists the values of both antenna weights that are used when transmitting the training symbols.

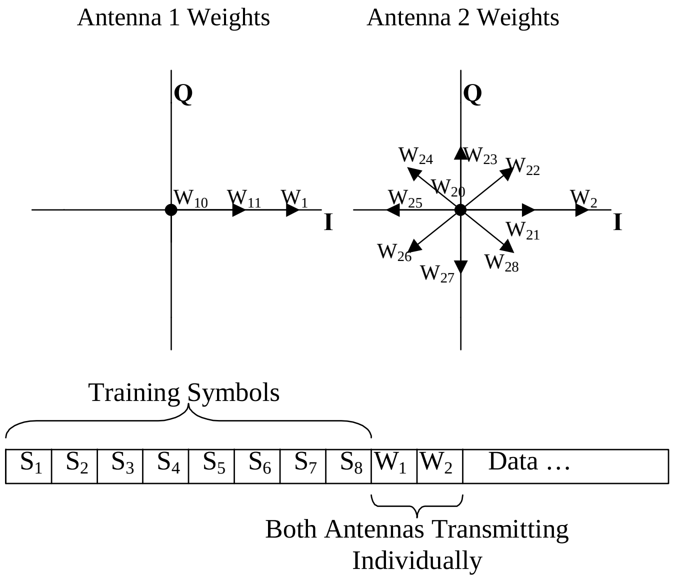

Figure 6.4. Constellation diagram of the weights applied to the individual antenna elements as well as the training symbol protocol used with the transmit diversity testbed.

Table 6.1. Antenna weights that were used for each of the training symbols

Symbol	**Weight on Antenna 1**	**Weight on Antenna 2**
S_1	W_{11}	W_{21}
S_2	W_{11}	W_{22}
S_3	W_{11}	W_{23}
S_4	W_{11}	W_{24}
S_5	W_{11}	W_{25}
S_6	W_{11}	W_{26}
S_7	W_{11}	W_{27}
S_8	W_{11}	W_{28}
W_1	W_1	W_{20}
W_2	W_{10}	W_2

The 9th symbol corresponds to the event with just the first antenna transmitting (w_1= W_1, w_2= W_{20}=0) and the 10th symbol is transmitted with just the second antenna on (w_1= W_{10}= 0, w_2= W_2). The 9th and 10th symbol are transmitted to compare the performance of a single element antenna to the two-element transmit array configuration. In order to make a fair comparison between a single antenna system and one that uses a two-element phase scanning system both systems are calibrated to transmit with equal power. This results in

$$|W_{11}| = |W_{21}| = \cdots\cdots = |W_{28}| = \frac{1}{\sqrt{2}}; |W_1| = |W_2| = 1$$

Receiver Setup

The Vector ImPulsE Response (VIPER) measurement system was used as the receiver. The system consisted of an oscilloscope and a PC. The multi-channel receiver consists of multiple RF/IF front ends driving a multi-channel analog-to-digital converter (ADC). A four-channel high-bandwidth oscilloscope serves as the high-speed ADC and memory storage device. The PC controls the system as well as stores the received signal data. The VIPER receiver is capable of receiving signals up to 400 MHz in bandwidth and processing these signals in software.

For the transmit diversity experiment, only a single channel of the VIPER receiver was used. Data was collected over all training symbols and the PC was used to evaluate the transmit antenna weight combination that produced the highest received signal-to-noise ratio at the receiver. The receiver displays instantaneous received signal power and generates plots of the cumulative distribution function (CDF) values. The plots display the instantaneous performance of the diversity system compared to a single-antenna system. As stated earlier, the single-antenna system transmits with twice the power as the individual elements of the two-antenna transmit diversity system to obtain fair comparisons.

Feedback System

The feedback system is comprised of a parallel port cable connection from the PC to the Altera board. The weight combination that produces that highest received SNR is sent back to the transmitter.

The receiver controls the phase stepping at the transmitter by sending appropriate control words to the CPLD board. Upon receiving the control word, the transmitter transmits with the proper weight combination for that control word. The receiver has a wait period of about 0.5 seconds to ensure that the transmitter has received the feedback signal and has started with the new weight vector. This helps the receiver resolve the weight vector and the corresponding received power. This process is iterated until the transmitter has stepped through all the phase settings. Once phase scanning is complete, the transmitter transmits on one antenna at a time to compare phase scanning technique with a single-antenna operation. After single-antenna performances are measured, the transmitter reverts back to transmission with training sequence and the cycle starts all over again.

The receiver examines the received signal-to-noise ratio of the first eight transmitted symbols and transmits the value of the symbol that is received with the highest SNR back to the transmitter through the feedback loop. The transmitter receives the optimal phase index and uses the appropriate weight combination to transmit the data through the channel.

6.3.4 Environment Description

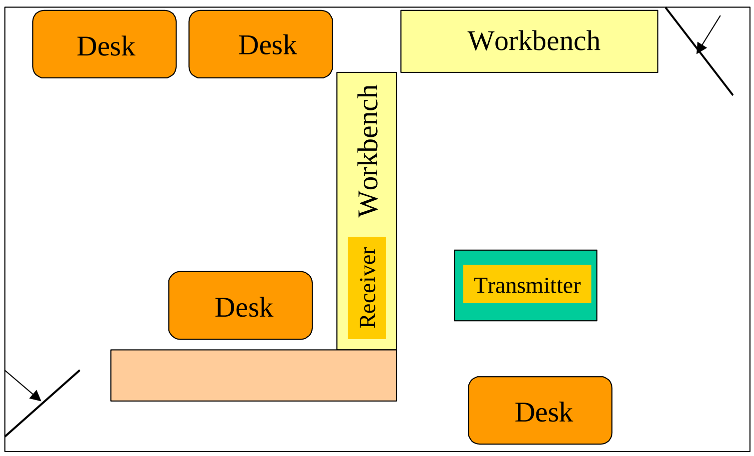

Figure 6.5. Demonstration environment

Figure 6.5 shows the indoor environment in which the demonstration was performed. The whole system was set up in room 618 of Whittemore Hall at Virginia Tech. The transmitter was set so that there was a line of sight (LOS) with the receiver. The channel provided a direct path as well as different multipaths bouncing off the walls, metallic objects, and other sources of scattering. The transmitter/receiver separation was about six feet. Figure 6.6(a) shows the transmitter hardware and 6.6(b) shows the complete setup.

(a) Transmitter hardware

(b) Complete setup

Figure 6.6 Pictures of measurement setup.

Measurement was also carried in a different indoor environment. This system was demonstrated in a big hall room with people moving around. This resulted in an indoor channel that provided some fading along with NLOS propagation.

6.3.5 Results

Power measurements were taken on the received signal for both the diversity system and single-antenna systems and CDF plots were generated from these measurements. Figure 6.7 shows the instantaneous received power plots and the corresponding CDF plots for a particular setting of the measurement system.

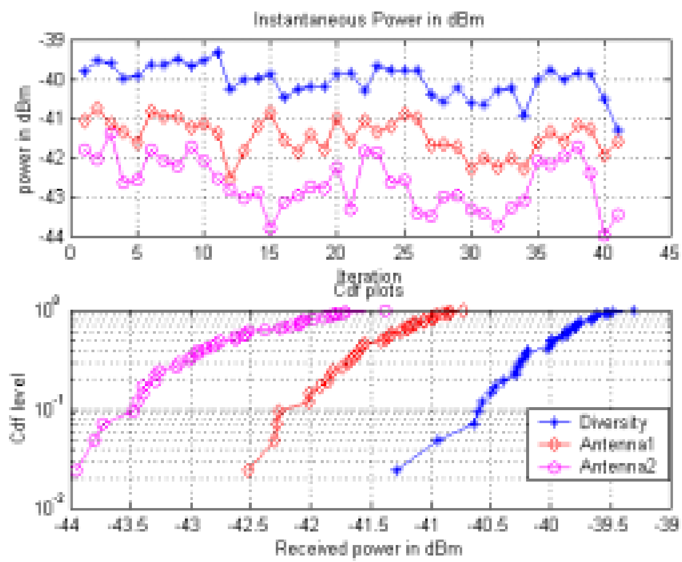

Figure 6.7. Instantaneous power plots and CDF plot for one data collection

Figure 6.7 shows that the diversity system provides better instantaneous performance than either of the two single-antenna systems. The received power goes through small-scale changes due to the lack of a strict static channel. The CDF plot reveals that the diversity system is also better in a statistical sense. At 10% outage level, the diversity system provides close to 2 dB of gain with respect to antenna 1 and about 3 dB of gain with respect to antenna 1.

Measurements were repeated by changing the location of the transmitter within a small area and by collecting data at each location. The received data was aggregated over several such repetitions. The mean and the standard deviation of aggregated data are presented in Table 6.2. From Table 6.2, the diversity system on the average provides a gain of 1 dB and 2 dB compared to antenna 2 and antenna 1, respectively. The small improvement is due to the fact that the measurements were carried out in LOS conditions where diversity gains tend to be small. NLOS environments were also studied, but the power amplifier of the transmitter was not strong enough to overcome propagation losses caused by blocking.

Table 6.2. Diversity gain from phase scanning technique

Transmission Scheme	**Mean Received power (dB)**	**Std. Dev. of Power (dB)**
Phase Scanning	-37.3	-40.5
Antenna 1	-39.2	-42.1
Antenna 2	-38.6	-40.4

The composite CDF plot from the aggregated data is shown in Figure 6.8. At the 1% outage level, the gain from the diversity system is about 2 dB compared to antenna 1 and about 6 dB compared to antenna 2 because although antenna 2 has higher average signal value than antenna 1 most of the time, it encountered some deep fades relative to antenna 1. This is reflected in the tails of the CDF curve.

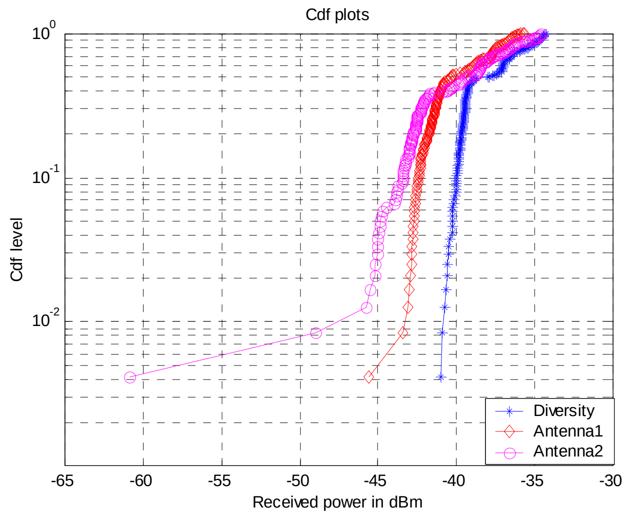

Figure 6.8. CDF plot of the aggregate data

A second set of measurements were taken in the second environment in the large hall room. The experiments were carried out for a relatively large number of iterations (> 120) to study the diversity gain. Figure 6.9 shows the diversity performance at a particular transmitter location.

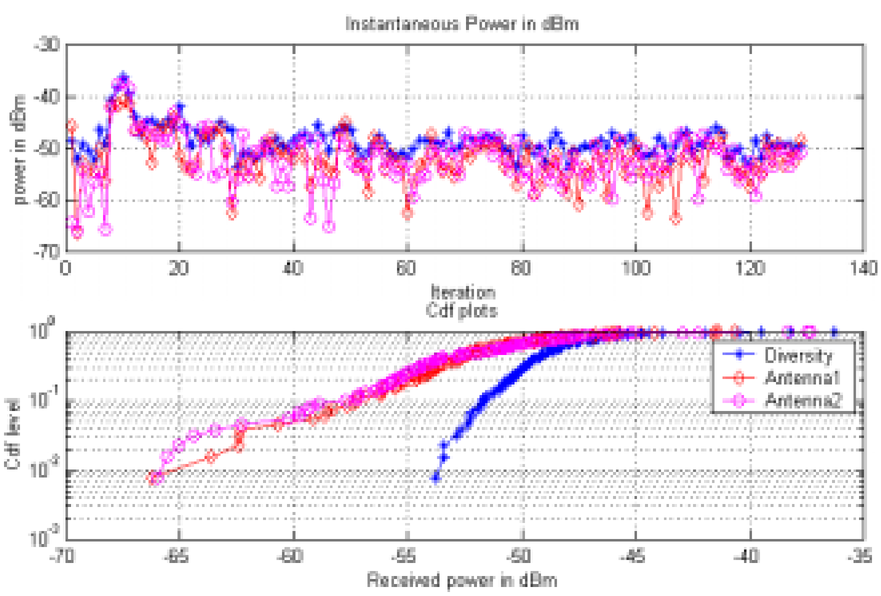

Figure 6.9. CDF plot of the aggregate data

The plots in Figure 6.9 reveal that the instantaneous behavior of the diversity may degrade at times, but the diversity system is better than either system in a fading environment from a statistical sense. At the 1% outage level, the diversity system provides a gain of more than 10 dB. However, it should be mentioned that, to assess the performance in a fading channel, a longer collect time and a large amount of data is required.

6.4 Conclusions

This chapter presented both narrowband and wideband transmit diversity implementations and demonstration carried out at Virginia Tech. The narrowband implementation provided a qualitative assessment of a transmit diversity system. The diversity system was based on a switched combining technique. The system was observed to offer better performance than a single-element system for a slow varying indoor fading channel.

For wideband implementation, a testbed was designed to provide a signal bandwidth of 5 MHz that was comparable to the W-CDMA standard. Measurements have been carried out in indoor environments. Results reveal that the transmit diversity system is better than the single-antenna system. For an LOS channel, the gain is at least about 2 dB at the 1% outage level compared to the best single-antenna case. Experiments also revealed a substantial gain when compared to a single-antenna system for an indoor channel with NLOS propagation and fading.

Chapter 7

MIMO Systems for flat fading and frequency-selective channel

This chapter provides an extension of the proposed TD techniques in Chapters 3 and 4 to a communications system that uses antenna array at both ends of the link. Using antenna arrays at transmitter and receiver generate a multiple-input-multiple-output (MIMO) system. Recently, MIMO systems are gaining popularity among researchers for their promise of enhanced receive SNR and throughput [FOS98]. The first part of the chapter presents proposed MIMO techniques for a flat-fading channel while the remainder is devoted to extension of DSNR solution (eq. 4.11, Chapter 4) to MIMO systems.

7.1 Flat fading channel

7.1.1 Introduction

This section proposes and evaluates a simple MIMO algorithm to enhance SNR at a handheld wireless device. The proposed algorithm combines classical phase scanning technique at the transmitter array with maximal ratio combining (MRC) at the receiver array. The operating environment is assumed to be indoor channels that experience flat fading. A 2×2 system is assumed in the study but an extension to a higher-order system is possible. The salient features of the proposed algorithm are: 1) minimal processing burden at both the transmitter and the receiver, 2) nominal feedback payload, and 3) novel combination of simple and proven techniques at both ends of the link for SNR enhancement.

7.1.2 Principle

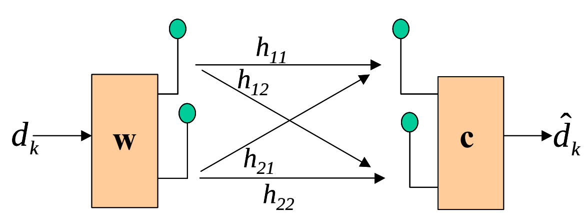

Figure 7.1. Setup for the proposed MIMO technique.

Figure 7.1 presents the setup for the proposed algorithm. The transmitter employs phase scanning technique by changing the phase of the individual elements in the weight vector, $\mathbf{w}$, for successive symbols. The transmitted symbols are scaled by the channel matrix, $\mathbf{H} = \{h_{ij}\}; i, j \in \{1, 2\}$, and combined linearly by $\mathbf{v}$ to generate received signals at each antenna element at the receiver. The magnitudes of the individual channel gains h_{ij} (*i*th transmit antenna to *j*th receive antenna) are assumed to be i.i.d. Rayleigh distributed and moreover, there is negligible signal correlation between antenna elements at both ends of the link. The wireless channel is assumed to be flat fading and quasi-stationary with time coherence that ensures proper closed loop operation. The receiver combines the signals in the different branches in a MRC fashion. It then stores the combined outputs for different weight vectors and finds the strongest output along with its index. This index is fed back to the transmitter to inform of it the phase setting that provides the maximum combined output. The transmitter transmits with this phase value for a certain period of time before engaging in periodic phase scanning. This periodic search provides re-initialization and helps to track slow fading in the channel.

7.1.3 Algorithm Development

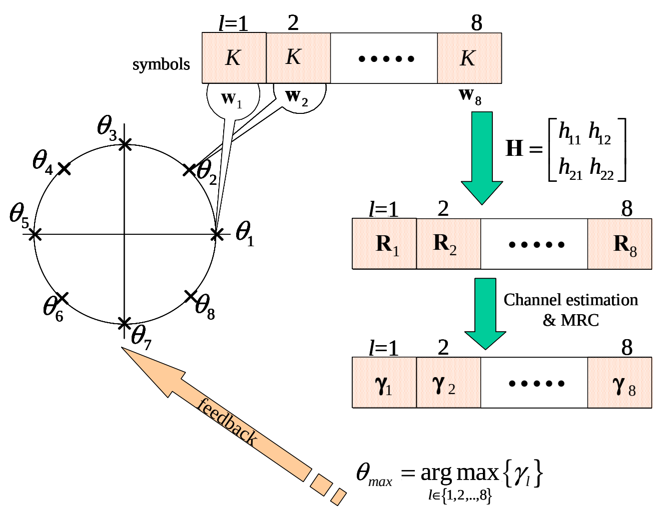

Figure 7.2. Functional block diagram of the proposed MIMO technique.

The functional block diagram of the proposed algorithm is shown in Figure 7.2. The phase scanning at the transmitter is performed by choosing discrete phase values from a set of uniformly spaced phase settings along a unit circle. For each phase setting, θ_l, the corresponding weight vector $\mathbf{w}_l$ is computed as

$$\mathbf{w}_l = \frac{1}{\sqrt{2}}\begin{bmatrix}1 \\ e^{-j\theta_l}\end{bmatrix}, \quad l \in \{1,2,..,L\}$$
$$\theta_l = \frac{2\pi}{L}(l-1) \tag{7.1}$$

The weight vector is normalized for maintaining a constant transmit power. A block of K symbols, $\mathbf{d}$, is transmitted for each $\mathbf{w}_l$ to generate a block of receive signal vectors, expressed collectively by a matrix $\mathbf{R}_l$ as follows

$$\left.\begin{aligned}\mathbf{R}_l &= \{\mathbf{r}_k\} \\ \mathbf{r}_k &= \mathbf{w}_l^\dagger \mathbf{H} d_k + \mathbf{n}_k = \mathbf{G}_l d_k + \mathbf{n}_k\end{aligned}\right\}; k \in \{1,2,\cdots,K\} \tag{7.2}$$

where, '†' denotes hermitian transpose. The noise at the receiver, $\mathbf{n}_k$, is assumed to be white additive gaussian, uncorrelated to the received signals. The gain vector $\mathbf{G}_l$ for the l-th block needs to be estimated before MRC can be performed on $\mathbf{R}_l$. Given $\mathbf{R}_l$ and $\mathbf{d}$, $\mathbf{G}_l$ can be estimated by least-squares (LS) based estimation technique as follows

$$\hat{\mathbf{G}}_l = \frac{\mathbf{R}_l^\dagger \mathbf{d}}{\mathbf{d}^\dagger \mathbf{d}} \tag{7.3}$$

By setting the receive weight vector as $\mathbf{v}_l = \hat{\mathbf{G}}_l^\dagger$, the combined received signal can be expressed as

$$y_k = \left(\hat{\mathbf{G}}_l^\dagger \mathbf{G}_l\right) d_k + \hat{\mathbf{G}}_l^\dagger \mathbf{n}_k \tag{7.4}$$

The resulting SNR for the l-th block is thus expressed as

$$\gamma_l = \frac{\left|\hat{\mathbf{G}}_l^\dagger \mathbf{G}_l\right|^2}{\left|\hat{\mathbf{G}}_l^\dagger\right|^2} \gamma_0 \tag{7.5}$$

where, γ_0 is the SNR per antenna element at the receiver.

The receiver stores the different γ_l and finds the maximum from the stored set after one complete scan of the weight vector at the transmitter. The index corresponding to the maximum SNR is fed back to the transmitter in the feedback channel. If L is set at eight, which is usually sufficient for a two-element array, only three bits are required to accommodate the feedback index.

Optimal Solutions

If perfect channel estimate is assumed, i.e., $\hat{\mathbf{G}} = \mathbf{G}$, the received SNR is given by

$$\gamma = |\mathbf{G}|^2 \gamma_0 . \tag{7.6}$$

The received combined SNR can be maximized with respect to **G**. From (7.2), it is evident that this maximization process involves choosing an optimal **w**. Writing γ in terms of **w**, we get

$$\gamma = \mathbf{w}^\dagger \left(\mathbf{h}_1\mathbf{h}_1^\dagger + \mathbf{h}_2\mathbf{h}_2^\dagger\right)\mathbf{w}\gamma_0 = \mathbf{w}^\dagger \left(\mathbf{H}\mathbf{H}^\dagger\right)\mathbf{w}\gamma_0 . \tag{7.7}$$

The optimal choice for **w** is the eigenvector of $\mathbf{H}\mathbf{H}^\dagger$ corresponding to the maximum eigenvalue. In this case, the optimal SNR is given by,

$$\gamma = \lambda_{max}\gamma_0 , \tag{7.8}$$

where λ_{max} is the maximum eigenvalue of $\mathbf{H}\mathbf{H}^\dagger$. The proposed MIMO scheme is an equal-gain (EG) based search algorithm (at the transmitter) which aims to attain optimal performance in (7.8). Since the optimal weight vector does not in general belong to EG weight vector, the performance from the proposed scheme is expected fall short of the optimal performance.

The solution in (7.8) assumes perfect estimate of **G** at the receiver and the optimal eigenvector of $\mathbf{H}\mathbf{H}^\dagger$ at the transmitter. However, a more general optimal solution can be derived for the given MIMO system. The received signal vector in this case is written as

$$\mathbf{r} = \mathbf{w}^\dagger \mathbf{H} d + \mathbf{n} . \tag{7.9}$$

The combined output can be expressed as

$$y = \mathbf{w}^\dagger \mathbf{H}\mathbf{v} d + \mathbf{n}\mathbf{v} . \tag{7.10}$$

The expression above shows that the combined receive SNR is maximized when **w** and **v** are chosen as the singular vectors of **H** that correspond to the maximum singular value. Additionally, $\mathbf{v}$ can be normalized to unity so that the filtered noise power does not change. Then optimum SNR is given by

$$\gamma = \sigma_{max}^2 \gamma_0 , \tag{7.11}$$

which is equivalent to the expression in (7.8) from the property $\lambda\left(\mathbf{H}\mathbf{H}^\dagger\right) = \sigma^2\left(\mathbf{H}\right)$. This indicates that the optimal solution in (7.8) is indeed the optimal solution for a given channel matrix **H**. Thus the proposed scheme aims at achieving the true optimal solution.

We can compare the optimal solutions to the one derived as a MRT solution proposed by Lo [LO99] as

$$\gamma = \frac{\sum_{p=1}^{L}\sum_{q=1}^{L}\left|\sum_{k=1}^{K} h_{pk} h_{qk}^{*}\right|}{L}\gamma_0 , \tag{7.12}$$

where, K and L are the number of antenna elements at the transmitter and receiver, respectively, and h_{pk} is the channel from transmit antenna k to receive antenna p. The MRT solution assumes EG combining at the receiver and transmit weight vector that is matched to the composite of channel matrix and the receive weight vector. The computation and application of transmit weight vector assumes perfect channel estimation and feedback of K complex values from the receiver to the transmitter which may not be feasible form practical implementation point of view. The SNR improvement from the proposed scheme has been compared with the MRT solution by simulation and is presented in the results section.

7.1.4 Open loop variations

Some open loop variations are possible with the proposed MIMO scheme. The combining scheme at the receiver can be based on selecting the antenna with the stronger signal for each packet received. Another possibility is the continuation of using phase scanning on the rest of the packet in addition to pilot symbols. The receiver can extract the estimate of channel gains from the received pilot symbols and use these estimated gains for MRC combining on the remaining, phase scanned symbols of the packet. A slow fading channel with large time coherence assures that the estimated gains are valid for the remainder of the packet. Both the selection and MRC schemes need not feed the optimal index back to the transmitter. This implies a system that is immune to mobility in the propagation media, and in addition to this, a simpler receiver design for the selection scheme. Since the transmitter does not have information on the optimal phase setting, and, thus, does not transmit with this setting, the performance improvement for the open loop system is expected to be lower than the close loop system.

There's an additional advantage with the selection scheme that the transmitter need not scan through a large number of phase settings; in fact, it need not scan at all. This can be shown be as follows. Let the gain vector at index l, G_l be expressed in terms of the channel and the transmit weight vector as

$$G_l = \begin{bmatrix} g_1 \\ g_2 \end{bmatrix} = \mathbf{H}\mathbf{w}_l = \begin{bmatrix} \mathbf{h}_1\mathbf{w}_l \\ \mathbf{h}_2\mathbf{w}_l \end{bmatrix} \tag{7.13}$$

The expect value of the SNR at any antenna element, say 1, at index l can be expressed as

$$\gamma_1 = E\left[|g_1|^2\right]\gamma_0 = \mathbf{w}_l{}^\dagger E\left[\mathbf{h}_1^\dagger \mathbf{h}_1\right]\mathbf{w}_l\gamma_0 \tag{7.14}$$

The expected operation $E\left[\mathbf{h}_1^\dagger \mathbf{h}_1\right]$ can be shown to yield an identity matrix multiplied by the channel variance when the MIMO channel matrix elements are i.i.d. according to a fading distribution profile. With the norm of transmit weight vector held at unity, the expected SNR then becomes

$$\gamma_1 = E\left[|h|^2\right]\gamma_0, \tag{7.15}$$

which is the independent of the number of phase settings used at the transmitter. Thus, unless, l_{max} among L indices is identified and fed back to the transmitter, any arbitrary phase setting suffices for the whole packet for open loop selection scheme.

7.1.5 Results

The algorithm has been tested in a Rayleigh channel, and the performance from gain estimation (7.3) and the resulting SNR (7.5) has been assessed and compared with optimal solutions in (7.8) and (7.12) in terms of outage probability.

Simulations have been performed for a 2×2-system operating in a stationary and i.i.d. Rayleigh channel. Each channel gain is composed of complex gaussian random variable with 0.5 variance per dimension. L, the total number of discrete phase values, is set at eight and the number of training symbols for each phase setting, K, is chosen as five. The operating SNR γ_0 is 15 dB. First, we assess the performance from channel estimation and compare that to the performance with perfect channel knowledge. Figure 7.3 shows cumulative distribution function (CDF) or outage probability curves for combined SNR for $\gamma_0 = 0, 5, 10 \text{ and } 15\,\text{dB}$. From the plots it can be seen that the difference between the performances from the estimate and perfect channel knowledge is insignificant for $\gamma_0 > 5\,\text{dB}$ and there is small performance degradation for $\gamma_0 = 0\,\text{dB}$.

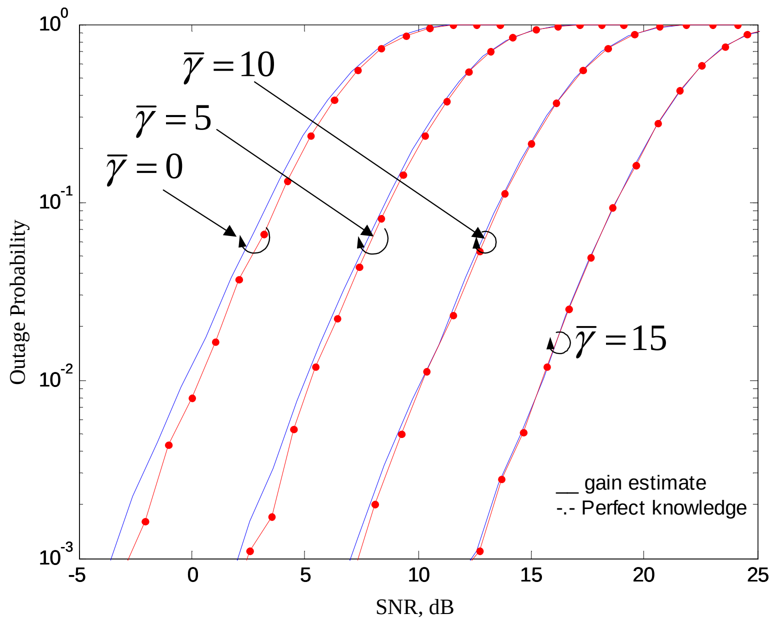

Figure 7.3 Outage probability plots of output SNR to compare channel estimate with perfect channel knowledge.

Figure 7.4 shows the outage probability curves from the computed SNR for the proposed algorithm. Single antenna case is provided as a benchmark while the ideal STBC technique is presented for comparison with the proposed technique.

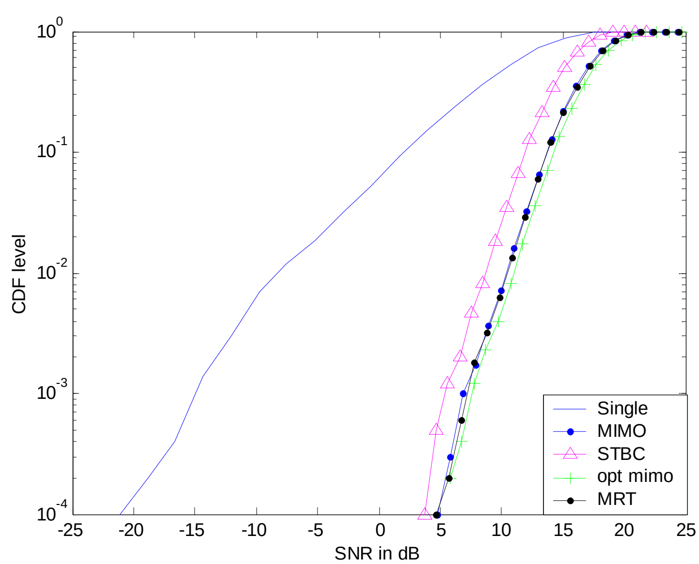

Figure 7.4 Outage probability plots for the proposed MIMO technique.

The proposed technique shows substantial diversity gain over the single antenna system. For example, at an outage probability of 10^{-2}, the proposed technique is better than the single antenna system by about 15 dB. The plots illustrate that the proposed MIMO scheme is within less than a dB of the optimal performance, and, it also essentially provides the same performance as the optimal MRT solution. The output from STBC technique with perfect channel estimate is also shown here for comparing with the proposed technique. Note that the proposed MIMO technique outperforms the STBC technique; e.g., at outage probability of 10^{-2}, the proposed MIMO technique is better by about 2 dB compared to the STBC technique.

The performance improvement from the open-loop variations of the proposed MIMO technique is shown in Figure 7.5 Outage probability curves have been generated at two different γ_0 for the selection and MRC techniques along with single antenna and optimal technique.

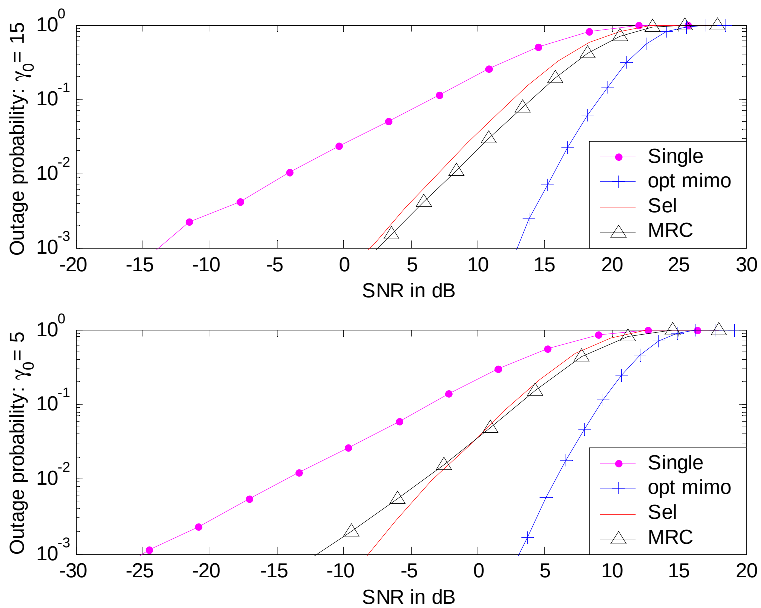

Figure 7.5. Outage probability plots for the selection and MRC technique for two different γ_0.

The plots show that the open-loop techniques provide SNR improvement over the single antenna case (e.g., a gain of about 15 dB for both the techniques for γ_0= 15 dB), and the improvement is lower than the proposed closed-loop technique, when compared to Figure 7.4, because of the absence of the feedback. The plots also reveal the contrast between the selection and the MRC techniques as a function of γ_0. The MRC technique is slightly better than the selection for higher

γ_0, but when γ_0 is lower (severe fading situation) the selection technique provides better performance at lower outage probability. This is mainly due to the channel estimation in the MRC case, which suffers when the operating SNR is degraded. This shows that the selection technique is robust to SNR variations compared to MRC and although its performance is slightly lower, it may provide a better choice between the two because of its simple implementation and its robustness.

The effect of L on the performance has been evaluated for the proposed closed-loop technique and the results are shown in Figure 7.6. Outage probability curves for different L reveal that the technique is relatively insensitive to changes in L. Choosing $L = 2$ will result in a small performance loss but will provide a simpler system design.

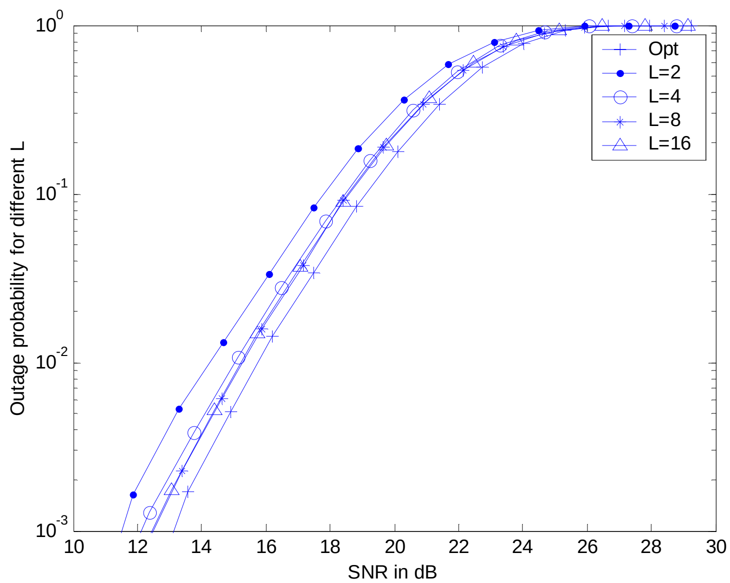

Fig. 7.6. Outage probability plots for different *L*.

A more robust identification of pilot bits can be achieved by using selection technique on the received signals from both the antenna elements during the phase scanning process (exact structure shown in Figure 8.16, Chapter 8). This is verified by studying the BER performance of the signal from one antenna and selection from both antenna elements as shown in Figure 7.7. For any operating SNR, the selection process enhances pilot symbol identification and thus may reduce the retransmission of previous packet.

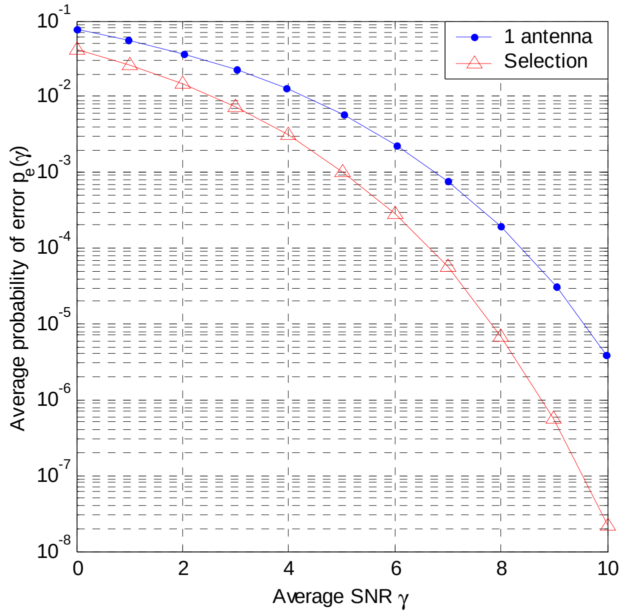

Figure 7.7. BER plots for comparing pilot symbol identification process from selection technique with single antenna systems.

7.2 Frequency selective channel

7.2.1 Introduction

There has been research reported on joint optimization of transmit and receive filters. Berger and Tufts presented joint transmitter-receiver design for a single-input-single-output (SISO) system in [BER67]. Their approach involves minimizing distortion with constant transmit power constraint and relies on iterative search over parametric curves of transmit power and minimum distortion. There is not a closed form solution and the channel characteristics have to be known a priori. The work in [YAN94a] follows the general pattern of [BER67] and provides an extension to multiple-input-multiple-output (MIMO) system. It discusses joint optimization of both transmit and receive filters subject to a power constraint. The scenario here is a fully cross-coupled transmitter and receiver systems, and the optimized transmitter-receiver system allows reliable estimates of transmitted data by reducing MSE. The authors provide an iterative solution similar to [BER67]. They extend their work to include a decision feedback receiver and provide a joint optimization over the transmitter and receiver [YAN94b]. Sampath and Paulraj [HEM99] addresses joint design of transmit and receive transfer matrices (i.e., zero-order filters) in a narrowband channel. Their result is similar to Berger and Yang in that the MIMO channel is shown to decouple into parallel sub-channels. Choi et. al. [CHO00] propose a joint transmitter-receiver filter design scheme based on optimizing SINR for a CDMA system. Their technique incorporates multi-user scenario and requires iterative solution for optimizing the transmit and receive MIMO equalizers. Choi and Cioffi [CHO99] combine ST-BC with a MIMO system to implement transmit diversity in a frequency selective channel. They propose a linear MSE equalizer at the receiver and provide optimal solutions for it. The ST-BC scheme is similar to the one proposed by Alamouti [ALA98].

7.2.2 Derivation of DSNR Solution

For a frequency selective channel, the channel is represented by an $N \times M$ size $\mathbf{C}$ matrix as $\mathbf{C}(t)=\{c_{ij}(t)\}$ for an *M*-element transmit array and *N*-element receive array where individual channel components (delayed multipaths) are $c_{ij}(t)=c^{0}_{ij}(t)+c^{1}_{ij}(t-\tau_1)+\cdots\cdots$ (*j*th transmit antenna to *i*th receive antenna). In frequency domain, the representation becomes $\mathbf{C}(f)=\{c_{ij}(f)\}$. The setup is an extension of the proposed transmitter and receiver structure in Chapter 4 where the receiver also employs an antenna array. The resulting structure is a MIMO space-time (MIMO-ST) one where the transmitter and the receiver pulse shaping filters are optimized regarding certain performance metrics. The usual performance metrics include DSNR or MMSE as mentioned in Chapter 4 and only the DSNR metric is addressed in this chapter. From Chapter 4, the DSNR optimization problem for the MIMO case can be formulated as

$$\max_{\mathbf{g}(f)} DSNR = \max_{\mathbf{g}(f)} \frac{d^2}{T_s}\cdot\left(T_s \int_{-\frac{1}{2T_s}}^{\frac{1}{2T_s}} \frac{df}{\sum_j \left|\mathbf{H}^*\left(f+\frac{j}{T_s}\right)\Phi_n^{-1}\left(f+\frac{j}{T_s}\right)\mathbf{H}\left(f+\frac{j}{T_s}\right)\right|^2}\right)^{-1} . \quad (7.16)$$

$$s.t. \qquad \frac{1}{T_s}\int_{-\frac{1}{2T_s}}^{\frac{1}{2T_s}} \sum_j \left\|\mathbf{g}\left(f+\frac{j}{T}\right)\right\|_2^2 \phi_I(f)\,df = P_{av}$$

Here Φ_n represents the noise covariance matrix at the receiver, and $\mathbf{g}(f)=\left[g_1(f) \quad g_2(f)\right]^T$.

Since $\mathbf{H}(f)=\mathbf{C}(f)\mathbf{G}(f)$, the optimization problem can be rearranged with the substitution of $\mathbf{C}^*(f)\mathbf{\Phi}_n^{-1}(f)\mathbf{C}(f)=\Theta(f)$ as follows

$$\begin{aligned}&\min_{\mathbf{g}(f)} \int_{-\frac{1}{2T_s}}^{\frac{1}{2T_s}} \frac{df}{\sum_j \left| \mathbf{g}^*\left(f+\frac{j}{T_s}\right)\Theta\left(f+\frac{j}{T_s}\right)\mathbf{g}\left(f+\frac{j}{T_s}\right)\right|^2},\\ &s.t.\ \ \frac{1}{T_s}\int_{-\frac{1}{2T_s}}^{\frac{1}{2T_s}} \sum_j \left\|\mathbf{g}\left(f+\frac{j}{T}\right)\right\|_2^2 \phi_I(f)\,df = P_{av}\end{aligned} \tag{7.17}$$

The optimal form of $\mathbf{g}(f)$ is of the form $\mathbf{g}(f)=p(f)\boldsymbol{\gamma}(f)$ where $\boldsymbol{\gamma}(f)$ is the singular vector corresponding to the maximum singular value $\sigma_{max}(f)$ of the matrix $\Theta(f)=\mathbf{C}^*(f)\mathbf{\Phi}_n^{-1}(f)\mathbf{C}(f)$. With this form of solution for the transmit filters, DSNR needs to be maximized with respect to the scalar $p(f)$ and the resulting optimization problem becomes

$$\begin{aligned}&\min_{p(f)} \int_{-\frac{1}{2T_s}}^{\frac{1}{2T_s}} \frac{df}{\sum_j p^2\left(f+\frac{j}{T}\right)\sigma_{max}\left(f+\frac{j}{T}\right)},\\ &s.t.\ \ \frac{1}{T_s}\int_{-\frac{1}{2T_s}}^{\frac{1}{2T_s}} \phi_I(f)\sum_j p^2\left(f+\frac{j}{T}\right)\left|\boldsymbol{\gamma}\left(f+\frac{j}{T}\right)\right|^2 df = P_{av}.\end{aligned} \tag{7.18}$$

The constraint in the above equation can be simplified by restricting the norm of $\boldsymbol{\gamma}(f)$ to unity as

$$\frac{1}{T_s}\int_{-\frac{1}{2T_s}}^{\frac{1}{2T_s}} \phi_I(f)\sum_j p^2\left(f+\frac{j}{T}\right)df = P_{av}\ .$$

Following the same procedures to derive (B-13) in the Appendix, it can be shown that the maximum DSNR is expressed as

$$DSNR_{max} = P_{av}T_s\left(T_s\int_{-1/2T_s}^{1/2T_s} \frac{\sqrt{\Phi_I(f)/d^2}\,df}{\sum_j\sqrt{\max_j \sigma_{max}^2\left\{\mathbf{C}^*\left(f+\frac{j}{T}\right)\mathbf{\Phi}_n^{-1}\left(f+\frac{j}{T}\right)\mathbf{C}\left(f+\frac{j}{T}\right)\right\}}}\right)^{-2} \tag{7.19}$$

If the receiver noise is assumed white and uncorrelated across the antenna branches, one can write $\mathbf{\Phi}_n(f)=N_0\mathbf{I}$ where N_0 is the noise variance in each receive antenna and $\mathbf{I}$ is an identity matrix. In this case, the maximum DSNR can be simplified as

$$DSNR_{max} = \frac{P_{av}T_s}{N_0}\left(T_s \int_{-1/2T_s}^{1/2T_s} \frac{\sqrt{\phi_I(f)/d^2}\,df}{\sum_j \sqrt{\max_j \sigma_{max}\left\{ \mathbf{C}^*\left(f+\frac{j}{T}\right)\mathbf{C}\left(f+\frac{j}{T}\right)\right\}}} \right)^{-2} . \qquad (7.20)$$

From the property of singular vector, the terms under the square root can be further simplified to $\max_j \sigma_{max}^2 \left\{ \mathbf{C}\left(f+\frac{j}{T}\right)\right\}$.

One can validate the above expression for a flat fading MIMO channel. For a flat fading channel and additive white gaussian noise at the receiver, $\mathbf{C}(f)=\mathbf{C} \quad |f| \le \frac{W}{2}$ and $\Phi_n(f) = N_0\mathbf{I}$, the expression under the square root in the denominator becomes

$$\max_j \sigma_{max}\left\{ \mathbf{C}^*\left(f+\frac{j}{T}\right)\mathbf{\Phi}_n^{-1}\left(f+\frac{j}{T}\right)\mathbf{C}\left(f+\frac{j}{T}\right)\right\} = \frac{1}{N_0}\sigma_{max}^2(\mathbf{C}). \qquad (7.21)$$

Assuming the signal PSD $\phi_I(f) = d^2$, it can be shown that

$$DSNR_{max} = \frac{P_{av}T_s}{N_0}\sigma_{max}^2(\mathbf{C}) = \gamma_0\sigma_{max}^2(\mathbf{C}), \qquad (7.22)$$

where, γ_0 is the average SNR per receive antenna branch. This is the expression for optimal SNR in a flat fading environment (MRT solution for MIMO system).

7.2.3. Results

The solution in (7.20) has been evaluated for WCDMA indoor channel (type-A) for a 2×2 system. Each multipath component undergoes Rayleigh fading and a bandwidth expansion factor of 5 is assumed in this case. An outage probability (CDF) plot of the resulting SNR is shown in Figure 7.8 for $\gamma_0 = 15$ dB. Compared to the single antenna system, the MIMO system provides a diversity gain of about 20 dB at 10^{-2} outage level.

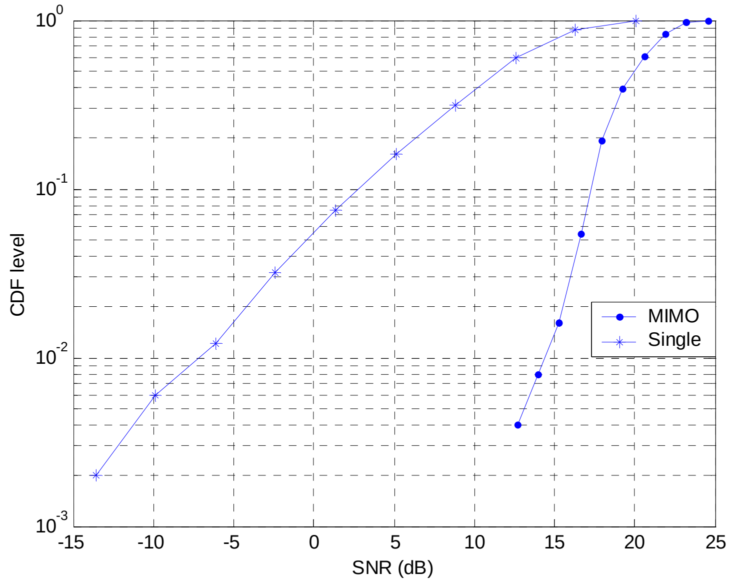

Figure 7.8. Outage probability plots from the 2×2 MIMO system and a single antenna system.

Chapter 8

Transmit Diversity in W-CDMA and WLAN

8.1 Introduction

Transmit diversity techniques have been proposed and their performance investigated in the previous chapters. Implementation for the W-CDMA standard was discussed briefly at the end of Chapter 2, and this chapter provides a concise description of this new standard and discusses the details of implementation of the proposed techniques in W-CDMA uplink (transmit diversity at the handset). The feasibility of diversity systems in Wireless Local Area Network (WLAN) standard is presented with regards to the framing structure of the common air interface.

8.2 W-CDMA

8.2.1. Background

The pursuit of extending the present-day mobile communications by including multimedia capabilities and global standardization has given rise to new a class of wireless standard. First-generation mobile communications, such as AMPS, TACS supported analog voice service. Second-generation systems were introduced to include digital voice and circuit-switched low rate data services. With the emergence of Internet, the vision for future mobile communication systems is to include multimedia service and provide seamless coverage across the globe. The International Telecommunications Union (ITU) and other standards bodies have been focusing on developing the next generation or "Third Generation (3G)" system standards. In Europe, the European Commission has been quite active in carrying out research to develop this new standard and their research has produced the Universal Mobile Telecommunications System (UMTS)/International Mobile Telecommunications in the year 2000 (IMT-2000) [DAH98]. Collaboration to define the standards for IMT-2000 drew participation from different standards bodies from around the world: European Telecommunications Standards Institute (ETSI) in Europe, Association of Radio Industries and Business (ARIB) in Japan, Telecommunications Industry Association (TIA) and T1P1 in USA, and Telecommunication Technology Association (TTA) in South Korea. This new standard supports both CDMA and TDMA systems. The

CDMA standard known as the W-CDMA system has both FDD and time division CDMA (TD-CDMA) in TDD implementation.

8.2.2 Brief Overview of Physical Layer

W-CDMA operates with a constant chip rate of 3.84 Mchips/sec and supports variable bit-rate services. This implies that the spreading gain varies with different services so that the resulting chip rate is always the same. The baseband signal bandwidth is about 5 MHz. Channels belong to a code-frequency grid of 200 KHz raster while the RF carrier spacing is 5 MHz. The RF carriers are limited to 1920-1980 MHz in the uplink (UL) and 2110-2170 MHz in the downlink (DL) according to one specification and 1850-1910 MHz (UL) and 1930-1990 MHz (DL) according to another specification.

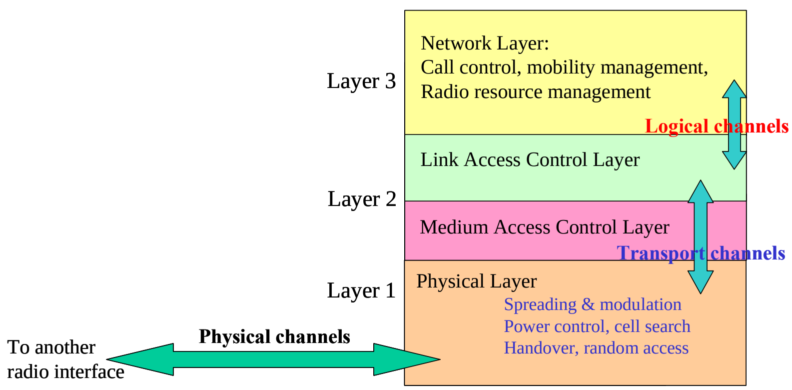

Figure 8.1. Radio Layer Architecture showing Layers 1, 2 and 3.

The basic structure of communications in W-CDMA follows a layered architecture as shown in Figure 8.1. The services required by a user are handled at the application layer, and the required processing, mapping onto physical layer, and transmitting to the air-interface are managed by different layers in the architecture. Data from the higher layers enters the layer 2 (link access control and MAC) by logical channels and then the physical layer by transport channels. The physical layer provides spreading and modulation, packaging the data into frames, power control, etc., to generate physical channels and subsequent transmission of physical channels onto the wireless medium. A detailed discussion of the different layers and their functions would be quite overwhelming and for the purpose of discussing transmit diversity, the relevant components of the physical layer will be given main focus.

The physical layer generates and transmits physical channels according to the instructions provided by the higher layers. A physical channel is characterized by the following parameters: specific carrier frequency, specific code, and relative phase (0 or $\pi/2$) in the uplink. A physical channel in the uplink or downlink can be divided into common and dedicated channels. The common channels usually carry system specific information and thus are available to all the users in the system. The dedicated channel carries information to a specific user and thus is dedicated to that user only. A dedicated physical channel (DPCH) contains both control information and user data. In the uplink the dedicated channels include DPCH and the common channel includes random access channel (RACH) and common packet channel (CPCH). In the downlink the dedicated channels include DPCH and dedicated shared channel (DSCH), and the common channels include primary and secondary common control physical channel (PCCPCH and SCCPCH), common pilot channel (CPICH), and synchronization channel (SCH). Among these, the DPCH and DSCH will be of importance in this chapter.

The basic structure of a physical channel is a 10 ms frame that contains fifteen slots. The structure of a DPCH in the uplink is shown in Figure 8.2.

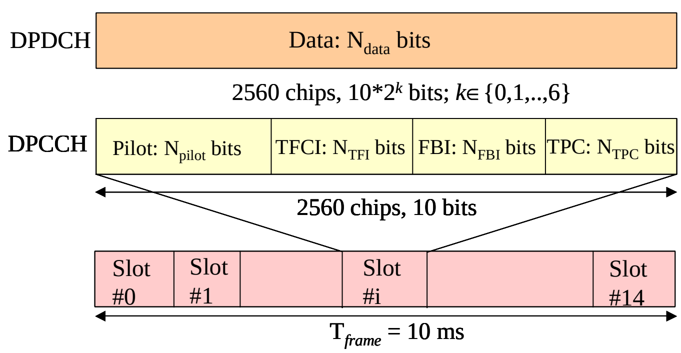

Figure 8.2. Frame structure for Uplink DPCH.

From Figure 8.2, a DPCH in the uplink is seen to contain two separate sub-channels, one for data (dedicated physical data channel, DPDCH) and one for control (dedicated physical control channel, DPCCH) respectively. The control channel contains pilot, transmit frame control indicator (TFCI), feedback information (FBI), and transmit power control (TPC) bits. The number of bits allotted for each of these categories can vary and is given in [ETS00a]. The pilot bits provide channel estimation and coherent demodulation, the FBI bits provide feedback information for a closed-loop transmit diversity system at the base station, and the TPC bits provide power control at the base station. It is interesting to see that the standard in its ongoing upgrading process has accommodated space for feedback information for implementing transmit diversity at the base station.

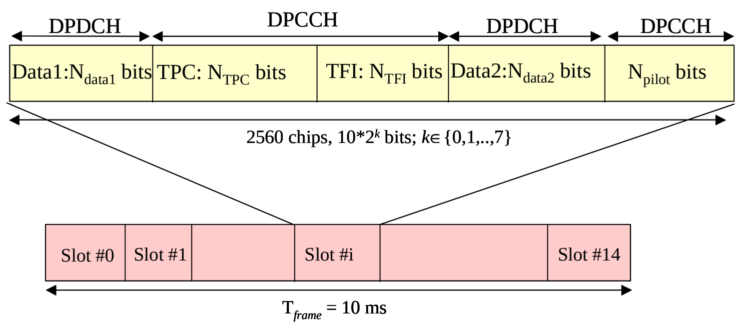

Figure 8.3. Frame structure for Downlink DPCH.

Figure 8.3 shows the structure of a DPCH in the downlink. Here unlike in the uplink, the data and control information are arranged in a single channel. User data is split into segments and placed at different locations in a slot. The control information contains Transmit Format Indicator (TFI), TPC, and pilot bits, and these are placed at different locations as well. The frame structure above indicates that the present standard cannot explicitly support a closed-loop transmit diversity at the handset, as there is no provision for feedback information in the downlink DPCH.

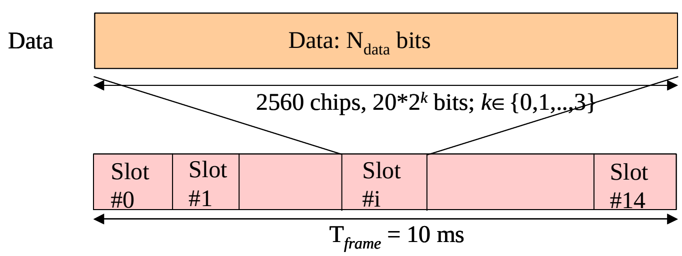

Figure 8.4. Frame structure for Downlink DSCH.

Figure 8.4 shows the frame structure of a DSCH. Several users usually share a DSCH through code multiplexing. A DSCH is always associated with one or several DCHs. A downlink channel can send additional information by using this shared channel, making it a good candidate for providing feedback to the mobile to support closed-loop transmit diversity at the handset.

8.3 Existing transmit diversity schemes in WCDMA

Transmit diversity techniques have been investigated for CDMA systems in [JAL99] and [HOT98]. Paper [JAL99] compares between Orthogonal Transmit Diversity (OTD) and Space-Time Transmit Diversity (STTD) and shows that the two techniques provide nearly the same level of performance. A selection-based technique that includes coherent multipath combining is proposed in [HOT98] and compared with Code Division Transmit Diversity (CDTD) and Time Division Transmit Diversity (TDTD). Simulation results show that the proposed selection-based technique is better than the other two in a two-path Rayleigh channel. Some authors have reported transmit diversity schemes for CDMA-2000 in [RAJ99], [CHE99] and present a simulation study of simple diversity techniques such as OTD, Phase Sweeping Transmit Diversity (PSTD), STD, and Time Switched Transmit Diversity (TSTD). Transmit diversity has been proposed in [HOT00], [RAI99] for W-CDMA systems to improve capacity and coverage without increasing the complexity of the receiver design at the mobile station (MS), i.e., without employing a secondary receiver chain to implement diversity reception. All the proposed transmit diversity schemes for W-CDMA require an antenna array at the BS and the MS with a single receive chain. OTD, TSTD and STTD belong to the open-loop category while STD and feedback mode transmit diversity (FBTD) belong to the closed-loop category.

The proposed transmit diversity techniques have an evolution associated with them. Transmit diversity techniques were first proposed in 1998 [ETS98] and contained OTD, TSTD and STD. Texas Instruments (TI) investigated the STTD techniques in 1999 [3GP99a]. The feedback mode transmit diversity also appeared in 1999 [3GP99b]. The proposed TSTD and STD are evaluated by simulation and results are reported in [3GP99c]. It is not clear from the Third Generation Project Partner (3GPP) documents whether the previously proposed transmit diversity techniques (OTD, TSTD and STD) have been completely replaced by the newly proposed techniques (STTD and FBTD).

8.4. Brief Descriptions of the Proposed Transmit Diversity Schemes

In the proposed techniques, it is ensured that orthogonality is maintained between the transmit antenna elements. The orthogonality can be maintained by using either code division or time division techniques. The transmit diversity techniques that employ delay transmit diversity are not proposed because of the self-interfering nature of the delayed signals and the requirement of rake fingers at the receiver.

OTD [ETS98]

When orthogonality is maintained by code, the technique is known as OTD. The orthogonality is maintained by employing orthogonal channelization codes for different antenna elements. The coded bits are split into separate data streams and provided to separate antenna elements. Orthogonal channelization codes are applied to antenna elements for spreading the data bits. It is noted that the effective number of channelization codes per user is the same as in the case without OTD since the coded data bits are split into separate data streams. The proposed structure is flexible and can be extended to antenna arrays having more than two antenna elements. OTD is seen as an optional feature that can be turned on as needed. It is also assumed that the system can support a mixture of mobiles with and without the OTD processing capability.

TSTD [ETS98]

The implementation of TSTD is shown in Figure 8.5. TSTD is implemented by transmitting successive slots through different antenna elements. The baseband signal is spread and scrambled and switched to different RF chains where up-conversion takes place. TSTD is intended to operate on DPCH, and all other downlink physical channels are transmitted in non-diversity mode, i.e., through a single antenna. The switching pattern for different users employing TSTD should aim to reduce peak transmit power and peak-to-average-power ratio in each RF amplifier.

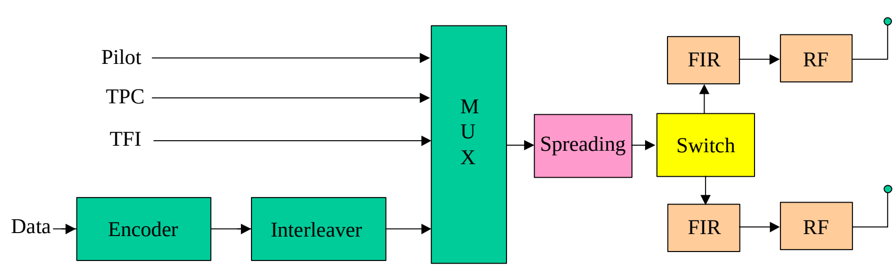

Figure 8.5. TSTD implementation

STD [ETS98]

STD offers an improved or more sophisticated version of TSTD by employing a selective switching mechanism. The switching occurs in accordance with a feedback signal from the MS. In the case of hard handover, antenna element selection is performed on a fast closed-loop control using an antenna selection (AS) signal from the MS. The MS performs signal quality measurements on individual antenna elements through antenna-specific PCCPCH. The pilot sequences on different antenna elements are chosen to be orthogonal to assist in antenna verification at the MS. Figure 8.6 shows a STD implementation.

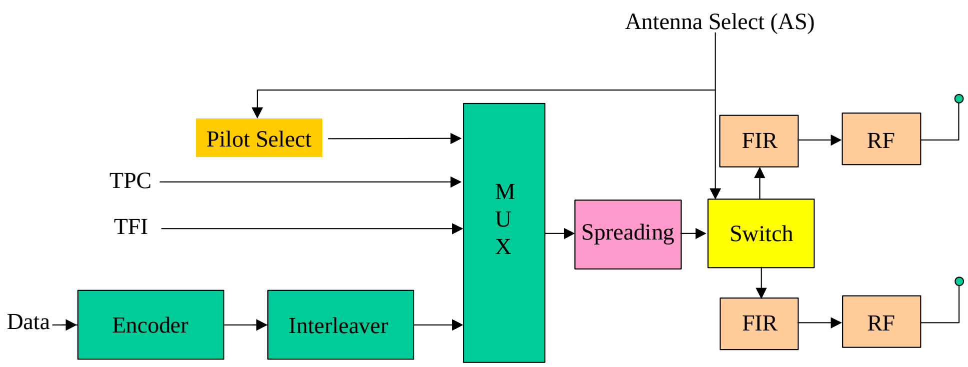

Figure 8.6. STD implementation

STTD:

The STTD mode is incorporated by employing Alamouti's scheme [ALA98]. The implementation of STTD [3GP99a] is shown for a downlink physical channel in Figure 8.7 (a) and the STTD encoding is shown in Figure 8.7 (b).

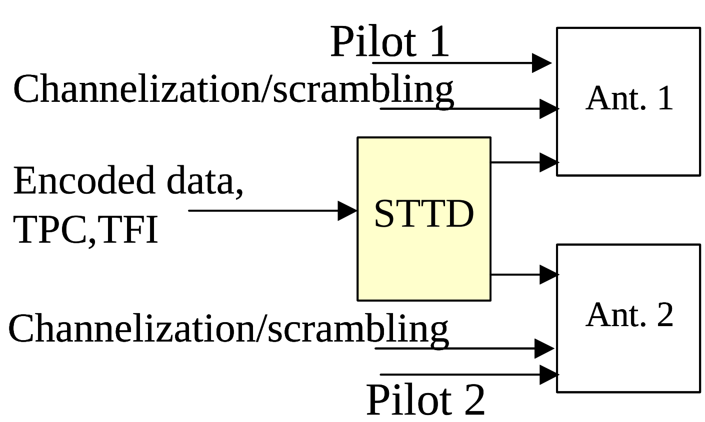

Figure 8.7(a). Implementation of STTD.

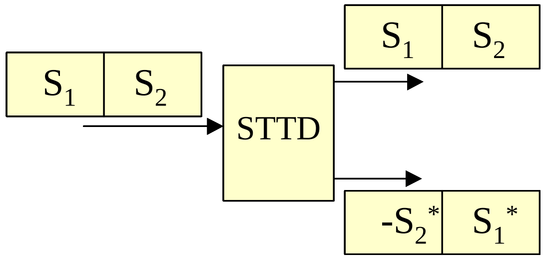

Figure 8.7 (b). STTD Encoding.

From the figures, it is seen that data, TFI and TPC bits are multiplexed and STTD encoded. There are two different pilot sequences, one for each antenna element. After the pilot information is multiplexed, the symbols are spread and scrambled. The receiver at the MS needs channel estimation from each of the elements to the MS to decode the encoded transmitted symbols.

FBTD [3GP99b]

The FBTD employs weighting on the transmitted signal and the weight vector is determined from power measurement at the receiver. The weight vector **W** is given by

$$\mathbf{w} = \begin{bmatrix} \sqrt{P_1} \\ \sqrt{P_2}\, e^{\frac{j\varphi\pi}{180}} \end{bmatrix}$$

where P_1 and P_2 are the power settings on the antenna elements and φ is the phase difference between the antenna elements. Clearly this representation of the weight vector corresponds to equal gain combining from a transmit diversity point of view.

The receiver, based upon the SINR measurement, determines the required weight vector and transmits the information back to the transmitter. The block diagram implementation of FBTD for a downlink DCH is shown in Figure 8.8.

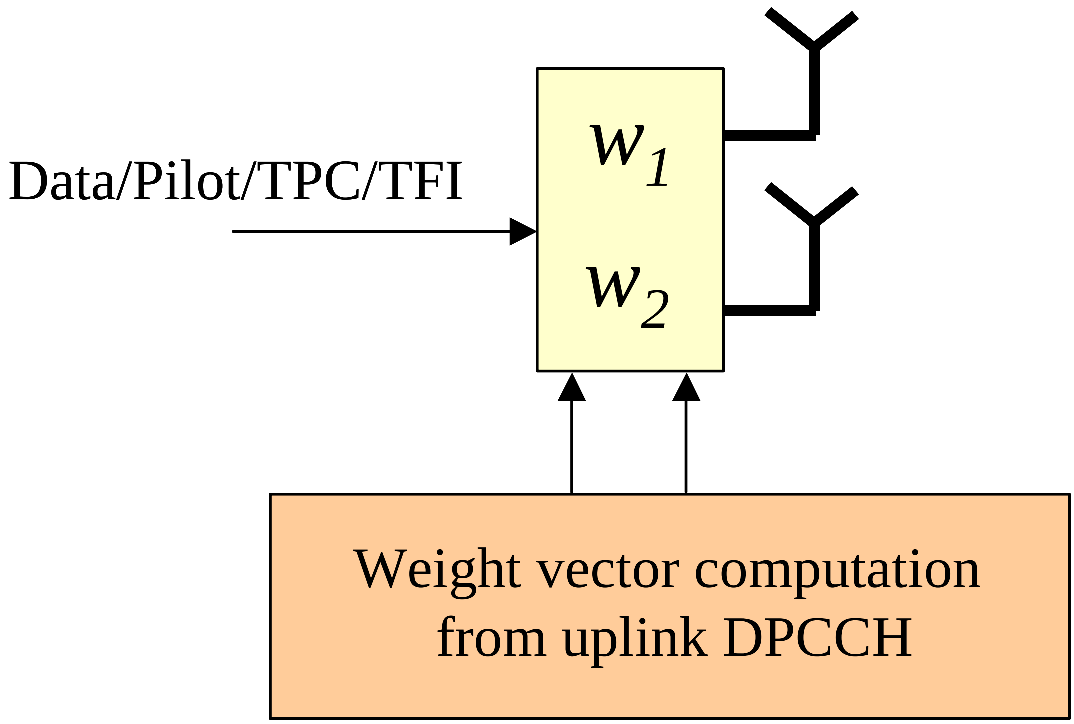

Figure 8.8. FBTD for a Downlink Channel.

The uplink feedback is provided in the FBI field of the DPCCH channel. The feedback is carried by the D sub-field within the FBI field as a feedback signaling message (FSM). Each FSM is comprised of N_w bits made up of N_{po} (power) and N_{ph} (phase) bits.

The FBI_D can have length belonging to the set {0,1,2}, and the length and arrangement of FSM bits can be determined according to different feedback modes. At present, there are two feedback modes available that define different bit allocations to the power and phase fields of a FSM.

For feedback mode 1, the N_{ph} bits can be either 0 or 1 referring to the value of the phase difference of 180° and 0°. For feedback mode 2, the power settings and the phase settings are given in [ETS00b].

8.5 Implementation of TD Techniques in Flat Fading Channel

This section discusses implementation in a flat fading scenario of the transmit diversity schemes proposed in Chapter 2. Transmit diversity at the handset is implemented with a two-element array. The uplink channel is designated as $\mathbf{a}=[a_1\ a_2]$. The principle of implementation is that the mobile transmits with the array and the base station receives the DPCH and decodes the pilot bits in the DPCCH to generate the required feedback information. It then places the feedback information in the DSCH. The mobile demodulates and decodes the DSCH to retrieve the feedback information. Since feedback information is carried by the DSCH, the system needs to establish a link for this channel whenever the mobile indicates the use of transmit diversity in the reverse link.

8.5.1 Bisection Method

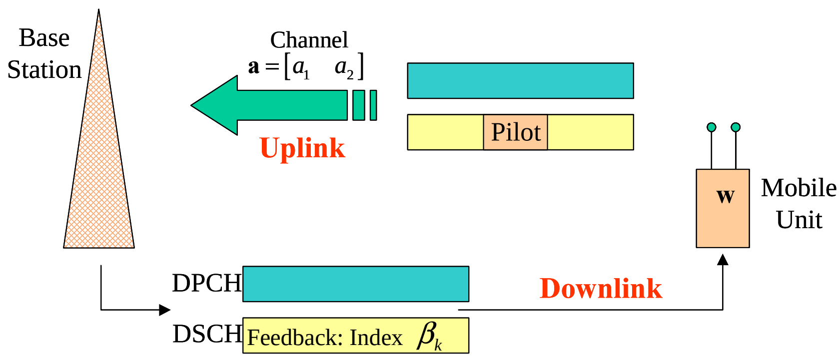

Figure 8.9. Bisection method in WCDMA uplink.

The operating principle as shown in Figure 8.9 is the same as in the phase scanning method. The pilot bits undergo three different weightings with three phase values corresponding to β_k, β_{k+1}, and β_{k-1} (see Section 2.3.1). If more than six pilot bits are employed, then there will be at least two bits for signal strength measurement for each phase and this will result in a better estimation of SNR and subsequently, a more reliable phase estimate (β_k) for feedback to the mobile. The feedback will be just an integer indicating the phase index corresponding to maximum SNR.

8.5.2 Early-Late Method

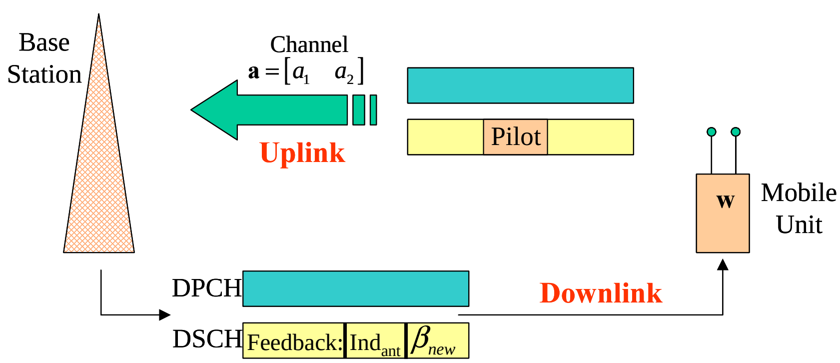

Figure 8.10. Early-Late Method in W-CDMA Uplink.

The implementation of the early-late method is the same as the previous two techniques in principle (Figure 8.10). Here the pilot bits undergo two phase variations corresponding to $\beta_1=\beta_k$ and $\beta_2=\beta_k+\Delta\beta$ (see Section 2.3.2). The SNR estimation for each phase value is better in this case since half the pilot bits are assigned to one phase (β_1) and the rest are assigned to the other phase (β_2). The feedback information now consists of the index of the phase that is going to change (1 or 2) and the value of the new phase β_{new} as well. This will require some quantization of β_{new} to accommodate the computed value in a finite number of bits and there may be some finite precision effects. If the number of bits in the DSCH is moderately large, the quantization error should be negligible.

8.5.3 Least Squares (LS) Method

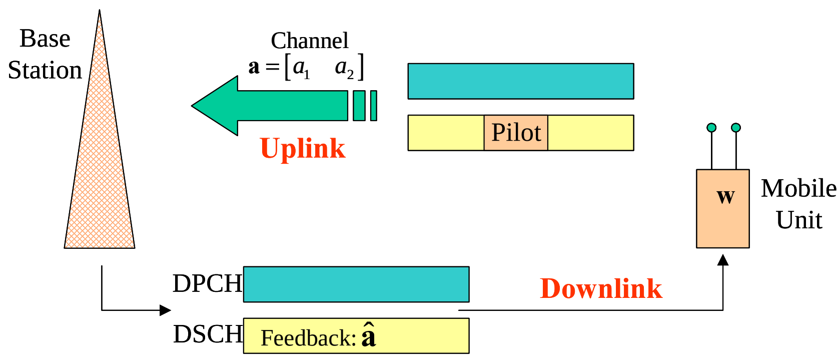

Figure 8.11. Least Squares Method in W-CDMA Uplink.

Figure 8.11 illustrates the least square method of transmit diversity at the handset. During the pilot bit sequence, the weight vector will be dithered according to some predefined sequence. This dithering sequence is known at the base station, and the base station will perform channel estimation from the pilot sequence with dithering. The estimated channel will be fed back to the mobile in the DSCH. Since the channel vector is a complex vector, each channel gain in the vector will be associated with a real and imaginary number and both numbers for each channel gain need to quantized. The DSCH is assumed to accommodate the quantized channel vector.

An alternative approach would be to transmit with a single antenna for half the duration of pilot bits and estimate the individual channel gain. This means that for half the total pilot bits, the mobile transmits with any one antenna, and for the other half, the mobile uses the other antenna. The base station processes these two halves of the pilot bits to estimate the channel independently. The quality of the channel estimates will depend upon the correlation properties of the spreading code and the amount of uplink interference at the base station. The attractive feature of this approach is that the pilot bits as well as the DPDCH do not undergo signal strength variations that may arise from weight dithering.

8.5.4 Subspace and LMS Method

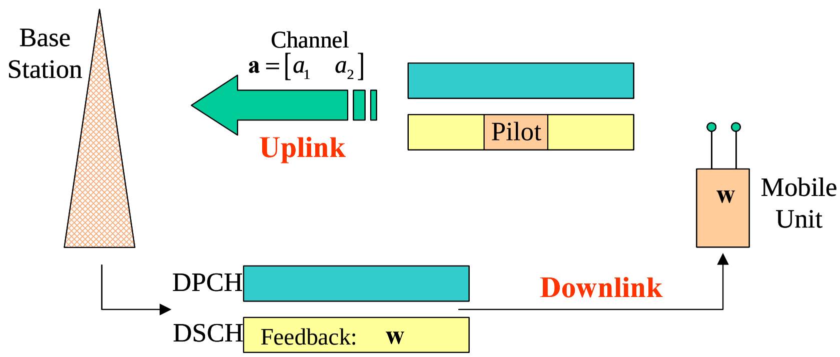

Figure 8.12. Subspace and LMS method in W-CDMA Uplink.

Both the subspace and the LMS methods require an estimate of the gradient of signal strength with respect to the weight vector at the transmitter. The estimate of the gradient provides the optimal weight vector in the subspace method and the new weight vector for the next iteration in the LMS method. Both these methods thus have the same principle of operation. The implementation for these two methods is shown in Figure 8.12. For a 2-element array, a total of five SNR measurements are needed to estimate the gradient. After the gradient is estimated, the optimal weight vector (subspace) or the updated weight vector (LMS) is fed back to the mobile. For a two-element complex weight vector, a total of four components need to be accommodated in the DSCH frame. This again requires some quantization and may introduce error.

8.6 Implementation of Frequency Selective Techniques

The transmit diversity techniques for a frequency selective channel involve filters at each antenna element at the transmitter as well as at the receiver. The filter coefficients are determined at the receiver from knowledge of the vector channel impulse response. The discrete time filter implementation or the sub-optimal implementations (see Section 4.3) can be designed once the base station has acquired the estimate of channel response from both the antenna elements at the transmitter. The computation of the filter coefficients may involve some iteration, but these iterations are carried out solely at the receiver and do not involve a closed-loop. Once the coefficients are determined, the base station feeds them back to the mobile. Figure 8.13 shows the implementation for transmit diversity when the channel is frequency selective.

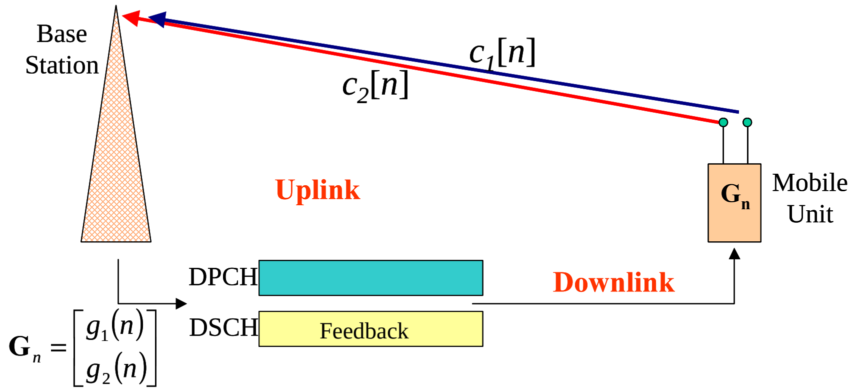

Figure 8.13. Transmit diversity in a frequency selective channel in W-CDMA Uplink.

The individual channel impulse responses $c_1[n]$ and $c_2[n]$ need to be estimated at the base station. This estimation can be done by the least square technique or by assigning two different pilot sequences in the DPCCH to the two antenna elements. Once the estimates are available, the base station can run the transmit diversity algorithm to generate the coefficients, $\mathbf{G}_n$. The amount of feedback information will depend directly on the length of the transmit filters $g_1[n]$ and $g_2[n]$. It may take more than one slot in the DSCH to accommodate the complete feedback information. This may limit the use of transmit diversity to low mobility environment.

8.7 WLAN

8.7.1 Introduction

WLAN is becoming increasingly popular for providing high data rate Internet services to low mobility users in indoor environments. The low infrastructure cost make it an attractive alternative to existing cellular systems in providing broadband services in places like coffee shops, airports and other public places. WLAN systems provide a vantage point for implementing smart antenna system because of its low-mobility and low-range environment. In the following subsections, a brief overview of this standard is provided with special emphasis on the version that is used in the USA. Antenna array systems have been studied for their applications in indoor wireless communications, e.g., in WLAN systems. They have been proposed for near-fixed indoor wireless systems under certain operating assumptions [MOC99] and sector-antenna base station in the forward link of a WLAN system [LEE00]. Near-field distortion for antenna arrays in WLAN applications has been addressed in [ABR00], and smart antenna at the mobile terminal has been proposed in [FUJ00]. With rapid progress in developing miniaturized RF components, faster and power efficient processors, antenna arrays can be quite feasible at mobile terminals, thus paving the way for the use of multiple antenna elements at both ends of the link.

The IEEE approved 802.11 standard for WLAN in June 1997 and the IEEE 802.11 was chosen as an International Standards Organization (ISO) in July 1997. The standard accommodates three different options for the physical layer: Frequency hopping spread spectrum (FHSS) with Gaussian frequency shift keying (GFSK), direct sequence spread spectrum (DSSS) with differential BPSK (DBPSK) and DSSS with DQPSK modulation. The IEEE 802.11 offers several data rates: 1, 2 5.5 and 11 MBPS operating in the 2.4 GHz industrial, scientific and medical (ISM) band. Between the two variations of 802.11a and 802.11b, the latter one is widely deployed in the USA.

8.7.2 Physical layer description

The physical layer (PHY) functionality is based on two basic protocol functions: physical layer convergence protocol (PLCP) and physical medium dependent protocol (PMD). The PLCP maps the MAC protocol data units (MPDU) into a framing format suitable for transmission in the channel using the associated PMD system. The MPDU is contained in the PLCP service data unit (PSDU) that is carried in the PHY protocol data unit (PPDU) of the PLCP frame. The PPDU is constructed from PLCP preamble, PLCP header and the PSDU. The preamble and the header contain control information and are transmitted at 1 MBPS with DBPSK modulation. The PSDU block operates at 1,2, 5.5 or 11 MBPS with DBPSK or DQPSK modulation.

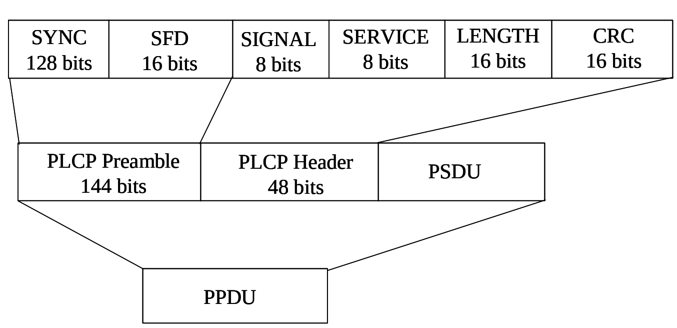

Figure 8.14. PLCP format

The PLCP preamble contain the following fields (see Figure 8.14):

1. Synchronization (SYNC): The SYNC field contains a 128-bit synchronization word created with a shift register with the scrambler polynomial $G(z) = z^{-7} + z^{-4} + 1$ operating on the seed sequence $[1101100]$.
2. Start frame delimiter (SFD): This field indicates the start of the PHY-dependent parameters within the PLCP preamble.

The PLCP header consists of the following four blocks:

1. Signal (SIGNAL): The 8-bit field indicates the type of modulation (along with rate) that is to be used with the PSDU. The date rate is derived by multiplying the SERVICE field value with 100 KBPS:
    a. X0A (msb to lsb) = 1 MBPS
    b. X14 (msb to lsb) = 2 MBPS
    c. X37 (msb to lsb) = 5.5 MBPS
    d. X6E (msb to lsb) = 11 MBPS
2. Service (SERVICE): Three bits (b_2, b_3 and b_4) of this 8-bit field are defined to support the high rate extension (Figure 8.15). The other bits are reserved for future use.

b_0	b_1	b_2	b_3	b_4	b_5	b_6	b_7

Figure 8.15. SERVICE field of PLCP frame.

3. Length (LENGTH): This field provides on the required transmission time (in microseconds) for the PSDU.
4. CRC: CRC is used to protect information in the SIGNAL, SERVICE and LENGTH fields using CCITT CRC-16 frame check sequence (FCS).

The 802.11 standard uses a data exchange mechanism between devices that is related to slotted-ALOHA. This is based on carrier sense multiple access with collision avoidance (CSMA-CA) where each device ‘listens’ for the presence of other devices through carrier sensing and transmits at given time slots only when the channel is free (no other device transmitting). If a collision occurs, retransmission occurs. A device sends a request-to-send (RTS) packet to the destination device and the destination device sends a clear-to-send (CTS) packet when it is ready to receive data. The RTS and CTS packets are derived from the PLCP frame (PCLP without

PSDU). When the source device receives CTS it starts transmission of the data packets (PCLP with PSDU).

This physical layer framing structure is suitable for supporting diversity applications. For example, the SYNC field is known to all the users and thus, can act as pilot or training sequence. Since the data exchange between the devices take place in slotted fashion in this protocol, the EGT algorithms or iterative algorithms in the MRT section (e.g., LMS or the subspace method) will take longer to converge depending upon traffic in the system. The higher the traffic, the longer it will take for one complete packet transmission (i.e., PLCP frame) because of collisions in the system. In such a case, mobility becomes more critical than in cellular type of systems. Fortunately, WLAN systems operate in quasi-stationary environment (people using their laptops or PDA) and convergence may not pose a big problem. These issues are less benign for LS algorithms since the channel can be estimated with the SYNC bits within one PLCP frame.

Feedback is not as straightforward in the 802.11 standard. The only place that can support feedback information is the reserved bits in the SERVICE field. These five bits can support phase index feedback in phase scanning or Bisection technique. These are inadequate for transmitting complex weight vector and some modifications may be needed in the PSDU to accommodate the feedback payload in this case.

This section treats the implementation of the proposed MIMO scheme (Chapter 7) in as much transparent manner as possible onto the IEEE 802.11b standard[1]. The PLCP frame is used to address the followings: i) utilization of bits from certain fields as pilot/training bits, ii) placement of feedback information, and iii) signaling method to incorporate the algorithm in this standard.

i) <u>Pilot Bits</u>: Two options are possible for choosing the pilots bits: use of SYNC field in the PLCP preamble or the use of address fields in the PSDU frame in the MAC layer. Assuming L = 8, phase scanning is applied on the synch word during the transmission of request to send (RTS) packet by arranging the 128 bits in to eight groups of 16 bits each and assigning each phase to

[1] This section is being worked as a full paper submission with Robert Max and Dr. Reed.

each of these of groups. Fig. 8.16 shows the required processing at the receiver to estimate the gain vector and thus θ_{max} from the phase-scanned synch word. Even though only one receiver chain can be used to synchronize with the synch word, the presence of another antenna provides a more robust synchronization process through selection between the two antennas (this is in fact verified in Chapter 7). The receiver uses information from both the antenna elements to select the received bits with higher signal strength, and, drives the synch correlator with this selected synch word. Meanwhile, the whole RTS packet received from the antenna elements are saved in a buffer for post-processing and computation of the optimal phase value. Once the correlator identifies the synch word it signals the buffer stage to process the stored synch word and derive the phase index associated with θ_{max}. The phase index is then converted to three equivalent bit representation and fed back to the transmitter in the clear to send (CTS) packet.

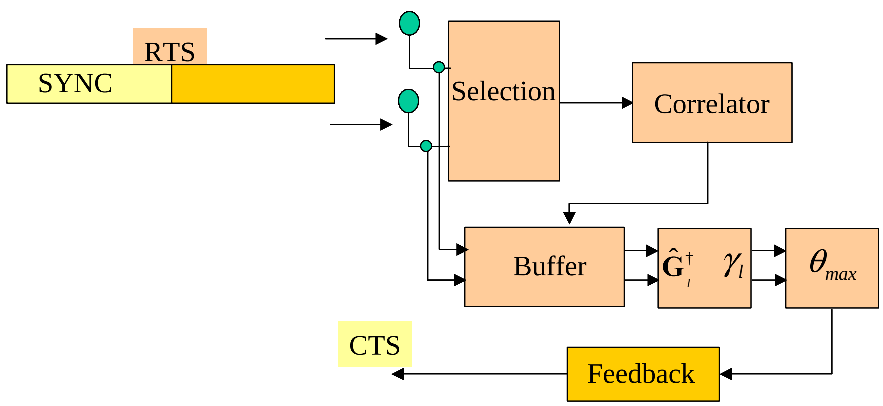

Fig 8.16. Processing at the receiver to derive feedback information.

The other option of deriving the optimal phase index is through the use of MAC PDU (MPDU) as shown in Fig. 8.17. The format of MPDU and the processing of this data unit at the receiver are illustrated in Figures 8.17a and 8.17b, respectively. The training bits are derived from the destination address in the address fields since the intended receiver knows the destination information in that field.

MPDU Header

	Frame Control	Duration /ID	Address 1	Address 2	Address 3	Sequence Control	Address 4	Frame Body	FCS
# bits:	16	16	48	48	48	16	48	0-18496	32

MAC Protocol Data Unit (MPDU)

Figure 8.17a. IEEE 802.11b MAC PDU

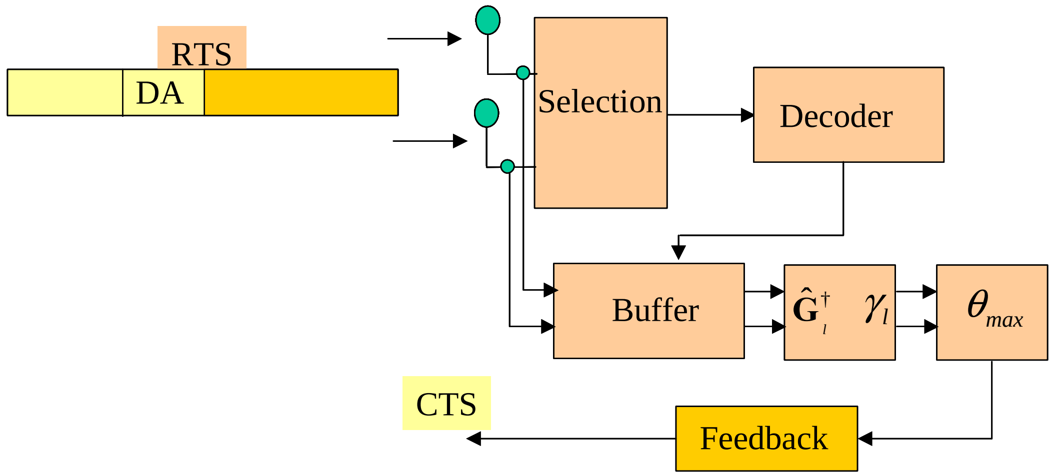

Figure 8.17b. Processing at the receiver to derive feedback information.

The transmitter employs phase scanning on the destination address bits by assigning each phase index to a group of 6 bits (assuming L = 8). The receiver generates soft decisions of the address fields in each antenna branch and a selection is made in favor of the decisions that have the higher signal strength. The selected address field information is decoded to generate the destination address information. Once the receiver validates that the MPDU is intended for it through the destination address, it signals post processing of the stored information to derive the gain vector estimate and subsequent estimation of the optimal phase index. The optimal phase index is then fed back to the transmitter.

ii) Feedback payload: In order to provide a level of transaction transparency, it is not possible to include the reply as part of the data payload transmitted by the devices. Furthermore, some packets contain no data, making this transport in both directions of the link difficult. The placement that was selected for this data is the service field in the PPDU as shown in Figure 8.18. Bits 4, 5, and 6, which are currently reserved on the IEEE 802.11b specifications, can be used to signal the correct phase to be used on the transmitter section of the MIMO system.

Recommended Change

Res.	Res.	Locked Clocks	Mod. Select	Res.	Res.	Res.	Length Bit Ext.

Figure 8.18. EEE 802.11b PLCP PPDU Service Field

iii) Signaling method: While the modifications are limited to the PLCP, the packets that were selected as the ones that would implement this algorithm were the RTS/CTS packets. The reason for the selection of these packets is that they signify the beginning of a data exchange between two devices, which would require the use of long packets. Once proper phase setting is identified through these packets, the trailing packets will benefit from the SNR improvement offered by the MIMO system. The signaling method that is suggested to provide the transparent implementation of the MIMO algorithm on an IEEE 802.11b device is as follows. Note that Device 1 is the MIMO "transmitter" and Device 2 is the MIMO "receiver".

- *Upon creation of RTS packet, modify the synchronization word of the PPDU such that eight separate blocks of 16 bits are transmitted with a separate phase. (Device 1)*
- *Upon receipt of the RTS packet, identify the phase index associated with the highest SNR. (Device 2)*
- *Create CTS packet with the PPDU service field bits 4 through 6 modified to signal the phase index value. (Device 2)*
- *Upon receipt of CTS, generate weight vector with feedback phase and apply it on the subsequent data packets. (Device 1)*
- *Upon receipt of CTS, generate weight vector with feedback phase and apply it on the subsequent data packets. Also, for every subsequent packet, modify the PPDU service field bits 4 through 6 to signal the phase index value that is desired for transmissions from Device 2. (Device 1)*
- *Upon correct receipt of the next data packet from Device 1, read the triplet in bits 4 through 6 of the service field of the PLCP PPDU and modify all subsequent acknowledgements to transmit at the corresponding phase. (Device 2)*

8.8 Conclusions

This chapter has studied the common air interface of the third generation W-CDMA standard and WLAN for implementation of the proposed diversity techniques. The implementations in WCDMA were discussed for transmit diversity techniques for both flat fading and frequency selective channels. The existing channel structure of the W-CDMA standard was found to be adequate to support the proposed schemes. The issues here are the length of pilot bits that act as the training sequence and the allowable number of bits in the DSCH that act as the source for accommodating feedback information. The amount of feedback required in the frequency selective channel case might limit transmit diversity application to low mobility environments. The physical layer of the WLAN standard allows long pilot sequence but feedback payload is limited. This implies that the proposed techniques can be feasible if the indoor channel is quasi-stationary, which is usually the case. The implementation of the proposed MIMO system is such a standard has been addressed in details.

Chapter 9

Selective nulling of dominant interferers (SNDI)

This chapter develops an analytical framework for characterizing the average symbol error rate and outage performance of a smart antenna system in cellular mobile radio environments. Specifically, the carrier to interference ratio statistics with N remaining (un-cancelled) "weakest" co-channel interference (CCI) signals from a total of N_I signals are derived given that both the desired user signal and the CCI signal amplitudes are subjected to Rayleigh, Rice, Nakagami-m or Nakagami-q fading. General expressions for the outage probability and the average symbol error rate performance of different digital modulation schemes in the presence of CCI signals are derived. Selected numerical results are presented to demonstrate the utility of the analysis in assessing the selective interference nulling performance in different fading environments.

9.1 Introduction

Smart antenna operations can be implemented either through adaptive beamforming or adaptive null steering. In the former approach, a beam is formed by shaping the antenna radiation pattern such that most of the energy is received from the desired user while steering nulls towards the co-channel interference (CCI) signals. Whereas in the adaptive null steering technique, the antenna gain pattern is shaped by placing deep nulls towards the CCI signals without significantly attenuating the desired user signal. Obviously, the objective of these two strategies is to improve the received carrier-to-interference ratio (CIR). These methods, however, place some constraints on the adaptive array with linear array processing algorithms in that an adaptive array with D elements can only effectively suppress at most (D-1) CCI signals. Often times, there may be residual interference signals as the number of CCI sources can be larger than the number of antenna elements for a practical array system. CCI suppression becomes even more challenging, as the antenna array needs to be small in size to conform to the form factor of a present day handset or mobile terminals. While some researchers are actively developing overloaded array processing algorithms [HIC01] to cope up with the above problems, computational complexity of the state-of-art algorithm may still be prohibitive for handset applications. In this paper, we study the theoretical performance of cellular radio networks that deploy an adaptive array to suppress a few dominant CCI signals using a linear array-processing algorithm. A mathematical framework is developed for deriving key statistical parameters such as the probability density function (pdf) and cumulative distribution function (cdf) of CIR as well as performance metrics including outage probability and average symbol error rate (ASER) of different digital modulation schemes.

Related studies on selective nulling of dominant interferers (SNDI) using smart antennas include [RAN95a], [RAN95b], [ALO99], [HAS00] and [ANN02]. The capacity of a narrowband TDMA system in which only the strongest CCI signal is cancelled is simulated in [RAN95a] and [RAN95b]. In [ALO99] and [HAS00], closed form expressions for the outage probability and average bit error rate of DPSK are derived with the assumption of independent and identically distributed (i.i.d) Rayleigh faded CCI signals, respectively. In [ALO99], the authors resort to the knowledge of the pdf of a sum ordered exponential random variables in closed-form [LIK62] in order to derive the outage probability of cellular mobile radio in interference-limited and minimum signal power constraint cases. While in [HAS00], they resort to the well-established result involving the sum of ordered exponential random variables as a linear combination of unordered exponential random variables [SUH37]-[ARN92]. In [ANN02], the authors extended the outage probability analysis in [ALO99] to i.i.d Nakagami-m faded CCI signals. Different from [ANN02], the main contribution of this paper is the derivation of generic formulas and closed-from expressions for the CIR statistics and their utility in the ASER and outage probability calculations in different fading environments. It is further noted that the analysis presented in [ANN02] does not facilitate ASER analysis of different digital modulation schemes.

9.2 CIR statistics

Consider a cellular mobile radio environment where a desired user cell is surrounded by total of N_I co-channel interfering cells in the first tier. Suppose the CCI signals are modeled as i.i.d. random variables $p_1, p_2, \ldots\ldots, p_{N_I}$, each with pdf $f(x)$ and cdf $F(x)$, and the receiver is able to selectively cancel out a few dominant interferers (i.e.,(N_I -N) strongest CCI signals) using an antenna array with (N_I –$N+1$) elements. As such, the resulting performance will be dictated by the sum of the remaining N “weakest” CCI signals, viz.,

$$I = \sum_{i=1}^{N} p_{i:N_I} \tag{9.1}$$

where $p_{i:N_I}$ denotes the i-th order statistic (obtained by arranging the CCI signal powers in ascending order of magnitude as $p_{1:N_I} \le p_{2:N_I} \le \ldots\ldots \le p_{N:N_I}$).

Notice that, in contrast to previous studies ([ALO99]- [HAS00]), both the desired user signal and the CCI signals can assume any common fading distributions. The only restriction that we impose here is that the CCI signals need to be i.i.d. for analytical tractability. Let us further denote the instantaneous received power for the desired user and interfering signals by p_d and p_i $\{i=1,2,..,N_I\}$ with the average values being $\overline{p}_d$ and $\overline{p}_i$, respectively ($\overline{p}_i$ being the same for all the CCI signals).

Suppose the CIR γ is defined as the ratio of p_d / I , service outage occurs when the operating CIR falls below a specified threshold or a protection ratio q, viz., $P_{out} = Pr\{\gamma < q\} = Pr\{p_d - qI < 0\}$. In the following, we will derive the pdf of CIR by utilizing a generic expression for the mgf $\phi_I(.)$ derived in [ANN02].

A. Generic Solution for $f_I(.)$

It is shown in [ANN01a] that calculating the outage probability of mobile cellular radio systems with a random number of interfering signals requires only the knowledge of the mgf of I and the desired user signal. Since a closed-form formula for the mgf of the desired signal is available when the signal amplitude is subject to flat Rayleigh, Rice, Nakagami-m or Nakagami-q fading (see Table 9.1), it is imperative to derive the mgf of I to compute the statistics of γ.

Table 9.1. pdf and *n*-th order derivative of the mgf of the signal power, $k \in \{d, i\}$ [ANN01a]

Channel Model	pdf and the *n*-th order derivative of the mgf of the signal power
Rayleigh	$f_k(x) = \frac{1}{\bar{p}_k} \exp\left(\frac{-x}{\bar{p}_k}\right), x \geq 0$ $\phi_k^{(n)}(s) = \frac{(-\bar{p}_k)^n n!}{(1+s\bar{p}_k)^{1+n}}$
Rician	$f_k(x) = \frac{(1+K_k)}{\bar{p}_k} \exp\left[-K_k - \frac{(1+K_k)x}{\bar{p}_k}\right] I_0\left[2\sqrt{\frac{K_k(1+K_k)x}{\bar{p}_k}}\right], x \geq 0, K_k \geq 0$ $\phi_k^{(n)}(s) = \frac{(-\bar{p}_k)^n (n!)^2 (1+K_k)}{(1+K_k+s\bar{p}_k)^{1+n}} \exp\left[\frac{-s\bar{p}_k K_k}{1+K_k+s\bar{p}_k}\right] \sum_{i=0}^{n} \frac{1}{(n-i)!(i!)^2} \left(\frac{K_k(1+K_k)}{1+K_k+s\bar{p}_k}\right)^i$
Nakagami-m	$f_k(x) = \frac{1}{\Gamma(m_k)} \left(\frac{m_k}{\bar{p}_k}\right)^{m_k} x^{m_k-1} \exp\left(\frac{-m_k x}{\bar{p}_k}\right), x \geq 0, m_k \geq \frac{1}{2}$ $\phi_k^{(n)}(s) = \frac{(-\bar{p}_k)^n m_k^{m_k} \Gamma(m_k+n)}{(m_k+s\bar{p}_k)^{m_k+n} \Gamma(m_k)}$
Nakagami-q	$f_k(x) = \frac{1}{\bar{p}_k\sqrt{1-b_k^2}} \exp\left[-\frac{x}{(1-b_k^2)\bar{p}_k}\right] I_0\left[\frac{b_k x}{(1-b_k^2)\bar{p}_k}\right], x \geq 0 \ \lvert b_k \rvert \leq 1$ $\phi_k^{(n)}(s) = \frac{n!}{2^{2n}\sqrt{[1+s\bar{p}_k(1+b_k)][1+s\bar{p}_k(1-b_k)]}} \left[\frac{-\bar{p}_k(1+b_k)}{1+s\bar{p}_k(1+b_k)}\right]^n$ $\times \sum_{w=0}^{n} \frac{(2w)![2(n-w)]!}{(w)!(n-w)!} \left[\frac{(1-b_k)[1+s\bar{p}_k(1+b_k)]}{(1+b_k)[1+s\bar{p}_k(1-b_k)]}\right]^w$

Notice that the computation of the mgf of I, $\phi_I(.)$, in [ANN01a] is relatively easy because the problem reduces to computing the mgf of unordered CCI signals. In our case, we need to compute the sum of $p_{1:N_I}, p_{2:N_I}, \ldots\ldots, p_{N:N_I}$ for $N < N_I$, which are not independent. Fortunately, simple solution for this is available for the special case of i.i.d. CCI signals [ANN02], viz.,

$$\begin{aligned} \phi_I(s) &= N!\binom{N_I}{N}\int_0^\infty e^{-sx_N}\left[1-F(x_N)\right]^{N_I-N} f(x_N)\int_0^{x_N} e^{-sx_{N-1}} f(x_{N-1})\cdots\int_0^{x_2} e^{-sx_1} f(x_1)\,dx_1 dx_2\ldots dx_N \\ &= N\binom{N_I}{N}\int_0^\infty e^{-sx_N}\left[1-F(x_N)\right]^{N_I-N} f(x_N)\left[H(s,x)\right]^{N-1} dx_N \end{aligned} \tag{9.2}$$

where $0 < x_1 < x_2 < \ldots\ldots < \infty$, and the marginal mgf for each of the CCI signal powers is defined as $H(s,y) = \int_0^y e^{-sx} f(x)\,dx$.

In arriving to (9.2), we have made use of the integral identity,

$$\int_0^{x_N} e^{-sx_{N-1}} f(x_{N-1}) \cdots \int_0^{x_2} e^{-sx_1} f(x_1)\,dx_1 dx_2 \ldots dx_{N-1} = \frac{1}{(N-1)!}\left(\int_0^{x_N} e^{-sx} f(x)\,dx\right)^{N-1}, N \geq 2 \quad (9.3)$$

A proof of (9.3) using the principle of mathematical induction is provided in the Appendix C1. It is evident from the second line of (9.2) that $\phi_I(s)$ can be computed easily by evaluating a single integral point-by-point wise instead of an *N*-fold nested integral. The net result is a significant reduction in the computational complexity for $\phi_I(s)$, and this is attributed to (9.3) and to the availability of a closed-form formula for the marginal mgf of signal power for all common fading distributions. The closed-form expressions for $H(s,x)$ in different fading environments are summarized in Appendix C2 for completeness. Furthermore, the cdf $F(.)$ in (9.2) may be computed directly from the marginal mgf as $F(x) = H(0,x)$.

It will be shown in Section 9.2B that the pdf of *I*, $f_I(x)$, is also needed to facilitate the derivation CIR statistics. Using [BEU90, eq. (37)], we obtain the desired pdf as

$$\begin{aligned} f_I(x) &= \frac{1}{2\pi}\int_{-\infty}^{\infty} \phi_I(-j\omega) e^{-j\omega x} d\omega \\ &\cong \frac{4}{T}\sum_{\substack{n=1 \\ n\ odd}}^{\infty} \mathrm{Re}\left[\phi_I\left(\frac{-j2\pi n}{T}\right)\exp\left(\frac{-j2\pi n x}{T}\right)\right] \end{aligned} \quad (9.4)$$

where $j = \sqrt{-1}$, the coefficient *T* is selected sufficiently large such that $\Pr(x > T) \leq \varepsilon$ and ε can be set a relatively small value.

Before concluding this subsection, we would like to point out that (9.2) can be evaluated in closed-form if $p_1, p_2, \ldots\ldots, p_{N_I}$ are i.i.d. exponential or Gamma variates. Assuming that the amplitudes of the CCI signals are subject to Nakagami-m fading with a positive integer fading severity index *m*, it is not difficult to show that (9.2) reduces to (9.5) [ANN02]:

$$\phi_I(s) = \frac{N}{\Gamma(m_i)}\binom{N_I}{N}\sum_{n=0}^{(N_I-N)(m_i-1)}\beta(n, N_I-N, m_i)\left(\frac{m_i}{\bar{p}_i}\right)^{n+Nm_i}\sum_{v=0}^{N-1}(-1)^v\binom{N-1}{v}\sum_{k=0}^{v(m_i-1)}\beta(k,v,m_i)$$
$$\times\frac{\Gamma(m_i+n+k)}{\left(s+\frac{m_i}{\bar{p}_i}\right)^{m_i(N-1)-k}\left[s(v+1)+\frac{m_i}{\bar{p}_i}(N_I-N+v+1)\right]^{m_i+n+k}} \tag{9.5}$$

where the coefficients $\beta(.,.,..)$ may be computed as

$$\beta(z,k,c) = \sum_{i=z-c+1}^{z}\frac{\beta(i,k-1,c)}{(z-i)!}I_{[0,(k-1)(c-1)]}(i) \tag{9.6}$$

where, $I_{[a,b]}(i) = \begin{cases}1 & a \le i \le b\\ 0 & otherwise\end{cases}$, $\beta(0,0,c) = \beta(0,k,c) = 1$, $\beta(z,1,c) = \frac{1}{z!}$, and $\beta(1,k,c) = k$. A closed-form expression for $f_I(x)$ can also be obtained from (9.5) by first expanding $\phi_I(s)$ using partial fractions and then performing an inverse Laplace transformation of the resultant terms. These results are omitted here for brevity. Nevertheless, they are also reported in [ANN02].

B. Derivation of pdf of CIR, $f_\gamma(.)$

In this subsection, we will derive an infinite series as well as closed-form formulas for the pdf of CIR. Since $\gamma = p_d / I$, it follows directly that

$$f_\gamma(\gamma) = \int_0^\infty x f_d(\gamma x) f_I(x)\,dx = \frac{1}{\gamma^2}\int_0^\infty u f_d(u) f_I\left(\frac{u}{\gamma}\right)du \tag{9.7}$$

where, $f_d(.)$ deontes the pdf of the desired user signal.

B.1 Generic Solution for $f_\gamma(.)$

Substituting (9.4) into (9.7), we obtain

$$f_\gamma(\gamma) \cong \frac{-4}{T\gamma^2}\sum_{\substack{n=1\\ n\ odd}}^{\infty}\mathrm{Re}\left[\phi_I\left(\frac{-j2\pi n}{T}\right)\phi_d^{(1)}\left(\frac{j2\pi n}{T\gamma}\right)\right] \tag{9.8}$$

where $\phi_d^{(1)}\left(\frac{j2\pi n}{T\gamma}\right) = \frac{d}{ds}\phi_d(s)\Big|_{s=\frac{j2\pi n}{T\gamma}}$ denotes the first-order derivative of the mgf of the desired signal power with respect to *s*, and then evaluated at $\left(\frac{j2\pi n}{T\gamma}\right)$. Closed-form formulas for $\phi_d^{(1)}(\cdot)$ are available for all common fading channel models and they are also summarized in Table I.

B.2 Closed-Form Expression for $f_\gamma(.)$

By exploiting the closed-form expressions for $f_I(x)$ derived in [ANN02] while the signals are i.i.d. exponential or Nakagami-m distributed (positive integer fading index), it is possible to simplify (9.7) into a closed-form formula. These results are summarized below:

$$f_\gamma(\gamma) = \frac{1}{\Gamma(m_i N_I)}\left(\frac{-m_i}{\overline{p}_i\gamma}\right)^{m_i N_I}\frac{1}{\gamma}\phi_d^{(m_i N_I)}\left(\frac{m_i}{\overline{p}_i\gamma}\right), \quad N = N_I \tag{9.9}$$

$$f_\gamma(\gamma) = \frac{N_I}{\Gamma(m_i)}\sum_{n=0}^{(N_I-1)(m_i-1)}\frac{\beta(n, N_I-1, m_i)}{\gamma^{m_i+n+1}}\left(-\frac{m_i}{\overline{p}_i}\right)^{n+m_i}\phi_d^{(n+m_i)}\left(\frac{m_i N_I}{\overline{p}_i\gamma}\right), \quad N=1 \tag{9.10}$$

$$\begin{aligned} f_\gamma(\gamma) = {} & \frac{N}{\Gamma(m_i)}\binom{N_I}{N}\sum_{n=0}^{(N_I-N)(m_i-1)}\beta(n, N_I-N, m_i)\left(\frac{m_i}{\overline{p}_i}\right)^{n+Nm_i}\sum_{v=0}^{N-1}(-1)^v\binom{N-1}{v}\sum_{k=0}^{v(m_i-1)}\beta(k,v,m_i)\frac{\Gamma(m_i+n+k)}{(v+1)^{m_i+n+k}} \\ & \times\left\{\sum_{r=1}^{m_i(N-1)-k}\frac{A_r}{\Gamma(r)}\frac{(-1)^r}{\gamma^{r+1}}\phi_d^{(r)}\left(\frac{m_i}{\overline{p}_i\gamma}\right) + \sum_{r=1}^{m_i+n+k}\frac{B_r}{\Gamma(r)}\frac{(-1)^r}{\gamma^{r+1}}\phi_d^{(r)}\left(\frac{m_i(N_I-N+v+1)}{\overline{p}_i(v+1)\gamma}\right)\right\}, \quad 1<N<N_I \end{aligned} \tag{9.11}$$

where

$$A_r = \binom{m_i N+n-r-1}{m_i+n+k-1}\frac{(-1)^{m_i(N-1)-k-r}}{\left[\frac{m_i}{\overline{p}_i}\left(\frac{N_I-N}{v+1}\right)\right]^{m_i N+n-r}}$$

$$B_r = \binom{m_i N+n-r-1}{m_i(N-1)-k-1}\frac{(-1)^{m_i(N-1)-k}}{\left[\frac{m_i}{\overline{p}_i}\left(\frac{N_I-N}{v+1}\right)\right]^{m_i N+n-r}}$$

To the best of our knowledge, all of the above results are new.

9.3 Outage probability

The outage probability is an important metric in analyzing the performance of cellular mobile radio systems. The outage probability can be obtained by simply computing the cdf of γ at a specified threshold γ_{th}:

$$P_{out}(N, N_I) = \int_0^{\gamma_{th}} f_\gamma(y)\,dy = F_\gamma(\gamma_{th}) \tag{9.12}$$

Alternatively, the outage probability can be evaluated as

$$P_{out}\left(N,N_I\right)=\Pr\left\{\gamma=\frac{p_d}{\sum_{i=1}^{N}p_{i:N_I}}<\gamma_{th}\right\}=\int_0^{\infty}f_d\left(p_d\right)\int_{\frac{p_d}{\gamma_{th}}}^{\infty}f_I\left(y\right)dydp_d \qquad (9.13)$$

A. Generic Solution for the Outage Probability

Substituting (9.4) into (9.13) and noting that $F_I\left(x\right)=\frac{1}{2}-\frac{2}{\pi}\sum_{\substack{n=1\\ n\ odd}}^{\infty}\frac{1}{n}\mathrm{Im}\left[\phi_I\left(\frac{-j2\pi n}{T}\right)e^{-\frac{j2\pi nx}{T}}\right]$, we obtain a generic infinite series expression for computing the outage probability, viz.,

$$P_{out}(N,N_I)\cong\frac{1}{2}+\frac{2}{\pi}\sum_{\substack{n=1\\ n\ odd}}^{\infty}\frac{1}{n}\mathrm{Im}\left[\phi_I\left(\frac{-j2\pi n}{T}\right)\phi_d\left(\frac{j2\pi n}{T\gamma_{th}}\right)\right] \qquad (9.14)$$

B. Closed-Form Solutions for the Outage Probability

It is also possible to derive a closed-form formula for the probability of outage when the i.i.d CCI signals are subject to Nakagami-m fading (positive integer fading index). Substituting (9.9), (9.10) and (9.11) into (9.12), we obtain the following expressions:

$$P_{out}\left(N_I,N_I\right)=\sum_{k=0}^{m_iN_I-1}\frac{1}{k!}\left(\frac{-m_i}{\overline{p}_i\gamma_{th}}\right)^k\phi_d^{(k)}\left(\frac{m_i}{\overline{p}_i\gamma_{th}}\right),\quad N=N_I \qquad (9.15)$$

$$P_{out}\left(1,N_I\right)=\frac{N_I}{\Gamma\left(m_i\right)}\sum_{n=0}^{(N_I-1)(m_i-1)}\beta\left(n,N_I-1,m_i\right)\frac{\Gamma\left(m_i+n\right)}{N_I^{m_i+n}}\sum_{k=0}^{m_i+n-1}\frac{1}{k!}\left(-\frac{m_iN_I}{\overline{p}_i\gamma_{th}}\right)^k\phi_d^{(k)}\left(\frac{m_iN_I}{\overline{p}_i\gamma_{th}}\right),\ N=1 \qquad (9.16)$$

$$\begin{aligned}P_{out}\left(N,N_I\right)=&\frac{N}{\Gamma\left(m_i\right)}\binom{N_I}{N}\sum_{n=0}^{(N_I-N)(m_i-1)}\beta\left(n,N_I-N,m_i\right)\left(\frac{m_i}{\overline{p}_i}\right)^{n+Nm_i}\\ &.\sum_{v=0}^{N-1}(-1)^v\binom{N-1}{v}\sum_{k=0}^{v(m_i-1)}\beta\left(k,v,m_i\right)\frac{\Gamma\left(m_i+n+k\right)}{(v+1)^{m_i+n+k}}\\ &.\left\{\begin{array}{l}\sum_{r=1}^{m_i(N-1)-k}A_r\left(\frac{\overline{p}_i}{m_i}\right)^r\sum_{z=0}^{r-1}\frac{1}{z!}\left(-\frac{m_i}{\overline{p}_i\gamma_{th}}\right)^z\phi_d^{(z)}\left(\frac{m_i}{\overline{p}_i\gamma_{th}}\right)\\ +\sum_{r=1}^{m_i+n+k}B_r\left(\frac{\overline{p}_i\left(v+1\right)}{m_i\left(N_I-N+v+1\right)}\right)^r\sum_{z=0}^{r-1}\frac{1}{z!}\left(\frac{-m_i\left(N_I-N+v+1\right)}{\overline{p}_i\left(v+1\right)\gamma_{th}}\right)^z\phi_d^{(z)}\left(\frac{m_i\left(N_I-N+v+1\right)}{\overline{p}_i\left(v+1\right)\gamma_{th}}\right)\end{array}\right\},1<N<N_I\end{aligned} \qquad (9.17)$$

It is important to note that above expressions are obtained at once (by observation) using identity

$$I_r\left(\beta,a\right)=\int_0^{\beta}\frac{(-1)^r}{\gamma^{r+1}}\phi_d^{(r)}\left(\frac{a}{\gamma}\right)d\gamma=\frac{1}{(-a)^r}\int_{\frac{a}{\beta}}^{\infty}y^{r-1}\phi_d^{(r)}\left(y\right)dy=\frac{(r-1)!}{a^r}\sum_{k=0}^{r-1}\frac{1}{k!}\left(-\frac{a}{\beta}\right)^k\phi_d^{(k)}\left(\frac{a}{\beta}\right)$$

where integer $r \geq 1$. In contrast, identical results were obtained in [ANN02] by exploiting the fact that $F_I(.)$ is of the form $1-\sum y^k e^{-y}$, and therefore $P_{out}(N, N_I)$ is expressed in terms of the derivatives of $\phi_d(s)$ through the use of the Laplace derivative formula:

$$\int_0^\infty y^k e^{-ay} f_d(y) dy = (-1)^k \frac{d^k}{ds}\left[\phi_d(s)\right]\Big|_{s=a} = (-1)^k \phi_d^{(k)}(a)$$

As a sanity check, the accuracies of the derivations for (9.15),(9.16),(9.17) have been verified with (9.14), and the results are in perfect agreement.

9.4 ASER Analysis

In this section we develop the analytical expressions for computing the ASER of cellular radio systems equipped with smart antennas (to suppress a few dominant interferers). In general, the ASER of a digital modulation scheme in wireless channels can be evaluated by averaging its conditional error probability $P_s(\gamma)$ (i.e., performance in AWGN channel) over the pdf of $f_\gamma(.)$, viz.,

$$\overline{P}_S = \int_0^\infty P_s(\gamma) f_\gamma(\gamma) d\gamma \tag{9.18}$$

Now, substituting (9.8) into (9.18), we obtain

$$\overline{P}_s \cong \frac{-4}{T} \sum_{\substack{n=1 \\ n\ odd}}^{\infty} \mathrm{Re}\left[\phi_I\left(\frac{-j2\pi n}{T}\right) \int_0^\infty \frac{1}{\gamma^2} P_s(\gamma) \phi_d^{(1)}\left(\frac{j2\pi n}{T\gamma}\right) d\gamma\right] \tag{9.19}$$

Further simplifications of (9.19) for the most general fading environments do not appear possible. However, when $P_s(\gamma)$ takes the form of $Ae^{-B\gamma}$ (A and B are scalars) and the desired user signal is subject to Rayleigh or Nakagami-m faded, (9.19) can be simplified as:

$$\overline{P}_s = \frac{-2A\Gamma(m_d+1)}{\pi} \sum_{\substack{n=1 \\ n\ odd}}^{\infty} \frac{1}{n} \mathrm{Im}\left[\phi_I\left(\frac{-j2\pi n}{T}\right) U\left(m_d, 0, \frac{j2\pi n B\overline{p}_d}{Tm_d}\right)\right] \tag{9.20}$$

Besides routine mathematical manipulations, we have also made use of the identity $\int_0^\infty \frac{e^{-px} x^{q-1}}{(1+ax)^\nu} dx = \frac{\Gamma(q)}{a^q} U\left(q, q+1-\nu; \frac{p}{a}\right)$ [ABR70] to arrive at (9.20) where $U(a,b,z)$ is the confluent hypergeometric function defines as $U(a,b,z) = \frac{1}{\Gamma(a)} \int_0^\infty e^{-zt} t^{a-1} (1+t)^{b-a-1} dt$. This special function can be evaluated efficiently using the generalized hypergeometric function as $U(a,b,z) = z^{-a}\,{}_2F_0(a, 1+a-b;\,;-1/z)$ or via its finite range integral representation as $U(a,b,z) = \frac{2}{\Gamma(a)} \int_0^{\frac{\pi}{2}} e^{-z\tan^2\theta} (\tan\theta)^{2a-1} (\sec\theta)^{2(b-a)}\, d\theta$.

Moreover, when both the desired user and the CCI signals are subject to Rayleigh or Nakagami-m fading (positive integer m_i and real $m_d \geq 0.5$), it is possible to derive a closed-form formula for the mgf of γ by taking the Laplace transformation of (9.9), (9.10) or (9.11) and using identity [ABR70, (13.2.5)]. The resulting expressions are summarized below:

$$\phi_\gamma(s) = \frac{\Gamma(m_d + m_i N_I)}{\Gamma(m_i N_I)} \quad U\left(m_d, 1 - m_i N_I, \frac{m_i \tilde{\gamma} s}{m_d}\right),\ N = N_I \tag{9.21}$$

$$\phi_\gamma(s) = \frac{N_I}{\Gamma(m_i)} \sum_{n=0}^{(N_I-1)(m_i-1)} \frac{\beta(n, N_I - 1, m_i)}{N_I^{\,m_i+n}} \Gamma(m_d + m_i + n) U\left(m_d, 1 - m_i - n, \frac{m_i N_I \tilde{\gamma}}{m_d} s\right),\ N = 1 \tag{9.22}$$

$$\begin{aligned}\phi_\gamma(s) = {} & \frac{N}{\Gamma(m_i)} \binom{N_I}{N} \sum_{n=0}^{(N_I-N)(m_i-1)} \beta(n, N_I - N, m_i) \left(\frac{m_i}{\overline{p}_i}\right)^{n+Nm_i} \sum_{v=0}^{N-1} (-1)^v \binom{N-1}{v} \sum_{k=0}^{v(m_i-1)} \beta(k, v, m_i) \frac{\Gamma(m_i + n + k)}{(v+1)^{m_i+n+k}} \\ & \times \left\{ \begin{array}{l} \displaystyle\sum_{r=1}^{m_i(N-1)-k} \frac{A_r}{\Gamma(r)} \frac{(\overline{p}_d)^r}{(m_i\tilde{\gamma})^r} \Gamma(m_d + r) U\left(m_d, 1-r, \frac{m_i \tilde{\gamma}}{m_d} s\right) \\ \displaystyle + \sum_{r=1}^{m_i+n+k} \frac{B_r}{\Gamma(r)} \frac{(\overline{p}_d)^r}{\left(\frac{m_i(N_I - N + v + 1)\tilde{\gamma}}{(v+1)}\right)^r} \Gamma(m_d + r) U\left(m_d, 1-r, \frac{m_i(N_I - N + v + 1)\tilde{\gamma}}{m_d(v+1)} s\right) \end{array} \right\},\ 1 < N < N_I \end{aligned} \tag{9.23}$$

where $\tilde{\gamma} = \frac{\overline{p}_d}{\overline{p}_i}$.

It is interesting to note that the above expressions can be used for ASER analysis of a broad range of digital modulation schemes using the mgf approach [SIM98]- [ANN01b]. For example, the ASER performance of coherent M-ary PSK modulation scheme in conjunction of a SNDI receiver is given by

$$\overline{P}_s = \frac{1}{\pi} \int_0^{\pi - \frac{\pi}{M}} \phi_\gamma\left(\frac{\sin^2(\pi/M)}{\sin^2\theta}\right) d\theta \tag{9.24}$$

It is also straightforward to extend this to other binary and M-ary modulation schemes. They are omitted here for brevity. It is also validated that the ASER curves generated using (9.19), (9.20) and (9.24) are in good agreement.

9.5 Computational Results

In this section, selected numerical results are presented to highlight the benefits of SNDI in cellular mobile radio systems. These results include a study on the dependence of CIR statistics on N and fading distributions as well as the assessment of outage probability and ASER of digital modulation schemes in the presence of CCI signals. Throughout this section we have assumed that the total number of CCI signals from the first tier is N_I = 6. Clearly the use of cell sectorization will reduce N_I; for example, with 120^0 sectorization, N_I becomes 2.

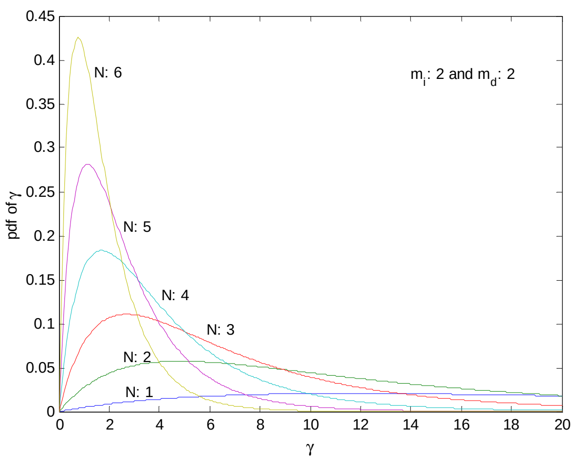

(a)

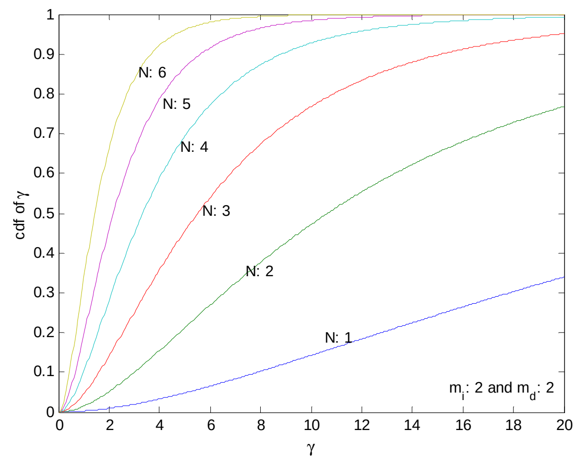

(b)

Figure 9.1. Statistics of CIR for different values of N (a) pdf plots, (b) cdf plots.

A family of curves for the pdf and cdf of γ with N as a parameter is plotted in Figures 9.1 (a) and 1(b), respectively. Figure 9.1(a) reveals that with an increase in number of antenna elements (or a corresponding decrease in N), the pdf curves become less skewed and flatter, which translates into an improvement in the mean CIR value. Figure 9.1(b) depicts the benefits of SNDI in the outage probability performance. It is clear that the outage probability $F_{\gamma}\left(\gamma_{th}\right)$ drops significantly as more dominant interferers are suppressed.

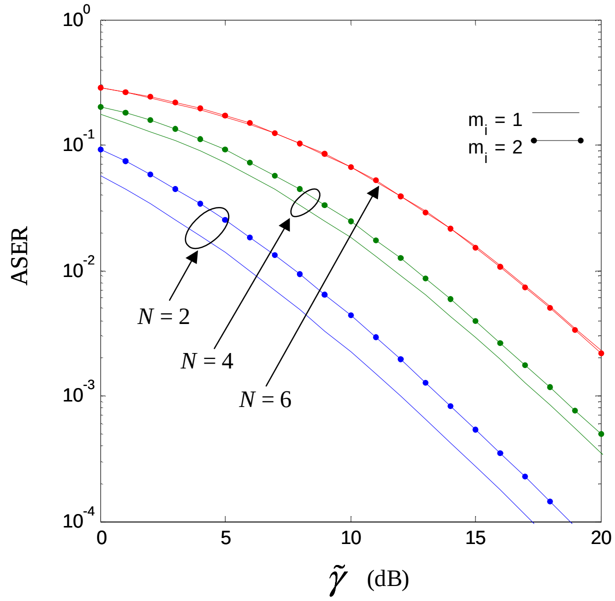

Figure 9.2. Plots of ASER for coherent BPSK signal for N = 2, 4 and 6; m_d = 2 and $m_i \in$ {1,2}.

Figure 9.2 shows the ASER plots for a coherent BPSK case for N= 2, 4, and 6 with m_d = 2 and $m_i \in \{1,2\}$. Two important observations can be made from the plots: (a) substantial performance gain can be achieved with nulling of dominant CCI signals; and (b) the influence of CCI fading index on the system performance becomes more prominent when more interferers are cancelled. For example, at ASER $=10^{-3}$, the gain achieved is at least 8 dB when four out of six interferers are cancelled. Even canceling out two interferers (N = 4) provides about 3 dB gain over the no-cancellation scenario. The effect of m_i on the ASER performance becomes more prominent with decreasing N as can be seen from the larger spread between the curves corresponding to different fading indices. This in turn suggests that the fading distributions do influence the ASER performance of a cellular mobile radio system equipped with smart antenna. When the CCI signals are subject to Rayleigh fading (m_i = 1), the ASER performance with SNDI is the most improved compared to the other values of m_i. This is expected, since higher values of m_i are associated with less severe fading on the CCI signals and the net result being a more adverse interference on the desired signal.

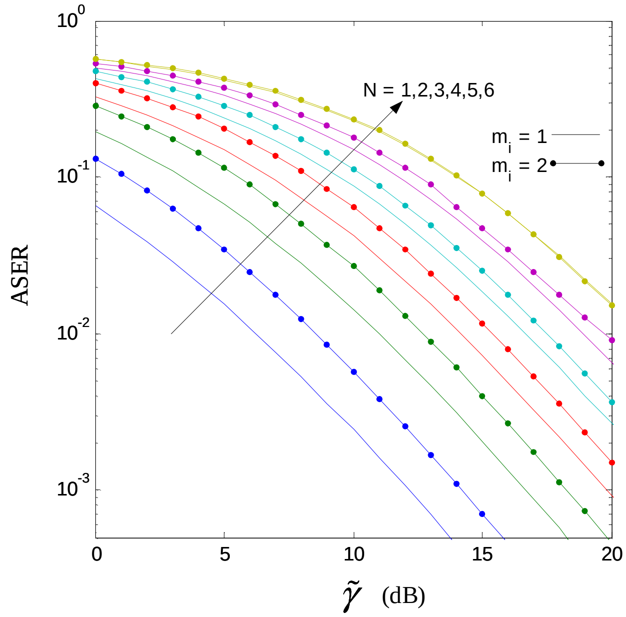

Figure 9.3. Plots of ASER for QPSK signal for N = 1 to 6; m_d =2 and $m_i \in$ {1,2}.

Figure 9.3 demonstrates the ASER performance for QPSK (M-ary constellation) modulation in a Nakagami-m channel with m_d = 2 and $m_i \in \{1,2\}$ for different values of N. The trends observed in Fig. 2 are also apparent in this figure.

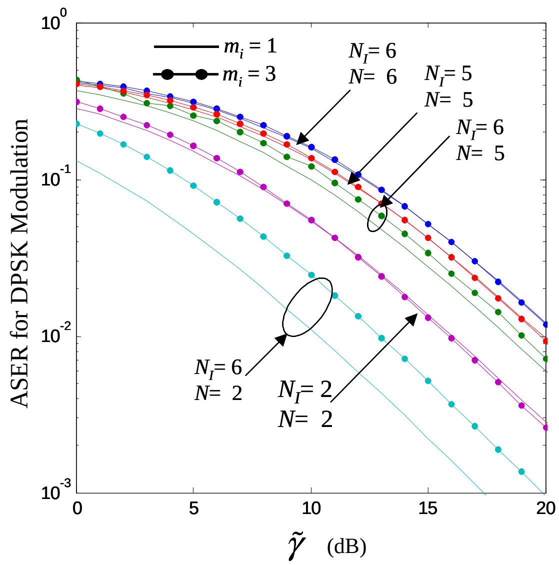

Figure 9.4. ASER performance plots for DPSK modulation for different $N_I \in$ {6,2}, $m_i \in$ {1,3}

Figure 9.4 shows a family of ASER curves for DPSK modulation assuming Nakagami-m faded desired user and CCI signals. The fading indices for the desired user and the CCI signals are chosen as m_d =2 and $m_i \in \{1,3\}$. The benefits of SNDI are evident even when the dominant CCI signal (at any given instant) is cancelled (N_I= 6, N=5) compared to a system where a CCI signal is cancelled in random (N_I = 5, N=5). The benefits become more prominent as more dominant interferers are suppressed (N_I = 6, N= 2) compared to arbitrarily canceling the CCI signals (N_I = 2, N=2). However, the relative improvement (i.e., discrepancy between these curves) diminishes as the fading index m_i gets larger.

In Section 9.3, we have derived analytical expressions for computing the probability of outage by assuming that all of the co-channel interferers N_I are active all the time, and therefore $L = N_I$ is fixed, where L denotes the number of active CCI signals. In practice, however, not all the CCI signals will be active at any given time. This is particularly true if the offered traffic load in the co-channel cells is not heavy or when a discontinuous transmission scheme is implemented to improve the spectral efficiency. Outage calculation in these situations can be shown to be [STU96],

$$P_{out} = \sum_{L=D}^{N_I} \binom{N_I}{L} B^{\frac{L}{N_c}} \left(1 - B^{\frac{1}{N_c}}\right)^{N_I - L} P_{out}(L - D + 1, L) \qquad (9.25)$$

where D denotes the number of antenna elements and N_c is different frequency voice channels with blocking probability B.

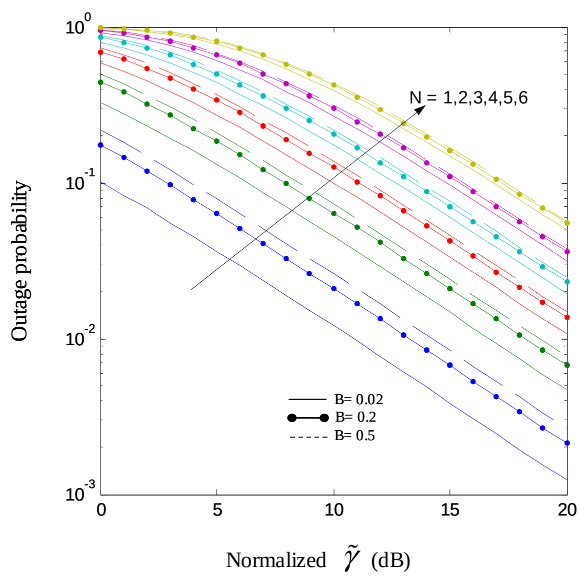

Figure 9.5(a). Outage probability plots with $\tilde{\gamma}/\gamma_{th}$ for random number of CCI signals. Desired user Rician distributed with K_d =0, interferers Nakagami-m with m_i = 2.

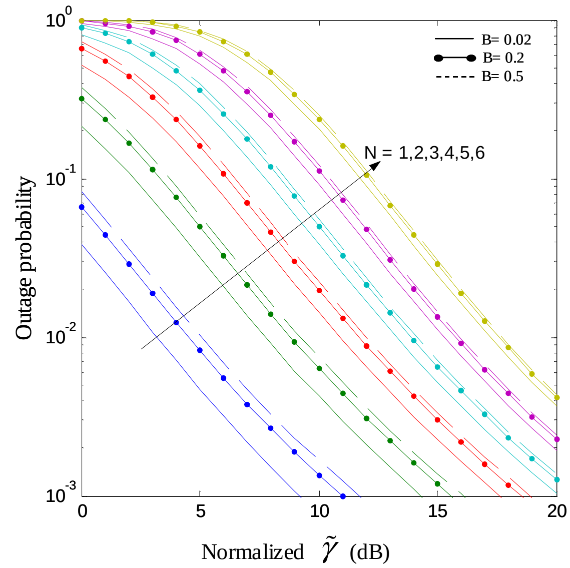

Figure 9.5(b). Outage probability plots with $\tilde{\gamma}/\gamma_{th}$ for random number of CCI signals. Desired user Rician distributed with K_d = 5, interferers Nakagami-m with m_i = 2.

Using (9.15)-(9.17) and (9.25), a family of curves is plotted in Figs. 5 (a) and (b) that show the effect of blocking probability on the outage probability performance. We have assumed that the desired signal amplitude is Rayleigh (K_d = 0) or Rician (K_d = 5) faded and the CCI signals are Nakagami-m faded with m_i = 2. The impact of B is negligible when the system is interference limited and its effect becomes more prominent as more dominant interferers are suppressed. However the spread between the different blocking probability curves tend to be relatively insensitive to the fading parameter of the desired user.

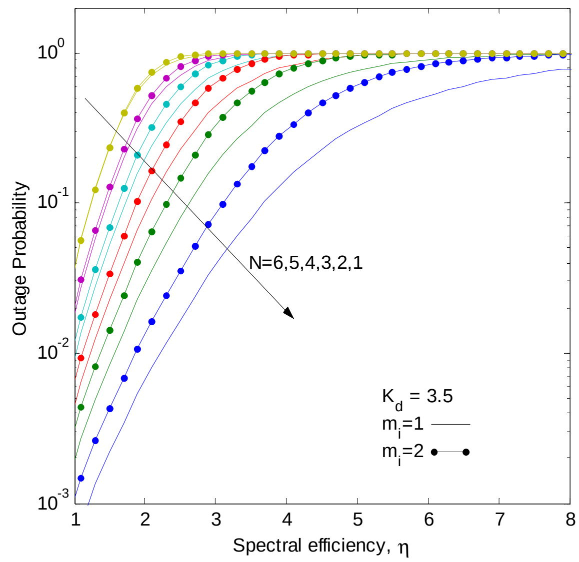

Figure 9.6. Plots of outage probability vs. spectral efficiency for different values of N and m_i.

Figure 9.6 shows the effect of spectral efficiency on the outage probability of a cellular system employing SNDI. Spectral efficiency is of primary concern to cellular system planners, and is measured in terms of the spatial traffic density per unit bandwidth. In a cellular system with a uniform deployment of hexagonal cells, the spectral efficiency is given by [PRA98]

$$\eta = \frac{G_c}{N_c W_c C A_{cell}} \text{ Erlang/MHz/km}^2 \tag{9.26}$$

where G_c is defined as the offered traffic per cell, N_c corresponds to the number of channels per cell, W_c is the bandwidth per channel (MHz), C denotes the cluster size and A_{cell} is the area per cell (km^2). Using geometric arguments, we can show that $A_{cell} = 3\sqrt{3}R^2/2$ and the co-channel reuse factor R_f is related to the cluster size C as $R_f = D/R = \sqrt{3C}$ for a regular hexagonal cell deployment while R is the distance from the center to the corner of a cell (i.e., cell radius) and D denotes the co-channel reuse distance (distance between the centers of the nearest neighboring co-channel cells). Considering a two-slope path loss model, [PRA98] has shown that $\overline{p}_d / \overline{p}_i$ in the worst-case scenario (in which the desired user is near the edge of its cell and the interfering users are on the cell edges closest to the desired user cell) is given by

$$\frac{\overline{p}_d}{\overline{p}_i} = \left(\frac{D-R}{R}\right)^a \left(\frac{1+(D-R)/g}{1+R/g}\right)^b = \left(R_f - 1\right)^a \left(\frac{g/R + R_f - 1}{g/R + 1}\right)^b \tag{9.27}$$

where a and b are the path loss exponents, and parameter g denotes the breakpoint range (typically, in the range of 150-300 meters). Substituting (9.27) into (9.15)-(9.17) and using the definition of spectral efficiency in (9.26), we can study the outage probability as a function of the reuse distance and spectral efficiency, respectively. Figure 9.6 shows the variation of outage probability with spectral efficiency with K_d = 3.5 and $m_i \in \{1,2\}$. The improvement in spectral efficiency is apparent as the strongest CCI signals are suppressed and the effect of m_i on the curves follows the trend observed in the earlier figures.

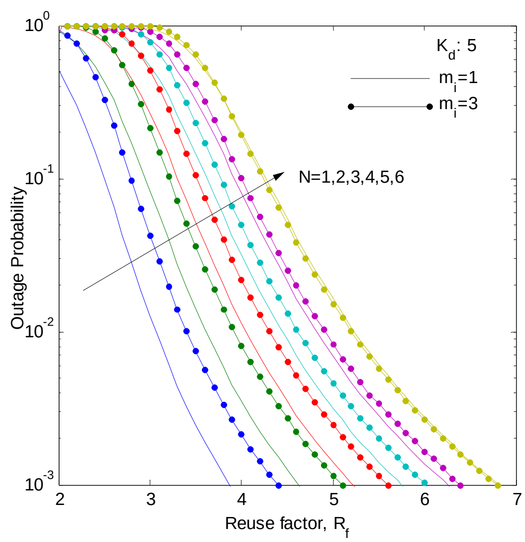

Figure 9.7. Plots of outage probability vs. reuse distance for different values of N, m_i with K_d = 5.

Figure 9.7 presents outage probability curves as a function of reuse distance when the desired user is Rician distributed with K_d = 5 and the CCI signals are Nakagami-m distributed $m_i \in \{1,3\}$. The plots show that reuse distance decreases as more interferers are cancelled, i.e., as N decreases. The benefits of reducing the reuse distance is significantly impacted by the fading index of CCI signals m_i.

9.6 Conclusions

In this chapter, a mathematical framework for studying the performance of a smart antenna system is outlined that employs selective nulling of dominant CCI signals in a mobile radio environment. Generic formulas for computing the outage probability and the average symbol error rate are also derived. For the special case of Rayleigh and Nakagami-m fading, several new closed-form formulas are derived. Numerical results show that the fading distributions of CCI signals can play a significant role in the performance assessment of a cellular radio system equipped with a SNDI receiver, especially as more interferers are suppressed. This observation contrasts the general assumption that the outage performance is insensitive to fading distributions of the CCI signals, and emphasizes the need to model both the desired user signal and CCI signals accurately for reliable performance prediction.

Chapter 10

Conclusions

This chapter provides a summary of the research contributions and accomplishments as presented in this dissertation. Section 10.1 touches upon the key aspects of different chapters and summarizes the contents in succeeding paragraphs. Section 10.2 discusses possible future work.

10.1 Review of the dissertation

Closed-loop transmit diversity techniques have been developed for both flat fading and frequency selective channels. The techniques were developed to provide fast convergence and simplicity in operation and implementation. The proposed techniques for flat fading channel are classified into two groups: EGT and MRT. For EGT category, the feedback information is either phase index or phase value and with quantization, the amount of feedback is expected to be small compared to the amount of information. For MRT, the amount of feedback is usually a complex weight vector the size of which depends on the number of antenna elements. The EGT techniques provide substantial improvement over a single antenna system, and the bisection method among the EGT category provided the best performance both in terms of convergence and SNR, coming almost within a dB of the optimal value (ideal MRT). The supervised LS technique among the MRT provides the best performance and almost achieves the performance from an ideal MRT technique. The EGT techniques offer the advantage of having fast convergence and requiring small feedback compared to the MRT techniques, except for the LS technique. Implementation issues that include quantization, latency and reverse channel impairment (feedback error) have been addressed. For a W-CDMA signal structure, the LS technique has been shown to be quite robust to channel dynamics for an indoor channel. Relatively coarse quantization (to accommodate feedback information) has been found to have small impact on the SNR performance of the LS technique.

Large signal strength fluctuation may occur during training period from weight perturbation and this may cause the signal fall close to the receiver noise floor. One suggestion to overcome this problem is to transmit at higher power during the training period for proper detection and estimation of the optimal weight vector and then reduce the transmit power to normal level during information transmission with the optimal weight vector.

For a frequency selective channel, optimal solution was derived in frequency domain for signals with excess bandwidth. Optimal and sub-optimal solutions were derived to maximize DSNR and a lower bound was derived for the minimum MSE case. All these solutions were expressed in terms of channel parameters. For example, the analysis shows that the optimal solution reduces to a MRC solution when the channel becomes frequency non-selective. Analysis was carried out in discrete time to come up with finite length filters that optimize the SINR performance. Several sub-optimal structures were proposed and they all performed better than a single antenna system. Simulation studies show that spatial processing at the transmitter and temporal processing at the receiver (structure 3) may provide a good compromise between performance and feedback bandwidth. Perfect channel knowledge was assumed at the receiver. The amount of feedback required to track a dynamic wireless channel may restrict the use of these techniques to low mobility or fixed point-to-point applications.

Several vector channel propagation measurements, mostly indoor, were made to assess transmit diversity at the SWT. Goals of these measurements include: i) showing channel reciprocity at the SWT, ii) determining the effect of antenna spacing on signal correlation, and iii) understanding wideband diversity. Measurements show that there is a strong reciprocal behavior between the transmitter and receiver implying that the performance of a transmit diversity system can be inferred from an existing receive diversity system. The study of inter-element spacing variation and its effect on diversity performance was done on the receive side. Low measured values of correlation coefficients indicate that the elements can be tightly spaced at the SWT without significantly hurting diversity performance. This is a promising result for implementing a smart antenna at the SWT. Wideband channel measurements spanning a bandwidth of 10 MHz showed that an indoor channel does not exhibit frequency selectivity and the coherence bandwidth was found to be about 10 MHz. Outdoor-to-indoor measurements showed that the coherence bandwidth is between 0.5 MHz and 1 MHZ. A direct measurement of narrowband transmit diversity was carried out for a two-element array at the handset.

Orientation of the transmitter with respect to the receiver was found to have impact on the diversity performance and this was explained in terms of antenna pattern distortion.

Results of hardware-based experiments of transmit diversity were presented in this report. For wideband experiments, a transmitter array testbed was designed to provide a signal bandwidth of 5 MHz to make the system comparable to the W-CDMA standard. The wideband measurements demonstrated that a statistical diversity gain in excess of 10 dB is possible for a slow fading, NLOS indoor channel.

MIMO structures were developed as an extension to the proposed diversity techniques for flat fading and frequency-selective channel. The reduced complexity structure for flat fading channel offered simplicity in implementation and significant performance gain.

The implementation of the proposed transmit diversity techniques in the next generation W-CDMA standard and WLAN IEEE802.1b was presented. The existing physical layer of W-CDMA standard was found to be adequate to support the proposed schemes. The issues here are the sufficient length of pilot bits for use as a training sequence and the needed number of bits in the DSCH that act as the source for accommodating feedback information.

The SNDI approach promises performance improvement for a SWT operating in an interference-limited environment. Results indicate often the nulling of one or two dominant interferers in enough to improve the performance.

10.2 Future work

The research presented in this dissertation can be extended to include the following:

1. Designing diversity algorithms in a multi-user ad-hoc networks.
2. Studying the impact of channel coding on the performance of the proposed algorithms.
3. Studying the impact of transmit beamforming in an IEEE802.11 system regarding user isolation and throughput enhancement.
4. Studying the physical layer of future high-data rate communications systems (e.g., 4G or Hiperlan) for implementing smart antenna.

5. The impact of the proposed scheme on the MAC layer performance.
6. Using the SDR-3000 testbed to perform wideband MIMO measurements and analyze the data to generate channel models and post-process it with proposed algorithms.

Appendix

Appendix A1: Optimal LS Solution

The problem statement given in equation (2.2) is a constrained optimization problem. Utilizing the method of LaGrange's multipliers converts the constrained optimization problem into an unconstrained optimization problem with cost function

$$L(\mathbf{w},\lambda) = \mathbf{w}^H \mathbf{a}^H \mathbf{a}\mathbf{w} + \lambda(-\mathbf{w}^H \mathbf{w} + 1)\,. \tag{A1-1}$$

Taking the gradient with respect to $\mathbf{w}^H$ and λ results in the following set of equations:

$$\begin{aligned} \nabla_{\mathbf{w}^H} L &= \mathbf{a}^H \mathbf{a}\mathbf{w} - \lambda \mathbf{w} = 0 \\ \nabla_\lambda L &= -\mathbf{w}^H \mathbf{w} + 1 = 0. \end{aligned} \tag{A1-2}$$

The second equation results in the expression for power constraint. However, the first equation is recognized as an eigenvalue problem:

$$\begin{aligned} \mathbf{a}^H \mathbf{a}\mathbf{w} &= \lambda \mathbf{w} \\ \mathbf{A}\mathbf{w} &= \lambda \mathbf{w} \end{aligned} \tag{A1-3}$$

Thus, (A1-3) is maximized for the largest eigenvalue λ of the matrix **A**. The vector **w** is the eigenvector corresponding to λ. In the following, the detailed solution for a two-element array is given; the extension to any arbitrary number of antennas is straightforward.

$$\mathbf{A} = \begin{bmatrix} a_1^* \\ a_2^* \end{bmatrix} \begin{bmatrix} a_1 & a_2 \end{bmatrix} = \begin{bmatrix} |a_1|^2 & a_1^* a_2 \\ a_1 a_2^* & |a_2|^2 \end{bmatrix}. \tag{A1-4}$$

The eigenvalues of **A** can be found by solving the following characteristic polynomial

$$\begin{aligned} \det\left(\mathbf{A} - \lambda \underline{I}\right) &= \lambda\left(\lambda - \left(|a_1|^2 + |a_2|^2\right)\right) \\ \lambda_1 &= 0 \\ \lambda_2 &= |a_1|^2 + |a_2|^2\,. \end{aligned} \tag{A1-5}$$

Eventually, the corresponding eigenvector can be found from

$$\left(\mathbf{A} - \lambda \mathbf{I}\right)\mathbf{w} = 0 \quad \Rightarrow \begin{bmatrix} -|a_2|^2 & a_1^* a_2 \\ a_1 a_2^* & -|a_1|^2 \end{bmatrix} \mathbf{w} = 0 \tag{A1-6}$$

where now **A** is a matrix of rank one and therefore singular. The solution for this class of matrices is known to be simply the Hermitian of **a**.

$$\mathbf{w}_{opt} = \mathbf{a}^H\,. \tag{A1-7}$$

It can be shown that this choice of optimal weight solves the eigenvalue problem. (A1-7) can be substituted into (A1-6) to generate

$$\mathbf{A}\mathbf{w}_{opt} = \begin{bmatrix} -|a_2|^2 & a_1^* a_2 \\ a_1 a_2^* & -|a_1|^2 \end{bmatrix} \begin{bmatrix} a_1^* \\ a_2^* \end{bmatrix}. \qquad \text{(A1-8)}$$

The expression in (A1-8) is expanded to show that it indeed solves the eigenvalue problem:

$$\begin{aligned} \left(-|a_2|^2\right) a_1^* + a_1^* |a_2|^2 &= 0 \\ |a_1|^2 a_2^* + \left(-|a_1|^2\right) a_2^* &= 0. \end{aligned} \qquad \text{(A1-9)}$$

Due to the power constraint, the optimum weight vector still needs to be scaled by the 2-norm of the channel. Thus, the final solution for the optimum weigh vector is

$$\mathbf{w}_{opt} = \frac{\mathbf{a}^H}{\|\mathbf{a}\|_2}. \qquad \text{(A1-10)}$$

Appendix A2: Vector Channel Estimation by LS Technique

With reference to Figure 2.1, the output observed over a period of N symbols is

$$\left[y_1 \; y_2 \cdots\cdots y_N\right] = \left[\mathbf{a}\mathbf{w}_1 s_1 \; \mathbf{a}\mathbf{w}_2 s_2 \cdots\cdots \mathbf{a}\mathbf{w}_N s_N\right] + \left[\eta_1 \; \eta_2 \cdots\cdots \eta_N\right]. \qquad \text{(A2-1)}$$

Here $\mathbf{a}$ is a row vector of size M, the number of antenna elements, and $\mathbf{w}$ is a column vector of the same size. This can be written in a compact form as

$$\tilde{\mathbf{y}} = \mathbf{a}\mathbf{W}\mathbf{S} + \left[\eta_1 \; \eta_2 \cdots\cdots \eta_N\right] \qquad \text{(A2 -2)}$$

where $\tilde{\mathbf{y}}$ is the vector containing all y_k and the noise samples, $\mathbf{W}$ is a $M\times N$ matrix and $\mathbf{S}$ is an $N\times N$ diagonal matrix comprising of the individual s_k. The problem of LS channel identification can be expressed as

$$\min_{\mathbf{a},\mathbf{S}} \|\tilde{\mathbf{y}} - \mathbf{a}\mathbf{W}\mathbf{S}\|_2^2. \qquad \text{(A2-3)}$$

For the ease of implementation, it is assumed that the input signal is BPSK-modulated and therefore has a finite alphabet structure, that is, $s_k \in \{1, -1\}$. Exploiting this property, formula (A2-3) can be rearranged as

$$\min_{\mathbf{a},\mathbf{S}} \left\| [s_1 \cdots s_N] \begin{bmatrix} y_1 & 0 & 0 \\ 0 & \ddots & \\ 0 & 0 & \ddots \\ 0 & 0 & y_N \end{bmatrix} - \mathbf{aW} \right\|_2^2 \tag{A2-4}$$

or as

$$\min_{\mathbf{a},\mathbf{S}} \left\| [s_1 \cdots s_N \mid a_1 \cdots a_N] \begin{bmatrix} y_1 & 0 & 0 \\ 0 & \ddots & \\ 0 & 0 & \ddots \\ 0 & 0 & y_N \\ \hline & -\mathbf{W} & \end{bmatrix} \right\|_2^2 . \tag{A2-5}$$

Interchanging the row and column vector leads to

$$\min_{\mathbf{a},\mathbf{S}} \left\| \left[\tilde{\mathbf{Y}} \mid -\mathbf{W} \right] \begin{bmatrix} s_1 \\ \vdots \\ s_N \\ a_1 \\ \vdots \\ a_N \end{bmatrix} \right\|_2^2 . \tag{A2-6}$$

Defining the concatenated matrix as **A** and the column vector as **x**, the expression above can be written as

$$\min_{\mathbf{x}} \|\mathbf{Ax}\|_2^2 \tag{A2-7}$$

The LS problem formulation with respect to **a** is

$$\mathbf{a} = \arg\min \left\| \mathbf{s}\tilde{\mathbf{Y}} - \mathbf{aW} \right\|_2^2 . \tag{A2-8}$$

Formulating the cost function results in

$$\begin{aligned} J &= \left(\mathbf{s}\tilde{\mathbf{Y}} - \mathbf{aW} \right) \left(\mathbf{s}\tilde{\mathbf{Y}} - \mathbf{aW} \right)^H \\ &= \left(\mathbf{s}\tilde{\mathbf{Y}} - \mathbf{aW} \right) \left(\tilde{\mathbf{Y}}^H \mathbf{s}^H - \mathbf{W}^H \mathbf{a}^H \right) \\ &= \mathbf{s}\tilde{\mathbf{Y}}\tilde{\mathbf{Y}}^H \mathbf{s}^H - \mathbf{s}\tilde{\mathbf{Y}}\mathbf{W}^H \mathbf{a}^H - \mathbf{aW}\tilde{\mathbf{Y}}^H \mathbf{s}^H + \mathbf{aWW}^H \mathbf{a}^H . \end{aligned} \tag{A2-9}$$

Taking the gradient of formula (A2-9) with respect to $\mathbf{a}^H$ leads to

$$\nabla_{\mathbf{a}^H} J = -\mathbf{s}\tilde{\mathbf{Y}}\mathbf{W}^H + \mathbf{aWW}^H = 0 . \tag{A2-10}$$

Eventually the solution for **a** can be found with

$$\mathbf{a} = \mathbf{s}\tilde{\mathbf{Y}}\mathbf{W}^H \left(\mathbf{W}\mathbf{W}^H\right)^{-1}. \tag{A2-11}$$

The inverse exists (because the weight vectors are dithered with random variations). Thus, if **s** and **W** are known and $\tilde{\mathbf{Y}}$ is available from observations, then the channel can be estimated. The knowledge of **s** can be established by transmitting a known training sequence. If **s** is unknown to the receiver, then the channel estimation can be modified to incorporate symbol estimation as well.

Appendix B1: Optimal Solution for DSNR

Let the transmit filters and channel filters be defined as vectors as

$$\mathbf{g}(f) = \begin{bmatrix} G_1(f) \\ G_2(f) \end{bmatrix}; \qquad \mathbf{c}(f) = \begin{bmatrix} \hat{C}_1^*(f) \\ \hat{C}_2^*(f) \end{bmatrix}. \tag{B1-1}$$

The problem now becomes to minimize the reciprocal of SNR defined as

$$\frac{T_s \sigma^2 W}{d^2} \cdot \left(T_s \int_{-\frac{1}{2T_s}}^{\frac{1}{2T_s}} \frac{df}{\sum_n \left| H\left(f + \frac{n}{T_s} \right) \right|^2} \right) \tag{B1-2}$$

with respect to **g**(f) subject to the power constraint written in terms of vector notation as

$$\frac{1}{T_s} \int_{-\frac{1}{2T_s}}^{\frac{1}{2T_s}} \sum_n \left\| \mathbf{g}\left(f + \frac{n}{T} \right) \right\|^2 \Phi_I(f)\, df = P_{av} \,. \tag{B1-3}$$

These equations indicate that the optimal choice for **g**(f) will be a vector that is aligned with **c**(f) so that $H(f)$ is maximized for all f. The form for **g**(f) can be expressed as **g**(f)= p(f)**c**(f) where $p(f)$ is a positive scalar weighting function of frequency. The minimization problem now can be written as

$$\min_{p(f)} \quad \frac{T_s \sigma^2 W}{d^2} \cdot \left(T_s \int_{-\frac{1}{2T_s}}^{\frac{1}{2T_s}} \frac{df}{\sum_n p^2\left(f + \frac{n}{T_s} \right) \left\| \mathbf{c}\left(f + \frac{n}{T_s} \right) \right\|^4} \right)$$

$$s.t. \quad \frac{1}{T_s} \int_{-\frac{1}{2T_s}}^{\frac{1}{2T_s}} \Phi_I(f) \sum_n p^2\left(f + \frac{n}{T_s} \right) \left\| \mathbf{c}\left(f + \frac{n}{T_s} \right) \right\|^2 df = P_{av}. \tag{B1-4}$$

Let $\begin{matrix} v(f) = p^2(f) \left\| \mathbf{c}(f) \right\|^2 \\ a(f) = \left\| \mathbf{c}(f) \right\|^2 \end{matrix}$, the minimization problem then becomes

$$\min_{v(f)} \quad \frac{T_s\sigma^2 W}{d^2}\cdot\left(T_s\int_{-\frac{1}{2T_s}}^{\frac{1}{2T_s}}\frac{df}{\sum_n a\left(f+\frac{n}{T_s}\right)v\left(f+\frac{n}{T_s}\right)}\right) \tag{B1-5}$$
$$s.t. \quad \frac{1}{T_s}\int_{-\frac{1}{2T_s}}^{\frac{1}{2T_s}}\Phi_I(f)\sum_n v\left(f+\frac{n}{T_s}\right)df = P_{av}.$$

Let k be the smallest integer greater than or equal to $(WT_s\text{-}1)/2$, and let the following k-dimensional vectors be defined as

$$\mathbf{x}(f)=\left[v\left(f-\frac{k}{T_s}\right)\cdots\cdots v(f)\;\; v\left(f+\frac{1}{T_s}\right)\cdots\cdots v\left(f+\frac{k}{T_s}\right)\right]^H$$
$$\mathbf{A}(f)=\left[a\left(f-\frac{k}{T_s}\right)\cdots\cdots a(f)\;\; a\left(f+\frac{1}{T_s}\right)\cdots\cdots a\left(f+\frac{k}{T_s}\right)\right]. \tag{B1-6}$$

With this change in notation, the minimization problem reduces to

$$\min_{\mathbf{x}(f)} \quad \frac{T_s\sigma^2 W}{d^2}\cdot\left(T_s\int_{-\frac{1}{2T_s}}^{\frac{1}{2T_s}}\frac{df}{\sum_n A(f)\mathbf{x}(f)}\right) \tag{B1-7}$$
$$s.t. \quad \frac{1}{T_s}\int_{-\frac{1}{2T_s}}^{\frac{1}{2T_s}}\Phi_I(f)\left\|x(f)\right\|_1 df = P_{av}.$$

From the properties of 1-norm, the optimal $\mathbf{x}(f)$ will have the form $\mathbf{x}(f)=z(f)\left[0\cdots\cdots 0 \quad 1 \quad 0\cdots\cdots 0\right]^H$ where $z(f)$ is a positive scalar weighting function of frequency and the "1" occurs in the ith position where i is a function of frequency expressed as $i(f)=\arg\max_{n\in[-k,k]} a\left(f+\frac{n}{T_s}\right)$. Now let $\hat{a}(f)=\max_{n\in[-k,k]} a\left(f+\frac{n}{T_s}\right)$. The minimization problem takes the form

$$\min_{z(f)} \quad \frac{T_s \sigma^2 W}{d^2} \cdot \left(T_s \int_{-\frac{1}{2T_s}}^{\frac{1}{2T_s}} \frac{df}{z(f)\hat{a}(f)} \right)$$

$$s.t. \quad \frac{1}{T_s} \int_{-\frac{1}{2T_s}}^{\frac{1}{2T_s}} \Phi_I(f) z(f) df = P_{av}. \tag{B1-8}$$

The constrained optimization problem stated above can be transformed into an unconstrained problem through the use of Lagrange's multiplier as

$$\min_{z(f)} \left(\int_{-\frac{1}{2T_s}}^{\frac{1}{2T_s}} \frac{1}{z(f)\hat{a}(f)} + \lambda \Phi_I(f) z(f) df \right) \tag{B1-9}$$

where λ is the Lagrange multiplier that is chosen to satisfy the power constraint. Using the calculus of variations, the optimal $z(f)$ can be found as the one that satisfies

$$\frac{-1}{z^2(f)\hat{a}(f)} + \lambda \Phi_I(f) = 0. \tag{B1-10}$$

This provides with the optimal $z(f)$ as

$$z(f) = \frac{1}{\sqrt{\lambda \Phi_I(f)\hat{a}(f)}}. \tag{B1-11}$$

The multiplier λ can be solved from the power constraint equation as

$$\lambda = \left(\frac{1}{P_{av} T_s} \int_{-\frac{1}{2T_s}}^{\frac{1}{2T_s}} \sqrt{\frac{\Phi_I(f)}{\hat{a}(f)}} df \right)^2. \tag{B1-12}$$

With the value of optimum $z(f)$ and λ, the minimization process yields

$$\begin{aligned} \min_{z(f)} \quad \frac{\sigma^2 W T_s^2}{d^2} \left(\int_{-\frac{1}{2T_s}}^{\frac{1}{2T_s}} \frac{1}{z(f)\hat{a}(f)} df \right) &= \frac{\sigma^2 W T_s}{P_{av} d^2} \left(\int_{-\frac{1}{2T_s}}^{\frac{1}{2T_s}} \sqrt{\frac{\Phi_I(f)}{\hat{a}(f)}} df \right)^2 \\ &= \frac{\sigma^2 W}{P_{av} T_s} \left(T_s \int_{-1/2T_s}^{1/2T_s} \frac{\sqrt{\Phi_I(f)/d^2} df}{\max_n \sqrt{\left|\hat{C}_1\left(f+\frac{n}{T}\right)\right|^2 + \left|\hat{C}_2\left(f+\frac{n}{T}\right)\right|^2}} \right)^2. \end{aligned} \tag{B1-13}$$

The optimum DSNR can be found by simply inverting this expression.

Appendix B2: Sub-optimal Solution for Sub-opt$_{I}$

Let

$$x_i = \frac{1}{P_{av}T_s}\int_{-\frac{W}{2}}^{\frac{W}{2}} \frac{\Phi_I(f)}{\left|\hat{C}_i(f)\right|^2} df \ . \tag{B2-1}$$

Then the optimization problem becomes

$$\begin{aligned} &\max_{\alpha_1,\alpha_2} \quad \frac{d^2}{\sigma^2}\left|\alpha_1+\alpha_2\right|^2 \\ &s.t. \quad \left|\alpha_1\right|^2 x_1^2 + \left|\alpha_2\right|^2 x_2^2 = 1. \end{aligned} \tag{B2-2}$$

Following the guidelines as in Appendix B1, this optimization problem can be solved to yield the sub-optimal SNR.

Appendix B3: Sub-optimal Solution for Sub-opt$_{II}$

Let the following definitions hold (as in Appendix B1):

$$\mathbf{g}(f) = \begin{bmatrix} G_1(f) \\ G_2(f) \end{bmatrix}; \qquad \mathbf{c}(f) = \begin{bmatrix} \hat{C}_1^*(f) \\ \hat{C}_2^*(f) \end{bmatrix}. \tag{B3-1}$$

The optimization problem in this case can be stated as to maximize the DSNR subject to the following constraints:

$$\begin{aligned} &H(f) = \mathbf{c}^*(f)\mathbf{g}(f) = \alpha \\ &\frac{1}{T_s}\int_{-\frac{1}{W}}^{\frac{1}{W}} \sum_n \left\|\mathbf{g}(f)\right\|^2 \Phi_I(f)\, df = P_{av}. \end{aligned} \tag{B3-2}$$

Plugging the expression for $H(f)$ in the expression for DSNR (B1-2), one can show that the DSNR is tightly upper-bounded by $\frac{d^2}{\sigma^2}\left|\alpha\right|^2$ (with equality holding when WT_s is an integer). This value is maximized when **g**(f) is aligned with $c(f)$ (as in appendix B1) so that the following form holds for **g**(f):

$$\mathbf{g}(f) = \alpha\frac{\mathbf{c}(f)}{\left\|\mathbf{c}(f)\right\|^2} \ . \tag{B3-3}$$

This expression for **g**(*f*) can be substituted in (B1-3) and the resulting expression can be solved for α. This follows the same guidelines as in Appendix B1to solve for λ and for optimum SNR. After solving for α, the corresponding expression can be found.

Appendix B4: Lower Bound on MMSE Solution

The proof for this section is analogous to the proof in Appendix B1. Assuming the same definitions as in Appendix B1, the problem can be stated as

$$\begin{aligned} &\min_{z(f)} \quad T_s\sigma^2 W\left(T_s\int_{-\frac{1}{2T_s}}^{\frac{1}{2T_s}}\frac{\Phi_I(f)\,df}{\Phi_I(f)z(f)\hat{a}(f)+T_s\sigma^2 W}\right) \\ &s.t. \quad \frac{1}{T_s}\int_{-\frac{1}{2T_s}}^{\frac{1}{2T_s}}\Phi_I(f)z(f)\,df=P_{av}. \end{aligned} \tag{B4-1}$$

This can be cast into an unconstrained minimization problem as

$$\min_{z(f)}\left(\int_{-\frac{1}{2T_s}}^{\frac{1}{2T_s}}\frac{\Phi_I(f)}{\Phi_I(f)z(f)\hat{a}(f)+T_s\sigma^2 W}+\lambda\Phi_I(f)z(f)\,df\right). \tag{B4-2}$$

where λ has the same interpretation. By invoking the calculus of variations, one can show that the optimal *z*(*f*) satisfies

$$\frac{-\Phi_I(f)}{\left(\Phi_I(f)z(f)\hat{a}(f)+T_s\sigma^2 W\right)^2}+\lambda=0 \tag{B4-3a}$$

$$\text{or,}\quad z(f)=\frac{1}{\sqrt{\lambda\Phi_I(f)\hat{a}(f)}}-\frac{T_s\sigma^2 W}{\Phi_I(f)\hat{a}(f)}. \tag{B4-3b}$$

Solving for λ gives

$$\lambda=\left(\int_{-\frac{1}{2T_s}}^{\frac{1}{2T_s}}\sqrt{\frac{\Phi_I(f)}{\hat{a}(f)}}\,df\Bigg/\left(P_{av}T_s+T_s\sigma^2 W\int_{-\frac{1}{2T_s}}^{\frac{1}{2T_s}}\sqrt{\frac{1}{\hat{a}(f)}}\,df\right)\right)^2. \tag{B4-4}$$

Solving for $z(f)$ and substituting in (B4-2) yields the desired lower bound for the MMSE. This is a lower bound, not an exact expression for the MMSE, because the solution for $z(f)$ in the above expression may not be non-negative as is required in the definition.

Appendix B5: Evaluation from CT Model to DT Model

Proposition 1

Let $y_k = y\left(\frac{k}{W}\right)$.

Then $y(t) = \sum_k y_k \sin c\pi W\left(t - \frac{k}{W}\right)$.

Proof

The channel output $y(t)$ can be written as $y(t) = \sum_k I_k h(t - kT)$ where the equivalent channel $h(t)$ is sampled at a rate of T^{-1}. The band-limited nature of $g(t)$ imposes band-limited characteristics on $h(t)$. This implies that

$$H(f) = 0, \qquad |f| > \frac{W}{2}.$$

With $h(t)$ being band-limited to W, its impulse response can be described as $h(t) = \sum_k h_k \sin c\pi W\left(t - \frac{k}{W}\right)$ where $h_k = h\left(\frac{k}{W}\right)$. Now the expression for $h(t)$ can be substituted in the expression for $y(t)$ to yield $y(t) = \sum_k \sum_n I_k h_n \sin c\pi W\left(t - \frac{km+n}{W}\right)$.

Now $y(t)$ can be sampled at a rate of W to generate the samples y_j as

$$\begin{aligned} y_j &= \sum_k \sum_n I_k h_n \sin c\pi\left(j - km - n\right) \\ &= \sum_k I_k h_{j-km} \end{aligned}$$

It can be shown that $y(t)$ can be reconstructed from these samples as shown below:

$$
\begin{aligned}
y_j &= \sum_j y_j \operatorname{sinc} \pi W\left(t - \frac{j}{W}\right) \\
&= \sum_k \sum_j I_k h_{j-km} \operatorname{sinc} \pi W\left(t - \frac{j}{W}\right) \\
&= \sum_k \sum_n I_k h_n \operatorname{sinc} \pi W\left(t - \frac{km+n}{W}\right) \\
&= y(t).
\end{aligned}
$$

Proposition 2

Channel output y_k is given by the system shown in Figure B5.1

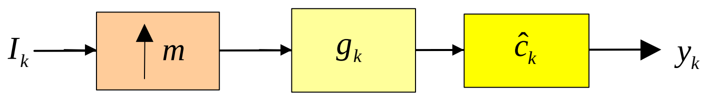

Figure B5.1: The Discrete Time Output y_k at the Receiver.

Proof

The system is shown in Figure B5.1. The pulse shaping filter $g(t)$ and the channel can be combined into a single filter $h(t)$ by using convolution operation. $h(t)$ can be further expanded as

$$
\begin{aligned}
h(t) &= \int c(\tau) \sum_k g_k \operatorname{sinc} \pi W\left(t - \tau - kT_s\right) d\tau \\
&= \sum_k g_k \int c(\tau) \operatorname{sinc} \pi W\left(t - \tau - kT_s\right) d\tau \\
&= \sum_k g_k \hat{c}\left(t - kT_s\right).
\end{aligned}
$$

Then $h(t)$ can be sampled at a rate of W to yield

$$
h_j = \sum_k g_k \hat{c}_{j-k} = g_k * \hat{c}_k .
$$

Now let up-sampling be defined as

$$
s_k = \begin{cases} I_{\frac{k}{m}} & if \quad \dfrac{k}{m} \quad is\ an\ integer \\ 0 \;\vdots\; else & \end{cases} .
$$

This implies $I_k = s_{km}$. Now the sampled version of $y(t)$ can be expressed as

$$
\begin{aligned}
y_j &= \sum_k I_k h_{j-km} \\
&= \sum_k s_{km} h_{j-km} \\
&= \sum_n s_n h_{j-n}.
\end{aligned}
$$

It can be seen from the expression above that y_n is a convolution of the sequences s and the filter h_n. Thus it follows that

$$y_n = s_n * h_n = s_n * g_n * \hat{c}_n .$$

Proposition 3

The receiver noise is expressed as

$$n(t) = \sum_k n_k \operatorname{sinc} \pi W \left(t - \frac{k}{W} \right).$$

Proof

Let the following expression hold true:

$$\hat{n}(t) = \sum_k n_k \operatorname{sinc} \pi W \left(t - \frac{k}{W} \right)$$

One can show from [PRO95] that $n(t)$ and $\hat{n}(t)$ are equal in the mean square sense. Since both of them belong to Gaussian distribution, equality in the mean square sense implies exact equality.

Proposition 4

The received signal is given by

$$r(t) = \sum_k r_k \operatorname{sinc} \pi W \left(t - \frac{k}{W} \right).$$

Proof

The propositions presented previously can be invoked to show that the expression above is true.

Proposition 5

The estimated symbol $\hat{I}_k$ is given as shown in Figure B5.2

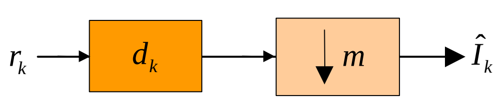

Figure B5.2: System for Down-sampling and Estimating Transmitted Symbol.

Proof

It can be seen that $a(t)$ is given by

$$a(t) = \int r(\tau)\, p(t-\tau) d\tau \, .$$

If $a(t)$ is sampled, then the sampled values can be expressed as

$$a_k \equiv a(kT) = \int r(\tau)\, p(kT-\tau) d\tau \, .$$

The expression above can be expanded as follows:

$$\begin{aligned} a_k &= \int r(\tau)\, p(kT-\tau)\, d\tau \\ &= \int p(kT-\tau) \sum_n r_n \, sinc \pi W \left(\tau - \frac{n}{W}\right) d\tau \\ &= \sum_n r_n \int p(kT-\tau)\, sinc \pi W \left(\tau - \frac{n}{W}\right) d\tau \\ &= \sum_n r_n \hat{p}\left(kT - \frac{n}{W}\right). \end{aligned}$$

Here $\hat{p}(t)$ is the band-limited version of $p(t)$ and is obtained by smoothing the original $p(t)$ with a sinc function of appropriate bandwidth. In other words,

$$\hat{p}(t) = \int p(t)\, sinc \pi W (t-\tau) d\tau$$

$$or \quad = \frac{1}{W} \int_{-\frac{W}{2}}^{\frac{W}{2}} P(f) e^{j2\pi f t} df \, .$$

With this, a_k is expressed by

$$a_k = \sum_n r_n p_{km-n}$$

where $p_k = \hat{p}\left(\frac{k}{W}\right)$.

Thus we have that I_k is given by Figure B5.3 or equivalently, in Figure B5.4.

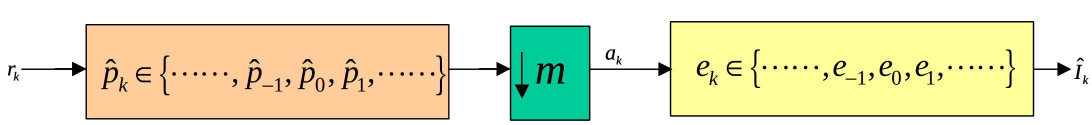

Figure B5.3 Discrete Time Filter at the Receiver.

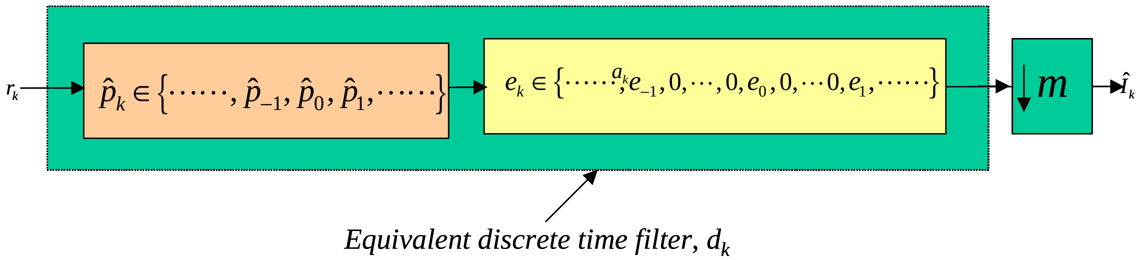

Figure B5.4 Equivalent Discrete Time Filter

Derivation of Discrete Time Model for the Channel

Let the continuous time description of a multipath channel be given as

$$c(t) = \sum_{i=1}^{M} \alpha_i \delta(t - t_i).$$

Then

$$\begin{aligned} c(t) &= \int c(\tau) \sin c\pi W (t-\tau) d\tau \\ &= \sum_{i=1}^{M} \alpha_i \int \delta(\tau - t_i) \sin c\pi W (t-\tau) d\tau \\ &= \sum_{i=1}^{M} \alpha_i \sin c\pi W (t - t_i). \end{aligned}$$

Therefore in the discrete time model, the sampled channel gains become

$$\hat{c}_k = \sum_{i=1}^{M} \alpha_i \sin c\pi W (k - Wt_i).$$

In the special case that the multipath delays t_i are some multiple of the sampling time ($1/W$), $t_i = \gamma_i / W$ where the γ_i is an integer and $0 \le \gamma_1 < \gamma_2 < \cdots\cdots < \gamma_M$. In this case, the sampled channel gains can be written as

$$\begin{aligned} \hat{c}_k &= \sum_{i=1}^{M} \alpha_i \sin c\pi W (k - Wt_i) \\ &= \sum_{i=1}^{M} \alpha_i \delta_{k-\gamma_i}. \end{aligned}$$

Thus given a continuous time model for a multipath channel, the discrete time model can be derived with the proper sampling rate as given by expressions for $\hat{c}_k$.

Appendix B6: DSNR for a Finite Length Receive Filter

The orthogonal projection of $\mathbf{x}_0$ onto $\mathbf{X}$ defined as a vector $\mathbf{a}$ can be expressed as [DAY00]

$$\mathbf{a} = \mathbf{X}\left(\mathbf{X}^*\mathbf{X}\right)^{-1}\mathbf{X}^*\mathbf{x}_0\,. \tag{B6-1}$$

The inverse exists, as X is a full rank matrix. The expression for **b** can be written as the component of $\mathbf{x}_0$ orthogonal to **X**:

$$\mathbf{b} = \mathbf{x}_0 - \mathbf{a} = \left[\mathbf{I} - \left(\mathbf{X}^*\mathbf{X}\right)^{-1}\mathbf{X}^*\right]\mathbf{x}_0\,. \tag{B6-2}$$

Now q_0 can be written as

$$q_0 = \mathbf{x}_0^*\mathbf{b} = \mathbf{x}_0^*\left[\mathbf{I} - \left(\mathbf{X}^*\mathbf{X}\right)^{-1}\mathbf{X}^*\right]\mathbf{x}_0\,. \tag{B6-3}$$

The square of the norm of **b** is

$$\begin{aligned}\mathbf{b}^*\mathbf{b} &= \mathbf{x}_0^*\left[\mathbf{I} - \mathbf{X}\left(\mathbf{X}^*\mathbf{X}\right)^{-1}\mathbf{X}^*\right]\left[\mathbf{I} - \mathbf{X}\left(\mathbf{X}^*\mathbf{X}\right)^{-1}\mathbf{X}^*\right]\mathbf{x}_0 \\ &= \mathbf{x}_0^*\left[\mathbf{I} - 2\mathbf{X}\left(\mathbf{X}^*\mathbf{X}\right)^{-1}\mathbf{X}^* + \mathbf{X}\left(\mathbf{X}^*\mathbf{X}\right)^{-1}\mathbf{X}^*\right]\mathbf{x}_0 \\ &= \mathbf{x}_0^*\left[\mathbf{I} - \mathbf{X}\left(\mathbf{X}^*\mathbf{X}\right)^{-1}\mathbf{X}^*\right]\mathbf{x}_0.\end{aligned} \tag{B6-4}$$

The SNR can now be written as

$$\begin{aligned}SNR &= \frac{d^2\left|q_0\right|^2}{E\left[\left|v_k\right|^2\right]} \\ &= \frac{d^2}{\sigma^2}\frac{\mathbf{x}_0^*\mathbf{b}\mathbf{b}^*\mathbf{x}_0}{\mathbf{b}^*\mathbf{b}} \\ &= \frac{d^2}{\sigma^2}\frac{\left(\mathbf{x}_0^*\left[\mathbf{I} - \left(\mathbf{X}^*\mathbf{X}\right)^{-1}\mathbf{X}^*\right]\mathbf{x}_0\right)\left(\mathbf{x}_0^*\left[\mathbf{I} - \left(\mathbf{X}^*\mathbf{X}\right)^{-1}\mathbf{X}^*\right]\mathbf{x}_0\right)}{\left(\mathbf{x}_0^*\left[\mathbf{I} - \left(\mathbf{X}^*\mathbf{X}\right)^{-1}\mathbf{X}^*\right]\mathbf{x}_0\right)} \\ &= \frac{d^2}{\sigma^2}\mathbf{x}_0^*\left[\mathbf{I} - \left(\mathbf{X}^*\mathbf{X}\right)^{-1}\mathbf{X}^*\right]\mathbf{x}_0.\end{aligned} \tag{B6-5}$$

Appendix B7: Sub-optimal SINR Solution for Structure 1

The optimization problem described in (4.27) is repeated here:

$$\begin{aligned}&\max \quad \frac{\mathbf{g}^H\mathbf{p}_0\mathbf{p}_0^H\mathbf{g}}{\mathbf{g}^H\mathbf{X}\mathbf{g}} \\ &s.t. \quad \mathbf{g}^H\mathbf{g} = T\end{aligned} \tag{B7-1}$$

where the matrix **X** is given by (4.28). Let $\mathbf{U\Sigma U}^{\mathrm{H}}$ be the singular value decomposition of **X.** Defining the vector $\hat{\mathbf{g}}$ with $\hat{\mathbf{g}} = \Sigma^{1/2}\mathbf{U}^H\mathbf{g}$ and expressing **g** in terms of $\hat{\mathbf{g}}$ leads to

$$\begin{aligned}\mathbf{g} &= \left(\mathbf{U}^H\right)^{-1}\Sigma^{-1/2}\hat{\mathbf{g}} = \mathbf{U}\Sigma^{-1/2}\hat{\mathbf{g}} \\ \hat{\mathbf{g}}^H &= \mathbf{g}\mathbf{U}\Sigma^{1/2}.\end{aligned} \tag{B7-2}$$

Substituting (B7-2) into (B7-1) changes the problem formulation to

$$\begin{aligned} &\max \frac{\hat{\mathbf{g}}^H \mathbf{\Sigma}^{-1/2}\mathbf{U}^H \mathbf{p}_0 \mathbf{p}_0^H \mathbf{U}\mathbf{\Sigma}^{-1/2}\hat{\mathbf{g}}}{\hat{\mathbf{g}}^H \hat{\mathbf{g}}} \\ &s.t. \quad \hat{\mathbf{g}}^H \mathbf{\Sigma}^{-1}\hat{\mathbf{g}} = T. \end{aligned} \tag{B7-3}$$

By defining a vector $\mathbf{y}^{\mathrm{H}}$ as $\mathbf{y}^H = \mathbf{p}_0^H \mathbf{U}\mathbf{\Sigma}^{-1/2}$, the problem in Equation (B7-3) becomes an eigenvalue problem

$$\begin{aligned} &\max \quad \frac{\hat{\mathbf{g}}^H \mathbf{y}\mathbf{y}^H \hat{\mathbf{g}}}{|\hat{\mathbf{g}}|^2} \\ &s.t. \quad \hat{\mathbf{g}}^H \mathbf{\Sigma}^{-1}\hat{\mathbf{g}} = T. \end{aligned} \tag{B7-4}$$

Clearly the maximum of (B7-4) is reached if vector $\mathbf{y}^H$ is aligned with $\hat{\mathbf{g}}$. Thus the optimal solution for $\hat{\mathbf{g}}$ has the form

$$\hat{\mathbf{g}} = k\mathbf{\Sigma}^{-1/2}\mathbf{U}^H \mathbf{p}_0 \tag{B7-5}$$

where the scalar constant k is used to meet the power constraint. The scalar k is determined by substituting Equation (B7-5) into the formulation for the power constraint in formula (B7-3):

$$\begin{aligned} k^2 &= \frac{T}{\mathbf{p}_0^H \mathbf{U}\mathbf{\Sigma}^{-2}\mathbf{U}^H \mathbf{p}_0} \\ k &= \frac{\sqrt{T}}{\left\|\mathbf{U}\mathbf{\Sigma}^{-1}\mathbf{U}^H \mathbf{p}_0\right\|_2}. \end{aligned} \tag{B7-6}$$

Incorporating (B7-6) and (B7-5) into (B7-2) gives the optimal vector $\mathbf{g}_{opt}$:

$$\begin{aligned} \hat{\mathbf{g}} &= \sqrt{T}\,\frac{\mathbf{\Sigma}^{-1/2}\mathbf{U}^H \mathbf{p}_0}{\left\|\mathbf{U}\mathbf{\Sigma}^{-1}\mathbf{U}^H \mathbf{p}_0\right\|_2} \\ \mathbf{g}_{opt} &= \sqrt{T}\,\frac{\mathbf{U}\mathbf{\Sigma}^{-1}\mathbf{U}^H \mathbf{p}_0}{\left\|\mathbf{U}\mathbf{\Sigma}^{-1}\mathbf{U}^H \mathbf{p}_0\right\|_2} = \sqrt{T}\,\frac{\mathbf{X}^{-1}\mathbf{p}_0}{\left\|\mathbf{X}^{-1}\mathbf{p}_0\right\|_2}. \end{aligned} \tag{B7-7}$$

Substituting the vector $\mathbf{g}_{opt}$ into the original problem formulation stated in Equation (B7-1) eventually gives the SINR for the optimum filters used:

$$\begin{aligned} SINR &= \frac{\mathbf{g}_{opt}^H \mathbf{p}_0 \mathbf{p}_0^H \mathbf{g}_{opt}}{\mathbf{g}_{opt}^H \mathbf{X}\mathbf{g}_{opt}} = \frac{T\left\|\mathbf{X}^{-1}\mathbf{p}_0\right\|_2^2 \left(\mathbf{p}_0^H \mathbf{X}^{-1}\mathbf{p}_0 \mathbf{p}_0^H \mathbf{X}^{-1}\mathbf{p}_0\right)}{T\left\|\mathbf{X}^{-1}\mathbf{p}_0\right\|_2^2 \left(\mathbf{p}_0^H \mathbf{X}^{-1}\mathbf{X}\mathbf{X}^{-1}\mathbf{p}_0\right)} \\ &= \frac{\mathbf{p}_0^H \mathbf{X}^{-1}\mathbf{p}_0 \mathbf{p}_0^H \mathbf{X}^{-1}\mathbf{p}_0}{\mathbf{p}_0^H \mathbf{X}^{-1}\mathbf{p}_0} = \mathbf{p}_0^H \mathbf{X}^{-1}\mathbf{p}_0. \end{aligned} \tag{B7-8}$$

Appendix B8: Sub-optimal SINR Solution for Structure 3

Let the weight vector be denoted by $\mathbf{w}_k$ at any given time instant k. Then from Figure 4.8, the weight vector and the channel vector can be composed into a composite channel. Then with this given composite channel, the receive filter can be designed to provide optimum SNR improvement at the output of the receiver. The overall channel can be expressed as

$$\begin{aligned} h_k &= w_1 c_k^{(1)} * d_k + w_2 c_k^{(2)} * d_k \\ &= w_1 \sum_n d_n c_{k-n}^{(1)} + w_2 \sum_n d_n c_{k-n}^{(2)} \\ &= \sum_n (w_1 c_{k-n}^{(1)} + w_2 c_{k-n}^{(2)}) d_n . \end{aligned} \tag{B8-1}$$

Proceeding as in the previous derivations, h_k can be written as

$$h_k = \mathbf{p}_k^H \mathbf{d} \tag{B8-2}$$

where the vectors $\mathbf{p}_k$ and $\mathbf{d}$ are defined appropriately. The expression for SNR or the cost function in this case becomes

$$J(\mathbf{d}) = SNR(\mathbf{d})\Big|_{\mathbf{w}_k} = \frac{\mathbf{d}^H \mathbf{p}_0 \mathbf{p}_0^H \mathbf{d}}{\mathbf{d}^H \sum_{k \neq 0} \mathbf{p}_k \mathbf{p}_k^H \mathbf{d} + \sigma^2 \mathbf{d}^H \mathbf{d}} . \tag{B8-3}$$

Now the optimization problem can be defined as

$$\begin{aligned} &\max_{\mathbf{d}} \quad J(\mathbf{d}) = \frac{\mathbf{d}^H \mathbf{p}_0 \mathbf{p}_0^H \mathbf{d}}{\mathbf{d}^H \sum_{k \neq 0} \mathbf{p}_k \mathbf{p}_k^H \mathbf{d} + \sigma^2 \mathbf{d}^H \mathbf{d}} \\ &s.t. \quad \|\mathbf{d}\|_2^2 = 1. \end{aligned} \tag{B8-4}$$

This optimization problem is similar to the problem described and solved in Appendix B7. The solution to this problem can thus be written as

$$\mathbf{d}_{opt} = \frac{\left[\sum_{k \neq 0} \mathbf{p}_k \mathbf{p}_k^H + \sigma^2 \mathbf{I} \right]^{-1} \mathbf{p}_0}{\left\| \left[\sum_{k \neq 0} \mathbf{p}_k \mathbf{p}_k^H + \sigma^2 \mathbf{I} \right]^{-1} \mathbf{p}_0 \right\|_2} . \tag{B8-5}$$

After solving for optimal $\mathbf{d}$, optimization is carried out for the weight vector. The receive filter now can be merged with the channel to form the composite channel. The overall channel gain at time k can be written as

$$
\begin{aligned}
h_k &= w_1 c_k^{(1)} * d_k + w_2 c_k^{(2)} * d_k \\
&= w_1 \mathbf{c}_k^{1,H} \underline{d} + w_2 \mathbf{c}_k^{2,H} \underline{d} \\
&= \left[w_1 \; w_2 \right] \begin{bmatrix} \mathbf{c}_k^{1,H} \underline{d} \\ \mathbf{c}_k^{2,H} \underline{d} \end{bmatrix} \\
&= \mathbf{w}^H \mathbf{q}_k .
\end{aligned} \tag{B8-6}
$$

In the above expression, different vectors are defined as

$$
\begin{aligned}
\mathbf{c}_k^{1,2} &= \left\{ c_{k-l}^{1,2} \right\} \; for \; l = -L, \cdots, 0, \cdots, L \\
\mathbf{w} &= \begin{bmatrix} w_1^* \\ w_2^* \end{bmatrix} .
\end{aligned} \tag{B8-7}
$$

As before, the optimum SNR can be expressed as

$$
\begin{aligned}
SNR &= \frac{\left| h_0 \right|^2}{\sum_{k \neq 0} \left| h_k \right|^2 + \sigma^2 \sum_{k \neq 0} \left| d_k \right|^2} \\
&= \frac{\mathbf{w}^H \mathbf{q}_0 \mathbf{q}_0^H \mathbf{w}}{\mathbf{w}^H \sum_{k \neq 0} \mathbf{q}_k \mathbf{q}_k^H \mathbf{w} + \sigma^2 \mathbf{d}^H \mathbf{d}} .
\end{aligned} \tag{B8-8}
$$

Now the SNR or the cost function can be written as (norm of **d** set to unity)

$$
J(\mathbf{w}) = \frac{\mathbf{w}^H \mathbf{q}_0 \mathbf{q}_0^H \mathbf{w}}{\mathbf{w}^H \left[\sum_{k \neq 0} \mathbf{q}_k \mathbf{q}_k^H + \sigma^2 \mathbf{I} \right] \mathbf{w}} . \tag{B8-9}
$$

The optimization problem for the weight vector can be expressed as

$$
\begin{aligned}
&\max_{\mathbf{w}} \quad J(\mathbf{w}) = \frac{\mathbf{w}^H \mathbf{q}_0 \mathbf{q}_0^H \mathbf{w}}{\mathbf{w}^H \left[\sum_{k \neq 0} \mathbf{q}_k \mathbf{q}_k^H + \sigma^2 \mathbf{I} \right] \mathbf{w}} \\
&s.t. \quad \left\| \mathbf{w} \right\|_2^2 = 1.
\end{aligned} \tag{B8-10}
$$

The optimization problem with respect to the weight vector has the same form for the problem with respect to the receive filter. The optimal solution in this case can be written directly as

$$
\mathbf{w}_{opt} = \frac{\left[\sum_{k \neq 0} \mathbf{q}_k \mathbf{q}_k^H + \sigma^2 \mathbf{I} \right]^{-1} \mathbf{q}_0}{\left\| \left[\sum_{k \neq 0} \mathbf{q}_k \mathbf{q}_k^H + \sigma^2 \mathbf{I} \right]^{-1} \mathbf{q}_0 \right\|_2} . \tag{B8-11}
$$

Appendix C1: Proof of equation (3) in Chapter 9

In this appendix, a proof for the identity using the principles of mathematical induction is provided.

Define $I_N(s, x_N)$ as

$$I_N(s, x_N) = \int_0^{x_N} e^{-sx_{N-1}} f(x_{N-1}) \cdots\cdots \int_0^{x_2} e^{-sx_1} f(x_1) dx_1 \cdots dx_{N-1}, \quad N \geq 2 \tag{C.1}$$

We will prove that the above multivariate nested integral can be transformed into a power of a univariate integral, viz.,

$$I_N(s, x_N) = \frac{1}{(N-1)!}\left(H(s, x_N)\right)^{N-1}, N \geq 2 \tag{C.2}$$

where $H(s, x) = \int_0^x e^{-sy} f(y)\, dy$ is the marginal mgf of a CCI signal power.

Let N= 2 in (C.1) and we obtain

$$I_2(s, x_2) = H(s, x_2) \tag{C.3}$$

implying that (C.2) holds for N=2.

Assume that (C.2) holds for N= D-1. This implies that

$$I_{D-1}(s, x_{D-1}) = \frac{1}{(D-2)!}\left(H(s, x_{D-1})\right)^{D-2} \tag{C.4}$$

Using the definition of (C.1) and the assumption of (C.4), we can write $I_D(s, x_D)$ as

$$I_D(s, x_D) = \int_0^{x_D} e^{-sx_{D-1}} f(x_{D-1}) \frac{\left[H(s, x_{D-1})\right]^{D-2}}{(D-2)!} dx_{D-1} \tag{C.5}$$

Since $\frac{d}{dx_{D-1}} H(s, x_{D-1}) = e^{-sx_{D-1}} f(x_{D-1})\, dx_{D-1}$, we can simplify (C.5) into

$$I_D(s, x_D) = \frac{1}{(D-1)!}\left[H(s, x_D)\right]^{D-1} \tag{C.6}$$

using the integral identity

$$\int_a^b \left[g(x)\right]^n \left[\frac{d}{dx} g(x)\right] dx = \frac{\left[f(b)\right]^{n+1} - \left[f(a)\right]^{n+1}}{n+1} \tag{C.7}$$

Equation (C.6) is identical to (C.2) implying that (C.2) holds for N=D. Therefore, by mathematical induction, (C.2) holds for arbitrary integer $N \geq 2$.

Appendix C2: Summary of common channel models

In this appendix, we provide a brief description of four different channel models as well as summarize the marginal mgf of signal power for each channel model, respectively.

A. Rayleigh channel model

Faded signal amplitudes in macro-cellular mobile radio environments, in the absence of a direct line of sight (LOS) component, are usually modeled as Rayleigh distribution [RAP96]. Tropospheric and ionospheric propagation based on reflection and refraction are also modeled by this distribution [SUG95]. The marginal mgf for an exponential distribution is expressed as

$$H(s,x) = \frac{1}{1+s\overline{p}_i}\left[1-e^{-x\left(s+1/\overline{p}_i\right)}\right] \tag{C.8}$$

where $\overline{p}_i$ denotes the average signal power.

B. Rice channel model

In microcellular environments, including urban and suburban land mobile, and indoor (picocell), there exists a dominant LOS propagation path in addition to numerous diffused multipath components between the transmitter and the receiver. The fade coefficients in this case are modeled with Rician distributions with the Rice factor K_i that indicates the ratio between the specular and the diffused components [BUL89]. For the limiting case of K_i = 0, Ricean distribution reduces to Rayleigh distribution. The marginal mgf for a non-central chi-square distribution is given by

$$H(s,x) = \frac{1+K_i}{1+K_i+s\overline{p}_i} e^{\frac{-s\overline{p}_i K_i}{1+K_i+s\overline{p}_i}}\left[1-Q\left[\sqrt{\frac{2K_i(1+K_i)}{1+K_i+s\overline{p}_i}},\sqrt{\frac{2(1+K_i+s\overline{p}_i)x}{\overline{p}_i}}\right]\right] \tag{C.9}$$

where, $Q\left(\sqrt{2a},\sqrt{2b}\right)=\int_b^{\infty} e^{(-t-a)} I_0\left(2\sqrt{at}\right)dt$ denotes the first-order Marcum Q-function and K_i is the Rice factor of the CCI signals.

C. Nakagami-m channel model

Indoor mobile propagation environments are best modeled as Nakagami-m distribution [AUL81] -[DER91]. This distribution includes other important fading distributions via the fading index m_i, e.g., $m_i = 1$ refers to Rayleigh distribution while $m_i = \infty$ indicates no fading. In this case, the marginal mgf of a gamma variate is given by

$$H(s,x) = \left(\frac{m_i}{m_i + s\overline{p}_i}\right)^{m_i} \left[1 - \frac{\Gamma\left[m_i, x\left(m_i + s\overline{p}_i\right)/\overline{p}_i\right]}{\Gamma(m_i)}\right] \qquad \text{(C.10)}$$

where $\Gamma(a,x) = \int_x^\infty e^{-t} t^{a-1} dt$ is the complementary incomplete Gamma function. If the fading index m_i assumes a positive integer value, (C.10) may be simplified as

$$H(s,x) = \left(\frac{m_i}{m_i + s\overline{p}_i}\right)^{m_i} \left[1 - e^{-sx - \frac{m_i x}{\overline{p}_i}} \sum_{u=0}^{m_i - 1} \frac{\left[x\left(m_i / \overline{p}_i + s\right)\right]^u}{u!}\right] \qquad \text{(C.11)}$$

D. Nakagami-q channel model

Satellite links subject to strong ionospheric scintillation tend to follow Nakagami-q distribution (also known as Hoyt distribution). The limiting values of the fading parameter $b_i = \frac{1 - q_i^2}{1 + q_i^2}$, $\left(0 \le q_i \le \infty\right)$ include Rayleigh $\left(b_i = 0\right)$ and one-sided Gaussian distribution $\left(b_i = 1\right)$. The marginal mgf for Nakagami-q fading is as follows

$$H(s,x) = \frac{\sqrt{1 - b_i^2}}{s\left(1 - b_i^2\right)\overline{p}_i + 1} I_e\left(\frac{b_i}{s\left(1 - b_i^2\right)\overline{p}_i + 1}, \frac{s\left(1 - b_i^2\right)\overline{p}_i}{s\left(1 - b_i^2\right)\overline{p}_i + 1} x\right) \qquad \text{(C.12)}$$

where $\left|b_i\right| \le 1$ and Rice's I_e-function is expressed as $I_e(k,x) = \int_0^x e^{-t} I_0(kt)\, dt$

Reference

[3GP99a] “TS 25.211 V2.1.0 (1999-06),” a 3GPP Technical Specification document on physical channels and mapping of Transport channels onto physical channels (FDD), 1999.

[3GP99b] “3GPP RAN 25.214 V1.1.2 (1999-08),” a 3GPP Radio Access Network document, August 1999.

[3GP99c] TS 25.211 v2.2.1, 3GPP TSG RAN document, August 1999.

[3GP99d] TS 25.214 v3.0.0 (1999-10), 3GPP TSG RAN document, 1999.

[ABR70] M. Abramowitz and I. A. Stegun, Handbook of Mathematical Functions, Dover Publications Inc., New York, 1970.

[ABR00] G. Abreu, and R. Kohno, “ Smart antenna for IEEE 802.11 wireless LAN II with near field distortion compensation,” 11th IEEE International Symposium on Personal Indoor and Mobile Radio Communications. PIMRC 2000 vol. 2, 2000, pp. 1454-1458.

[ADN00] N. Adnani, and R. J. C. Bultitude, ‘Analysis of Wideband Measurement Data to Assess and Predict System Performances for IMT2000 Systems’, *IEEE RAWCON*, 2000, pp. 55-58.

[ALA98] S. M. Alamouti, “A Simple Transmit Diversity Technique for Wireless Communications,” *IEEE Journal on Selected Areas in Communications*, vol. 16, no. 8, October 1998.

[ALA98] S. M. Alamouti, V. Tarokh, and P. Poon, “Trellis-Coded Modulation and Transmit Diversity: Design Criteria and Performance Evaluation,” *IEEE International Conference on Universal Personal Communications*, vol. 1, 1998.

[ALO99] M-S. Alouini, A. Bastami and E. Ebbini, “Outage Probability of Cellular Mobile Radio Systems with Successive Interference Cancellation,” *Proc. 1999 Asilomar Conference on Signals, Systems and Computers*, pp. 192-196.

[ANN99] M. Dell’Anna and A. H. Aghvami, “Performance of Optimum and Suboptimum Combining at the Antenna Array of a W-CDMA System,” *IEEE Journal on Selected Transactions*, vol. 17, no. 12, December, 1999.

[ANN01a] A. Annamalai, C. Tellambura and V. K. Bhargava, “Simple and Accurate Methods for Outage Analysis in Cellular Mobile Radio Systems — A Unified Approach,” *IEEE Transactions on Communications*, Vol. 49, No. 2, Feb. 2001, pp. 303-316.

[ANN01b] A. Annamalai and C. Tellambura, “Error Rates for Nakagami-m Fading Multichannel Reception of Binary and M-ary signals,” *IEEE Transactions on Communications*, vol. 49, no. 1, January 2001, pp. 58-68.

[ANN02] A. Annamalai and V. Srivastava, “Outage Probability of Cellular Mobile Radio Systems Employing a Selective Co-channel Interference Cancellation Scheme,” *IEEE VTS 54th Vehicular Technology Conference*, Fall 2001, Volume 1, pp. 492 –496. (Also appeared in the Journal on Wireless Communications and Mobile Computing, vol. 2, pp. 421-438, 2002.)

[ARN92] B. C. Arnold, N. Balakrishnan and H. N. Nagaraja, *A First Course in Order Statistics*, Wiley, New York: 1992.

[AUL81] T. Aulin, “Characteristics of a Digital Mobile Radio Channel,” *IEEE Trans. Vehicular Technology*, vol. VT-30, May 1981, pp. 45-53.

[BER67] T. Berger and D. W. Tufts, “Optimum Pulse Amplitude Modulation Part I: Transmitter-Receiver Design and Bounds from Information Theory,” *IEEE Transactions on Information Theory*, vol. IT-13, no. 2, April 1967, pp. 196-208.

[BER95] R. C. Bernhardt, “The Use of Multiple-Beam Directional Antennas in Wireless Messaging Systems,” *Vehicular Technology Conference*, 1995, pp. 858-861.

[BEU90] N.C. Beaulieu, “An Infinite Series for the Computation of the Complementary Probability Distribution Function of a Sum of Independent Random Variables and Its Application to the Sum of Rayleigh Random Variables,” *IEEE Transactions on Communications*, Volume: 38 Issue: 9, Sept. 1990, pp.: 1463 –1474.

[BON99] C. S. Bontu and D. D. Falconer, “Diversity Transmission and Adaptive MLSE for Digital Cellular Radio,” *IEEE Transactions on Vehicular Technology*, vol. 48, no. 5, September 1999, pp. 1488-1502.

[BRA98] C. Braun, G. Engblom and C. Beckman, “Antenna Diversity for Mobile Telephones,” *IEEE Antennas and Propagation Society International Symposium*, vol. 4, 1998, pp. 2220-2203.

[BRA99] C. Braun, G. Engblom and C. Beckman, “Evaluation of Antenna Diversity Performance for Mobile Handsets using 3-D Measurement Data,” *IEEE Transactions on Antennas and Propagation*, vol. 47, No. 11, November 1999, pp. 1736-1738.

[BRE59] D. G. Brennan, “Linear Diversity Combining Techniques,” *Proceedings of the IRE*, June 1959, pp. 1075-1102.

[BUL89] R. J. C. Bultitude, S. A. Mahmoud, and W. A. Sullivan, “A Comparison of Indoor Radio Propagation Characteristics at 10 MHz and 1.75 GHz,” *IEEE J. Select Areas Comm.*, vol. 7, no. 1, Jan. 1989, pp. 20–30.

[CHE99] A. Chheda and D. Paranchych, “Performance Evaluation of Two Transmit Diversity Techniques for CDMA-2000,” 1999, pp. 893-897.

[CHO00] R. L.-U Choi, K. B. Letaief and R. D. Murch, “MIMO CDMA antenna systems,” IEEE International Conference on Communications, vol.2, 2000, pp(s): 990 –994.

[CHO02a] J. Choi, “Performance Analysis for Transmit Antenna Diversity with/without Channel Information,” *IEEE Transactions on Vehicular Technology*, vol. 51, no. 1, pp. 101-113, January 2002.

[CHO02b] J. Choi, H.K. Choi and H.W. Lee, “An Adaptive Technique for Transmit Antenna Diversity with Feedback,” *IEEE Transactions on Vehicular Technology*, vol. 51, no. 4, pp. 617-623, July 2002.

[CHO99] W.-J. Choi and J. M. Cioffi, “Multiple Input/Multiple Output (MIMO) Equalization for Space-Time Block Coding,” IEEE Pacific Rim Conference on Communications, Computers and Signal Processing, 1999, pp. 341-344.

[COL96] J. S. Colburn, Y. Rahmat-Samii, M. A. Jensen and G. J. Pottie, “Diversity Performance of Dual Antenna Personal Communications Handsets,” *IEEE Antennas and Propagation Society International Symposium 1996 Digest*, vol. 1, pp. 730-733.

[DAH98] E. Dahlman, B. Gudmundson, M. Nilsson, and J. Skold, “UMTS/IMT-2000 Based on Wideband CDMA,” *IEEE Communications Magazine*, vol. 36, no. 9, September 1998, pp. 70-80.

[DAS95] V. M. DaSilva and E. S. Sousa, “Fading-resistant Transmission from Several Antennas,” 1995, pp. 1218-1222.

[DAY00] M. Day, “Matrix Theory (MATH 5524),” a collection of lecture notes for teaching MATH5524 in the Spring 2000 semester at Virginia Tech.

[DER91] U. Dersch and W. R. Braun, “A Physical Mobile Radio Channel Model,” *IEEE Vehicular Technology Conference* 1991, pp. 289-294.

[DES00] B. Desplanches, A. Sharaiha, J. F. Diouris, and C. Terret, “Experimental Study of 2-Dimensioal Rake Receiver with Transmit Diversity,” *Antennas and Propagation*, 2000, Abstract #1129 (a01129), http://www.estec.esa.nl/ap2000/abstracts.

[DIE01] C. B. Dietrich, Jr., K. Dietze, J. R. Nealy, and W. L. Stutzman, “Spatial, Polarization, and Pattern Diversity for Wireless Handheld Terminals,” IEEE Transactions on Antennas and Propagation, vol. 49, (9), September 2001, pp. 1271-1281.

[EGG00] P.C.F. Eggers, I. Z. Kovács, K. Olesen, and G. Kuijpers, ‘Measurements of Wideband Multi-element Transmit-Receive Diversity Channels in the UMTS-band’, VTC 2000, pp. 1683-1689.

[ETS98] “UMTS (XX.08) V0.0.2 1998-09,” an ETSI document on air interface, 1998.

[ETS00a]. ETSI TS 125 211 v3.2.0 (2000-3).

[ETS00b]. *Physical Layer Procedure* (*FDD*), ETSI TS 125 214 v3.2.0 (2000-3).

[FAR98] F. Rashid-Farrokhi, R. Liu, and L. Tassiulas, “Transmit Beamforming and Power Control for Cellular Wireless Systems,” *IEEE Journal on Selected Areas in Communications*, vol.16, No.8, October 1998, pp. 1437-1449.

[FAR95] C. Farsakh and J. Nossek, “Channel Allocation and Downlink Beamforming in an SDMA Mobile Radio System,” *International Symposium on Personal Indoor and Mobile Radio Communications*, 1995.

[FOS98] G. J. Foshcini and M. J. Gans, “On Limits of Wireless Communications in a Fading Environment when using Multiple Antennas,” Wireless Personal Communications vol.6, pp. 311-335, 1998.

[FUJ00] T. Fujii and M. Nakagawa, “Indoor multi-base stations system with simultaneous transmission using OFDM adaptive array antenna,” 11th IEEE International Symposium on Personal Indoor and Mobile Radio Communications. PIMRC 2000, vol.2, pp. 1241-1245.

[GER94] D. Gerlach and A. Paulraj, “Adaptive Transmitting Antenna Arrays with Feedback,” *IEEE Signal Processing Letters*, vol.1, no.10, October 1994.

[GOL93] G. H. Golub, and C. F. Van Loan, *Matrix Computations*, John Hopkins University Library Press, 2nd Edition, 1993.

[GRE00] B. M. Green and M. A. Jensen, “Diversity performance of dual-antenna handsets near operator tissue,” *IEEE Transactions on Antennas and Propagation*, Volume: 48 Issue: 7, July 2000, pp. 1017 –1024.

[HAS00] M. O. Hasna and M-S. Alouini, “Performance Evaluation of Cellular Mobile Radio Systems with Successive Co-Channel Interference Cancellation,” *Proc. 2000 IEEE Vehicular Technology Conference (Fall)*, pp. 1506-1513.

[HAY96] S. Haykin, *Adaptive Filter Theory*, Upper Saddle River, New Jersey: Prentice Hall, 1996.

[HEA98] R. W. Heath and A. Paulraj, "A Simple Scheme for Transmit Diversity Using Partial Channel Feedback," *Conference Record of 32nd Asilomar Conference on Signals, Systems and Computers*, vol. 2, 1998, pp. 1073-1077.

[HEA99]. R. W. Heath and A. Paulraj, "Transmit Diversity Using Decision-Directed Antenna Hopping," *IEEE* (?) 1999, pp. 141-145.

[HEI98] T. Heikkinen and A. Hottinen, "On Downlink Power Control and Capacity with Multi-Antenna Transmision," *Vehicular Technology Conference*, 1998, pp. 475-479.

[HEM99] H. Sampath and A. J. Paulraj, "Joint transmit and receive optimization for high data rate wireless communication using multiple Antennas," Thirty-Third Asilomar Conference on Signals, Systems, and Computers, vol.1, 1999, pp: 215 –219.

[HIC01] J. Hicks, S. Bayram, W.H. Tranter, R. J. Boyle, J. H. Reed, "Overloaded array processing with spatially reduced search joint detection," *IEEE Journal on Selected Areas in Communications*, Volume: 19 Issue: 8, Aug. 2001 pp.1584 –1593.

[HIR92] A. Hiroike, F. Adachi, and N. Nakajima, "Combined effects of Phase Sweeping Transmitter Diversity and Channel Coding," *IEEE Transactions on Vehicular Technology*, vol. 41, no. 2, May 1992, pp. 170-176.

[HOT98] A. Hottinen and R. Wichman, "Transmit Diversity by Antenna Selection in CDMA Downlink," *IEEE International Symposium on Spread Spectrum Techniques & Applications*, vol.3, pp. 767-770, 1998.

[HOT00] A. Hottinen and R. Wichman, "Transmit Diversity Using Filtered Feedback Weights in the FDD/WCDMA System," *2000 International Zurich Seminar on Broadband Communications- Accessing, Transmission, Networking*, 2000, pp. 15-21.

[JAK74]. W. C. Jakes, *Mobile Microwave Communications*, New York: John Wiley, 1974.

[JAL99] L. M. A. Jalloul, K. Rohani, K. Kuchi, and J. Chen, "Performance Analysis of CDMA Transmit Diversity Methods," 1999, pp. 1326-1330.

[KAR99]. P. Karlsson, C. Bergljung, E. Thomsen, and H. Börjeson, 'Wideband Measurement and Analysis of Penetration Loss in the 5 GHz Band', *IEEE VTC*, 1999, pp. 2323-2328.

[KOR97] I. A. Korisch, M. Sumetskii, and S. S. Patel, "Analysis of Handset antenna Performance in a Multipath Environment," *IEEE Antennas and Propagation Society International Symposium*, 1997, vol. 1, pp. 402-405.

[KTF03] http://www.3g.co.uk/PR/Jan2003/4667.htm.

[LEE00] K. Lee and M. Nakagawa. "Adaptive base station sector antenna pre-selection transmitter diversity using CDMA forward link signal for indoor wireless LAN," IEICE Transactions on Communications, vol. E83-B, no.11, Nov. 2000, pp.2464-73.

[LEF97] M. LeFevre, M. A. Jensen, and M. D. Rice, "Indoor Measurement of Handset Dual-Antenna Diversity Performance," *Vehicular Technology Conference*, 1997.

[LIA95] J-W. Liang and A. Paulraj, "Forward Link Antenna Diversity Using Feedback for Indoor Communication Systems," *ICASSP* 1995, pp. 1753-1755.

[LIK62] J. Likes, "On the Distribution of Certain Linear Functions of Ordered Sample from Exponential Population," *Annals Inst. Stat. and Math*., Vol. 13, 1962, pp. 225-230.

[LIN00] E. Lindskog and A. Paulraj, "A Transmit Diversity Scheme for Channels with Intersymbol Interference," *International Conference on Communications-2000*, pp. ?

[LIT96] J. Litva and T. K. Y. Lo, *Digital Beamforming in Wireless Communications*, Boston: Artech House, 1996.

[LO99] T. K. Y. Lo, "Maximum Ratio Transmission," *IEEE Transactions on Communications*, vol.47, no.10, October 1999.

[LOM98]. G. Lombardi, V. Degli-Esposti, and C. Passerini, 'Wideband Measurement and Simulation of the DECT Indoor Propagation Channel', IEEE 48th VTC, 1998, vol. (1), pp. 11-15.

[MAJ] M. V. Majmundar, "Pre-Slot Selection Antenna Diversity at the Mobile Handset for TDMA Systems," ?.

[MAN96] S. Mano, M. Kimata, N. Inagaki and N. Kikuma, "Application of Planar Multibeam Array Antennas to Diversity Reception," *Electronics and Communications in Japan*, Part 1, Vol. 79, no. 11, 1996, pp. 104-112.

[MEC95] H. K. Mecklai and R. S. Blum, "Transmit Antenna Diversity for Wireless Communications," *IEEE International Conference on Communications*, vol. 3, 1995.

[MOC99] H. Mochizuki, T. Sugiyama, and R. Kohno "A simplified adaptive array antenna system for FH/SS indoor radio communications" 10th International Symposium on Personal, Indoor and Mobile Radio Communications (PIMRC'99), vol.2, 1999, pp.792-796.

[MOS00] T. Biedka, C. Dietrich, K. Dietze, R. B. Ertel, B-K. Kim, R. Mostafa, W. Newhall, U. Ringel, J. H. Reed, D. Sweeney, W. L. Stutzman, R. J. Boyle, and A. Tikku, "Smart Antenna for Handsets," *TI DSPFest*, Houston, August 2000.

[OGA94] K. Ogawa and T. Uwano, “A Diversity Antenna for Very Small 800-MHz Band Portable Telephones,” *IEEE Transactions on Antennas and Propagation*, 1994, pp. 1342-1345.

[PAN03] http://www.thevideodoctor.com/pages/KX-TG2593B.htm

[PAR00] S. Parkvall, M. Karlsson, M. Samuelsson, L. Hedlund, and B. Göransson, “Transmit Diversity in WCDMA: Link and System Level Results,” *VTC 2000*, pp. 864-868.

[PAU] E. Pauliina and E. Bonek, “Diversity Arrangements for Internal Handset Antennas,” *IEEE Vehicular Technology Conference* (?), pp. 589- 593.

[PED] G. F. Pederson, S. Widell and T. Østervall, “Handheld Antenna Diversity Evaluation in a DCS-1800 Small Cell,” *IEEE Vehicular Technology Conference* (?), pp. 584-588.

[PRA98] R. Prasad, “Universal Wireless Personal Communications”, Chapter 6, Artech House Publishers, Boston London, 1998.

[PRO95]. J. G. Proakis, *Digital Communications*, 3rd edition, New York: McGraw Hill, 1995.

[QUA01] QCTEST, 1xEV-DO Trial phone product from Qualcomm, 2001, http://www.qualcomm.com/qctest/products/qtp5500.html

[RAG00] B. Raghothaman, G. Mandyam, and R. T. Derryberry, “Performance of closed loop Transmit Diversity with Feedback Delay,” *34th Asilomar Conference on Signals, Systems and Computers*, 2000, vol.1, pp. 102 –105.

[RAI99] M. Raitola, A. Hottinen, and R. Wichman, “Transmission Diversity in Wideband CDMA,” *IEEE Vehicular Technology Conference*, 1999.

[RAJ99] D. Rajan and S. D. Gray, “Transmit Diversity Schemes for CDMA-2000,” 1999, pp. 669-673.

[RAN95a] P. Ranta, Z. Honkasalo and Tapanien, “TDMA Cellular Network Application of an Interference Cancellation Technique,” *Proc. IEEE Vehicular Technology Conference*, Chicago, May 1995, pp. 296-300.

[RAN95b] P. Ranta, A. Hottinen and Z. Honkasalo, “Co-channel Interference Cancelling Receiver for TDMA Mobile Systems,” *Proc. IEEE International Conference on Communications*, Seattle, June 1995.

[RAP96] T. S. Rappaport, *Wireless Communications- Principles and Practice*, Prentice Hall, 1996.

[RAY95] G. G. Rayleigh, S. N. Diggavi, V. K. Jones, and A. Paulraj,"A Blind Adaptive Transmit Antenna Algorithm for Wireless Communication," *IEEE ?*, 1995.

[SAM03] http://www.promediamemphis.com/samson.htm

[SIM98] M. K. Simon and M-S., Alouini, "A Unified Approach to the Performance Analysis of Digital Communication over Generalized Fading Channels," *Proceedings of the IEEE*, vol. 86, no. 9, September 1998, pp. 1860-1877.

[STU96] G. L. Stuber, *Principles of Mobile Communications*, Kluwer Academic Publisher, Boston: 1996.

[SUG95] G. R. Sugar, "Some Fading Characteristics of Regular VHF Ionospheric Propagation," *Proc. IRE*, October 1995, pp. 1432-1436.

[SUH37] P. V. Suhatme, "Tests of Significance for Samples of the Population with Two Degrees of Freedom," *Annals of Eugenics*, Vol. 8, 1937, pp. 52-56.

[TAN97] S. Tanaka, M. Sawahashi, and F. Adachi, "Pilot Symbol-Assisted Decision-Directed Coherent Adaptive Array Diversity for DS-CDMA Mobile Radio Reverse Link," *IEICE Transactions Fundamentals*, vol. E80-A, No. 12, pp. 2445-2453, December, 1997.

[TAR98] V. Tarokh, S. M. Alamouti, and P. Poon, "New Detection Schemes for Transmit Diversity with no Channel Estimation," *IEEE International Conference on Universal Personal Communications*, vol. 2, 1998.

[TSU89] K. Tsunekawa, "Diversity antennas for portable telephones," *Vehicular Technology Conference*, 1989, pp. 50-56.

[VAU93] R. G. Vaughan, "Closely spaced monopoles for mobile communications," *Radio Science*, vol. 28, no. 6, November-December, 1993, pp. 1259-1266.

[VAU99] R. Vaughan, "Switched Parasitic Elements for Antenna Diversity," *IEEE Transactions on Antennas and Propagation*, vol. 47, No. 2, February 1999, pp. 399-405.

[WEE93] V. Weerackody, "Diversity for the Direct-Sequence Spread Spectrum System Using Multiple Transmit Antennas," *IEEE* (?) 1993, pp. 1775-1778.

[WIN94] J. H. Winters, "The Diversity Gain of Transmit Diversity in Wireless Systems with Rayleigh Fading," *IEEE International Conference on Communications*, vol. 3, 1994.

[WIN98] J. H. Winters, “The Diversity Gain of Transmit Diversity in Wireless Systems with Rayleigh Fading,” *IEEE Transactions on Vehicular Technology*, vol. 47, No. 1, February 1998, pp. 119-123.

[WIT93] A. Wittneben, “A new bandwidth Efficient Transmit Antenna Modulation Diversity Scheme for Linear Digital Modulation,” *IEEE International Conference on Communications*, 1993, vol. 3, pp. 1630-1634.

[WIT94] A. Wittneben and T. Kaltenschnee, “TX Selection Diversity with Prediction: Systematic Nonadaptive Predictor Design”, *IEEE 44th Vehicular Technology Conference*, vol.1, 1994, pp. 1246-1250.

[YAN94a] J. Yang and S. Roy, “On Joint Transmitter and Receiver Optimization for Multiple-Input-Multiple-Output (MIMO) Transmission Systems,” *IEEE Transaction on Communications*, vol. 42, no. 12, December 1994, pp. 3221-3231.

[YAN94b] J. Yang and S. Roy, “Joint Transmitter and Receiver Optimization for Multiple-Input-Multiple-Output Systems with Decision Feedback,” *IEEE Transaction on Information Theory*, vol. 40, no. 5, September 1994, pp. 1334-1347.

[YAN98] W. Yang and G. Xu, “Design of Smart Antenna Downlink Weighting Vectors,” *31st Asilomar Conference Record*, 1998, p.1018-1022.

[ZET94] P. Zetterberg and B. Ottersten, “The Spectrum Efficiency of a Base station Antenna Array System for Spatially Selective Transmission,” *IEEE 44th Vehicular Technology Conference*, 1994.

Vita

Raqibul Mostafa

Raqibul Mostafa was born on June 8, 1966, in Dhaka, Bangladesh. He received his Bachelor of Science degree in Electrical and Electronics Engineering in 1991 from Bangladesh University of Engineering and Technology. He worked as a Lecturer in the department of Electrical and Electronics Engineering of the same university for a year and a half before coming to Virginia Tech for graduate study. He obtained his MS degree in Electrical Engineering from Virginia Tech in 1995. He joined MPRG for his doctoral program in January 1997. He is doing research with Dr. Jeffrey H. Reed in antenna array algorithms and applications.